IMPROVED RESPONSE SPECTRUM ANALYSIS PROCEDURE FOR DESIGN OF REINFORCED CONCRETE TALL BUILDINGS

Mr. Kimleng Khy

จุฬาลงกรณ์มหาวิทยาลัย
CHULALONGKORN UNIVERSITY

A Dissertation Submitted in Partial Fulfillment of the Requirements
for the Degree of Doctor of Philosophy in Civil Engineering
Department of Civil Engineering
Faculty of Engineering
Chulalongkorn University
Academic Year 2018

Copyright of Chulalongkorn University

การปรับปรุงวิธีวิเคราะห์สเปกตรัมผลตอบสนองเพื่อการออกแบบอาคารสูง

นายคิมเล็ง คี

จุฬาลงกรณ์มหาวิทยาลัย
Chulalongkorn University

วิทยานิพนธ์นี้เป็นส่วนหนึ่งของการศึกษาตามหลักสูตรปริญญาวิศวกรรมศาสตรดุษฎีบัณฑิต
สาขาวิชาวิศวกรรมโยธา ภาควิชาวิศวกรรมโยธา
คณะวิศวกรรมศาสตร์ จุฬาลงกรณ์มหาวิทยาลัย
ปีการศึกษา 2561

ลิขสิทธิ์ของจุฬาลงกรณ์มหาวิทยาลัย

Thesis Title	IMPROVED RESPONSE SPECTRUM ANALYSIS PROCEDURE FOR DESIGN OF REINFORCED CONCRETE TALL BUILDINGS
By	Mr. Kimleng Khy
Field of Study	Civil Engineering
Thesis Advisor	Assistant Professor Chatpan Chintanapakdee, Ph.D.
Thesis Co Advisor	Associate Professor Anil C. Wijeyewickrema, Ph.D.

Accepted by the Faculty of Engineering, Chulalongkorn University in Partial Fulfillment of the Requirement for the Doctor of Philosophy

..... Dean of the Faculty of Engineering
(Associate Professor SUPOT TEACHAVORASINSKUN, D.Eng.)

DISSERTATION COMMITTEE

..... Chairman
(Associate Professor TOSPOL PINKAEW, D.Eng.)

..... Thesis Advisor
(Assistant Professor Chatpan Chintanapakdee, Ph.D.)

..... Thesis Co-Advisor
(Associate Professor Anil C. Wijeyewickrema, Ph.D.)

..... Examiner
(Associate Professor Anat Ruangrassamee, Ph.D.)

..... Examiner
(Assistant Professor Watanachai Smittakorn, Ph.D.)

..... External Examiner
(Associate Professor Sutat Leelataviwat, Ph.D.)

จุฬาลงกรณ์มหาวิทยาลัย
Chulalongkorn University

คิมเล็ง คี : การปรับปรุงวิธีวิเคราะห์สเปกตรัมผลตอบสนองเพื่อการออกแบบอาคารสูง. (IMPROVED RESPONSE SPECTRUM ANALYSIS PROCEDURE FOR DESIGN OF REINFORCED CONCRETE TALL BUILDINGS) อ.ที่ปรึกษาหลัก : ผู้ช่วยศาสตราจารย์ ดร.ฉัตรพันธ์ จินตนาภักดี, อ.ที่ปรึกษาร่วม : รองศาสตราจารย์ ดร.เอนิล ไวเจวิเครมา

ผลการวิจัยจำนวนมากพบว่าวิธีสเปกตรัมผลตอบสนอง (Response Spectrum Analysis, RSA) ที่วิศวกรนิยมใช้ออกแบบอาคารสูงในปัจจุบันให้ค่าแรงเฉือนสำหรับการออกแบบองค์อาคารแนวดิ่งที่ต่ำเกินไป ในเหตุการณ์แผ่นดินไหวจริงในต่างประเทศมีการสังเกตพบการวิบัติและความเสียหายของกำแพงรับแรงเฉือนคอนกรีตเสริมเหล็กในอาคารสูงปานกลางและอาคารสูง งานวิจัยนี้จึงได้พัฒนาและปรับปรุงวิธีสเปกตรัมผลตอบสนอง เรียกว่า วิธี Modified Response Spectrum Analysis (MRSA) ซึ่งมีการเสนอวิธีการคำนวณแรงเฉือนสำหรับการออกแบบองค์อาคารแนวดิ่งและวิธีประมาณค่าความเครียดเนื่องจากผลของแรงตามแนวแกนร่วมกับโมเมนต์ดัดด้วยเพื่อหาตำแหน่งในองค์อาคารแนวดิ่งที่ต้องเสริมเหล็กรายละเอียดให้มีความเหนียว การศึกษานี้ใช้อาคารตัวอย่างที่มีกำแพงรับแรงเฉือนเป็นระบบต้านทานแรงด้านข้าง 6 หลัง สูง 15 ถึง 39 ชั้น และอาคารโครงต้านแรงดัด 4 หลัง สูง 3 ถึง 15 ชั้น และใช้คลื่นแผ่นดินไหวที่คาดว่าจะเกิดขึ้นที่กรุงเทพมหานครและเชียงใหม่กระทำ โดยออกแบบอาคารเหล่านั้นตามวิธี RSA แบบเดิม จากนั้นทำการวิเคราะห์ด้วยวิธีแบบประวัติเวลาไม่เชิงเส้น (Nonlinear Response History Analysis, NLRHA) ซึ่งเป็นวิธีการวิเคราะห์ที่ถือว่ามีความถูกต้องที่สุดและใช้ผลเป็นค่าอ้างอิงในการประเมินความถูกต้องของวิธี RSA และ MRSA ผลการศึกษาพบว่า วิธี RSA ให้ค่าการกระจัดและการเคลื่อนตัวสัมพัทธ์ระหว่างชั้นที่ถูกต้องดีสำหรับโครงสร้างกำแพงรับแรงเฉือน แต่ให้ค่าที่ต่ำเกินไปสำหรับอาคารโครงต้านแรงดัด หากใช้ผลการวิเคราะห์แบบยืดหยุ่นเชิงเส้นจะมีความถูกต้องดีกว่า ส่วนการคำนวณแรงเฉือนในองค์อาคารแนวดิ่ง วิธี MRSA สามารถให้ค่าแรงเฉือนที่ถูกต้องใกล้เคียงกับค่าจากวิธี NLRHA ซึ่งทำให้วิธี MRSA ดีกว่าวิธี RSA แบบเดิมในทุกกรณี โดยการออกแบบกำลังต้านทานโมเมนต์ดัดในวิธี MRSA ยังคงเหมือนกับวิธี RSA แบบเดิมแต่เพิ่มขั้นตอนการตรวจสอบความเครียดในองค์อาคารแนวดิ่งเพื่อหาตำแหน่งที่จำเป็นต้องเสริมเหล็กรายละเอียดให้มีความเหนียวหากความเครียดมากเกินเกณฑ์ที่กำหนด จากการตรวจสอบพบว่าวิธีประมาณค่าความเครียดที่เสนอใหม่สามารถให้ค่าใกล้เคียงกับผลการวิเคราะห์ด้วยวิธี NLRHA

สาขาวิชา	วิศวกรรมโยธา	ลายมือชื่อนิสิต .....
ปีการศึกษา	2561	ลายมือชื่อ อ.ที่ปรึกษาหลัก .....
		ลายมือชื่อ อ.ที่ปรึกษาร่วม .....

5971454121 : MAJOR CIVIL ENGINEERING

KEYWORD: Tall buildings, Shear forces, Response spectrum analysis, Modified response spectrum analysis, Nonlinear response history analysis

Kimleng Khy : IMPROVED RESPONSE SPECTRUM ANALYSIS PROCEDURE FOR DESIGN OF REINFORCED CONCRETE TALL BUILDINGS. Advisor: Asst. Prof. Chatpan Chintanapakdee, Ph.D. Co-advisor: Assoc. Prof. Anil C. Wijeyewickrema, Ph.D.

Response spectrum analysis (RSA) procedure commonly used in design practice has been found to underestimate design forces in tall buildings. Failure and damage of reinforced concrete (RC) shear walls in mid-rise and high-rise buildings have been observed in recent earthquakes. In this dissertation, a modified RSA (MRSA) procedure to compute shear forces and strains in RC walls and columns to identify locations requiring ductile detailing was proposed. Six tall RC shear-wall buildings of 15 to 39 stories and four RC moment-frame buildings of 3 to 15 stories subjected to earthquake ground motions expected in Bangkok and Chiang Mai were first designed using seismic demands determined by conventional RSA procedure. Results from nonlinear response history analysis (NLRHA), which is the most accurate method, were used as reference values to evaluate the accuracy of the RSA and MRSA procedures. For floor displacements and story drifts, RSA provides good estimates for shear-wall buildings but underestimates for moment-frame buildings, and linear RSA is recommended for moment-frame buildings. The proposed MRSA method can significantly improve the underestimation of RSA in computing shear forces in vertical members for all cases, i.e., MRSA provides good accuracy when compared with NLRHA. In MRSA procedure, bending moments are computed and designed for in the same way as conventional RSA but ductile detailing in RC walls and columns is to be provided at the locations where combined axial-bending strains exceed a certain limit. The proposed method in MRSA to compute strains can predict well NLRHA results.

Field of Study:	Civil Engineering	Student's Signature .....
Academic Year:	2018	Advisor's Signature .....
		Co-advisor's Signature .....

ACKNOWLEDGEMENTS

I would like to express my sincere gratitude to my advisor, Asst. Prof. Chatpan Chintanapakdee, for his productive guidance, good advice and strong support during my research study for this doctoral degree program. I highly appreciate his valuable time, encouragement and attention to discuss about the research issue with me.

My sincere gratitude is extended to my co-advisor, Assoc. Prof. Anil C. Wijeyewickrema, for his kind support and good advice during my six-month collaborative research in Tokyo Institute of Technology (TIT). His suggestions, corrections and critical comments are highly acknowledged.

I gratefully acknowledge the ASEAN University Network/Southeast Asia Engineering Education Development Network (AUN/SEED-Net) program for granting me the scholarship for my doctoral degree in Chulalongkorn University (CU). The kind support from JICA in Tokyo during my collaborative research in TIT is gratefully acknowledged.

My profound thanks are extended to all committee members, Assoc. Prof. Tospol Pinkaew, Assoc. Prof. Anat Ruangrassamee, Asst. Prof. Watanachai Smittakorn and Assoc. Prof. Sutat Leelataviwat for their thoughtful comments and suggestions for this research.

I would like to thank Prof. Pennung Warnitchai for the helpful suggestions for this research, Assoc. Prof. Nakhorn Poovarodom for the ground motion data and Asst. Prof. Fawad Ahmed Najam for the guidance on nonlinear structural modeling used in this study.

I would also like to acknowledge my Cambodian friends studying in CU and TIT and all my colleagues in the Center of Excellent in Earthquake Engineering and Vibration in CU, and Anil Lab in TIT for their friendship and moral support.

Last but not least, I would like to deeply thank my parents, brothers and especially my wife for their endless encouragement and support which motivate me to complete my research successfully.

Kimleng Khy

TABLE OF CONTENTS

Page

ABSTRACT (THAI) iii

ABSTRACT (ENGLISH) iv

ACKNOWLEDGEMENTS v

TABLE OF CONTENTS vi

LIST OF TABLES x

LIST OF FIGURES xii

CHAPTER 1 INTRODUCTION 1

1.1 Background 1

1.2 Statement of research problem 3

1.3 Objectives of research 4

1.4 Scope of research 5

1.5 Research methodology 5

1.6 Research significance 6

1.7 Outline of dissertation 6

CHAPTER 2 LITERATURE REVIEW 8

2.1 Analysis methods 8

2.1.1 Linear response history analysis and response spectrum analysis 8

2.1.2 Nonlinear response history analysis 10

2.1.3 Modal pushover analysis 11

2.2 Causes of excessive shear demands 11

2.3 Improved estimations of seismic force demands 13

จุฬาลงกรณ์มหาวิทยาลัย
CHULALONGKORN UNIVERSITY

2.3.1 Amplification factor method 13

2.3.2 Higher-mode-elastic method 21

2.3.3 Equivalent linearization method 25

2.4 Summary 30

CHAPTER 3 STRUCTURAL SYSTEMS AND EARTHQUAKE GROUND MOTIONS 32

3.1 Description of studied buildings 32

3.1.1 Tall RC shear-wall buildings 32

3.1.2 RC moment-frame buildings 36

3.2 Analytical models 38

3.2.1 Linear analytical model 39

3.2.2 Nonlinear analytical model 40

3.3 Description of earthquake ground motions 45

3.3.1 Earthquake ground motions in Bangkok 45

3.3.2 Earthquake ground motions in Chiang Mai 49

3.4 Application of conditional mean spectrum in NLRHA 51

3.4.1 Seismic demands from NLRHA using CMS as target spectrum 53

3.4.2 Seismic demands from NLRHA using CMS and UHS as target spectrum .. 54

3.4.3 Summary 60

CHAPTER 4 MODIFIED RESPONSE SPECTRUM ANALYSIS FOR DESIGN OF TALL RC SHEAR-WALL BUILDINGS 61

4.1 Introduction 61

4.2 Response spectrum analysis 61

4.3 Nonlinear response history analysis 66

4.4 Design demands by RSA and NLRHA 67

4.5 Inelasticity of response in each mode 75

4.6 Modified response spectrum analysis 78

4.6.1 Computation of shear forces 79

4.6.1.1 Modified RSA based on higher-mode-elastic approach 79

4.6.1.2 Modified RSA based on higher-mode inelastic approach 81

4.6.2 Computation of strains in RC walls and columns 81

4.6.3 Summary of modified RSA procedure 84

4.7 Evaluation of modified RSA procedure 84

4.7.1 Shear forces 84

4.7.2 Strains in RC walls and columns 92

4.8 Summary 97

CHAPTER 5 MODIFIED RESPONSE SPECTRUM ANALYSIS FOR DESIGN OF RC FRAME BUILDINGS 98

5.1 Introduction 98

5.2 Accuracy of response spectrum analysis procedure 99

5.3 Inelasticity of response in each mode 105

5.4 Accuracy of modified RSA procedure 107

5.4.1 Shear forces 107

5.4.2 Strains in columns 111

5.5 Summary 113

CHAPTER 6 CONCLUSIONS AND RECOMMENDATIONS 114

6.1 Conclusions 114

จุฬาลงกรณ์มหาวิทยาลัย
CHULALONGKORN UNIVERSITY

6.1.1 Seismic demands from NLRHA using CMS and UHS as target spectrum 114

6.1.2 Modified response spectrum analysis procedure 114

6.2 Suggestions for design practice 116

6.3 Recommendations for future studies 117

APPENDIX A DETAILS OF STUDIED BUILDINGS 118

APPENDIX B TIME HISTORY OF EARTHQUAKE GROUND ACCELERATIONS 136

APPENDIX C LINEAR RESPONSE SPECTRUM ANALYSIS AND LINEAR RESPONSE HISTORY ANALYSIS 145

APPENDIX D EXAMPLE OF MODIFIED RESPONSE SPECTRUM ANALYSIS PROCEDURE 153

REFERENCES 176

VITA 184

จุฬาลงกรณ์มหาวิทยาลัย
CHULALONGKORN UNIVERSITY

LIST OF TABLES

Page

Table 2.1 Higher-mode factor and base overturning moment reduction factor (NBCC 2010). 18

Table 2.2 Proposed base shear amplification factor value (Boivin and Paultre 2012). ... 19

Table 3.1 Structural parameters of tall RC shear-wall buildings. 35

Table 3.2 Structural parameters of RC moment-frame buildings. 38

Table 3.3 Effective stiffness of structural members in linear and nonlinear analytical models. 40

Table 3.4 Material cyclic degradation parameters (Kolozvari et al. 2017). 44

Table 3.5 List of ground motions for six periods of interest: 0.2, 0.5, 1, 1.5, 2, and 3 sec. 47

Table 3.6 List of selected ten pairs of ground motions for Chiang Mai. 50

Table 4.1 Scaling factors for tall RC shear-wall buildings in Bangkok. 64

Table 4.2 Scaling factors for tall RC shear-wall buildings in Chiang Mai. 64

Table 4.3 Modal mass participating ratio of the first-four translational modes used in RSA for tall RC shear-wall buildings. 65

Table 4.4 Spectral accelerations at fundamental periods used in ELF and RSA for X-direction of tall RC shear-wall buildings. 65

Table 4.5 Spectral accelerations at fundamental periods used in ELF and RSA for Y-direction of tall RC shear-wall buildings. 66

Table 5.1 Scaling factors for RC frame buildings. 100

Table 5.2 Modal mass participating ratio of each mode used in RSA for RC frame buildings. 100

จุฬาลงกรณ์มหาวิทยาลัย
Chulalongkorn University

Table 5.3 Spectral accelerations at fundamental periods for ELF and RSA for RC frame buildings. 100

จุฬาลงกรณ์มหาวิทยาลัย
CHULALONGKORN UNIVERSITY

LIST OF FIGURES

Page

Figure 2.1 Moment design envelope of NZS 3101 (2006). 14

Figure 2.2 Wall design envelope (a) shear force; and (b) bending moment (Priestley et al. 2007) 16

Figure 2.3 Design shear envelope proposed by (a) Rutenberg and Nsieri (2006); (b) Boivin and Paultre (2012); and (c) Luu et al. (2014). 17

Figure 2.4 Design moment envelope of CSA-A23.3 (2004). 18

Figure 2.5 Moment design envelope (Priestley 2003). 23

Figure 2.6 (a) Computation of modal responses according to the proposed EMS method and (b) definition of the effective stiffness in the substitute structure (Pennucci et al. 2015). 28

Figure 2.7 Design envelope of (a) shear forces; and (b) bending moments (Pennucci et al. 2015). 28

Figure 3.1 Floor plans and three-dimensional models of tall RC shear-wall buildings. ... 34

Figure 3.2 Floor plans and two-dimensional models of RC moment-frame buildings. 37

Figure 3.3 Concrete stress-strain relationship. 42

Figure 3.4 Steel stress-strain relationship. 42

Figure 3.5 Hysteretic behavior of concrete material. 43

Figure 3.6 Hysteretic behavior of steel material. 43

Figure 3.7 Comparison of load-deformation hysteresis loops from fiber model and experiment of U-shape RC wall: (a) E-W direction; and (b) N-S direction (Kolozvari et al. 2017). 43

Figure 3.8 Tri-linear moment-hinge rotation back bone curve (ASCE 41-13). 44

จุฬาลงกรณ์มหาวิทยาลัย
CHULALONGKORN UNIVERSITY

Figure 3.9 Hysteresis loop of moment-rotation relationship. 44

Figure 3.10 Uniform hazard spectrum (UHS) and conditional mean spectrum (CMS) conditioned at 0.2, 0.5, 1, 1.5, 2, and 3 sec at rock outcrop for 5% damping ratio. 48

Figure 3.11 Uniform hazard spectrum (UHS) and average spectra of rock outcrop ground motions matching conditional mean spectrum (CMS) at rock outcrop for 5% damping ratio. 48

Figure 3.12 Conditional mean spectrum (CMS) at rock outcrop, average spectrum of input ground motions at rock outcrop, and average spectrum of output ground motion at soft-soil site for conditioning period of 2 sec. 48

Figure 3.13 Uniform hazard spectrum (UHS) and average spectra of soft-soil ground motions considered as conditional mean spectrum (CMS) at soft-soil site for 5% damping ratio. 48

Figure 3.14 Original spectra of CMS ground motions conditioned at 3 sec and target spectrum of soft-soil ground motions for 2.5% damping ratio. 49

Figure 3.15 Individual matching spectra, mean matching spectrum, and target spectrum of soft-soil ground motions for 2.5% damping ratio. 49

Figure 3.16 Individual original spectra, mean original spectrum, and target spectrum for 2.5% damping ratio in Chiang Mai. 50

Figure 3.17 Individual matching spectra, mean matching spectrum, and target spectrum for 2.5% damping ratio in Chiang Mai. 50

Figure 3.18 Conditional mean spectrum (CMS) conditioned at 0.5, 1, and 3 sec of soft-soil ground motions for 2.5% damping ratio used in NLRHA for the 39-story building (SWB4). 53

Figure 3.19 (a) Story shear force; (b) story overturning moment; (c) story drift ratio; and (d) floor displacement computed from NLRHA for X-direction seismic excitation using three sets of CMS ground motions. 56

CHULALONGKORN UNIVERSITY

Figure 3.20 (a) Story shear force; (b) story overturning moment; (c) story drift ratio; and (d) floor displacement computed from NLRHA for Y-direction seismic excitation using three sets of CMS ground motions. 57

Figure 3.21 (a) Story shear force; (b) story overturning moment; (c) story drift ratio; and (d) floor displacement computed from NLRHA for X-direction seismic excitation using CMS and UHS as the target spectrum. 58

Figure 3.22 (a) Story shear force; (b) story overturning moment; (c) story drift ratio; and (d) floor displacement computed from NLRHA for Y-direction seismic excitation using CMS and UHS as the target spectrum. 59

Figure 4.1 Seismic demands from RSA, $LRSA_{cracked}$, $LRSA_{uncracked}$ and NLRHA due to seismic excitation in X-direction for case studies in Bangkok: (a) floor displacement; (b) story drift ratio; (c) story shear force; and (d) story overturning moment. 70

Figure 4.2 Seismic demands from RSA, $LRSA_{cracked}$, $LRSA_{uncracked}$, and NLRHA due to seismic excitation in Y-direction for case studies in Bangkok: (a) floor displacement; (b) story drift ratio; (c) story shear force; and (d) story overturning moment. 71

Figure 4.3 Seismic demands from RSA, $LRSA_{cracked}$, $LRSA_{uncracked}$, and NLRHA due to seismic excitation in X-direction for case studies in Chiang Mai: (a) floor displacement; (b) story drift ratio; (c) story shear force; and (d) story overturning moment. 72

Figure 4.4 Seismic demands from RSA, $LRSA_{cracked}$, $LRSA_{uncracked}$, and NLRHA due to seismic excitation in Y-direction for case studies in Chiang Mai: (a) floor displacement; (b) story drift ratio; (c) story shear force; and (d) story overturning moment. 73

Figure 4.5 Ratios between NLRHA and RSA results: base overturning moment, base shear force, and roof displacement for buildings in Bangkok: (a) X-direction; (b) Y-direction. 74

Figure 4.6 Ratios between NLRHA and RSA results: base overturning moment, base shear force, and roof displacement for buildings in Chiang Mai: (a) X-direction; (b) Y-direction. 74

จุฬาลงกรณ์มหาวิทยาลัย
CHULALONGKORN UNIVERSITY

Figure 4.7 Design strength, nominal strength, actual strength, and seismic demands computed from RSA and NLRHA of a core wall in the 39-story building (SWB4) in Bangkok: (a) base axial force and bending moment; (b) bending moment; and (c) shear force along the height of the wall. The arrow in (b) indicates the direction of seismic excitation. 75

Figure 4.8 Linear and nonlinear pushover curves along with the target roof displacements of the first-three translational modes in X-direction of buildings in Bangkok: (a) first mode; (b) second mode; and (c) third mode. The black dots in each figure indicate the target roof displacement. 77

Figure 4.9 Force response reduction factor of the first-three translational modes for case studies in Bangkok: (a) X-direction; and (b) Y-direction. 78

Figure 4.10 Force response reduction factor of the first-three translational modes for case studies in Chiang Mai: (a) X-direction; and (b) Y-direction. 78

Figure 4.11 Mean values of peak seismic demands (a) shear force; and (b) bending moment of a core wall in the 39-story building (SWB4) in Bangkok with flexural strength designed by RSA and HE. The arrow indicates the direction of seismic excitation. 80

Figure 4.12 Shifting of neutral axis in an L-shaped wall of the 15-story building (SWB1) in Bangkok: (a) relative shifting distance of neutral axis computed by using strains from NLRHA; (b) before shifting of neutral axis; (c) neutral axis shifted toward Edge 1; and (d) neutral axis shifted toward Edge 2. 83

Figure 4.13 Mean values of peak story shear forces computed by RSA, $MRSA_{HE}$, $MRSA_{HI,}$ MMPA, EC8, and NLRHA procedures for buildings in Bangkok due to seismic excitation in: (a) X-direction; and (b) Y-direction. 87

Figure 4.14 Mean values of peak story shear forces computed by RSA, $MRSA_{HE}$, $MRSA_{HI}$, MMPA, EC8, and NLRHA procedures for buildings in Chiang Mai due to seismic excitation in: (a) X-direction; and (b) Y-direction. 88

จุฬาลงกรณ์มหาวิทยาลัย
Chulalongkorn University

Figure 4.15 Mean values of peak shear forces in RC walls computed by RSA, $MRSA_{HE}$, $MRSA_{HI}$, MMPA, and NLRHA procedures for buildings in: (a) Bangkok; and (b) Chiang Mai. The arrow in each figure indicates the direction of seismic excitation. 90

Figure 4.16 Mean values of peak shear forces in RC columns computed by RSA, $MRSA_{HE}$, $MRSA_{HI}$, MMPA, and NLRHA procedures for buildings in: (a) Bangkok; and (b) Chiang Mai. The arrow in each figure indicates the direction of seismic excitation and the circle indicates the location of the column considered. 91

Figure 4.17 Mean values of peak vertical axial strains in RC walls computed by MRSA and NLRHA procedures for buildings in Bangkok. The arrow in each figure indicates the direction of seismic excitation and the black dot indicates the location of strain considered in the wall. 93

Figure 4.18 Mean values of peak vertical axial strains in RC columns computed by MRSA and NLRHA procedures for buildings in Bangkok. The arrow in each figure indicates the direction of seismic excitation and the circle indicates the location of the column considered. 94

Figure 4.19 Mean values of peak vertical axial strains in RC walls computed by MRSA and NLRHA procedures for buildings in Chiang Mai. The arrow in each figure indicates the direction of seismic excitation and the black dot indicates the location of strain considered in the wall. 95

Figure 4.20 Mean values of peak vertical axial strains in RC columns computed by MRSA and NLRHA procedures for buildings in Chiang Mai. The arrow in each figure indicates the direction of seismic excitation and the circle indicates the location of the column considered. 96

Figure 5.1 Original spectra of CMS ground motions conditioned at 3 sec and target spectrum for 2.5% damping ratio in Bangkok zone 5. 99

Figure 5.2 Individual matching spectra, mean matching spectrum, and target spectrum for 2.5% damping ratio in Bangkok zone 5. 99

Chulalongkorn University

Figure 5.3 Mean values of peak seismic demands computed from RSA, $LRSA_{cracked}$, $LRSA_{uncracked}$, and NLRHA for RC frame buildings in Bangkok: (a) floor displacement; (b) story drift ratio; (c) story shear force; and (d) story overturning moment. 103

Figure 5.4 Mean values of peak seismic demands computed from RSA, $LRSA_{cracked}$, $LRSA_{uncracked}$, and NLRHA for RC frame buildings in Chiang Mai: (a) floor displacement; (b) story drift ratio; (c) story shear force; and (d) story overturning moment. 104

Figure 5.5 Ratio between NLRHA and RSA results: base overturning moment, base shear force, and roof displacement for RC frame buildings in: (a) Bangkok; (b) Chiang Mai. 105

Figure 5.6 Lateral over-strength factors for RC frame buildings. 105

Figure 5.7 Linear and nonlinear pushover curves along with the target roof displacements of the first-three translational modes of RC frame buildings in Bangkok: (a) first mode; (b) second mode; and (c) third mode. The black dots in each figure indicate the target roof displacement. 106

Figure 5.8 Force response reduction factor of each mode for RC frame buildings in: (a) Bangkok; and (b) Chiang Mai. 107

Figure 5.9 Mean values of peak story shear forces computed by RSA, $MRSA_{HE}$, capacity design, and NLRHA procedures for RC frame buildings in: (a) Bangkok; and (b) Chiang Mai. 109

Figure 5.10 Mean values of peak shear forces in RC columns computed by RSA, $MRSA_{HE}$, capacity design, and NLRHA procedures for RC frame buildings in: (a) Bangkok; and (b) Chiang Mai. The circle indicates the location of column considered. 110

Figure 5.11 Mean values of peak shear forces in RC beams computed by RSA, $MRSA_{HE}$, capacity design, and NLRHA procedures for RC frame buildings in: (a) Bangkok; and (b) Chiang Mai. The circle indicates the location of beam considered. 111

จุฬาลงกรณ์มหาวิทยาลัย
CHULALONGKORN UNIVERSITY

Figure 5.12 Mean values of peak vertical axial strains in RC columns computed by MRSA and NLRHA procedures for RC frame buildings in (a) Bangkok; (b) Chiang Mai. The circle indicates the location of the column considered. 112

จุฬาลงกรณ์มหาวิทยาลัย
CHULALONGKORN UNIVERSITY

CHAPTER 1
INTRODUCTION

1.1 Background

Reinforced concrete (RC) shear walls are often used as a lateral force resisting system in tall buildings. To design such structures to resist earthquakes, there are primarily four analysis methods: linear static analysis by means of the equivalent lateral force (ELF) procedure; linear dynamic analysis using the response spectrum analysis (RSA) procedure or linear response history analysis (LRHA); nonlinear static procedure (NSP) known as pushover analysis; and nonlinear dynamic analysis by means of nonlinear response history analysis (NLRHA). Among the four analysis methods, NLRHA is recognized as the most accurate method but is not always used in current practice because of its difficulties involving limited understanding of inelastic behavior of a structure, creation of a realistic nonlinear structural model, selection of appropriate earthquake ground motions for the site of interest, significant computational effort, data processing, and result interpretation. The RSA procedure is usually used by design engineers in practice.

As allowed in ASCE 7-10, the RSA procedure is widely used in current practice to compute design demands on structures. This method uses response modification factor (R) and deflection amplification factor (C_d) to provide a rational relationship between elastic and inelastic demand of a given structural system. The R factor is used to reduce elastic demands to design demands and the C_d factor is used to scale up the displacement and drift demands after reducing the elastic demands by R factor. To compute the design force demands on an inelastic RC wall with an acceptable ductility demand using the RSA procedure, the elastic response computed from many vibration modes is combined and then reduced by a single R factor, assuming that all modes are equally affected by the same inelastic action. A structural wall is normally designed to experience flexural yielding by providing flexural strength corresponding to the elastic demand divided by the R factor, and the RSA procedure permits the elastic shear force

to be reduced by the same *R* factor (which assumes that shear force is reduced by the same factor as bending moment, or in other words, that flexural yielding of the wall limits shear force in the same manner as it limits bending moment). However, previous experimental studies have shown that shear forces in the wall subjected to earthquake motions can continue to increase after flexural yielding occurs at the base of the wall (Ghorbanirenani et al. 2011, Panagiotou et al. 2011, Jimenez and Massone 2018). Moreover, several numerical studies have demonstrated that higher modes are not significantly affected by inelasticity as much as the first mode (Eibl and Keintzel 1988, Priestley 2003, Calugaru and Panagiotou 2012, Munir and Warnitchai 2012, Maniatakis et al. 2013, Najam and Warnitchai 2018). These evidences suggest that using a single *R* factor to reduce the elastic shear forces of all modes in the RSA procedure is likely the primary reason for the underestimation of shear forces contributed from higher modes. As demonstrated in recent studies (Leng et al. 2014, Khy and Chintanapakdee 2017, Najam and Warnitchai 2018, Khy et al. 2019), shear force computed from NLRHA was significantly larger than the design shear force computed from RSA procedure. Since shear dominant response leads to brittle failure, the shear response is normally modeled as elastic in the design process (PEER 2017). Shear strength designed with the shear demand from RSA procedure may be less than the shear demand computed from NLRHA, which could lead to shear failure in structural walls. The accurate prediction of shear forces is important to prevent brittle failure.

In real earthquake events, failure and damage of RC shear walls in mid-rise and high-rise buildings have been observed due to recent earthquakes and common failure mode of RC walls includes shear failure, concrete crushing and spalling, vertical rebar buckling, and lateral instability of shear walls (Wallace et al. 2012, Marius 2013, Telleen et al. 2017). The failure of RC walls could cause failure of buildings resulting in human injury and economic loss. One of the most efficient way to mitigate destructive effects due to earthquake is to improve the design method commonly used in design practice.

1.2 Statement of research problem

Brittle shear failure of lateral force resisting system has captured many interests from researchers around the world. For moment resisting frames, shear forces from capacity design approach using probable flexural strengths at both ends of a beam or column are used instead of shear forces from RSA procedure for design of a beam or column (ACI 318M-14). For shear walls, the capacity design approach will not work because the lateral forces at each floor level corresponding to flexural strengths are unknown and vary during nonlinear response. Many simplified equations to estimate shear demands of RC walls have been developed. The improved estimations of shear forces for RC cantilever walls were proposed by Blakeley et al. (1975), Eibl and Keintzel (1988), Ghosh and Markevicius (1990), Paulay and Priestley (1992), Priestley (2003), Rutenberg and Nsieri (2006), Yathon (2011), Boivin and Paultre (2012), Calugaru and Panagiotou (2012), Rejec et al. (2012), Luu et al. (2014); for RC coupled walls were proposed by Fox et al. (2014) and Pennucci et al. (2015); for RC wall-frame structures were proposed by Kappos and Antoniadis (2007), Sullivan et al. (2008), and Kazaz and Gülkan (2016). Most of the formulas and methods developed by researchers as mentioned above are based on parametric studies; hence, they are appropriate only with structures and ground motions similar to those used in their studies. As reported by Khy and Chintanapakdee (2017) that an empirical equation was not appropriate for every site because the same building situated in different locations and subjected to different ground motions have quite different shear amplification factors. None of these studies utilized real buildings to evaluate their proposed methods. For real tall buildings, an improved method was proposed by Najam and Warnitchai (2018) but it seems quite difficult for practical application and is more appropriate for assessment rather than design. Hence, a more rational and practical analysis procedure conducted on real case-study buildings should be developed.

This study is part of a project on improving the seismic analysis and design procedure for buildings in Thailand. Although ASCE 7-05, which is the model standard of Thai seismic code (DPT 1302, 2009), has not yet addressed the shear demand problem

in shear walls, several seismic design codes such as Eurocode 8 (CEN 1998-1, 2004) of Europe, NBCC (2010) of Canada, and Appendix D1 in NZS 3101 (2006) of New Zealand have already addressed the shear problem in RC walls by multiplying design shear forces with an amplification factor to account for higher-mode effects and flexural over-strength factor inherent in design. One of reasons that the United States has not dealt with this problem in ASCE 7 (even for the latest version, ASCE 7-16) for design of tall buildings may be that NLRHA is directly used for verification of the design of tall buildings according to Tall Building Initiative (PEER, 2017) and an Alternative Procedure for Seismic Analysis and Design of Tall Buildings Located in the Los Angeles Region (LATBSDC, 2017). However, most structural engineers in Thailand are not familiar with time history analysis and still prefer the RSA procedure to analyze and design of tall buildings. Hence, the design of shear resistance in structural walls is not safe if the conventional RSA procedure is used. Therefore, it is necessary to improve the calculation method for computing shear force demands for use in design of vertical structural members.

The research questions are whether it is safe to design a tall building with seismic demands computed from the RSA procedure in ASCE 7 and which methods from the past studies related to shear demands should design engineers adopt to if NLRHA is not conducted.

จุฬาลงกรณ์มหาวิทยาลัย
CHULALONGKORN UNIVERSITY

1.3 Objectives of research

The objectives of this study are the followings:

(1) To investigate higher-mode contribution of tall RC shear-wall buildings and RC moment-frame buildings.

(2) To evaluate the accuracy of RSA procedure by using NLRHA.

(3) To evaluate the accuracy of previously proposed amplification methods when applied to real tall buildings.

(4) To develop a modified response spectrum analysis (MRSA) procedure for design of tall RC shear-wall buildings and RC moment-frame buildings. Here, two versions of MRSA method to compute shear forces together with a method to

compute strains in RC walls and columns to identify locations that require ductility detailing are proposed.

1.4 Scope of research

The scope of this study is the followings:

- Two types of lateral force resisting systems, RC shear wall and RC moment frame are used.
- Six tall RC shear-wall buildings of 15 to 39 stories are used.
- Four RC moment-frame buildings of 3 to 15 stories are employed.
- Large-magnitude long-distance soft-soil ground motions in Bangkok and moderate-magnitude short-distance stiff-soil ground motions in Chiang Mai cities of Thailand are used.
- Structures are designed according to ASCE 7-10 and ACI 318M-14.
- Structures are assumed to have fixed support at the base.
- Earthquake ground motions are applied in each principal horizontal direction separately.

1.5 Research methodology

The procedure adopted in this study is outlined as the followings:

จุฬาลงกรณ์มหาวิทยาลัย
CHULALONGKORN UNIVERSITY

(1) Design the structural systems according to ACI 318M-14, such that the design strengths are approximately equal to the demands from factored load combinations including gravity load, wind load, and earthquake load using the RSA procedure in ASCE 7-10. The design task of the structural system is accomplished by using ETABS (CSI 2015).

(2) Analyze the structures subjected to gravity loads and earthquake ground motions by using NLRHA procedure with PERFORM-3D (CSI 2011) to evaluate the accuracy of the RSA procedure used in the design.

(3) Investigate inelasticity of response in each mode using pushover analysis.

(4) Develop two modified response spectrum analysis methods $MRSA_{HE}$ based on higher-mode-elastic assumption and $MRSA_{HI}$ base on higher-mode-inelastic assumption to compute the design shear forces in a structure.

(5) Develop a method based on the equal-displacement rule (Veletsos and Newmark 1960), which uses strain from elastic analysis to predict inelastic strain computed from NLRHA to predict locations of yielding of vertical reinforcement and crushing of concrete in RC walls or columns.

(6) Evaluate accuracy of the conventional RSA method, the previously proposed methods, and the proposed MRSA method by comparing the computed demands with NLRHA results.

1.6 Research significance

- The findings of this study will be considered as possible revision to existing Thai seismic design standard (DPT 1302, 2009).
- The proposed method will be to ensure that the computed design demands on tall buildings are reasonably accurate and safe to use while maintaining the suitability for practical application.
- The proposed method can be used in performance based-design application which can ensure adequate shear demands and shear strength before conducting NLRHA.
- The proposed method can be used to predict the location of yielding in RC walls and columns so that ductile detailing should be implemented. Such method is not yet available in the conventional RSA procedure.

จุฬาลงกรณ์มหาวิทยาลัย
Chulalongkorn University

1.7 Outline of dissertation

There are six chapters in this dissertation, which are briefly summarized below:

Chapter 1 presents background and problems of using the conventional RSA procedure. It includes statement of research problem, objectives and scope of research, research methodology, and research significances.

Chapter 2 describes about analysis methods and up-to-date literature review of problems being addressed in this study. Previously proposed methods to improve the estimation of force demands on structures are included.

Chapter 3 provides description of studied buildings, analytical models, and earthquake ground motions. It also addresses about application of conditional mean spectrum (CMS) in NLRHA for design purposes of tall buildings. Seismic demands computed from NLRHA, where the ground motions are selected and scaled using CMS and uniform hazard spectrum (UHS) as target spectrum, are compared.

Chapter 4 evaluates accuracy of the RSA procedure and investigates inelasticity of response in each mode for tall RC shear-wall buildings. Then, it presents two MRSA methods to compute shear forces together with a method to compute strains in RC walls and columns.

Chapter 5 applies the proposed MRSA method developed in Chapter 4 to RC moment-frame buildings. The accuracy of the RSA procedure, the capacity design method, and the proposed MRSA method is evaluated for RC moment-frame buildings.

Chapter 6 summarizes the important findings of this dissertation. It consists of conclusions, suggestions for design practice, and recommendations for future studies.

จุฬาลงกรณ์มหาวิทยาลัย
CHULALONGKORN UNIVERSITY

CHAPTER 2
LITERATURE REVIEW

2.1 Analysis methods

2.1.1 Linear response history analysis and response spectrum analysis

The equation of motion of a linear multi-degree of freedom (MDOF) system subjected to earthquake ground motion $\ddot{u}_g(t)$ is defined as:

$$\mathbf{m}\ddot{\mathbf{u}}(t)+\mathbf{c}\dot{\mathbf{u}}(t)+\mathbf{k}\mathbf{u}(t)=-\mathbf{m}\boldsymbol{\iota}\ddot{u}_g(t) \tag{2.1}$$

where **m**, **c** and **k** are mass, damping and stiffness matrix, respectively, $\boldsymbol{\iota}$ is the influence vector. The right-hand side of Eq. (2.1) is interpreted as effective earthquake force.

$$\mathbf{p}_{\text{eff}}(t)=-\mathbf{m}\boldsymbol{\iota}\ddot{u}_g(t) \tag{2.2}$$

The spatial distribution of effective earthquake forces over the height of the building is defined by the vector $\mathbf{s}=\mathbf{m}\boldsymbol{\iota}$. This force distribution can be expanded as a summation of modal inertia force distribution.

$$\mathbf{m}\boldsymbol{\iota}=\sum_{n=1}^{N}\mathbf{s}_n=\sum_{n=1}^{N}\Gamma_n\mathbf{m}\boldsymbol{\phi}_n \tag{2.3}$$

where $\boldsymbol{\phi}_n$ is the nth mode shape of the structure and

$$\Gamma_n=\frac{L_n}{M_n}\quad L_n=\boldsymbol{\phi}_n^T\mathbf{m}\boldsymbol{\iota}\quad M_n=\boldsymbol{\phi}_n^T\mathbf{m}\boldsymbol{\phi}_n \tag{2.4}$$

The contribution of nth mode to excitation vector $\mathbf{m}\boldsymbol{\iota}$ is:

$$\mathbf{s}_n=\Gamma_n\mathbf{m}\boldsymbol{\phi}_n \tag{2.5}$$

For a linear system, the displacement **u** of an *N*-DOF system can be expressed as the superposition of the modal contributions.

จุฬาลงกรณ์มหาวิทยาลัย
CHULALONGKORN UNIVERSITY

$$\mathbf{u}(t) = \sum_{n=1}^{N} \phi_n q_n(t) \tag{2.6}$$

where $q_n(t)$ is the modal coordinate. By substituting Eq. (2.6) into Eq. (2.1), multiplying both sides by ϕ_n^T, then dividing the obtained equation by normalized mass, M_n, and finally utilizing the orthogonal properties of modes, $\phi_n^T \mathbf{m} \phi_r = 0,\ \phi_n^T \mathbf{c} \phi_r = 0,\ \phi_n^T \mathbf{k} \phi_r = 0$, the equation governing each modal coordinate is:

$$\ddot{q}_n + 2\zeta_n \omega_n \dot{q}_n + \omega_n^2 q_n = -\Gamma_n \ddot{u}_g(t) \tag{2.7}$$

where ω_n is the modal natural frequency, and ζ_n is the modal damping ratio of the nth mode.

Then, the modal equation can be obtained by substituting $q_n(t) = \Gamma_n D_n(t)$ into Eq. (2.7).

$$\ddot{D}_n + 2\zeta_n \omega_n \dot{D}_n + \omega_n^2 D_n = -\ddot{u}_g(t) \tag{2.8}$$

The displacement due to the nth mode is computed by:

$$\mathbf{u}_n(t) = \phi_n q_n(t) = \Gamma_n \phi_n D_n(t) \tag{2.9}$$

The response contributed from the nth mode is determined by:

$$r_n(t) = r_n^{st} A_n(t) \tag{2.10}$$

where r_n^{st} is the modal static response determined by static analysis due to external force $\mathbf{s}_n$ and $A_n(t) = \omega_n^2 D_n(t)$, where $D_n(t)$ is obtained from dynamic analysis of SDOF system by solving Eq. (2.8). Alternatively, the peak value of $A_n(t)$ of the nth-mode SDOF system can be computed from ordinate of response spectra, $A(\mathrm{T}_n, \zeta_n)$.

The total response is computed by combining the contributions of all the modes. If the direct summation in time history of response from all modes as defined by Eq. (2.11) is used, the method is called modal response history analysis (RHA). If modal combination rule such as square root of the sum of the squares method (SRSS) or the complete

quadratic combination method (CQC) is used to combine modal peak responses, the method is called modal response spectrum analysis (RSA).

$$r(t) = \sum_{n=1}^{N} r_n(t) = \sum_{n=1}^{N} r_n^{st} A_n(t) \tag{2.11}$$

2.1.2 **Nonlinear response history analysis**

For an inelastic system, the relationship between lateral force ($\mathbf{f}_s$) and lateral displacement ($\mathbf{u}$) depends on the displacement and velocity of the mass relative to the ground.

$$\mathbf{f}_s = \mathbf{f}_s(\mathbf{u}, \dot{\mathbf{u}}) \tag{2.12}$$

The governing equation for inelastic system is obtained by modifying the stiffness term in Eq. (2.1) to recognize the inelastic behavior of the structure.

$$\mathbf{m}\ddot{\mathbf{u}}(t) + \mathbf{c}\dot{\mathbf{u}}(t) + \mathbf{f}_s(\mathbf{u}, \dot{\mathbf{u}}) = \mathbf{p}_{eff}(t) \tag{2.13}$$

Substituting Eq. (2.6) into Eq. (2.13) and formulating in the same way as in elastic system, the modal coordinate equation is obtained as:

$$\ddot{q}_n + 2\zeta_n \omega_n \dot{q}_n + \frac{F_{sn}}{M_n} = -\Gamma_n \ddot{u}_g(t) \tag{2.14}$$

where F_{sn} is the inelastic resisting force which is a function of all modal coordinates as shown in Eq. (2.15) implying that all modes are coupled; therefore, the modal analysis is no longer theoretically applicable to nonlinear inelastic system unless some approximation is adopted.

$$F_{sn} = F_{sn}(q, \dot{q}) = \phi_n^T \mathbf{f_s}(u, \dot{u}) \tag{2.15}$$

Normally, Eq. (2.13) is solved directly by a numerical method to determine displacement response history at several time steps and that is called nonlinear response history analysis (NLRHA).

2.1.3 Modal pushover analysis

The modal pushover analysis (MPA) (Chopra and Goel 2002) was developed under two main assumptions: (1) the invariant lateral load distribution and (2) the uncoupling of modal responses during inelastic response. The peak modal response can be obtained by static analysis of the structure subjected to lateral force distributed over the building height as $\mathbf{s}_n^* = \mathbf{m}\phi_n$.

Nonlinear static analysis is conducted by pushing the building to reach the peak roof displacement ($\mathbf{u}_{rno}$) of the nth mode estimated by:

$$\mathbf{u}_{rno} = \Gamma_n \phi_{rn} D_n \tag{2.16}$$

where $D_n = A_n / \omega_n^2$. For elastic system, A_n is obtained from response spectra in the same way as in RSA procedure. For inelastic system, the target roof displacement can be computed by displacement coefficient method (ASCE 41-13), capacity spectrum (ATC 40), inelastic response spectra (Chopra and Goel 2001), or NLRHA of equivalent SDOF system using uncouple modal response history analysis (UMRHA) (Chopra and Goel 2002).

CHULALONGKORN UNIVERSITY

Any response for each mode can be extracted from pushover analysis corresponding to the target roof displacement, and the modal peak response can be combined by SRSS or CQC rule to estimate the total peak response. For linear elastic system, MPA is identical to RSA procedure. For inelastic system, MPA is a simplification of UMRHA (Chopra and Goel 2002).

2.2 Causes of excessive shear demands

Higher-mode effects are taken into account when using RSA procedure, but the building code assumes that all modes of response are equally affected by inelastic action by using a single response modification factor (*R*) for all modes to reduce the elastic

forces. However, previous researchers have found that inelastic behaviors of each mode were not identical, and higher modes were not significantly affected by inelasticity as the first mode.

As stated by Rejec et al. (2012) that energy dissipation was predominantly limited to the flexural response in the first mode because it contributes most of the bending moment at the base, which is limited by its flexural capacity. While plastic hinge constrained the first-mode responses to the level equal to its flexural capacity, the responses of higher modes behaved primarily in the elastic range. This observation was also confirmed by Munir and Warnitchai (2012) from their cyclic pushover analysis on tall core-wall buildings that yielding occurred in the first mode was more significant than that occurred in the second mode, and the responses of the third and fourth modes were in the elastic range. Similarly, Maniatakis et al. (2013) concluded from the study of a 9-story RC moment-frame building that the reduction factors for each mode were different and generally decreased with increasing mode order.

The significant contributions of higher-mode responses for structural shear wall were also observed in the experimental studies (Ghorbanirenani et al. 2011, Panagiotou et al. 2011, Jimenez and Massone 2018). The full-scale shaking table test of a 7-story rectangular wall done by Panagiotou et al. (2011) showed that the location of lateral force resultant varied considerably and became lower at 46% of the building height, while the base bending moment remained almost constant between 90% and 100% of its peak value. This lowering of resultant force resulted in significant increase of the base shear force, which is mainly due to second-mode contribution. The amplification of base shear force was also observed in the small-scale testing of an 8-story cantilever RC shear wall by Ghorbanirenani et al. (2011), which showed that the peak base shear force occurred in the test was 1.82 times the value used in design. When the amplitude of ground motion was increased beyond the design level, the base shear force continued to increase; although, the base moment remained about constant. A recent experimental study on five small-scale RC cantilever walls conducted by Jimenez and Massone (2018) revealed that

จุฬาลงกรณ์มหาวิทยาลัย
Chulalongkorn University

after flexural yielding at the base of the wall, the base shear force could continue to increase by a factor of 1.7.

2.3 Improved estimations of seismic force demands

Higher-mode shear amplification has been first recognized since 1975 by Blakeley et al. (1975). Many subsequent studies have proposed different approaches to account for higher-mode contribution of inelastic RC shear walls. Here, the proposed methods were classified into three approaches: amplification factor method, higher-mode-elastic method, and equivalent linearization method. These proposed methods were developed based on different parametric studies such as structural configurations and ground motions; obviously, the results depend on these choices. Most of them have mainly focused on the estimation of shear forces in RC cantilever walls designed to accommodate a concentrated plastic hinge at the base of the walls.

2.3.1 Amplification factor method

Blakeley et al. (1975) conducted a study on RC cantilever walls from 6 to 20 stories tall. They found that the base shear force from nonlinear dynamic analysis was larger than that from equivalent static analysis method. They proposed a simple formula to compute base shear amplification factor which is used to multiply with static shear force to get the design shear force of the RC cantilever wall.

จุฬาลงกรณ์มหาวิทยาลัย
CHULALONGKORN UNIVERSITY

$$\omega_v = \begin{cases} 0.9 + \dfrac{n}{10} & \text{for n} \le 6 \\ 1.3 + \dfrac{n}{30} \le 1.8 & \text{for n} > 6 \end{cases} \tag{2.17}$$

where n is the number of stories and ω_v is the base shear amplification factor to be applied to the static shear force.

Paulay and Priestley (1992) modified the design shear force of Blakeley et al. (1975) by including flexural over-strength factor ϕ_o . The proposed design shear force V_u of the wall was limited by elastic shear force from equivalent static analysis as shown in the last term in Eq. (2.18).

$$V_u = \omega_v \phi_o V_E \leq \mu_\Delta V_E \tag{2.18}$$

where μ_Δ is the displacement ductility ratio and V_E is shear force from equivalent static analysis.

NZS 3101 (NZS 2006) followed the formula proposed by Paulay and Priestley (1992), but the standard does not limit the design shear force of the wall by elastic shear force. The design shear force of the wall in this standard shall not be less than the shear force determined by Eq. (2.19).

$$V_o^* = \omega_v \phi_o V_E \tag{2.19}$$

where V_o^* is the design shear force at any level of the wall and ϕ_o is the over-strength factor related to flexural action at any level of the wall. To account for higher-mode effects on flexural demand, NZS 3101 includes the design moment envelope as shown in Figure 2.1 by linear interpolation of values between the nominal flexural strength ($M_{n,B}$) at the top of the plastic hinge length of the wall, mid-height moment (M_c^*) calculated by Eq. (2.20) and zero moment at the top.

$$\frac{M_{n.B}}{2} < M_c^* = \frac{M_{E,C}}{0.85}\left[1 + \frac{n_t - 1}{4}\right] \leq 2M_{E,C} \tag{2.20}$$

where n_t is the total number of stories and $M_{E,C}$ is the bending moment at mid-height computed from equivalent static or response spectrum analysis.

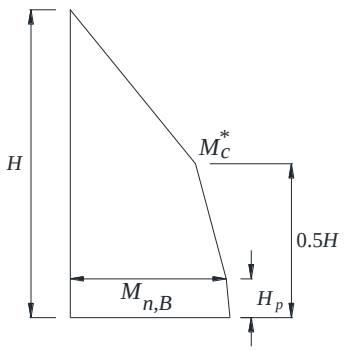

Figure 2.1 Moment design envelope of NZS 3101 (2006).

Priestley et al. (2007) proposed capacity design shear force of RC cantilever wall in a similar form to that of NZS 3101 (2006). This method amplifies shear force from direct displacement-based design (DDBD) with shear amplification factor characterized by initial period (T_i) and displacement ductility demand (μ).

$$V_{Base}^{o} = \omega_v \phi_o V_{Base} \tag{2.21}$$

where V_{Base}^{o} is the design base shear force of the wall; V_{Base} is the base shear force from DDBD; ϕ_o is base flexural over-strength factor; and ω_v is base shear amplification computed from Eq. (2.22).

$$\omega_v = 1 + \frac{\mu}{\phi_o} C_{2,T} \tag{2.22}$$

$$C_{2,T} = 0.067 + 0.4\left(T_i - 0.5\right) \leq 1.15$$

Priestley et al. (2007) proposed the capacity design shear force along the height as shown in Figure 2.2a which is computed by a linear envelope between base shear of the wall and shear at roof level (V_n^o) computed by Eq. (2.23).

$$V_n^o = C_3 V_{Base}^o \tag{2.23}$$

$$C_3 = 0.9 - 0.3T_i \geq 0.3$$

To prevent yielding to occur in upper stories, Priestley et al. (2007) proposed bi-linear envelope of design moment as shown in Figure 2.2b which consists of linear interpolation between over-strength base moment capacity ($\phi_o M_{Base}$, where M_{Base} is the base bending moment demand from DDBD) and mid-height over-strength moment demand $(M_{0.5H}^o)$ in the lower half and between $M_{0.5H}^o$, and zero moment at the top of the wall in the upper half of the building height. The mid-height moment is related to base moment capacity as in Eq. (2.24).

$$M^{o}_{0.5H} = C_{1,T}\phi_o \mathrm{M}_{Base} \tag{2.24}$$

$$C_{1,T} = 0.4 + 0.075T_i\left(\frac{\mu}{\phi_o} - 1\right) \geq 0.4$$

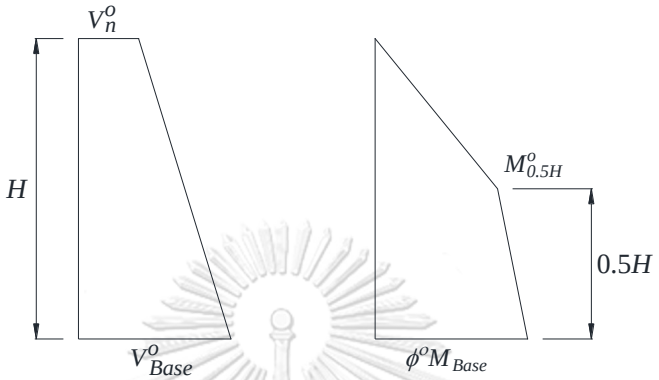

(a) Shear force (b) Bending moment

Figure 2.2 Wall design envelope (a) shear force; and (b) bending moment (Priestley et al. 2007)

Rutenberg and Nsieri (2006) conducted a research on RC cantilever walls ranging from 5- to 25-story in order to provide possible revisions to EC8 (2004) procedure to compute shear forces (see Section 2.2.3). From their parametric study, the base shear amplification factor can be represented by a function that is linear in the fundamental period *T* and the behavior factor *q*. Consequently, the following formula was proposed for computing the base shear force, V_a, of the wall.

$$V_a = \omega_v^* V_d \tag{2.25}$$

$$\omega_v^* = 0.75 + 0.22(T + q + Tq)$$

where ω_v^* is base shear amplification factor and V_d is the base shear obtained from Eq. (2.26).

$$V_d = \frac{M_y}{\frac{2}{3}H\left(1+\frac{1}{2n}\right)} \tag{2.26}$$

where M_y is the yielding moment at the base of the wall; H is the building height; and n is the number of stories.

Rutenberg and Nsieri (2006) also proposed the design envelope of shear force distributing over the height of the wall as function of the fundamental period as shown in Figure 2.3(a), where ξ is defined by Eq. (2.27).

$$\xi = 1.0 - 0.3T \geq 0.5 \tag{2.27}$$

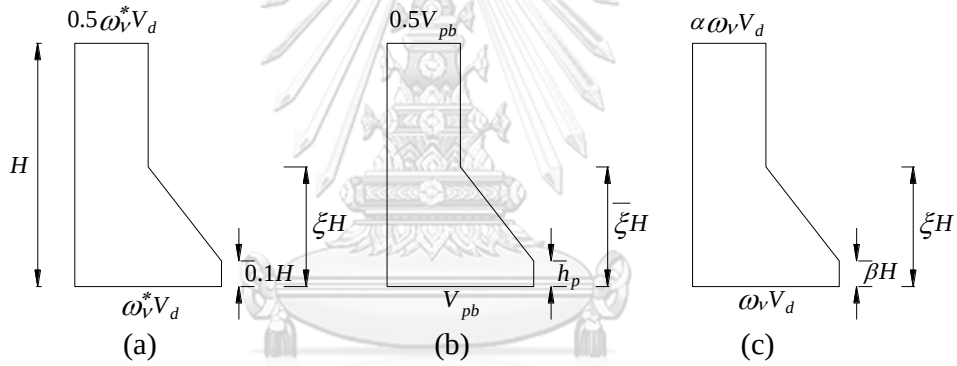

Figure 2.3 Design shear envelope proposed by (a) Rutenberg and Nsieri (2006); (b) Boivin and Paultre (2012); and (c) Luu et al. (2014).

NBCC (2010) has explicitly considered higher-mode effects when using equivalent static force procedure by applying higher-mode factor, M_v and base overturning moment reduction factor, J, to the base shear and moment envelope, respectively. These factors depend on the structural type, fundamental period of the structure and the shape of design spectrum as shown in Table 2.1. In addition to NBCC (2010), CSA-A23.3 (2004) requires that for ductile wall, the design base shear force shall be increased by the base flexural over-strength factor which is computed by the ratio between the base probable bending moment capacity and base bending moment demand. For moderately ductile wall, base over-strength factor is computed by the ratio

between the base nominal bending moment capacity and base bending moment demand. Based on Adebar et al. (2014), the design shear force of the wall in CSA-A23.3 (2014) shall not be greater than elastic shear force from RSA reduced by force reduction factor equal to 1.3. To prevent yielding in upper floors for shear wall, CSA A23.3 (2004) requires that design bending moment at location above the plastic hinge is amplified by the ratio between the design moment resistance (M_r) and the moment demand determined from the analysis (M_f), which are calculated at the top of the plastic hinge region. The design moment envelope of the wall is shown in Figure 2.4.

Table 2.1 Higher-mode factor and base overturning moment reduction factor (NBCC 2010).

$S_a(0.2)/S_a(2.0)$	Type of Lateral Resisting Systems	M_v for $T_a \leq 1.0$	M_v for $T_a = 2.0$	M_v for $T_a \geq 4.0$	J for $T_a \leq 0.5$	J for $T_a = 2.0$	J for $T_a \geq 4.0$
< 8.0	Moment-resisting frames	1.0	1.0	(3)	1.0	0.9	(3)
	Coupled walls(4)	1.0	1.0	1.0	1.0	0.9	0.8
	Braced frames	1.0	1.0	(3)	1.0	0.8	(3)
	Walls, wall-frame systems	1.0	1.2	1.6	1.0	0.6	0.5
	Other systems(5)	1.0	1.2	(3)	1.0	0.6	(3)
≥ 8.0	Moment-resisting frames	1.0	1.2	(3)	1.0	0.7	(3)
	Coupled walls(4)	1.0	1.2	1.2	1.0	0.7	0.6
	Braced frames	1.0	1.5	(3)	1.0	0.6	(3)
	Walls, wall-frame systems	1.0	2.2	3.0	1.0	0.4	0.3
	Other systems(5)	1.0	2.2	(3)	1.0	0.4	(3)

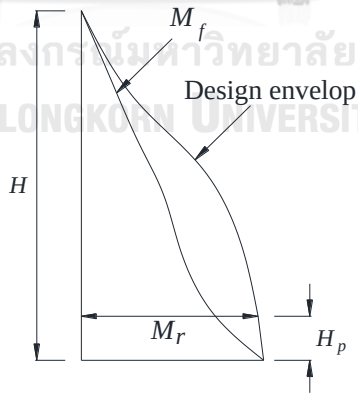

Figure 2.4 Design moment envelope of CSA-A23.3 (2004).

Boivin and Paultre (2012) proposed capacity design method for shear strength design of regular ductile RC cantilever walls for CSA-A23.3 (2004). Their proposed method was based on a parametric study for ductile walls subjected to Western North

America ground motions. They concluded that seismic base shear force was primarily influenced by wall over-strength factor and fundamental period. A new base shear amplification factor value, $\bar{\omega}_v$, was proposed as shown in Table 2.2. The design base shear force, V_{pb} , was calculated by Eq. (2.28).

$$V_{pb} = \bar{\omega}_v V_{Pbase} \leq V_{\text{limit}_{base}} \tag{2.28}$$

$$V_{Pbase} = V_f \left(\frac{M_p}{M_f} \right)_{base}$$

where V_{Pbase} is the probable shear force at the base of the wall as required in CSA-A23.3 (2004); $V_{\text{limit}_{base}}$ is the base share force limit (elastic shear force reduced by 1.3); V_f and M_f are the design base shear force and base bending moment, respectively; and M_p is the base probable moment capacity of the wall.

Boivin and Paultre (2012) also suggested using the design shear envelope proposed by Rutenberg and Nsieri (2006), with a new equation for $\bar{\xi}$. Their proposed design shear envelope is shown in Figure 2.3(b).

$$\bar{\xi} = 1.5 - T_1; \quad 0.5 \leq \bar{\xi} \leq 1 \tag{2.29}$$

Table 2.2 Proposed base shear amplification factor value (Boivin and Paultre 2012).

$R_d R_o / \gamma_w$	$T_1 \leq 0.5$	$T_1 \geq 1.0$
2.80	1.0	2.0
1.87	1.0	1.5
≤1.40	1.0	1.0

Luu et al. (2014) performed a parametric study to examine the seismic demands of moderately ductile (MD) RC cantilever walls of 5 to 25 stories subjected to high-frequency Eastern North America earthquakes. A new base shear amplification factor, ω_v , applied to the base shear, V_d , obtained from RSA was proposed for NBCC (2010) and CSA-A23.3 (2004) for MD RC shear walls.

$$V_b = \omega_v V_d \tag{2.30}$$

$$\omega_v = \begin{cases} 1.6+0.7\left(\gamma_w - 1\right)+0.2\left(T-0.5\right) & \text{if } 0.5\text{ sec} \le T \le 1.5\text{ sec} \\ 1.8+0.7\left(\gamma_w - 1\right)-0.1\left(T-1.5\right) & \text{if } 1.5\text{ sec} < T \le 3.5\text{ sec} \end{cases}$$

where V_b is the design base shear force of the wall; *T* is the fundamental period; and γ_w is the base flexural over-strength factor of the wall.

Luu et al. (2014) also proposed design shear envelope as shown in Figure 2.3c similar to Rutenberg and Nsieri (2006) and Boivin and Paultre (2012) with few modification as presented in Eq. (2.31).

$$\begin{aligned} &\xi = 1.2 - 0.4T \quad 0.6 \le \xi \le 1 \\ &\alpha = 0.4 \\ &\beta = 1/n \end{aligned} \tag{2.31}$$

where *n* is the number of stories and *T* is the fundamental period.

Kazaz and Gülkan (2016) investigated the shear amplification factor in regular RC frame-wall systems of 4, 8, and 12 stories. They found that the level of inelastic demand was the primary source of amplification, and amplification factor diminished with decreasing of force reduction factor. Base shear amplification (β_v) was proposed from parametric study by using regression analysis on actual reduction factor (R_{exist}) and number of stories (*n*). The design base shear force of the wall is computed by Eq. (2.32).

$$V_{de} = \beta_v \lambda_d V_d \tag{2.32}$$

$$\beta = \begin{cases} 0.95 + 0.01n + 0.1R_{exist} & \text{for } R_{exist} > 2 \\ 1 + (R_{exist} - 1)(0.15 + 0.01n) & \text{for } R_{exist} \le 2 \end{cases}$$

$$R_{exist} = \frac{M_e}{M_{yd}}$$

where V_{de} is the design base shear force of the wall; V_d is the base shear force obtained from equivalent static analysis; λ_d is the flexural over-strength factor; M_{yd} is the design bending moment capacity; and M_e is the elastic bending moment.

2.3.2 Higher-mode-elastic method

Eibl and Keintzel (1988) conducted a study on 2- to 5-story RC cantilever walls and proposed base shear magnification factor which is used to multiply with shear force obtained from RSA before used as design demand value. They assumed that higher-mode contributions remained elastic and the first-two modes were dominant modes. The design shear force at the base of structural walls was computed by Eq. (2.33).

$$V_{Ed} = \sqrt{\left(V'_{Ed,1}\right)^2 + \left(qV'_{Ed,2}\right)^2} \tag{2.33}$$

where V_{Ed} is the design shear force at the base of the wall; $V'_{Ed,1}$ and $V'_{Ed,2}$ are the reduced base shear forces of the first and second modes, respectively; q is the behavior factor used in design. They further simplified Eq. (2.33) such that the ratio of the base shear from the second mode to that from the first mode was equal to $\sqrt{0.1}S_e(T_c)/S_e(T_1)$ and that the flexural over-strength factor, $\gamma_{Rd}M_{Rd}/M_{Ed}$, was added to the first-mode shear, and that the base shear magnification ε was limited by factor, q. The following expressions could be derived.

$$V_{Ed} = V'_{Ed,1}q\sqrt{\left(\frac{\gamma_{Rd}}{q}\frac{M_{Rd}}{M_{Ed}}\right)^2 + 0.1\left(\frac{S_e(T_C)}{S_e(T_1)}\right)^2}$$

$$V_{Ed} = \varepsilon V'_{Ed,1}$$

$$\varepsilon = q\sqrt{\left(\frac{\gamma_{Rd}}{q}\frac{M_{Rd}}{M_{Ed}}\right)^2 + 0.1\left(\frac{S_e(T_C)}{S_e(T_1)}\right)^2} \le q \tag{2.34}$$

where ε is the base shear magnification factor, M_{Rd} is the design flexural resistance at the base of the wall, M_{Ed} is the base bending moment demand of the wall obtained from ELF or RSA procedure, γ_{Rd} is the over-strength factor to account for steel strain-hardening $(\gamma_{Rd} = 1.2)$, T_c is the upper-limit period of the constant spectral acceleration

region of the spectrum, T_1 is the fundamental period in the direction of shear force and $S_e(T)$ is the ordinate of the elastic response spectrum.

Equation (2.34) was introduced in Eurocode 8 (EC8) (CEN 2004) under two modifications. First, EC8 amplified the design shear force of the wall by total shear force from RSA, $V_{Ed}^{'}$. Second, EC8 uses Eq. (2.34) as constant magnification factor along the height of the wall. As required by EC8, for moderately ductile wall (q<3), the value of ε is taken as 1.5 , while for highly ductile walls, it is calculated from Eq. (2.35) and the value of ε has to be at least 1.5, but needs not be larger than q.

$$V_{Ed} = \varepsilon V_{Ed}^{'}$$

$$\varepsilon = q\sqrt{\left(\frac{\gamma_{Rd}}{q}\frac{M_{Rd}}{M_{Ed}}\right)^2 + 0.1\left(\frac{S_e(T_C)}{S_e(T_1)}\right)^2} \tag{2.35}$$

Priestley (2003) proposed a modified modal superposition (MMS) approach based on a study of RC cantilever walls of 2 to 20 stories to determine the design shear forces of the walls, as shown in Eq. (2.36). This method was developed based on the assumption that inelastic action limits the shear force from only the first mode which is computed using DDBD approach, and shear forces from higher modes behave elastically.

จุฬาลงกรณ์มหาวิทยาลัย
CHULALONGKORN UNIVERSITY

$$V_i = \left(V_{1i}^2 + V_{2Ei}^2 + V_{3Ei}^2 + ...\right)^{0.5} \tag{2.36}$$

where V_i is the design shear force of the wall at level i; V_{1i} is the lesser of elastic first-mode and inelastic first-mode shear computed by DDBD at level i; V_{2Ei} and V_{3Ei} are the elastic modal shear at level i for 2nd and 3rd modes, respectively. The same combination rule cannot be used for bending moment because it will increase bending moment to be larger than moment capacity of the wall at the base. For bending moment above mid-height, a similar modal combination to that of shear force was proposed by multiplying a factor of 1.1 over the upper haft of the wall height. The moment design (Figure 2.5) was

defined by linear variation from moment capacity at the base to mid-height moment calculated from Eq. (2.37) in the lower half of the wall height.

$$M_i = 1.1\left(M_{1i}^2 + M_{2Ei}^2 + M_{3Ei}^2 + ...\right)^{0.5} \tag{2.37}$$

where M_i is the design moment of the wall at level *i* starting from the mid-height to the top; M_{1i} is the lesser of elastic first mode moment and ductile design moment from DDBD at level *i*; M_{2Ei} and M_{3Ei} are the elastic modal moment at level *i* for 2nd and 3rd modes, respectively.

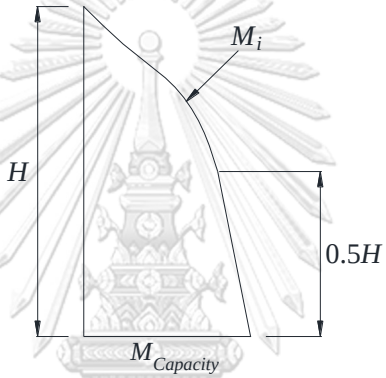

Figure 2.5 Moment design envelope (Priestley 2003).

Chopra et al. (2004) suggested a modified modal pushover analysis (MMPA) which was simplified from the MPA method of Chopra and Goel (2002) (see Section 2.1.3). The MMPA assumed that higher-mode responses were within elastic range. The total responses were computed by combining inelastic first-mode responses from MPA and elastic higher-mode responses from RSA.

Sullivan et al. (2008) proposed a transitory inelastic modal superposition (TIMS) method to account for inelastic higher mode for design of RC frame-wall structure. This study was conducted on 4- to 20-story RC frame-wall structures. They stated that elastic higher-mode assumption was suitable for RC wall but not for frame. TIMS method was proposed in a similar form to MMS method of Priestley (2003), but inelastic higher-mode responses were considered by higher-mode period lengthening which was approximated

by eigenvalue analysis using very small rotational spring stiffness (10kN/m) at the support. The TIMS method was applicable to only the base shear which is computed by Eq. (2.38).

$$V_{bTIMS} = \sqrt{V_{b1}^2 + V_{bTIM2}^2 + V_{bTIM3}^2 + \cdots + V_{bTIMn}^2} \tag{2.38}$$

where V_{bTIMS} is the design base shear from TIMS method; V_{b1} is the ductile 1st mode base shear obtained from DDBD; V_{bTIM2}, V_{bTIM3}, and V_{bTIMn} are the modal base shear associated with the 2nd, 3rd, and *n*th transitory inelastic mode, respectively.

Rejec et al. (2012) demonstrated from a study of RC cantilever walls of 4 to 20 stories that the design base shear force in EC8 should be computed from the first-mode shear, $V'_{Ed,1}$, amplified by the magnification factor, ε_a , and this is the basis of Eibl and Keintzel (1988)'s approach. They limit the base shear force of the wall by total elastic shear force from RSA. So, they modified Eq. (2.35) to be Eq. (2.39).

$$V_{Ed,a} = \varepsilon_a V'_{Ed,1} \tag{2.39}$$

$$\varepsilon_a = q\sqrt{\left(\min\left[\frac{\gamma_{Rd}}{q}\frac{M_{Rd}}{M_{Ed}};1\right]\right)^2 + 0.1\left(\frac{S_e(T_C)}{S_e(T_1)}\right)^2} \geq 1.5$$

Rejec et al. (2012) showed that constant magnification factor in EC8 was too conservative around mid-height of the wall; therefore, by replacing the constant ratio between the contribution of second mode to that of the first mode found by Eibl and Keintzel (1988) with a variable ratio, *m(z)* along the height of the wall, they proposed formula as shown in Eq. (2.40) to compute design shear force along the height of the wall.

$$\varepsilon_a(z) = q\sqrt{\left(\min\left[\frac{\gamma_{Rd}}{q}\frac{M_{Rd}}{M_{Ed}};1\right]\right)^2 + m(z)^2\left(\frac{S_e(T_C)}{S_e(T_1)}\right)^2} \geq 1.5 \tag{2.40}$$

where *z* is the vertical coordinate of the wall; *H* is the total height of the wall; and *m(z)* is the ratio between the higher modes (second and third modes) and the first mode.

Calugaru and Panagiotou (2012) conducted a research using a central RC core wall of 10-, 20- and 40-story buildings. They found that using a single *R* factor to reduce all modes of force responses as in ASCE 7-10 is not conservative for tall buildings because higher-mode response should not be reduced as much as the first mode. Modified modal response spectrum analysis (MMRSA), which uses different reduction factors for the first mode and higher mode, was proposed as shown in Eq. (2.41). The reduction factor for higher modes was found to be much smaller than the first mode and generally varied from 1 to 2.

$$Q^i = \sqrt{\left[Q_1^i \frac{\Omega_{b,0}}{R_1}\right]^2 + \frac{\left[Q_2^i\right]^2 + \left[Q_3^i\right]^2}{\left[R_H\right]^2}} \tag{2.41}$$

where Q^i is the design shear force of the wall at level *i*; Q_q^i is the qth mode elastic shear force at level *i*; $\Omega_{b,0}$ is the base flexural over-strength factor; R_1 and R_H are the reduction factor for the first and higher modes, respectively.

2.3.3 Equivalent linearization method

The main concept of the equivalent linearization method is to convert a nonlinear multi-degree-of-freedom (MDOF) structure to an equivalent linear single-degree-of-freedom (SDOF) system (Priestley et al. 2007, Panagiotou and Restrepo 2011, Fox et al. 2014, Pennucci et al. 2015) or to many equivalent linear SDOF systems (Najam and Warnitchai 2018). The equivalent linear SDOF system is characterized by an equivalent natural period computed using the secant stiffness at maximum displacement of the nonlinear structure and a level of equivalent viscous damping that combines elastic damping and hysteretic damping to represent overall energy dissipation. Elastic spectra reduced for the equivalent damping value was used in this approach (Priestley et al. 2007). Equivalent viscous damping to be used to characterize the design displacement spectrum for the SDOF structure was proposed by Priestley et al. (2007) for many types of structural systems. All approaches were based on the design displacement limit state, which is defined by material strain limits or drift limits. The capacity design was also

required to ensure that plastic hinge will occur only at the intended locations and that shear failure will not occur (Priestley 2003, Priestley et al. 2007).

Panagiotou and Restrepo (2011) proposed displacement-based method for regular RC walls, which was verified by a shaking table test of a full-scale 7-story rectangular RC wall. The proposed method combined the effect of inelastic first-mode response, kinematic system over-strength, and elastic higher-mode response. The first-mode response was computed by converting MDOF system to inelastic SDOF using effective stiffness at yield point. The target roof displacement was determined by performance objective limit state, which was calculated from geometric and material properties of the wall. The period of the equivalent SDOF can be calculated from displacement design spectrum. Beside flexural over-strength factor, this method considered kinematic system over-strength caused by deformation compatibility between walls and elements framing into them. The design force envelope was computed by SRSS combination rule.

$$U_i = \sqrt{\left(\Omega U_{1,i} + U_{K,i}\right)^2 + \left(U_{2,i}\right)^2} \tag{2.42}$$

where U_i is the design force (structure overturning moments, shear forces, and axial forces) at level *i*; $U_{1,i}$ and $U_{2,i}$ are the force associated with the first and second modes, respectively; $U_{K,i}$ is the force resulted from kinematic system over-strength. For bending moment of the wall, Eq. (2.42) was used for *i*=2 to *n* (roof level) because bending moment at the base of the wall already included flexural over-strength factor in establishing this method.

Pennucci et al. (2015) proposed two methods to estimate inelastic response of higher mode for RC cantilever and coupled wall systems. The first method is the effective modal superposition (EMS) method, which is based on the substitute structure method. The first-mode response is computed by reducing response spectrum analysis, while higher-mode responses are estimated using a substitute elastic structure as shown in Figure 2.6, in which the stiffness of plastic hinges is equivalent to the secant stiffness of

the original structure at maximum response, and the damping is equal to the elastic damping of the original structure. Secant stiffness of structural member was proposed as a function of design ductility (μ_Δ).

$$EI_{bh,eff} = \frac{EI_w}{\mu_\phi} = \frac{EI_w}{1+\frac{H}{3L_p}(\mu_\Delta - 1)} \tag{2.43}$$

$$EI_{\mathrm{CB},eff} = \frac{EI_{CB}}{\mu_\Delta} \tag{2.44}$$

where $EI_{bh,eff}$ and $EI_{\mathrm{CB},eff}$ are the effective flexural rigidity of wall at the base and coupling beams, respectively; EI_w and EI_{CB} are elastic gross flexural rigidity of wall and coupling beam, respectively; *H* is the total height of the wall; and L_p is the plastic hinge length.

The second method of Pennucci et al. (2015) was the weighted capacity design (WCD) method, which estimated inelastic higher-mode shears, $V_n(x)$ and bending moments, $M_n(x)$ from simplified closed-form equations based on structural dynamic theory. The higher-mode forces were then combined with the first-mode reduced response as in EMS method to obtain the design forces.

$$V_n(x) = m_{tot}\left[\rho c_{n,f}(x) Sa_{n,f} + (1-\rho) c_{n,p}(x) Sa_{n,p}\right] \tag{2.45}$$

$$M_n(x) = m_{tot} H\left[\rho d_{n,f}(x) Sa_{n,f} + (1-\rho) d_{n,p}(x) Sa_{n,p}\right] \tag{2.46}$$

where Sa_n is the spectral acceleration for mode *n*; m_{tot} is the total mass of the system; *H* is the total height of the system; $c_n(x)$ and $d_n(x)$ are the modal shear and moment distribution parameters at level x, respectively; ρ is the weight factor that equals to 1 for elastic structure and decreases linearly to zero at ductility of 3.5; and the subscripts *f* and *p* indicate parameters for fixed- and pinned-based solution, respectively. The shear force envelope as shown in Figure 2.7a was constructed by linear interpolation between base shear and mid-height shear for the lower half of the wall height, and it equals to mid-height shear for the upper half of the wall height. Bending moment envelope as shown in Figure

2.7b was constructed by linear function between base, mid-height, 80% of the height where moment was assumed equal to 60% of mid-height moment, and zero moment at the top.

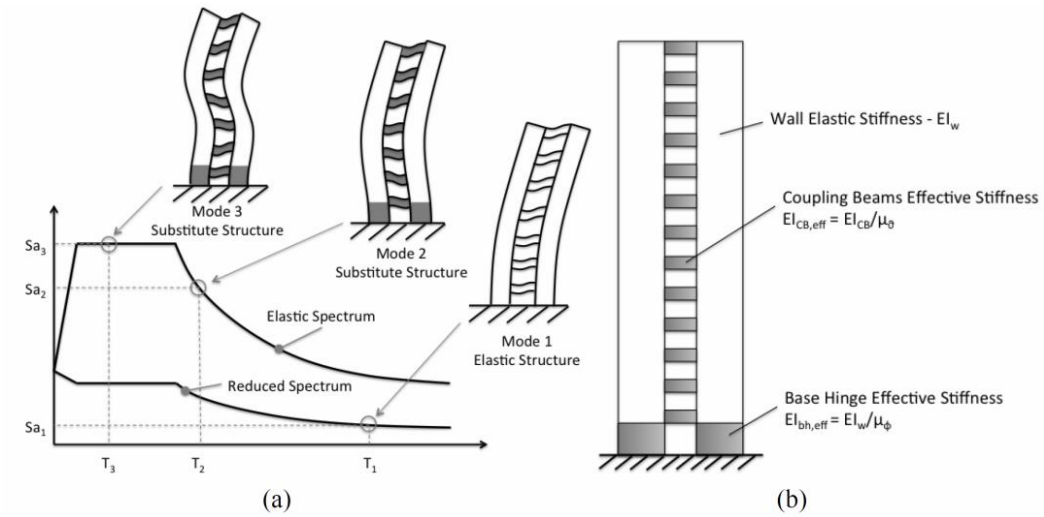

Figure 2.6 (a) Computation of modal responses according to the proposed EMS method and (b) definition of the effective stiffness in the substitute structure (Pennucci et al. 2015).

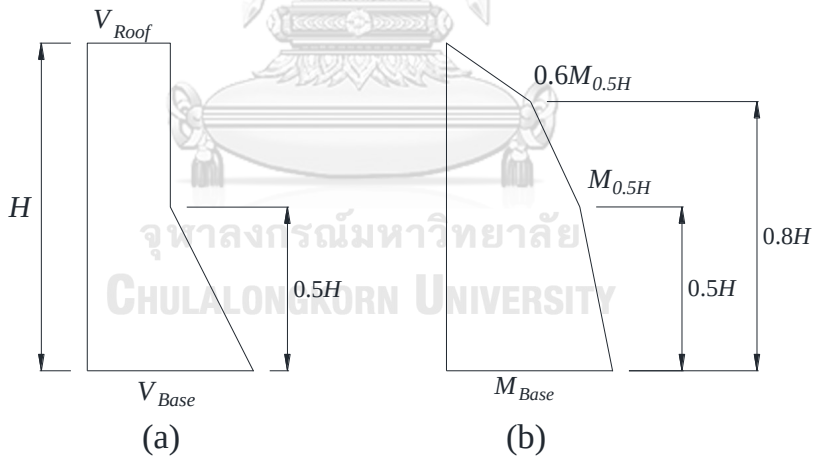

Figure 2.7 Design envelope of (a) shear forces; and (b) bending moments (Pennucci et al. 2015).

Fox et al. (2014) proposed a shear force capacity design method for RC coupled walls, which was simplified from the WCD method of Pennucci et al. (2015). The study used RC coupled walls of 5 to 30 stories. The main assumption used to simplify the WCD method was that the fixed- and pinned-base spectral accelerations of the higher modes

were assumed to lie in certain ranges of the acceleration spectrum. For short periods, all higher-mode components were assumed to have periods of vibration within the constant acceleration branch. For long periods, it was assumed the components of the first-higher mode were on the constant velocity branch of the spectrum, while the components of the second-higher mode were on the constant acceleration branch. The capacity-design base shear and mid-height shear forces are calculated from Eq. (2.47) and Eq. (2.48), respectively.

$$V_{base} = \sqrt{\left(\phi^o V_d\right)^2 + C_2\left(mSa_{PL}\right)^2} \tag{2.47}$$

$$V_{m-h} = \sqrt{\left(0.85\phi^o V_d\right)^2 + C_3\left(mSa_{PL}\right)^2} \tag{2.48}$$

$$C_1 = \frac{2T_C^2 EI}{mH_n^3} \tag{2.49}$$

$$C_2 = \min\begin{cases} 0.048 - 0.008\mu \\ \left(0.56 - 0.125\mu\right)\left(C_1 + 0.01\right) \end{cases} \tag{2.50}$$

$$C_3 = \min\begin{cases} 0.022 + 2\times10^{-4}\mu \\ \left(0.0019\mu - 2.8\times10^{-4}\right)C_1 + 0.0026 \end{cases} \tag{2.51}$$

where Sa_{PL} is the spectral acceleration on the plateau of the design spectrum; *EI* is the flexural rigidity of a single wall (calculated from the secant stiffness); H_n is the total height of the structure; and V_d is the design base shear. The shear envelope is defined in the same manner as the method proposed by Pennucci et al. (2015).

Najam and Warnitchai (2018) proposed a modified response spectrum analysis based on the equivalent linearization approach. The study was conducted using three tall buildings with RC shear walls. This method converts a nonlinear MDOF system to many equivalent linear SDOF systems representing many uncoupled vibration modes. For each vibration mode, the equivalent linear stiffness was set equal to the secant stiffness of a nonlinear system at maximum displacement and damping value was computed from equal energy concept. Among all methods described above, only this method was

developed using real tall buildings with RC shear walls; however, this method seems to be difficult for practical application and is more appropriate for seismic evaluation of a building rather than design of a new building.

2.4 Summary

Many previous studies have proposed different approaches for estimating higher-mode effects by means of simple amplification factor method, higher-mode elastic method and equivalent linearization method. Most researchers focused on RC cantilever walls designed to have concentrated yielding at the base region. This may not be appropriate when applied to real tall buildings where yielding and cracking could occur anywhere along the height of the building due to higher-mode effects.

Amplification factor method is appropriate in design practice as it is simple and has been adopted in several seismic design codes, EC8 (2004), NZS 3101 (2006), and NBCC (2010). However, the accuracy offered by this method is not warranted as the higher-mode responses variably depend on structural systems, ductility demands, and shapes of design response spectrum.

Equivalent linearization method is difficult in design practice because it uses the displacement-based design concept where ductility is used rather than force reduction factor, and that it requires an iteration process to compute the properties of the equivalent linear system. The design displacement requires significant computational effort in which geometry and material properties of member cross sections must be known. Moreover, there is no computer software to readily implement such method yet.

Higher-mode elastic assumption is convenient for practical application, once the inelastic first-mode response is already determined. Up to present time, the inelastic first-mode response can be computed using DDBD (Priestley 2003), pushover analysis (Chopra et al. 2004), or reducing elastic first-mode response with the corresponding force reduction factor (Calugaru and Panagiotou 2012). The method proposed by Calugaru and Panagiotou (2012) is more appropriate in design practice, since it requires only a linear structural model. However, this method was based on a study of RC cantilever core walls

designed to have concentrated yielding at the base of the wall, which resulted in a large bending moment and shear force amplification due to higher-mode effects. The effects of higher-mode responses can be reduced by allowing yielding to occur in upper stories of a tall building, and this can be numerically implemented by using nonlinear elements over the entire height of the structure (PEER 2017). When multiple plastic hinges are allowed, their locations must be identified so that ductile detailing can be provided. However, a method to predict such yielding locations is not yet available.

Although EC8 (2004), NZS 3101 (2006), and NBCC (2010) have already been modified to account for shear amplification in RC walls, there is not yet such shear amplification in ASCE 7-10. Therefore, this study aims to evaluate the accuracy of RSA procedure in ASCE 7-10. Two versions of modified response spectrum analysis (MRSA) method, (1) $MRSA_{HE}$ based on a higher-mode-elastic approach similar to MMS method of Priestley (2003) and MMPA method of Chopra et al. (2004) and (2) $MRSA_{HI}$ based on a higher mode inelastic approach, to compute shear forces were proposed together with a novel method based on an equal displacement rule to compute strains to predict ductile detailing locations in RC walls and column. The proposed method strives to ensure that the computed design demands on tall buildings are reasonably accurate and safe to use while maintaining the suitability for practical application.

จุฬาลงกรณ์มหาวิทยาลัย
CHULALONGKORN UNIVERSITY

CHAPTER 3
STRUCTURAL SYSTEMS AND EARTHQUAKE GROUND MOTIONS

3.1 Description of studied buildings

There were two types of lateral force resisting system considered in this study: RC shear wall and RC moment-resisting frame. The structural members were designed according to ACI 318M-14 considering all factored load combinations including gravity load, wind load using the Bangkok Building Control Law (2001), and earthquake load using the RSA procedure in ASCE 7-10. The buildings were assumed to be in Bangkok (soft soil, site class F) and Chiang Mai (stiff soil, site class D) cities of Thailand. The design loads, load combinations, and detail of the buildings can be found in Appendix A.

3.1.1 Tall RC shear-wall buildings

Six tall buildings with RC shear walls were considered in this study. Four of these buildings are 15-, 20-, 31-, and 39-story existing buildings in Bangkok denoted by SWB1, SWB2, SWB3, and SWB4, respectively. These tall buildings were selected to represent a wide range of typical tall buildings in Bangkok. Buildings SWB2, SWB3, and SWB4 have a podium consisting of the first few stories and a tower, which is a typical style for tall buildings in many countries around the world. Buildings SWB5 (20-story) and SWB6 (39-story) were modifications of building SWB4, with building SWB5 having the same floor plans as building SWB4, but with a shortened 20-story tower and wall thickness and column size reduced to represent a typical 20-story building; and building SWB6 has two additional RC core walls and an enlarged podium, so that building SWB6 has more vertical irregularity. The primary lateral force resisting system of buildings SWB1-SWB6 consists of RC core walls and a number of RC shear walls. The gravity load carrying system consists of RC columns and post-tensioned flat slabs for buildings SWB1, SWB3-SWB6 and consists of RC shear walls and post-tensioned flat slabs for building SWB2. The typical floor plans and three-dimensional models of the buildings are shown in Figure 3.1.

The buildings were modeled using the as-built building drawing plans. The concrete section sizes of the structural members were kept the same as in the existing

buildings, but the steel reinforcement of the structural members was re-designed with demands from all factored load combinations. For all buildings, the columns in each story resist less than 25% of the total lateral force; hence, the seismic force resisting system was considered to be RC shear walls and the design parameters for buildings SWB1-SWB6 were taken from ASCE 7-10: response modification factor $R = 5,$ deflection amplification factor $C_d = 4.5,$ and over-strength factor $\Omega_0 = 2.5$. The earthquake load governed the design of steel reinforcement for the 15-story (SWB1), 20-story (SWB2 and SWB5), and 31-story (SWB3) buildings. For the 39-story buildings (SWB4 and SWB6), the wind load resulted in a larger bending moment than the earthquake load, but required less than minimum reinforcement; hence, the minimum reinforcement was used in these two buildings. The basic structural parameters of buildings SWB1-SWB6 are summarized in Table 3.1. The periods of the buildings shown in Table 3.1 were computed from cracked cross section properties of the buildings as described in Section 3.2.1. The seismic weight of the buildings was computed from all dead loads and super-imposed dead loads. The details of each building can be found in Appendix A.

จุฬาลงกรณ์มหาวิทยาลัย
CHULALONGKORN UNIVERSITY

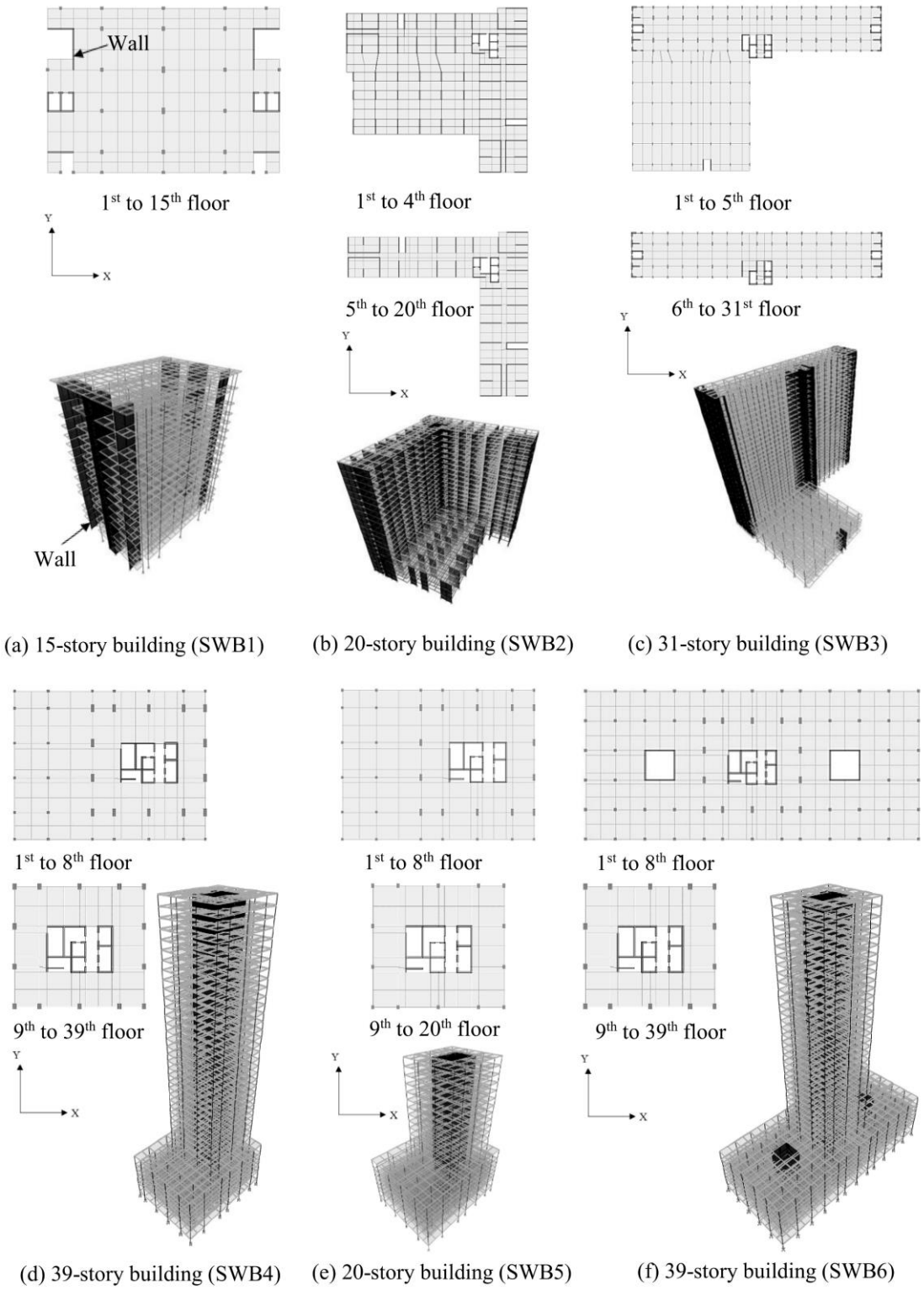

Figure 3.1 Floor plans and three-dimensional models of tall RC shear-wall buildings.

Table 3.1 Structural parameters of tall RC shear-wall buildings.

Building			SWB1	SWB2	SWB3	SWB4	SWB5	SWB6
No. of stories			15	20	31	39	20	39
Total height (m)			55.4	54.5	90.0	125.5	64.7	125.5
Podium height (m)			-	10.0	15.3	26.5	26.5	26.5
Typical story height (m)			3.2	2.75	2.85	3.2	3.2	3.2
Seismic weight (kN)			200216	324090	694887	375997	212759	553556
RC wall section area / floor area at the base (%)			1.2	2.2	1.2	1.5	1.2	1.5
RC column section area / floor area at the base (%)			1.2	-	1.3	1.3	1.4	1.9
Maximum RC wall thickness (m)			0.25	0.20	0.30	0.35	0.25	0.35
Maximum RC column size (m x m)			1.2x0.6	-	1.8x0.5	1.8x0.8	1.5x0.6	1.8x0.8
Maximum axial load ratio in RC wall $P / A_g f_c'$ (%) *			9.8	13.8	14.6	21.0	12.0	21.0
Compressive strength of concrete f_c' (MPa)			35	28	32	32	32	32
Yield strength of longitudinal steel reinforcement f_y (MPa)			400	400	400	400	400	400
Natural periods of translational modes (sec)	X-direction	T_{x1}	2.97	1.38	4.55	4.85	2.06	4.40
		T_{x2}	0.60	0.32	1.23	1.16	0.52	1.06
		T_{x3}	0.24	0.14	0.57	0.53	0.22	0.55
	Y-direction	T_{y1}	2.39	1.58	3.05	5.31	2.12	4.79
		T_{y2}	0.50	0.36	0.73	1.06	0.40	0.98
		T_{y3}	0.20	0.16	0.34	0.42	0.17	0.46

* $P =$ axial load, $A_g =$ gross section area of wall

จุฬาลงกรณ์มหาวิทยาลัย
CHULALONGKORN UNIVERSITY

3.1.2 RC moment-frame buildings

Four generic RC moment-frame buildings of 3-, 6-, 9- and 15-story denoted by MFB1, MFB2, MFB3, and MFB4, respectively were employed. Regular two-dimensional frames of three bays with span length of 6m, and typical story height of 3.5m were used. The concrete cross sections of columns were changed every three stories, and the concrete cross sections of beams are the same for all floors in a building. The lateral force resisting system was special RC moment-resisting frame whose design factor according to ASCE 7-10 are: R=8, C_d=5.5, Ω_0=3.0. The floor plan and two-dimensional models of RC frame buildings are shown in Figure 3.2.

The concrete sections of structural members were designed to satisfy strong column-week beam requirement and that the story drift is lower than the allowable story drift of 2% according to ASCE 7-10. The structural parameters of building MFB1-MFB4 are presented in Table 3.2. The periods shown in Table 3.2 were computed from cracked cross section properties of the buildings as described in Section 3.2.1. The details of each building can be found in Appendix A.

จุฬาลงกรณ์มหาวิทยาลัย
CHULALONGKORN UNIVERSITY

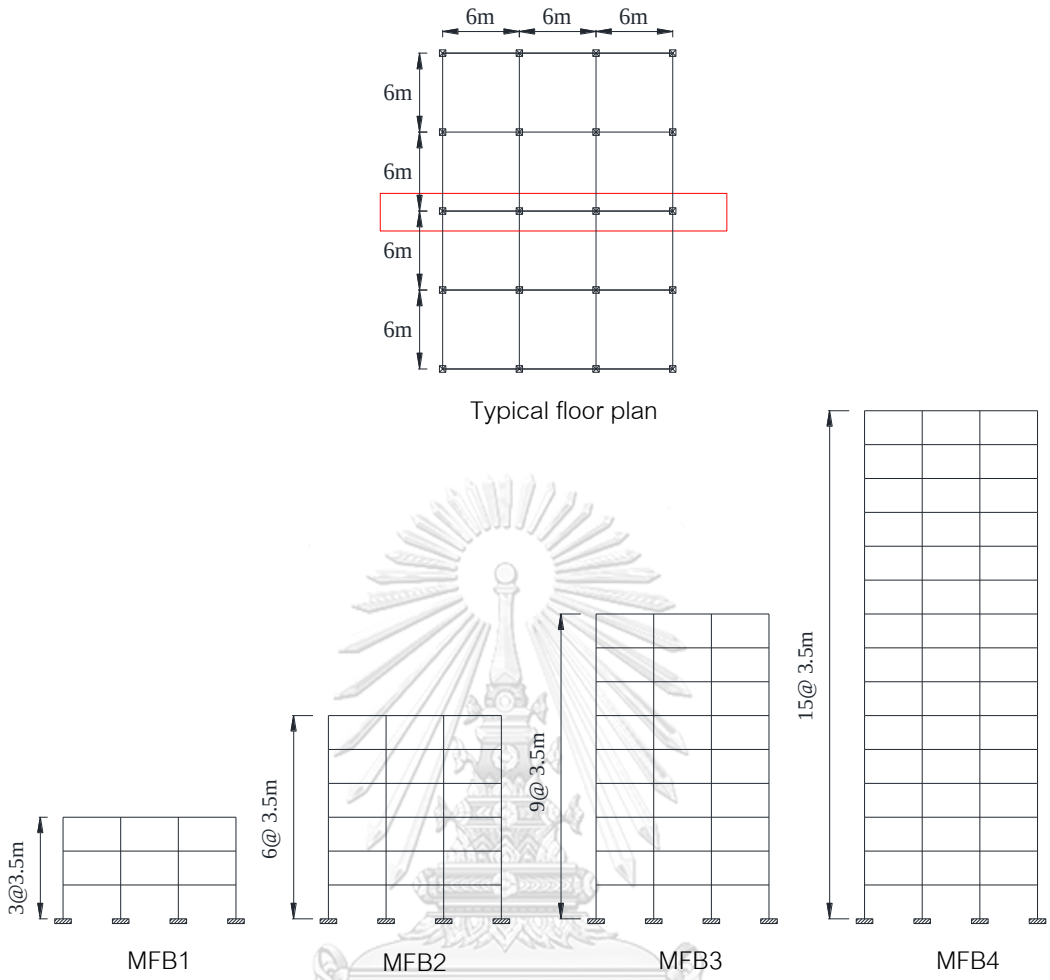

Figure 3.2 Floor plans and two-dimensional models of RC moment-frame buildings.

จุฬาลงกรณ์มหาวิทยาลัย
CHULALONGKORN UNIVERSITY

Table 3.2 Structural parameters of RC moment-frame buildings.

Building		MFB1	MFB2	MFB3	MFB4
No. of stories		3	6	9	15
Total height (m)		10.5	21	31.5	52.5
Typical story height (m)		3.5	3.5	3.5	3.5
Seismic weight (kN)		2253	4712	7492	12424
Compressive strength of concrete (MPa)		30	30	30	30
Yield strength of reinforcement (MPa)		400	400	400	400
Beam size (m x m)		0.25x0.5	0.3x0.6	0.3x0.6	0.3x0.6
Column size (m x m)	13th-15th	-	-	-	0.4x0.4
	10th-12th	-	-	-	0.45x0.45
	7th-9th	-	-	0.4x0.4	0.5x0.5
	4th-6th	-	0.4x0.4	0.5x0.5	0.6x0.6
	1st-3rd	0.35x0.35	0.4x0.4	0.6x0.6	0.7x0.7
Natural periods of translational modes (sec)	T_1	1.23	1.85	2.31	3.91
	T_2	0.38	0.59	0.79	1.34
	T_3	0.21	0.34	0.44	0.77

จุฬาลงกรณ์มหาวิทยาลัย
CHULALONGKORN UNIVERSITY

3.2 Analytical models

The design of the structural system was accomplished by using ETABS (CSI 2015) and the analyses were carried out using PERFORM-3D (CSI 2011). The design strength and structural model in ETABS were exported to PERFORM-3D. The followings were assumed in the mathematical model of structural systems:

- For real tall buildings SWB1-SWB6, three-dimensional structural models with all structural members: beams, columns, slabs, and shear walls were included in the analytical model.
- For generic RC frame buildings MFB1-MFB4, two-dimensional frame was considered in the analytical model.

- Shear behavior of structural members was considered to be elastic and was modeled using uncracked gross shear stiffness.
- Rigid floor diaphragm was assigned to each floor level assuming that the floor is rigid in plane.
- Joints between members were assumed to be rigid connection.
- Foundation was assumed to be fixed support.

3.2.1 **Linear analytical model**

A linear structural model considering cracked cross sections of RC structural members according to ACI 318M-14 was prepared for RSA procedure used for computing design demands of structural systems. The effective moment of inertia for RC walls was assumed to be 35% and 70% of the gross moment of inertia for cracked walls and uncracked walls, respectively. A cracked wall was considered at the locations where tensile stress from an analysis exceeds the modulus of rupture of concrete computed by Eq. (3.1) according to ACI 318M-14 (Section 19.2.3). The effective moment of inertia of 70%, 35%, and 25% of the gross moment of inertia was used for RC columns, beams, and slabs, respectively. Table 3.3 summarizes the effective stiffness values of structural members.

จุฬาลงกรณ์มหาวิทยาลัย
CHULALONGKORN UNIVERSITY

$$f_r = 0.62\lambda\sqrt{f_c^{'}} \tag{3.1}$$

where f_r is the modulus of rupture of concrete in MPa; $f_c^{'}$ is the compressive strength of concrete in MPa; and $\lambda = 1$ for normal weight concrete.

Table 3.3 Effective stiffness of structural members in linear and nonlinear analytical models.

Elements	Linear model			Nonlinear model		
	Flexural	Axial	Shear	Flexural	Axial	Shear
Shear wall (in-plane)	Cracked: 0.35 E_cI_g Uncracked: 0.70 E_cI_g	1.0 E_cA_g	1.0 GA_g	Fiber	Fiber	1.0 GA_g
Shear wall (out-of-plane)	0.25 E_cI_g	-	-	0.25 E_cI_g	-	-
Column	0.70 E_cI_g	1.0 E_cA_g	1.0 GA_g	Fiber	Fiber	1.0 GA_g
Beam	0.35 E_cI_g	1.0 E_cA_g	1.0 GA_g	0.35 E_cI_g	1.0E_cA_g	1.0 GA_g
Slab (in-plane)	1.0 E_cI_g	1.0 E_cA_g	1.0 GA_g	1.0 E_cI_g	1.0E_cA_g	1.0 GA_g
Slab (out-of-plane)	0.25 E_cI_g	-	-	0.25 E_cI_g	-	-

E_c is the Young's modulus of concrete; I_g is the gross moment of inertia; A_g is the gross cross section of structural member; G is the shear modulus of concrete.

3.2.2 Nonlinear analytical model

A nonlinear structural model was created in PERFORM-3D program (CSI 2011) for pushover analysis and NLRHA. The RC walls were modeled using nonlinear fiber elements represented by concrete and steel material properties to capture the in-plane axial-bending interaction behavior. The shear stiffness was modeled by a horizontal linear elastic shear spring assuming that the shear capacity of the wall is large enough that shear failure does not occur. The out-of-plane behavior of the wall was assumed to be elastic with small effective stiffness of $0.25E_cI_g$ to allow for stiffness reduction when concrete cracks. Nonlinear fiber modeling was used over the entire height of the walls to capture flexural cracking and yielding which could occur at any location due to higher-mode effects in tall buildings. The material stress-stain relationship for concrete proposed by Mander et al. (1988) was adopted and represented by a tri-linear relationship in PERFORM-3D as shown in Figure 3.3. A bilinear inelastic model (Figure 3.4) proposed by

Menegotto and Pinto (1973) was used for steel. The steel material properties were taken from material specification of Thailand industrial standard (SD40 in TIS 24-2548). The expected material strength was used in the model, as the actual material strength is usually greater than the nominal strength specified by the designer. The compressive strength of concrete was taken as 1.25 times the nominal strength, the yield strength of steel was taken as 1.25 times the nominal yield strength, and the ultimate strength of steel was taken as 1.18 times the nominal ultimate strength (Research and Consultancy Institute of Thammasat University, 2009). The cyclic degradation parameters of steel and concrete material in PERFORM-3D were taken from Kolozvari et al. (2017) as shown in Table 3.4. The hysteresis loop of concrete and steel resulted from the proposed cyclic degradation parameter of Kolozvari et al. (2017) are shown in Figures 3.5 and 3.6, respectively. It should be noted that the proposed parameters of Kolozvari et al. (2017) were obtained by calibrating fiber model of the wall in PERFORM-3D with experimental results of U-shape RC wall (Figure 3.7).

The RC columns were modeled by a linear elastic frame element with nonlinear plastic hinge zones at both ends. The plastic zones were modeled by nonlinear fiber elements similar to those used for RC walls. The length of the plastic zone was assumed equal to 0.5 times the depth of the column section (Paulay and Priestley 1992). The effective flexural stiffness of 0.7 times the gross stiffness was considered for the elastic portion of the columns.

จุฬาลงกรณ์มหาวิทยาลัย
CHULALONGKORN UNIVERSITY

The conventional RC beams and coupling beams were modeled by a linear elastic frame element at the middle portion and rotational plastic hinge elements at both ends with modeling parameters given by ASCE 41-13. Plastic hinge properties were defined by a tri-linear moment-hinge rotation relationship (Figure 3.8) whose cyclic degradation parameters in PERFORM-3D were taken from Naish et al. (2013). An example of plastic moment-hinge rotation model with hysteresis loop is shown in Figure 3.9. The effective flexural stiffness of 0.35 times the gross stiffness was considered for the elastic portion of the beams. Coupling beams were connected to the walls by using embedded rigid beams

to ensure the rigid connections between the coupled walls and the coupling beams as recommended by PERFORM-3D documentation.

Slabs were assumed to be elastic and were modeled by elastic shell elements with the out-of-plane effective stiffness of $0.25E_cI_g$ as used in linear analytical model. All nodes in each floor are constrained such that the slab acts as a rigid floor diaphragm. The joints between members are considered to be rigid connections.

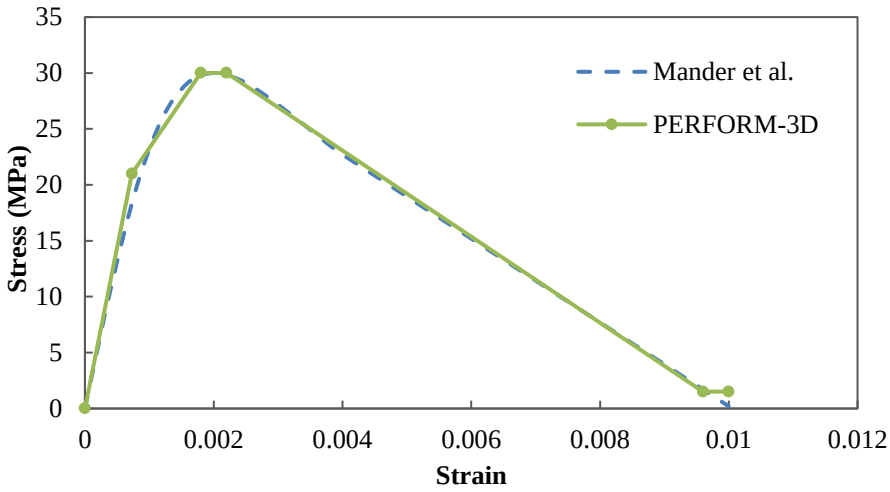

Figure 3.3 Concrete stress-strain relationship.

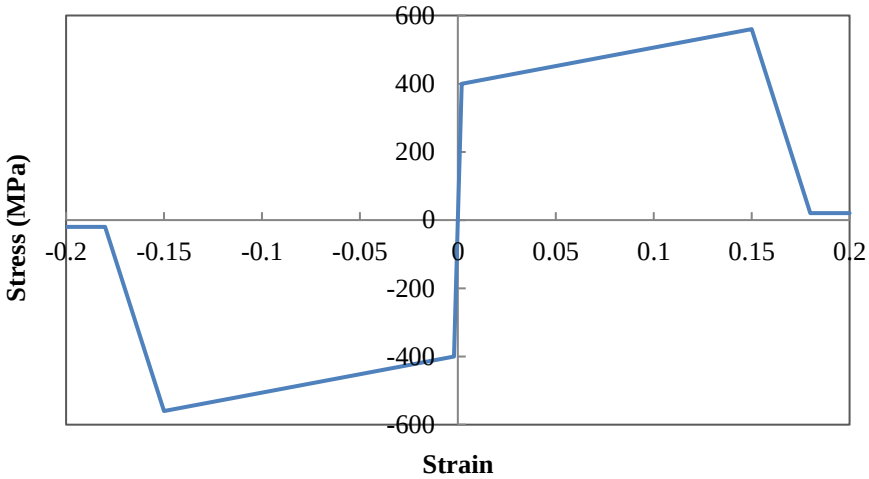

Figure 3.4 Steel stress-strain relationship.

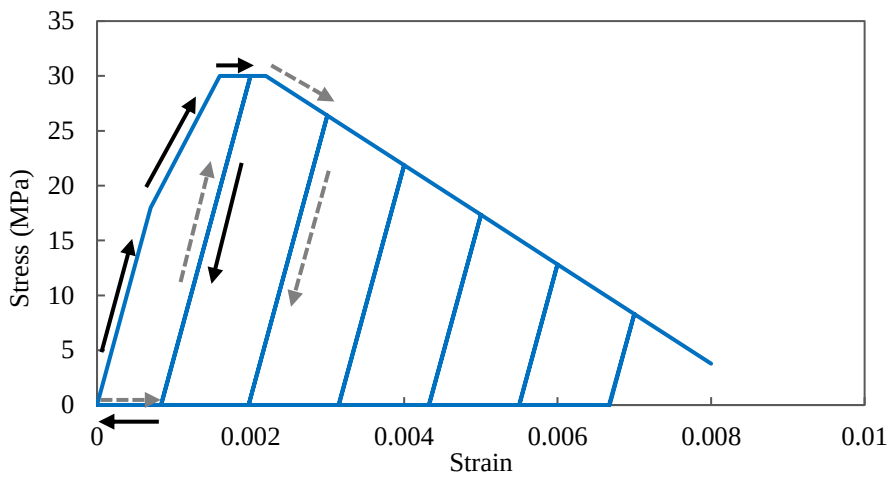

Figure 3.5 Hysteretic behavior of concrete material.

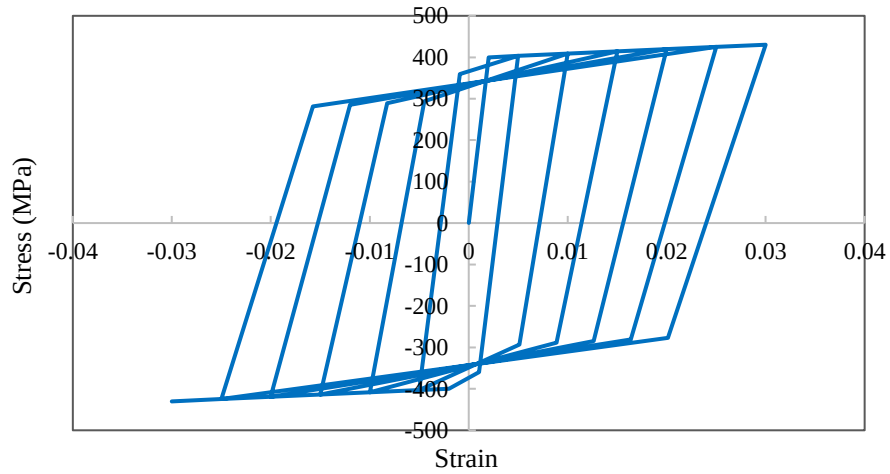

Figure 3.6 Hysteretic behavior of steel material.

จุฬาลงกรณ์มหาวิทยาลัย

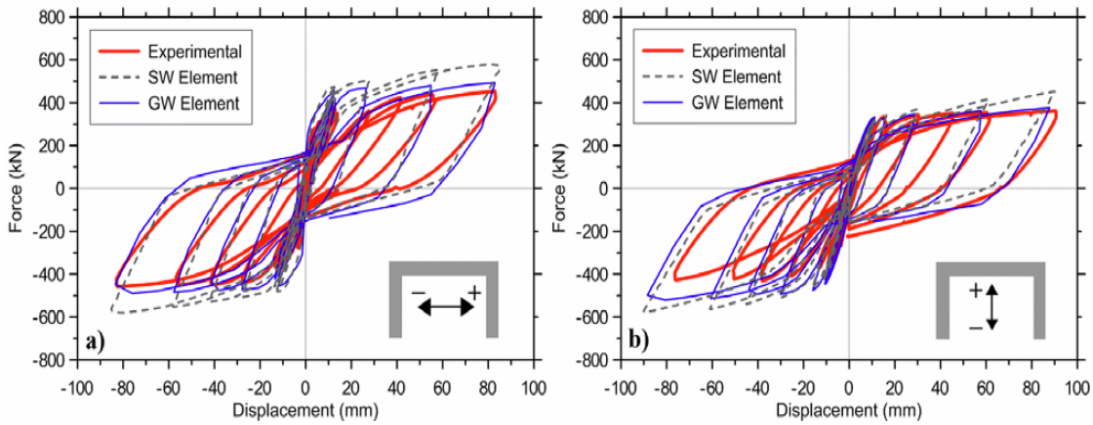

Figure 3.7 Comparison of load-deformation hysteresis loops from fiber model and experiment of U-shape RC wall: (a) E-W direction; and (b) N-S direction (Kolozvari et al. 2017).

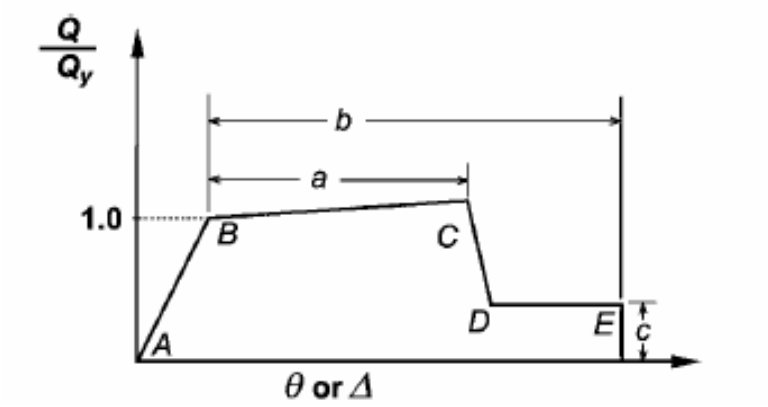

Figure 3.8 Tri-linear moment-hinge rotation back bone curve (ASCE 41-13).

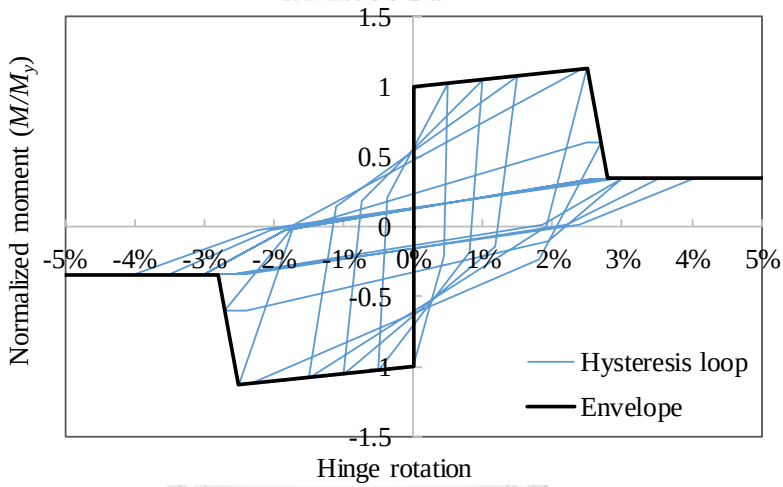

Figure 3.9 Hysteresis loop of moment-rotation relationship.

Table 3.4 Material cyclic degradation parameters (Kolozvari et al. 2017).

Cyclic Degradation Parameters	Unconfined Concrete	Confined Concrete	Steel D6 & D12
Deformation			
1	0.0014	0.0019	0.01
2	0.003	0.003	0.03
3	0.004	0.004	0.03
Energy Factor			
Y	0.001	0.001	1.00
1	0.001	0.001	0.75
2	0.001	0.001	0.75
3	0.001	0.001	0.75
X	0.001	0.001	0.75

3.3 Description of earthquake ground motions

Large-magnitude long-distance soft-soil ground motions in Bangkok (low seismicity) and moderate-magnitude short-distance stiff-soil ground motions in Chiang Mai (moderate seismicity) of Thailand were used. Ground motions having similar seismic mechanisms to Bangkok and Chiang Mai were selected from PEER ground motion database. The time history of earthquake ground accelerations can be found in Appendix B.

For the RSA and the proposed MRSA methods, uniform hazard spectrum (UHS) was used, while for NLRHA, consistent ground motions need to be used to ensure that the analysis results from different methods are compatible for comparison; hence, UHS spectral matching ground motions were used in NLRHA. It should be noted that ASCE 7 RSA procedure uses a design spectrum referring to design basic earthquake (DBE) having 10% probability of exceedance in 50 years, while NLRHA generally uses ground motions corresponding to maximum considered earthquake (MCE) having 2% probability of exceedance in 50 years to evaluate the performance of structures to prevent collapse. DBE is computed by multiplying MCE with a factor of 2/3. However, for the case of low seismicity in Bangkok, MCE was used for both RSA and NLRHA because the structures did not yield much under DBE. For the case of moderate seismicity in Chiang Mai, DBE was employed for all analyses.

จุฬาลงกรณ์มหาวิทยาลัย
CHULALONGKORN UNIVERSITY

3.3.1 Earthquake ground motions in Bangkok

For Bangkok site located on soft soil (site class F), due to its special tectonic setting and geological features, Bangkok faces a risk from distant large earthquakes, with the ground motions in Bangkok expected to be long-period, long-duration, and low-acceleration but large-displacement type motions. The UHS for Bangkok is significantly different from a typical code spectrum. The UHS at a hypothetical rock outcrop site in Bangkok was obtained from probabilistic seismic hazard analysis (PSHA) which was carried out by Ornthammarath et al. (2011). Six conditional mean spectrum (CMS) at the rock outcrop site for six periods of interest: 0.2, 0.5, 1, 1.5, 2, and 3 seconds were

determined using the procedure proposed by Baker (2011). It should be noted that for rock outcrop sites, a CMS matches the UHS only at its conditioning period and is lower than the UHS at other periods as shown in Figure 3.10. These rock outcrop CMSs were used as the target spectra to select appropriate rock outcrop ground motions to be used as inputs for site response analysis. Six sets of ground motions having similar seismic mechanisms as in Bangkok were selected from the PEER ground motion database as listed in Table 3.5. Each set comprises three pairs of ground motions. The first-three sets correspond to short conditioning period (0.2, 0.5, and 1 sec) ground motions from earthquakes having moderate magnitudes of 6.7 to 7.6 with epicentral distances of 80-186 km. The other three sets correspond to long conditioning period (1.5, 2, and 3 sec) ground motions from earthquakes of large magnitudes of 8.3 to 9, recorded at large epicentral distances of 550-1625 km. Since Bangkok is located on soft-soil layers, the selected ground motions for each of the six periods of interest were first scaled by amplitude scaling method to match the target CMS for rock outcrop site and then, simulated to propagate through soft-soil layers underlying downtown area of Bangkok by using SHAKE2000 software (Ordonez 2012). Detailed information of the development of design spectrum, ground motion selections, site response analysis, and soil properties used in this study can be found in Poovarodom et al. (2017) and Jirasakjamroonsri et al. (2018). The average spectra of input ground motions scaled to match each of the CMS at rock outcrop are shown in Figure 3.11 and an example of output ground motions at soft-soil surface from the site response analysis of input ground motions matching rock outcrop CMS conditioned at 2 sec is presented in Figure 3.12. The six sets of output ground motions were considered as CMS soft-soil ground motions. The average spectral acceleration of the six output ground motions in each set of period of interest represents UHS spectral ordinate at that period of interest, as CMS usually matches UHS at the period of interest. The UHS and six CMSs of soft-soil ground motions for 5% damping ratio are shown in Figure 3.13.

To obtain the UHS spectral matching ground motions to be used in NLRHA, CMS ground motions in the set for conditioning period of 3 sec (Figure 3.14) were modified by

SeismoMatch (SeismoSoft 2016) to have spectral shape fitted to the UHS. The individual matching spectra, the mean value of matching spectra, and the target spectrum (UHS) of soft-soil ground motions for 2.5% damping ratio are shown in Figure 3.15. For tall buildings, damping ratio of 2.5% recommended by PEER (2017) was used in this study.

Table 3.5 List of ground motions for six periods of interest: 0.2, 0.5, 1, 1.5, 2, and 3 sec.

T^* (sec)	Pair no.	Earthquake event	Year	Station	Magnitude M_w	Distance (km)
0.2	1	Kobe, Japan	1995	OKA	6.9	87
	2	Hector Mine	1999	Anza-Tripp Flats Training	7.1	102
	3	Northridge-01	1994	Rancho Cucamonga-Deer Canyon	6.7	80
0.5	1	Kocaeli, Turkey	1999	Tekirdag	7.5	165
	2	Hector Mine	1999	Anza-Tripp Flats Training	7.1	102
	3	Hector Mine	1999	Pacoima Kagel Canyon	7.1	186
1.0	1	Hector Mine	1999	Pacoima Kagel Canyon	7.1	186
	2	Chi-Chi, Taiwan	1999	TAP078	7.6	120
	3	Hector Mine	1999	Anza-Tripp Flats Training	7.1	102
1.5	1	Tokachi-oki	2003	YMT015	8.3	550
	2	Tohoku	2011	SIG007	9.0	689
	3	Tohoku	2011	HKD06	9.0	663
2.0	1	Tohoku	2011	HKD048	9.0	655
	2	Tohoku	2011	SIG007	9.0	689
	3	Tokachi-oki	2003	FKS02	8.3	550
3.0	1	Tohoku	2011	OSK004	9.0	747
	2	Tohoku	2011	HKD06	9.0	663
	3	W. Coast of Northern Sumatra	2004	PYAY	9.0	1625

จุฬาลงกรณ์มหาวิทยาลัย
CHULALONGKORN UNIVERSITY

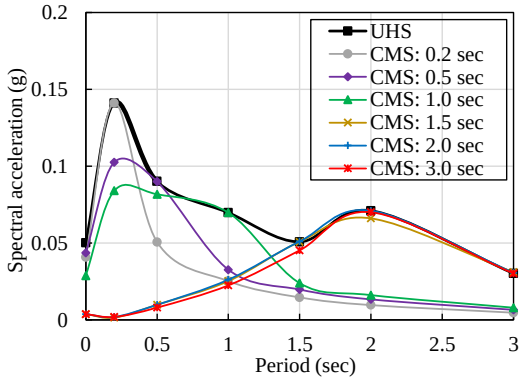

Figure 3.10 Uniform hazard spectrum (UHS) and conditional mean spectrum (CMS) conditioned at 0.2, 0.5, 1, 1.5, 2, and 3 sec at rock outcrop for 5% damping ratio.

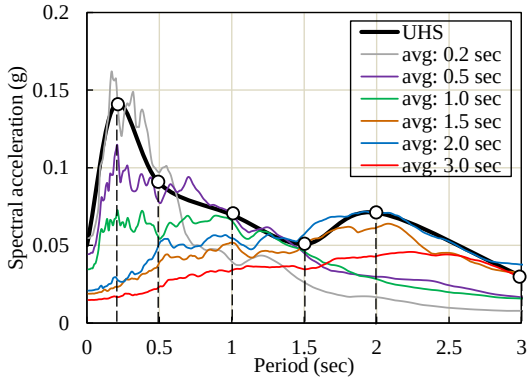

Figure 3.11 Uniform hazard spectrum (UHS) and average spectra of rock outcrop ground motions matching conditional mean spectrum (CMS) at rock outcrop for 5% damping ratio.

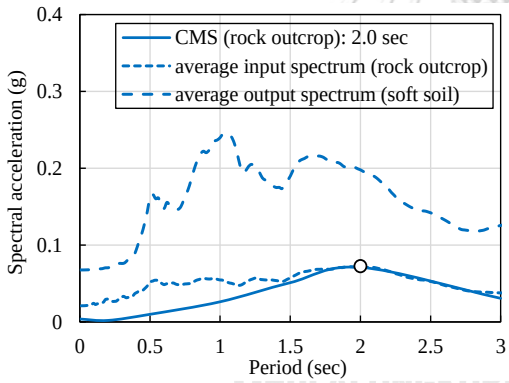

Figure 3.12 Conditional mean spectrum (CMS) at rock outcrop, average spectrum of input ground motions at rock outcrop, and average spectrum of output ground motion at soft-soil site for conditioning period of 2 sec.

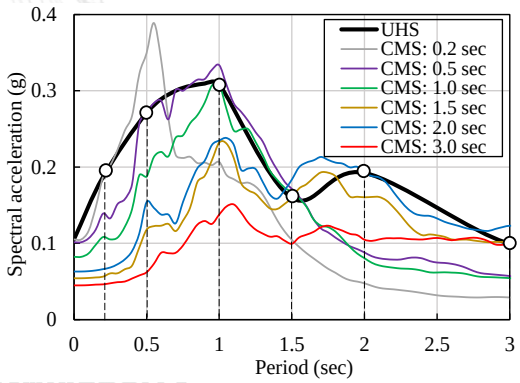

Figure 3.13 Uniform hazard spectrum (UHS) and average spectra of soft-soil ground motions considered as conditional mean spectrum (CMS) at soft-soil site for 5% damping ratio.

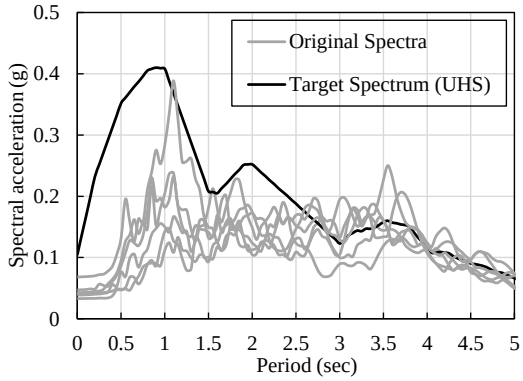

Figure 3.14 Original spectra of CMS ground motions conditioned at 3 sec and target spectrum of soft-soil ground motions for 2.5% damping ratio.

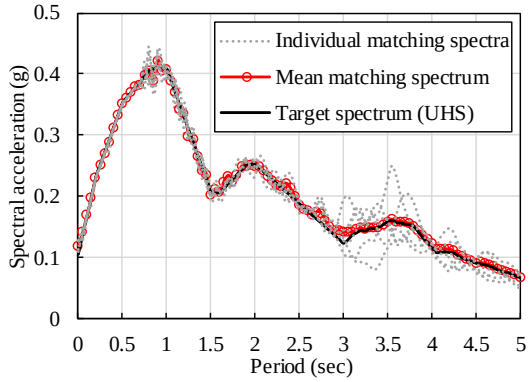

Figure 3.15 Individual matching spectra, mean matching spectrum, and target spectrum of soft-soil ground motions for 2.5% damping ratio.

3.3.2 Earthquake ground motions in Chiang Mai

For Chiang Mai site located on stiff soil (site class D), the UHS was developed using prescriptive code procedure in ASCE 7-10 with known spectral accelerations (S_s=0.878g and S_1=0.248g). It should be noted that design spectrum in ASCE 7 is for 5% damping ratio. To obtain spectrum with 2.5% damping ratio as recommended by PEER (2017) for tall buildings, the damping factor formula in ASCE 41-13 was adopted. Ten pairs of ground motions having seismic mechanism similar to Chiang Mai were selected from PEER ground motion database. The detailed information of these ground motions is shown in Table 3.6. The component with larger peak ground acceleration (PGA) was selected from each of the ten pairs to make a set of the ten ground motions, which were then modified by SeismoMatch (SeismoSoft 2016) to obtain a set of ten UHS spectral matching ground motions to be used in NLRHA. The individual and the mean of ten unscaled ground motions are shown in Figure 3.16. The individual matching spectra, the mean matching spectrum, and the target spectrum in Chiang Mai are shown in Figure 3.17.

Table 3.6 List of selected ten pairs of ground motions for Chiang Mai.

NGA no.	Earthquake	Year	Station	Magnitude M_w	Distance (km)	V_{s30} (m/s)
30	Parkfield	1966	Cholame-Shandon Array #5	6.19	9.6	290
95	Managua-Nicaragua-01	1972	Managua-ESSO	6.24	4.1	289
147	Coyote Lake	1979	Gilroy Array #2	5.74	9	271
148	Coyote Lake	1979	Gilroy Array #3	5.74	7.4	350
149	Coyote Lake	1979	Gilroy Array #4	5.74	5.7	222
159	Imperial Valley-06	1979	Agrarias	6.53	0.7	275
161	Imperial Valley-06	1979	Brawley Airport	6.53	10.4	209
162	Imperial Valley-06	1979	Calexico Fire Station	6.53	10.4	231
179	Imperial Valley-06	1979	El Centro Array #4	6.53	7	209
185	Imperial Valley-06	1979	Holtville Post Office	6.53	7.7	203

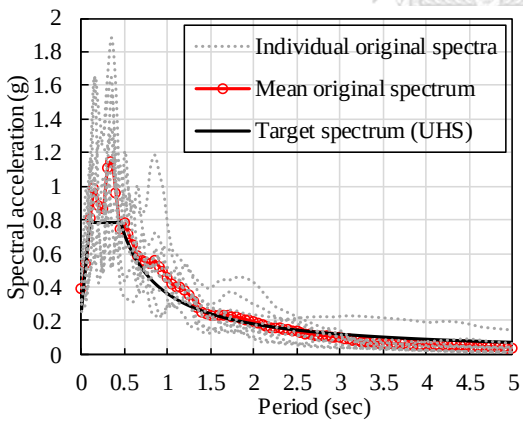

Figure 3.16 Individual original spectra, mean original spectrum, and target spectrum for 2.5% damping ratio in Chiang Mai

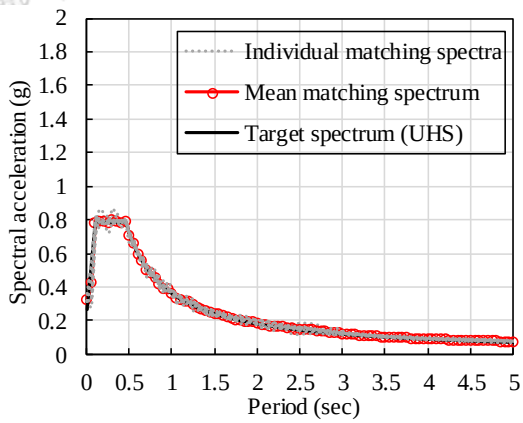

Figure 3.17 Individual matching spectra, mean matching spectrum, and target spectrum for 2.5% damping ratio in Chiang Mai.

3.4 Application of conditional mean spectrum in NLRHA

NLRHA is generally performed by using ground motion records that are selected and scaled to match a defined target spectrum. The most commonly used target spectrum is uniform hazard spectrum (UHS) and conditional mean spectrum (CMS) (Haselton et al. 2017). The UHS has the same probability of exceedance at all periods from consideration of many scenarios of earthquakes. The spectral shape of the UHS may not be resembled to that of a real ground motion. It is unlikely for one ground motion from the earthquake scenario contributing to the UHS at a period of interest to have as large spectral values as the UHS at all other periods (Bommer et al. 2000). Using the UHS as the target spectrum would be overly conservative to estimate responses to an earthquake scenario or develop a fragility function (Baker and Cornell 2006, Baker 2011, Koopaee et al. 2017, Sinković et al. 2018). On the other hand, CMS approach proposed by Baker (2011) is attractive as it can preserve more realistic spectral shape of earthquakes. The CMS will match the ordinate of the UHS only at the period of interest, T^*. However, the choice of the period of interest when using CMS with tall buildings is not definite as higher modes could be as important as the fundamental mode. Higher modes could be more dominant for some response parameters such as base shear force and mid-height overturning moment (Klemencic et al. 2007, Khy and Chintanapakdee 2017).

จุฬาลงกรณ์มหาวิทยาลัย
Chulalongkorn University

The main concerns when using CMS are that the results from an analysis using a single CMS vary with the choice of the conditioning period, and that it may underestimate response parameters significantly influenced by multiple vibration modes of the building (NIST 2011). To address these concerns, multiple sets of CMS has been suggested and adopted by several design guidelines and codes (CTBUH 2008, PEER 2010, ASCE 7-16). ASCE 7-16 (Method 2 in Chapter 16) suggests using two or more conditioning periods of vibration contributing significantly to the inelastic dynamic response of the building. According to the commentary of ASCE 7-16, the selected periods might include lengthened first-mode period, e.g., $1.5T_1$, period close to elastic first-mode period, and translational second-mode period of the building in the direction of analysis. More specifically for tall buildings, CTBUH (2008) recommends using three CMSs which in

aggregate can envelop the UHS over the period range from 0 to 1.5 times the fundamental period of the building, and the long-period CMS spectral ordinates shall not fall below the UHS in the period range from 1 to 1.5 times the fundamental period of the building. Similarly, PEER (2010) recommends using a minimum of three CMSs conditioned at the first-three translational periods of the building in each direction of analysis. When using CMS as the target spectrum for tall buildings, the numbers of analysis increase with a factor equal to the numbers of conditioning periods considered; hence, significant computational effort will be required. When using spectral matching ground motions and UHS as the target spectrum, only one set of analysis is required. The comparison of seismic demands of tall buildings situated on soft soil computed from NLRHA using CMS ground motions and UHS spectral matching ground motions has not yet been available.

This study aimed at investigating the application of CMS ground motions in NLRHA to estimate seismic demands for design of tall buildings located on soft soil. Seismic demands of tall buildings computed from NLRHA using CMS ground motions at multiple conditioning periods were compared to those computed from NLRHA using ground motions selected, scaled, and modified to match UHS at all periods. This study tried to confirm the acceptability of using only a single set of UHS spectral matching ground motions to compute design force and displacement demands instead of multiple sets of CMS ground motions corresponding to multiple conditioning periods.

จุฬาลงกรณ์มหาวิทยาลัย
Chulalongkorn University

Four existing tall buildings SWB1-SWB4 (Figure 3.1) with CMS ground motions in Bangkok (Figure 3.13) were used in this section. PERFORM-3D was used to conduct NLRHA. For each building, two different types of ground motions were used in NLRHA. The first type consists of three sets of CMS ground motions corresponding to conditioning periods closest to periods of the first-three translational modes of the building in the direction of excitation considered. For instance, CMS ground motions conditioned at the periods of 3, 1, and 0.5 sec were used for the 39-story building (SWB4) whose periods of the first-three translational modes in the X-direction are 4.85, 1.16, and 0.53 sec as shown in Figure 3.18. The second type is the set of six UHS spectral matching ground motions as shown in Figure 3.15. The ground motions were applied in each direction separately

for all analyses considered. Gravity load of all dead loads plus 25% of live loads were applied before NLRHA.

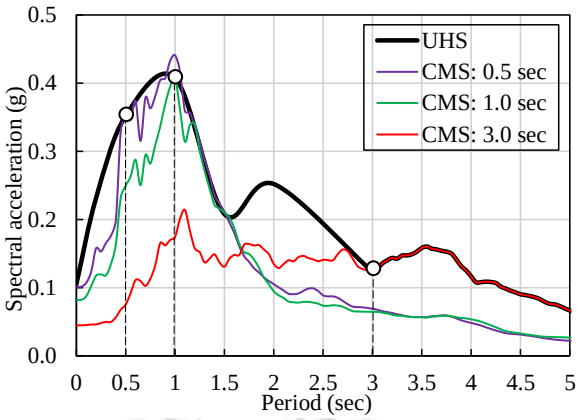

Figure 3.18 Conditional mean spectrum (CMS) conditioned at 0.5, 1, and 3 sec of soft-soil ground motions for 2.5% damping ratio used in NLRHA for the 39-story building (SWB4).

3.4.1 Seismic demands from NLRHA using CMS as target spectrum

The results presented were the mean values of peak responses considered: story shear force normalized by seismic weight of the building (V_{story}/W), story overturning moment (M_{story}), floor displacement, and story drift ratio. Responses to excitation in the X- and Y-directions of the building were presented.

The comparison of seismic demands computed from NLRHA using three sets of CMS ground motions conditioned at three different periods closest to the periods of the first-three translational modes of the building in X- and Y-directions is shown in Figures 3.19 and 3.20, respectively. It was found that the CMSs conditioned at short periods (CMS $(T^* \approx T_2)$ and CMS $(T^* \approx T_3)$) resulted in larger force demands than the CMS conditioned at long period (CMS $(T^* \approx T_1)$) for some locations along the height of the building. For instance, the CMSs conditioned at short periods caused significantly larger shear forces at the base region of the 15-story (SWB1) and 20-story (SWB2) buildings, and throughout the height of the 31-story (SWB3) and 39-story (SWB4) buildings as shown in Figures 3.19(a) and 3.20(a), and they caused larger overturning moments at the upper stories of the 31-story and 39-story buildings as shown in Figures 3.19(b) and 3.20(b), compared to the CMS conditioned at long period. This is because the base shear forces and mid-

height overturning moments in a tall building are significantly contributed from higher-mode responses (see Appendix C). Therefore, the design demand values should conservatively consider the envelope of force demands from NLRHA using CMS ground motions conditioned at multiple periods. This finding was consistent with the recommendations of the recent guidelines and standards (CTBUH 2008, PEER 2010, ASCE 7-16). For story drift ratios (Figures 3.19(c) and 3.20(c)) and floor displacements (Figures 3.19(d) and 3.20(d)), the CMS conditioned at the fundamental period was sufficient for conducting the evaluation as it provided larger results than the CMSs conditioned at higher-mode periods throughout the height of the building because floor displacements and story drift ratios are dominantly contributed by the first-mode response (see Appendix C).

3.4.2 Seismic demands from NLRHA using CMS and UHS as target spectrum

The comparison of seismic demands computed from NLRHA using CMS and UHS as target spectrum is shown in Figures 3.21 and 3.22 for seismic excitation in X- and Y-directions, respectively. The results from analysis using CMS as target spectrum refer to the envelope of results (Envelope CMS in Figures 3.21 and 3.22) from NLRHA using three sets of CMS ground motions as discussed in the preceding section. When using UHS as target spectrum, the computed results (UHS in Figures 3.21 and 3.22) are the mean values of peak response computed from NLRHA using six UHS spectral matching ground motions. It was found that using UHS spectral matching ground motions provided very similar seismic demands for most cases and slightly larger floor displacements and story drift ratios for Y-direction of the 20-story (SWB2) building (Figures 3.22(c) and 3.22(d)), compared to the envelope of results from NLRHA using CMS conditioned at multiple periods. Therefore, using UHS as target spectrum to select and scale ground motions together with spectral-matching modification can take care of the enveloping task required when using CMS; hence, it can significantly reduce the computational effort because only one set of analysis is required as opposed to three sets of analysis required when using CMS as target spectrum. This finding was different from the results of Kwong and Chopra (2017) who conducted a study on a 20-story RC frame building located on

จุฬาลงกรณ์มหาวิทยาลัย
Chulalongkorn University

stiff soil, and reported that using UHS as the target spectrum to select and scale earthquake records to be used in intensity-based assessment of a building provided over-conservative estimates for computing seismic design demands. This difference could be due to many reasons as many parameters in the present study and their study were not the same. For instance, (1) the UHS in their study was generally larger than CMS at most periods, except at the conditioning periods where UHS and CMS values were equal; (2) when using UHS, ground motions in their study were scaled to match UHS at the fundamental period, whereas ground motions in the present study were scaled and modified to match UHS at all periods; and (3) the lateral force resisting system and site class were different. A future study using the same conditions and parameters is recommended to clarify inconsistency between the two studies.

จุฬาลงกรณ์มหาวิทยาลัย
CHULALONGKORN UNIVERSITY

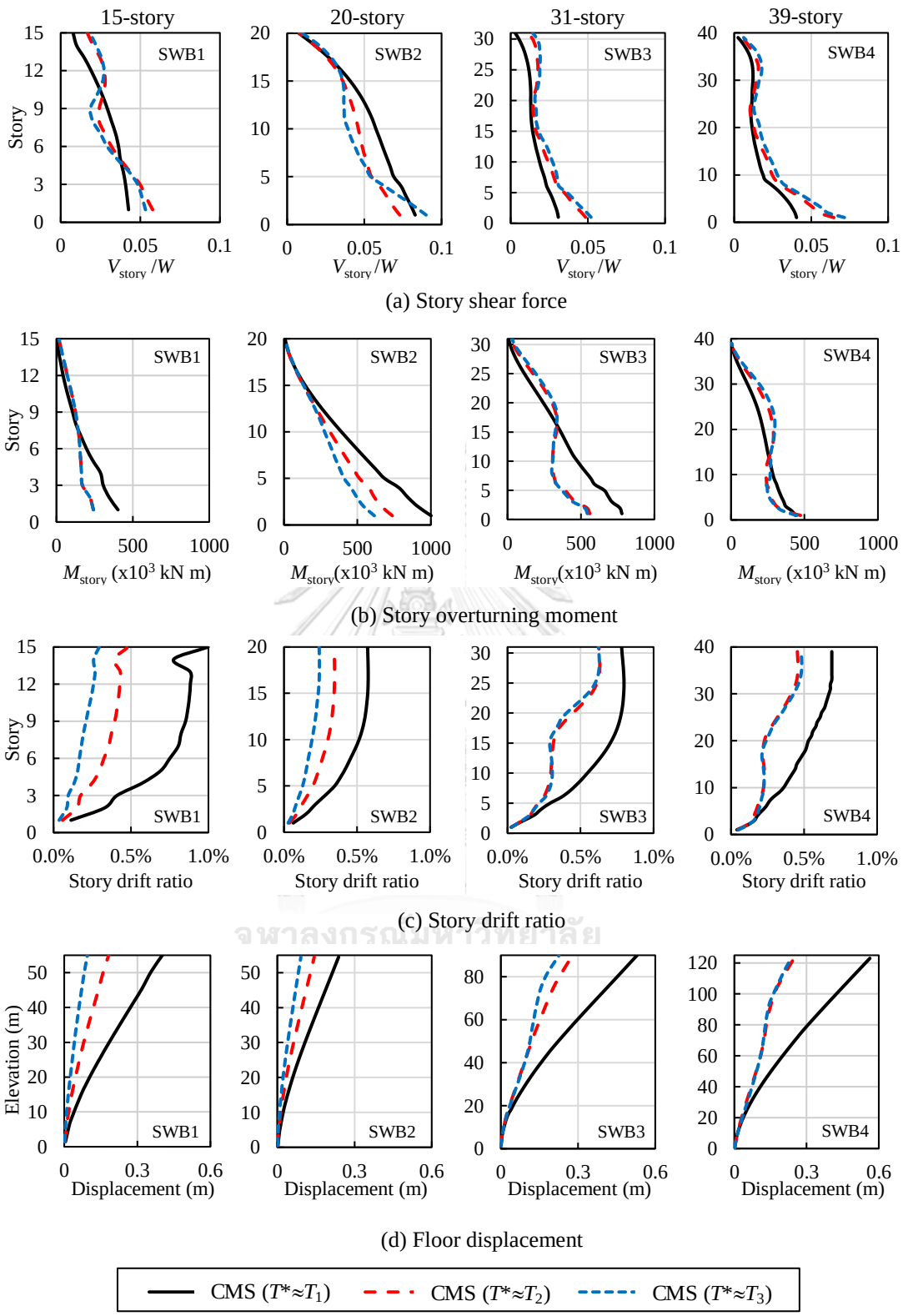

Figure 3.19 (a) Story shear force; (b) story overturning moment; (c) story drift ratio; and (d) floor displacement computed from NLRHA for X-direction seismic excitation using three sets of CMS ground motions.

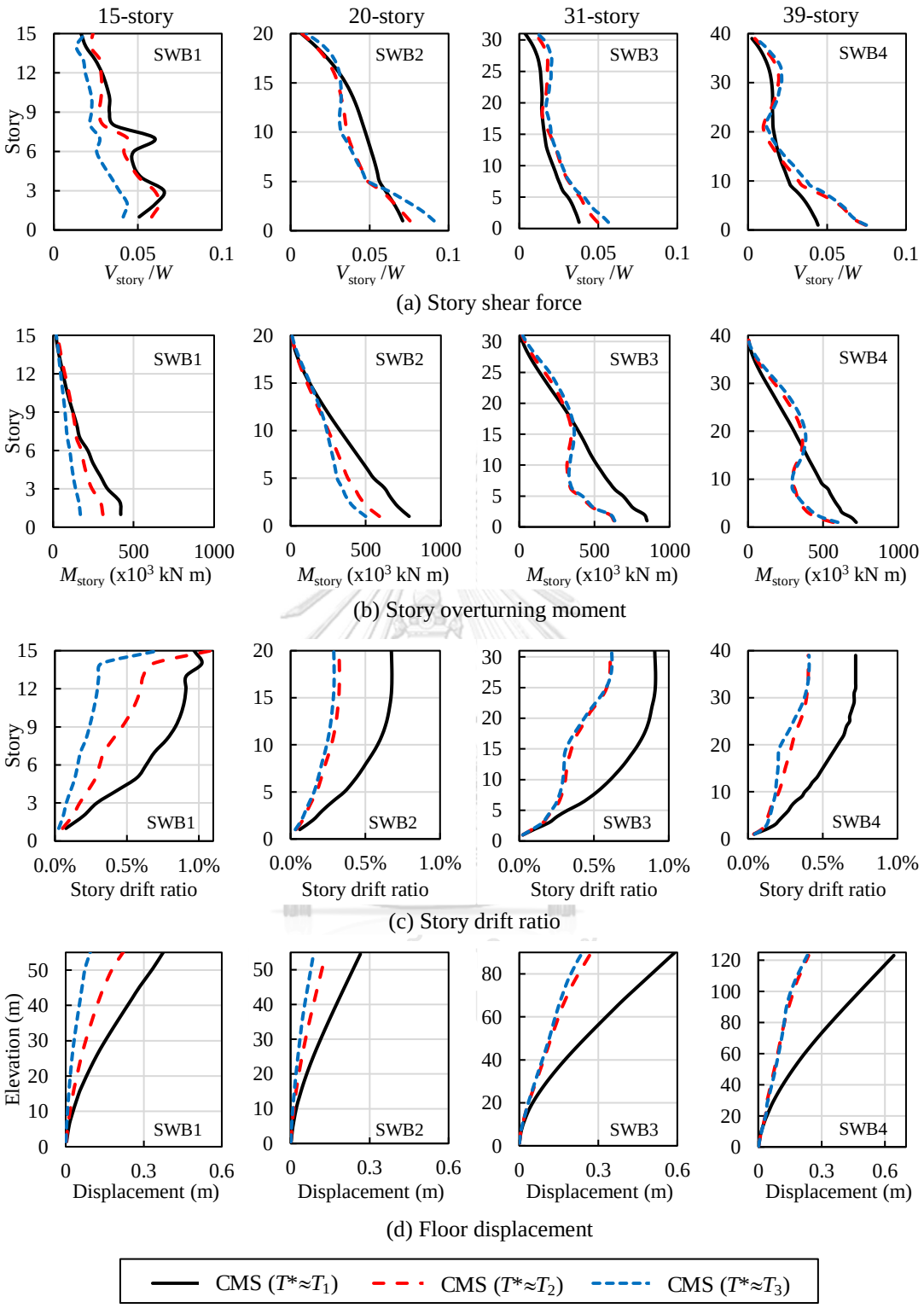

Figure 3.20 (a) Story shear force; (b) story overturning moment; (c) story drift ratio; and (d) floor displacement computed from NLRHA for Y-direction seismic excitation using three sets of CMS ground motions.

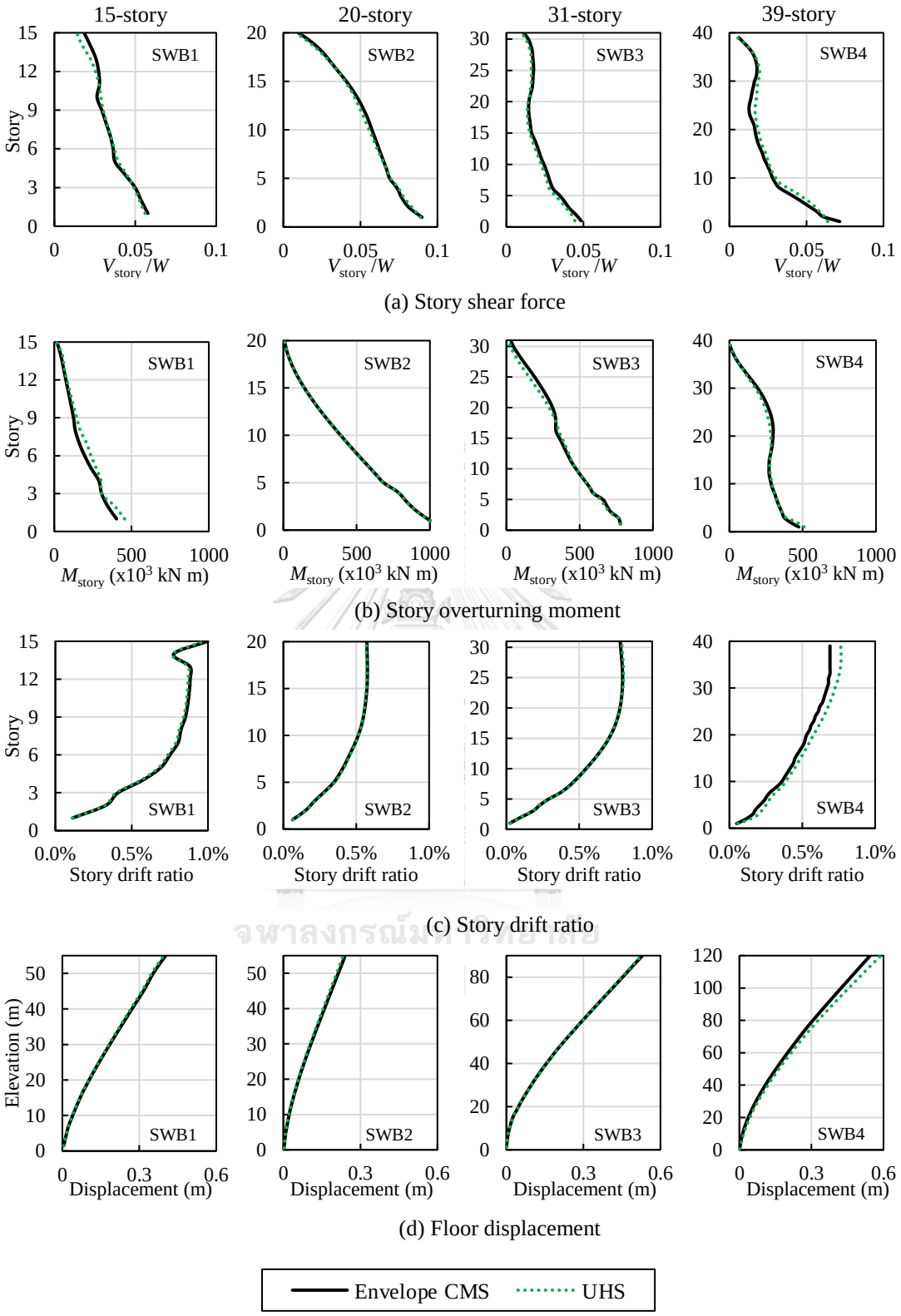

Figure 3.21 (a) Story shear force; (b) story overturning moment; (c) story drift ratio; and (d) floor displacement computed from NLRHA for X-direction seismic excitation using CMS and UHS as the target spectrum.

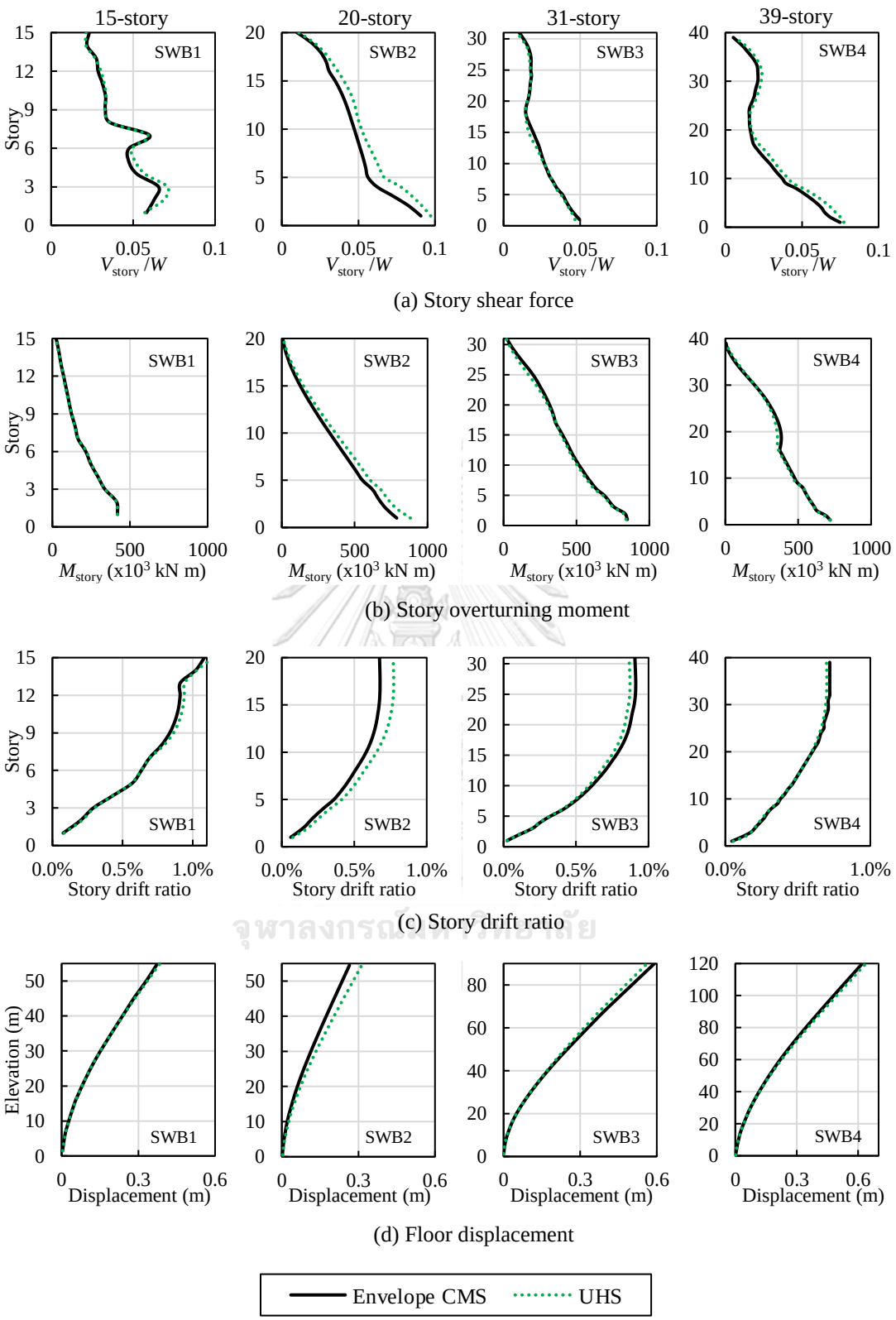

Figure 3.22 (a) Story shear force; (b) story overturning moment; (c) story drift ratio; and (d) floor displacement computed from NLRHA for Y-direction seismic excitation using CMS and UHS as the target spectrum.

3.4.3 Summary

The main findings are summarized as the followings:

(1) When using CMS as target spectrum for tall buildings, higher-mode periods should also be considered for response parameters dominated by higher modes such as base shear forces and mid-height overturning moments. Enveloping of force demands computed from NLRHA using CMS ground motions conditioned at multiple periods should be undertaken before used as design demand values.

(2) For response quantities dominated by the fundamental mode such as floor displacements and story drift ratios, CMS ground motions conditioned at the fundamental period are sufficient to be used in the analysis.

(3) Using UHS spectral matching ground motions can avoid enveloping of results and significantly reduce the computational effort as required when using multiple sets of CMS ground motions conditioned at multiple periods.

จุฬาลงกรณ์มหาวิทยาลัย
CHULALONGKORN UNIVERSITY

CHAPTER 4
MODIFIED RESPONSE SPECTRUM ANALYSIS FOR DESIGN OF TALL RC SHEAR-WALL BUILDINGS

4.1 Introduction

This chapter first evaluated the accuracy of the RSA procedure in ASCE 7-10. The inelasticity of response in each mode was investigated using modal pushover analysis (MPA). Then, two MRSA methods to compute shear forces together with a method to compute strains in RC walls and columns to identify the locations that require ductile detailing were developed. Here, six tall RC shear-wall buildings (Figure 3.1) in Section 3.1.1 and earthquake ground motions in Bangkok and Chiang Mai in Section 3.3 were employed. NLRHA was conducted to obtain benchmark results which were used to evaluate the accuracy of the RSA and the proposed MRSA procedures. The ground motions were applied separately in each principle direction of the building at a time for all analysis methods and vertical earthquake was not considered.

4.2 Response spectrum analysis

The RSA procedure in ASCE 7-10 was adopted in this study. A linear analytical model described in Section 3.2.1 was used. A constant modal damping ratio of 2.5% was used, which is different from the ASCE 7 RSA procedure that uses a design spectrum with a 5% damping ratio. However, a damping ratio of 2.5% is recommended for tall buildings by PEER (2017). The design spectral accelerations for 2.5% damping ratio in Bangkok and Chiang Mai used in the RSA procedure are shown in Figures 3.15 and 3.17, respectively.

In RSA procedure, the elastic response computed from many vibration modes is combined to get the total elastic response, which is then reduced by a response modification factor (*R*) to compute the design forces of structures. The first-four translational modes of the tall buildings in the direction of excitation considered in this study constituted around 90% of the total participating mass. According to ASCE 7-10, it is required that the modal base shear determined from the RSA procedure is at least equal

to 85% of the base shear computed from the equivalent lateral force (ELF) procedure. For story drifts, ASCE 7-10 employs a deflection amplification factor (C_d) to scale up the results computed from the RSA procedure. The design bending moment (M), shear force (V), floor displacement (δ), and story drift (Δ) in the RSA procedure are computed from

$$M = \frac{SF \times I}{R}\sqrt{M_{1e}{}^2 + M_{2e}{}^2 + M_{3e}{}^2 + \cdots} \tag{4.1}$$

$$V = \frac{SF \times I}{R}\sqrt{V_{1e}{}^2 + V_{2e}{}^2 + V_{3e}{}^2 + \cdots} \tag{4.2}$$

$$\delta = \frac{C_d}{R}\sqrt{\delta_{1e}{}^2 + \delta_{2e}{}^2 + \delta_{3e}{}^2 + \cdots} \tag{4.3}$$

$$\Delta = \frac{C_d}{R}\sqrt{\Delta_{1e}{}^2 + \Delta_{2e}{}^2 + \Delta_{3e}{}^2 + \cdots} \tag{4.4}$$

where M_{ie}, V_{ie}, δ_{ie}, and Δ_{ie} are the elastic bending moment, shear force, floor displacement, and story drift of mode i, respectively; I is the importance factor taken equal to 1 in this study; and SF is the scaling factor required to ensure the RSA modal base shear (V_t) is at least equal to 85% of the ELF base shear (V_s) and is computed by Eq. (4.5) and is not less than 1.

$$SF = 0.85V_s / V_t \tag{4.5}$$

The RSA modal base shear is computed from

$$V_t = \frac{I}{R}\sqrt{V_{1b}{}^2 + V_{2b}{}^2 + V_{3b}{}^2 + \cdots} \tag{4.6}$$

where V_{ib} is the base shear force of mode i.

The ELF base shear according to Thailand seismic design standard (DPT 1301/1302-61, 2018) was adopted and is computed from

$$V_s = C_s W \tag{4.7}$$

where W is the seismic weight of the building and C_s is the seismic response coefficient computed by (4.8) and is not less than 0.01.

$$C_s = S_a \frac{I}{R} \tag{4.8}$$

where S_a is the spectral acceleration at the fundamental period used in ELF procedure which is computed from

$$T = \min(C_u T_a, T_{1,\text{eigen}}) \tag{4.9}$$

$$T_a = 0.02H \tag{4.10}$$

where T_a is the approximated period from DPT 1301/1302-61; H is the total height of the building; C_u is the coefficient of upper limit period equal to 1.5; $T_{1,\text{eigen}}$ is the fundamental period computed from eigenvalue analysis.

The scaling requirement in ASCE 7 results in an effective response modification factor (R_{eff}) which is the ratio of elastic base shear to design base shear. The R_{eff} factor is computed from

$$R_{eff} = \frac{R}{SF \times I} \tag{4.11}$$

The RSA modal base shears, ELF base shears, effective response modification factors, and scaling factors for each building are summarized in Tables 4.1 and 4.2 for case studies in Bangkok and Chiang Mai, respectively. The scaling factors varied generally from 1.1 to 1.7 and 1.0 to 1.6 for case studies in Bangkok and Chiang Mai, respectively, which depends on the structural modal properties and the characteristic of the design spectrum. It should be noted that the ELF considers only the fundamental mode, while the RSA takes into account for higher mode contributions. However, the ELF uses total mass participation, but the mass participation used in the RSA is in average 55% for the first mode, 20% for the second mode, 10% for the third mode, and 5% for the fourth mode as shown in Table 4.3. The fundamental period used in the ELF was much smaller than the first-mode period used in the RSA and the design spectral acceleration in the ELF was generally larger than that used in the RSA for all buildings as shown in Tables 4.4 and 4.5 for X- and Y-directions, respectively.

The detail modal contribution of each linear response for each building can be found in Appendix C. The linear RSA and linear response history analysis (RHA) were compared in Appendix C to see the bias error of modal SRSS combination rule used in RSA procedure. It was found that linear RSA using SRSS combination rule generally provides results similar to linear RHA.

Table 4.1 Scaling factors for tall RC shear-wall buildings in Bangkok.

Building	X-direction				Y-direction			
	$0.85V_s/W$	V_t/W	SF	R_{eff}	$0.85V_s/W$	V_t/W	SF	R_{eff}
SWB1	0.036	0.022	1.66	3.01	0.036	0.026	1.37	3.65
SWB2	0.046	0.030	1.50	3.33	0.035	0.025	1.38	3.61
SWB3	0.027	0.015	1.78	2.81	0.027	0.021	1.30	3.83
SWB4	0.026	0.017	1.57	3.19	0.026	0.018	1.42	3.53
SWB5	0.041	0.033	1.23	4.05	0.041	0.029	1.41	3.56
SWB6	0.026	0.023	1.11	4.50	0.026	0.024	1.08	4.62

Table 4.2 Scaling factors for tall RC shear-wall buildings in Chiang Mai.

Building	X-direction				Y-direction			
	$0.85V_s/W$	V_t/W	SF	R_{eff}	$0.85V_s/W$	V_t/W	SF	R_{eff}
SWB1	0.037	0.023	1.66	3.02	0.037	0.029	1.29	3.86
SWB2	0.046	0.042	1.09	4.59	0.041	0.042	1.00	5.00
SWB3	0.030	0.019	1.58	3.16	0.030	0.027	1.11	4.50
SWB4	0.030	0.023	1.29	3.88	0.030	0.022	1.33	3.76
SWB5	0.034	0.043	1.00	5.00	0.034	0.036	1.00	5.00
SWB6	0.030	0.035	1.00	5.00	0.030	0.039	1.00	5.00

จุฬาลงกรณ์มหาวิทยาลัย
CHULALONGKORN UNIVERSITY

Table 4.3 Modal mass participating ratio of the first-four translational modes used in RSA for tall RC shear-wall buildings.

Building	X-direction				Y-direction			
	Mode 1	Mode 2	Mode 3	Mode 4	Mode 1	Mode 2	Mode 3	Mode 4
SWB1	64%	17%	8%	4%	67%	17%	6%	4%
SWB2	56%	20%	10%	5%	55%	21%	10%	5%
SWB3	58%	17%	9%	4%	57%	19%	8%	4%
SWB4	53%	19%	12%	6%	51%	22%	11%	5%
SWB5	56%	27%	7%	3%	56%	26%	6%	3%
SWB6	35%	21%	22%	7%	34%	23%	22%	7%

Table 4.4 Spectral accelerations at fundamental periods used in ELF and RSA for X-direction of tall RC shear-wall buildings.

Building	T_1 (sec)		S_a (T_1) (Bangkok)		S_a (T_1) (Chiang Mai)	
	ELF	RSA	ELF	RSA	ELF	RSA
SWB1	1.66	2.97	0.21	0.13	0.22	0.12
SWB2	1.38	1.38	0.27	0.27	0.27	0.27
SWB3	2.70	4.55	0.16	0.09	0.14	0.08
SWB4	3.77	4.85	0.15	0.08	0.10	0.08
SWB5	1.88	2.06	0.24	0.25	0.20	0.18
SWB6	3.77	4.40	0.15	0.10	0.10	0.08

จุฬาลงกรณ์มหาวิทยาลัย
Chulalongkorn University

Table 4.5 Spectral accelerations at fundamental periods used in ELF and RSA for Y-direction of tall RC shear-wall buildings.

Building	T_1 (sec)		S_a (T_1) (Bangkok)		S_a (T_1) (Chiang Mai)	
	ELF	RSA	ELF	RSA	ELF	RSA
SWB1	1.66	2.39	0.21	0.21	0.22	0.16
SWB2	1.58	1.58	0.21	0.21	0.24	0.24
SWB3	2.70	3.05	0.16	0.12	0.14	0.12
SWB4	3.77	5.31	0.15	0.07	0.10	0.07
SWB5	1.88	2.12	0.24	0.24	0.20	0.17
SWB6	3.77	4.79	0.15	0.08	0.10	0.08

4.3 Nonlinear response history analysis

NLRHA was conducted using PERFORM-3D (CSI 2011). A nonlinear analytical model was created as described in Section 3.2.2. NLRHA was carried out using average-acceleration Newmark's method to numerically solve the governing equations (Eq. (2.13)) of motion for inelastic system as demonstrated in Section 2.1.2. The size of time step used in the analysis was taken equal to the time interval of each earthquake record generally varying from 0.005 to 0.01 sec. Gravity loads of all deal loads plus 25% of live loads were applied before NLRHA. For Bangkok, six UHS spectral matching ground motions (Figure 3.15) were used, while for Chiang Mai, ten UHS spectral matching ground motions (Figure 3.17) were employed.

For NLRHA, the modal viscous damping model recommended by Chopra and McKenna (2016) was adopted because the Rayleigh damping model based on initial stiffness could cause spurious damping forces, resulting in unbalanced moments at beam-column joints. A constant damping ratio of 2.49% was assigned to all significant modes of the initial elastic structure. Since the modes that were not included in the modal damping formulation would be undamped, PERFORM-3D recommends that Rayleigh damping with a small damping ratio is also included, to make sure that all modes have

some damping. Hence, Rayleigh damping with a specified damping ratio of 0.01% for the first and third translational modes of the building in the direction of seismic excitation was used. It is normal practice to specify damping ratios for the first and third modes to result in similar damping ratios in the first few significant modes.

4.4 Design demands by RSA and NLRHA

The structural response of the buildings was presented in terms of the mean values of peak normalized floor displacement, peak story drift ratio, peak normalized story shear force, and peak normalized story overturning moment. The peak floor displacement δ_i is normalized by the building total height H, the peak story drift Δ_i is normalized by story height h_i, the peak story shear force V_i is normalized by the seismic weight W, and the peak story overturning moment M_i is normalized by WH. The responses were presented in both X- and Y-directions.

Results from linear RSA (without R and C_d) computed using cracked ($LRSA_{cracked}$) and uncracked ($LRSA_{uncracked}$) section properties of structural members were also presented. Note that results from RSA procedure were computed using $LRSA_{cracked}$ results. The results from $LRSA_{uncracked}$ were not used in design and were computed using gross stiffness of linear elastic structural model having the same stiffness as the initial stiffness of nonlinear structural model used in NLRHA. $LRSA_{uncracked}$ was included to approximately reflect the level of nonlinearity occurred in structures by comparing force demands from NLRHA and $LRSA_{uncracked}$, and this cannot be confirmed by $LRSA_{cracked}$ because it has smaller stiffness than that used in NLRHA at linear elastic behavior. It should be remarked that LRSA cannot be used to accurately estimate the level of nonlinearity in structures because error can be from the use of modal combination rule such as SRSS. However, this error was found to be minor as results from LRSA and linear response history analysis (LRHA) were found to be similar for these studied buildings (see Appendix C).

Results from $LRSA_{uncracked}$, $LRSA_{cracked}$, and RSA are compared with mean values of peak demands from NLRHA as shown in Figures 4.1 to 4.4. For floor displacements and story drift ratios, it was found that $LRSA_{cracked}$ provided similar results while

$LRSA_{uncracked}$ generally underestimated results, when compared with NLRHA for most studied buildings. For force demands, $LRSA_{uncracked}$ generally provided larger results than $LRSA_{cracked}$, and NLRHA resulted in the lowest demands because structures experienced inelasticity. The ratios between NLRHA and RSA results in terms of base overturning moment, base shear force, and roof displacement are shown in Figures 4.5 and 4.6 for buildings in Bangkok and Chiang Mai, respectively. It was found that floor displacements and story drift ratios from RSA ($LRSA_{cracked}$ x C_d/R where C_d=4.5; R=5) and NLRHA were similar. The ratios of roof displacement were about 0.9 to 1.1 for most studied buildings. The story shear forces and story overturning moments computed from RSA ($LRSA_{cracked}/R_{eff}$ where R_{eff} is shown in Tables 4.1 and 4.2 for buildings in Bangkok and Chiang Mai, respectively) were significantly lower than those computed from NLRHA for all case studied buildings. The ratios of base overturning moment were about 1.8 to 2.5 and 2.3 to 3.5 for buildings in Bangkok (Figure 4.5) and Chiang Mai (Figure 4.6), respectively. The ratios of base shear force were about 2.2 to 3.5 and 3 to 4.3 for buildings in Bangkok and Chiang Mai, respectively. The underestimation of force demands computed from RSA could be mainly due to the use of a single R factor to reduce the force response of all modes, which was also observed by previous studies (Priestley 2003, Calugaru and Panagiotou 2012, Munir and Warnitchai 2012, Najam and Warnitchai 2018).

However, the structural members are normally designed to experience ductile flexural yielding. Bending moment computed from NLRHA cannot be larger than the actual flexural strength, but it can exceed the design flexural strength which is larger than the design bending moment computed from RSA due to the factor of safety used during the design. Here, actual strength refers to nominal strength that considers material over-strength as explained in Section 3.2.2; nominal strength is computed using nominal material strength; and design strength is nominal strength multiplied by the strength reduction factor (ϕ) according to ACI 318M-14. In the example shown in Figure 4.7a, axial force and bending moment response history at the base of a core wall in the building SWB4 computed from NLRHA varied inside the actual P-M interaction curve and slightly exceeded the design P-M interaction curve. For this core wall, minimum vertical

reinforcement criterion governed the design, as flexural strength associated with this minimum reinforcement was about two times larger than RSA design demand at the base of the wall (Figure 4.7a). The actual flexural strengths according to the minimum reinforcement were larger than the bending moments computed from NLRHA along the height of the wall as shown in Figure 4.7b.

Unlike bending moment, shear action has brittle failure mode and shear behavior of structural members is preferably designed to remain elastic. In this nonlinear structural analysis, shear capacity was assumed to be large enough that shear failure did not occur. But the shear force demand from NLRHA will be compared against the shear strength that would be provided if it were designed by RSA procedure. As minimum shear reinforcement governed the design of a core wall in the building SWB4, the design shear strength was larger than the RSA shear demand, but it was still considerably smaller than the shear demand computed from NLRHA at the first few stories as seen in Figure 4.7c, which can cause shear failure in structural walls. It should be noted that the concrete shear capacity of the wall presented in Figure 4.7c was computed using the simplified equation in Table 11.5.4.6 of ACI 318M-14 which ignores the contribution from axial load, shear force, and bending moment. The underestimation in computing shear force in the walls using RSA procedure is the main problem that this study attempts to address to avoid shear failure in the walls.

จุฬาลงกรณ์มหาวิทยาลัย
CHULALONGKORN UNIVERSITY

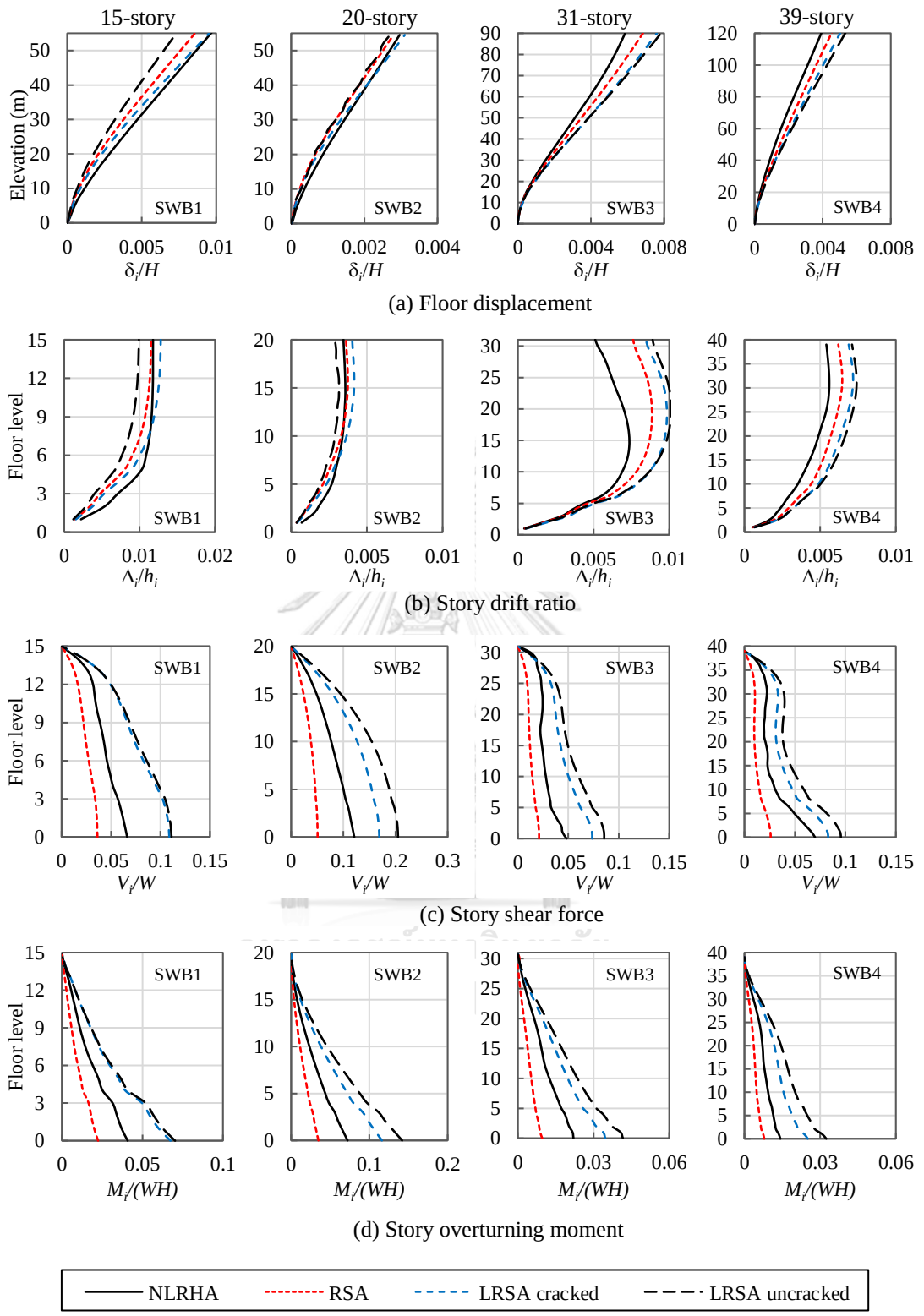

Figure 4.1 Seismic demands from RSA, $LRSA_{cracked}$, $LRSA_{uncracked}$ and NLRHA due to seismic excitation in X-direction for case studies in Bangkok: (a) floor displacement; (b) story drift ratio; (c) story shear force; and (d) story overturning moment.

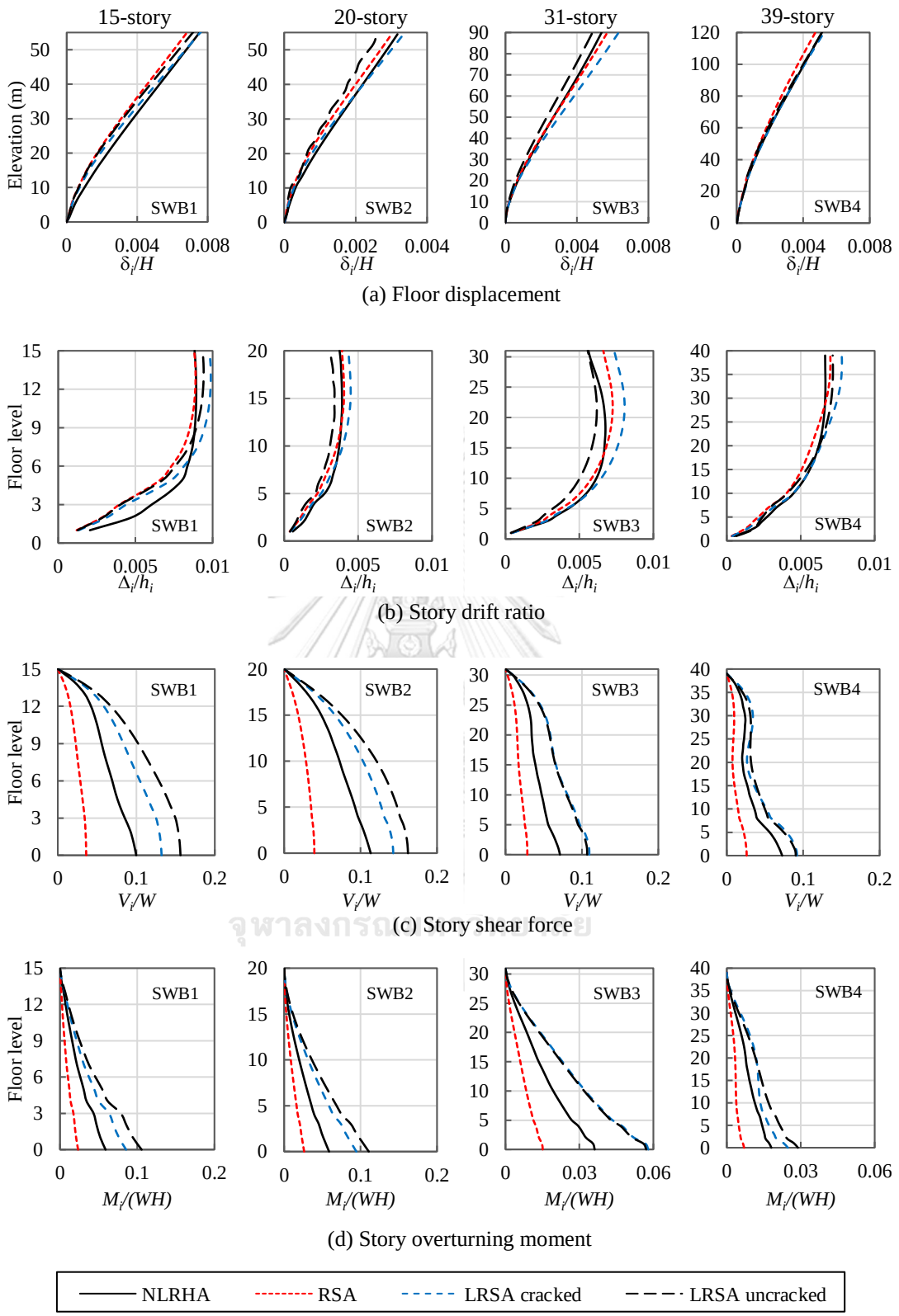

Figure 4.2 Seismic demands from RSA, $LRSA_{cracked}$, $LRSA_{uncracked}$, and NLRHA due to seismic excitation in Y-direction for case studies in Bangkok: (a) floor displacement; (b) story drift ratio; (c) story shear force; and (d) story overturning moment.

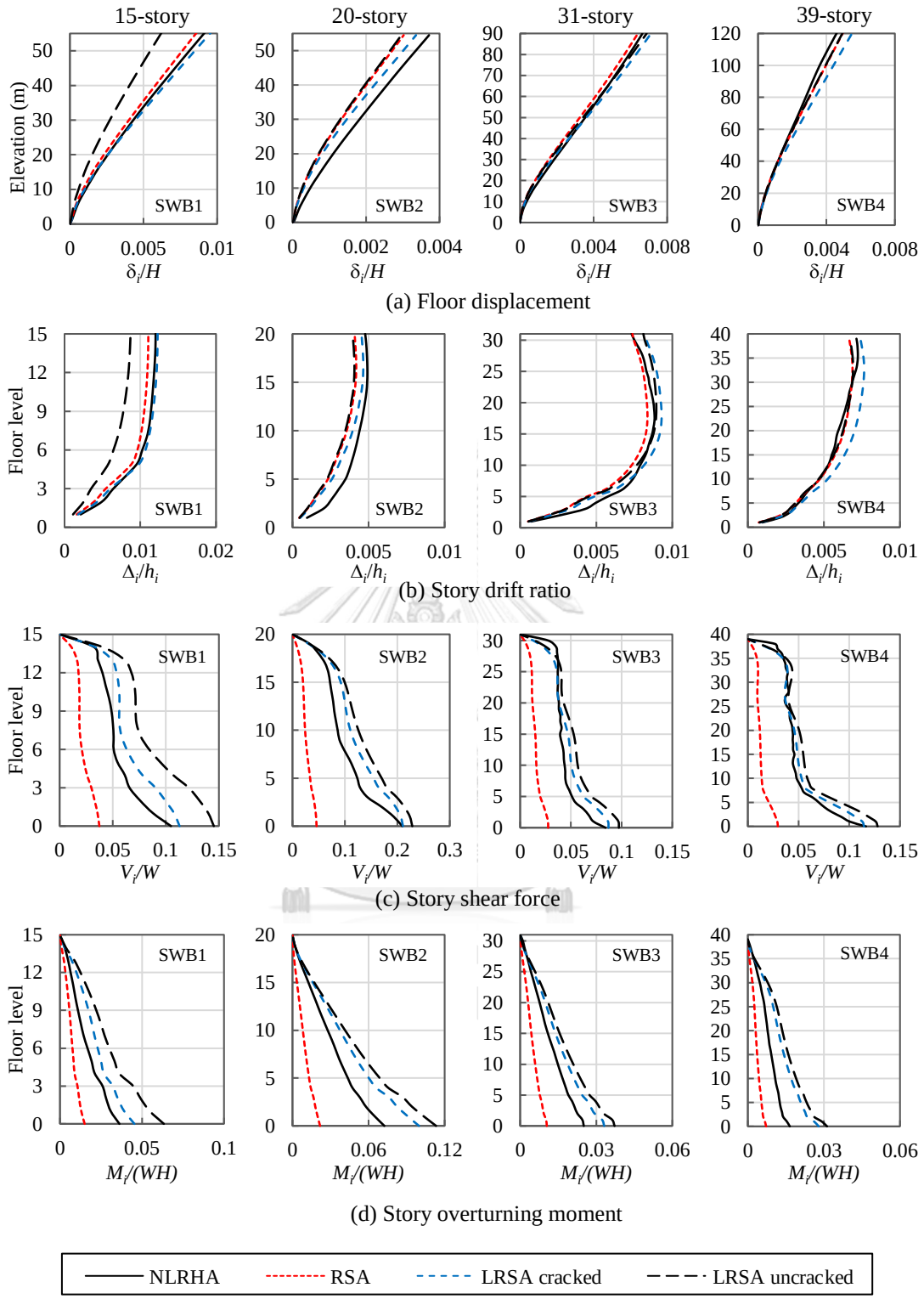

Figure 4.3 Seismic demands from RSA, $LRSA_{cracked}$, $LRSA_{uncracked}$, and NLRHA due to seismic excitation in X-direction for case studies in Chiang Mai: (a) floor displacement; (b) story drift ratio; (c) story shear force; and (d) story overturning moment.

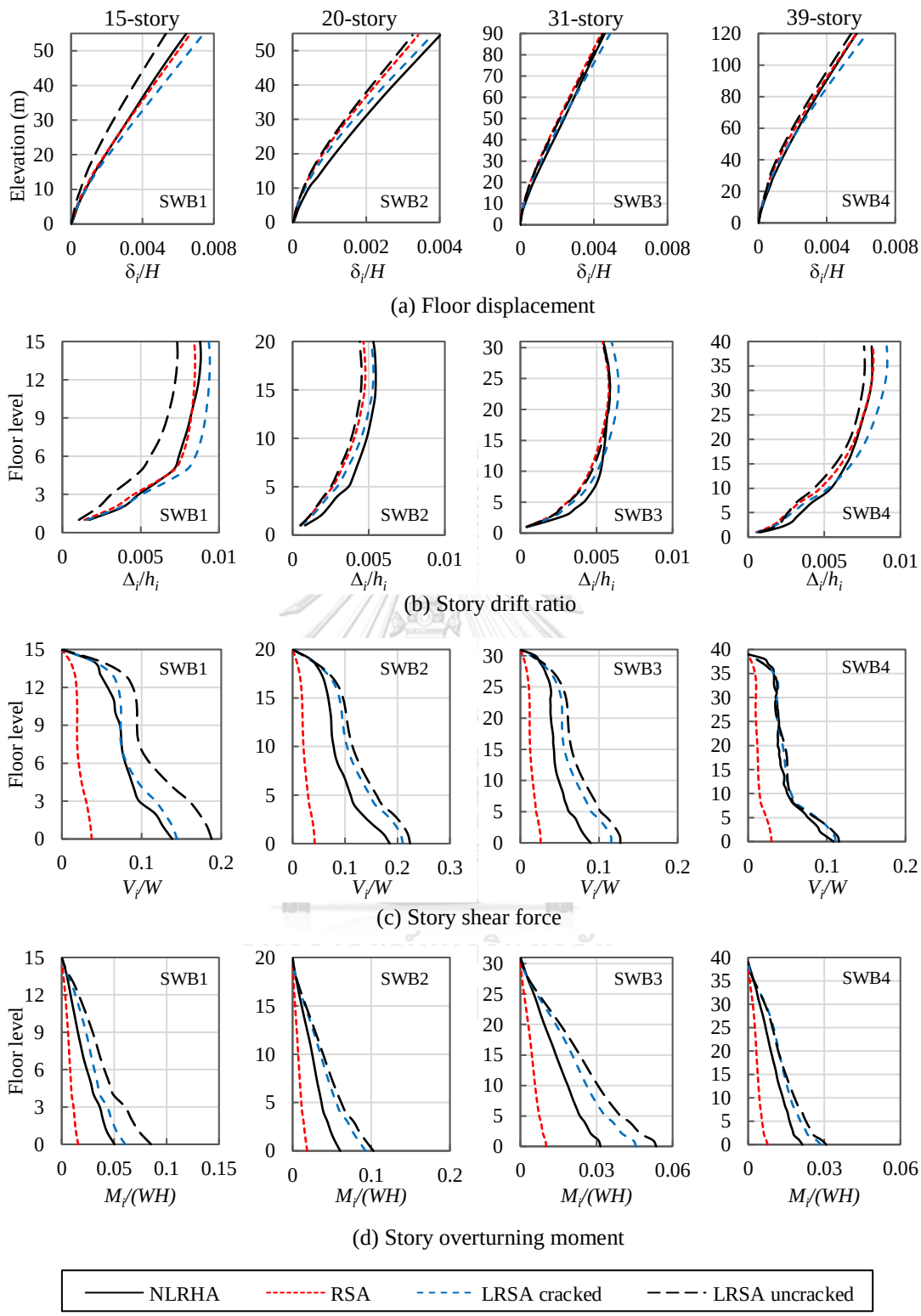

Figure 4.4 Seismic demands from RSA, $LRSA_{cracked}$, $LRSA_{uncracked}$, and NLRHA due to seismic excitation in Y-direction for case studies in Chiang Mai: (a) floor displacement; (b) story drift ratio; (c) story shear force; and (d) story overturning moment.

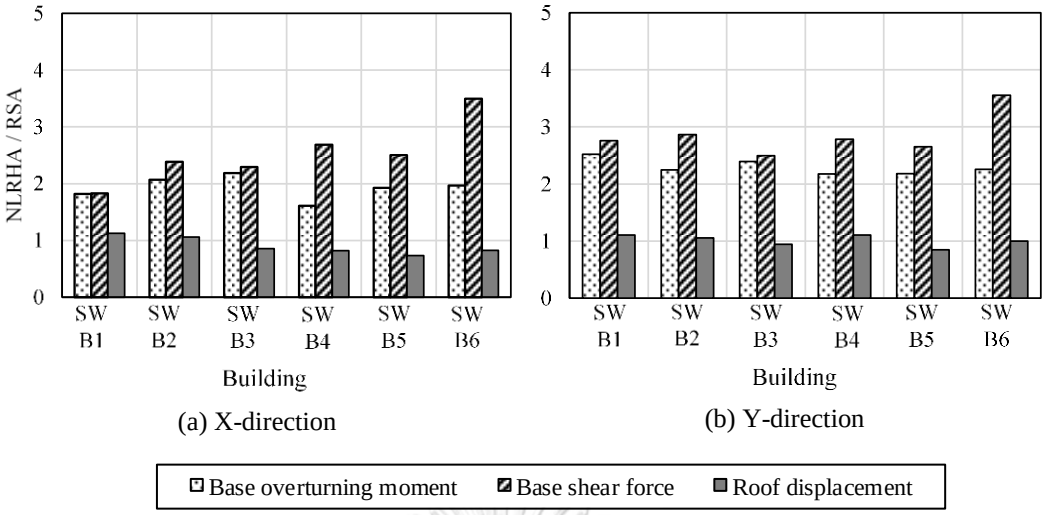

Figure 4.5 Ratios between NLRHA and RSA results: base overturning moment, base shear force, and roof displacement for buildings in Bangkok: (a) X-direction; (b) Y-direction.

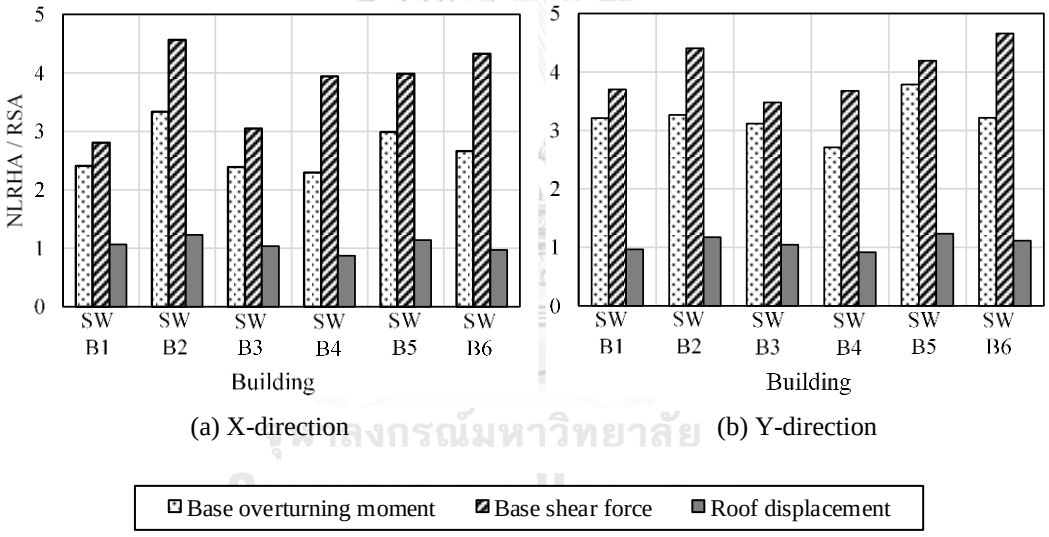

Figure 4.6 Ratios between NLRHA and RSA results: base overturning moment, base shear force, and roof displacement for buildings in Chiang Mai: (a) X-direction; (b) Y-direction.

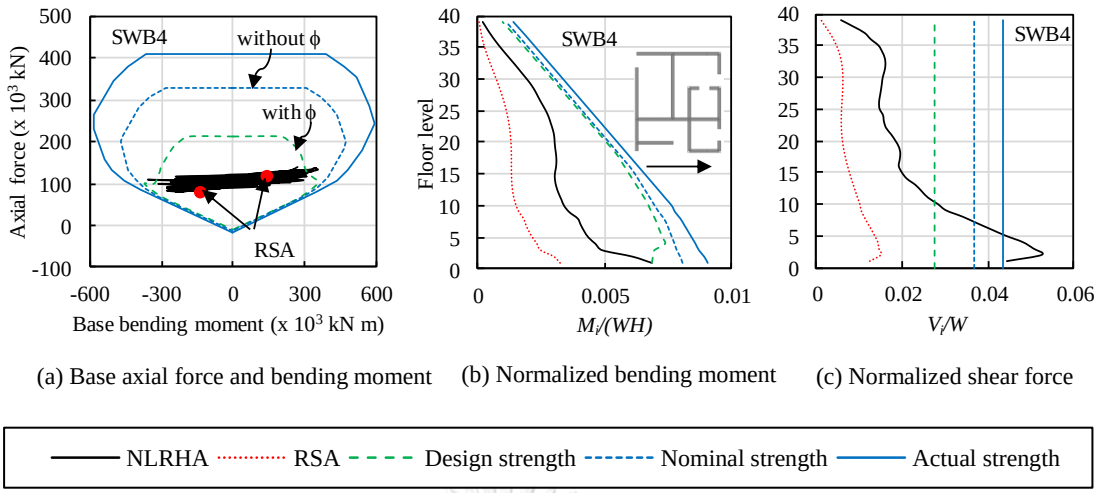

(a) Base axial force and bending moment (b) Normalized bending moment (c) Normalized shear force

Figure 4.7 Design strength, nominal strength, actual strength, and seismic demands computed from RSA and NLRHA of a core wall in the 39-story building (SWB4) in Bangkok: (a) base axial force and bending moment; (b) bending moment; and (c) shear force along the height of the wall. The arrow in (b) indicates the direction of seismic excitation.

4.5 Inelasticity of response in each mode

To investigate inelasticity of response in each mode, modal pushover analysis (MPA) (Chopra and Goel 2002) was conducted with both linear and nonlinear structural models. The stiffness of the linear structural model was equal to the initial stiffness of the nonlinear structural model. Note that this linear structural model adopted uncracked section properties of structural members, which was different from the one used for RSA in Section 4.2. This is because using a linear structural model with cracked section properties as considered for RSA will provide a lower stiffness than that of a nonlinear structural model in the low deformation range, which is not appropriate for the purpose of investigating inelasticity of each mode. The target roof displacement of the first mode was computed by the displacement coefficient method in ASCE 41-13, while the target roof displacement of higher modes was assumed equal to the elastic response computed by modal analysis of the linear structural model considering cracked cross section of structural members. The first-three translational modes were considered in this study. The lateral load pattern based on each mode shape was used for pushover analysis. The gravity loads of all dead loads plus 25% of live loads were applied before pushover

analysis. The force response reduction factor of each mode (R_i) is defined as the ratio between elastic base shear and inelastic base shear computed from modal pushover analysis at the target roof displacement of each mode.

Figure 4.8 presents base shear-roof displacement curves computed from linear and nonlinear pushover analysis along with the target roof displacements. Here, base shear (V_b) is normalized by the seismic weight (W) and roof displacement (δ_{roof}) is normalized by the total height of the building (H). The force response reduction factor of each mode is summarized in Figures 4.9 and 4.10 for case studies in Bangkok and Chiang Mai, respectively. It was found that inelasticity of response in different modes was not the same. The force response reduction factor (R_i) decreased with increasing mode order for most buildings, except for building SWB6 where the R factor of higher modes were larger than that of the first mode, maybe because the mass participating ratios of higher modes for this building (23% for 2nd mode and 22% for 3rd mode) were also significant compared to mass participating ratio of the first mode (35%) (see Table 4.3). The R factor of the first mode was generally from 1.5 to 2 for most buildings considered in this study, which is about 2.5 to 3 times lower than the response modification factor (R=5) used in the design of these buildings, because of the scaling factor required by ASCE 7-10 and the over-strength factor inherent in the design process. For 15-story (SWB1) and 20-story (SWB2 and SWB5) buildings, the higher modes behaved almost elastically as the R factors of the second and third modes were equal to one for case studies in Bangkok (Figure 4.9) and slightly larger than one for case studies in Chiang Mai (Figure 4.10). For 31-story (SWB3) and 39-story (SWB4 and SWB6) buildings, the R factors of the higher modes were larger than one indicating that higher modes deformed beyond linear elastic limit. Therefore, using the higher-mode-elastic assumption is appropriate for 15- and 20-story buildings and is conservative for 31- and 39-story buildings in estimating force demands.

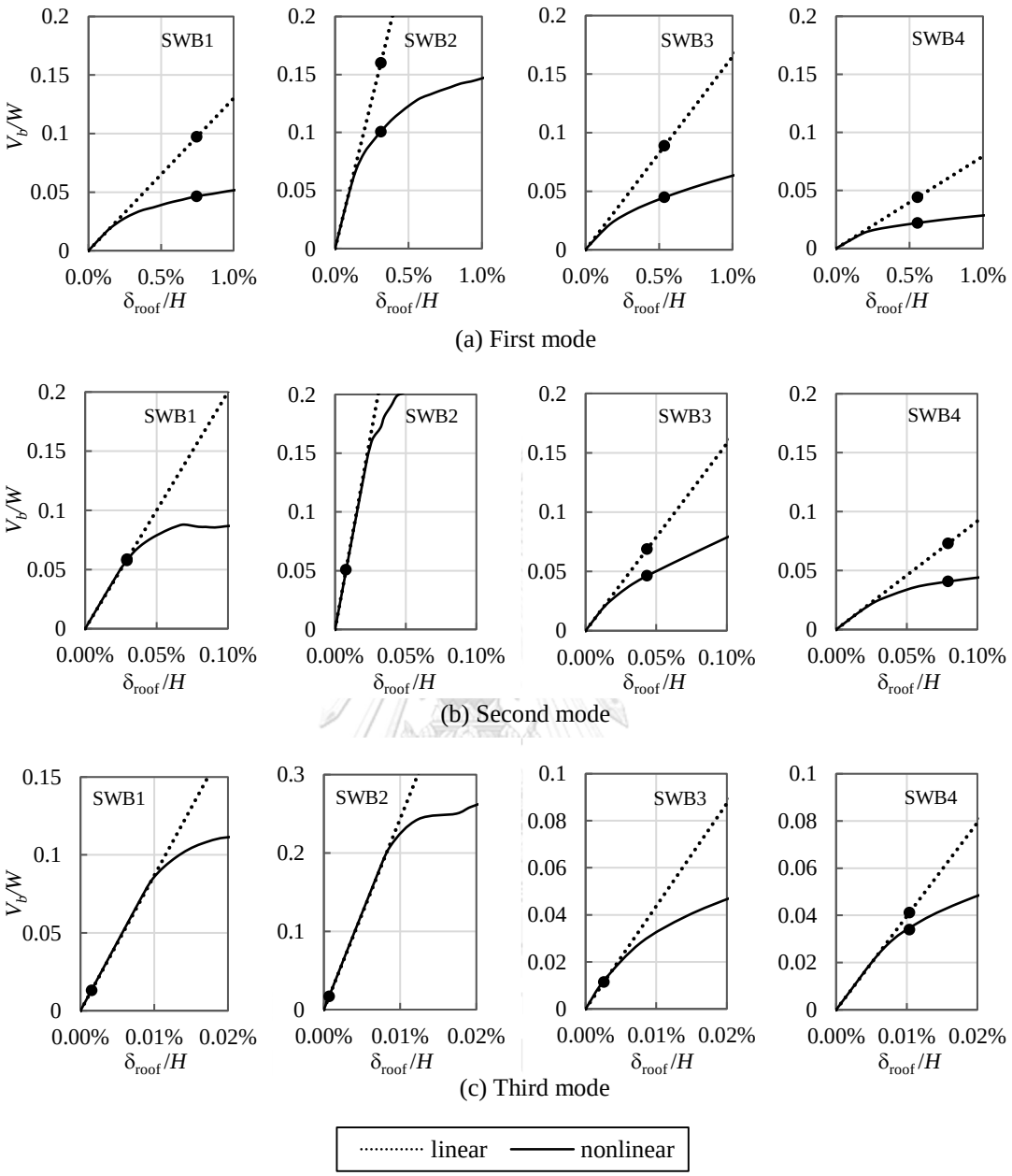

Figure 4.8 Linear and nonlinear pushover curves along with the target roof displacements of the first-three translational modes in X-direction of buildings in Bangkok: (a) first mode; (b) second mode; and (c) third mode. The black dots in each figure indicate the target roof displacement.

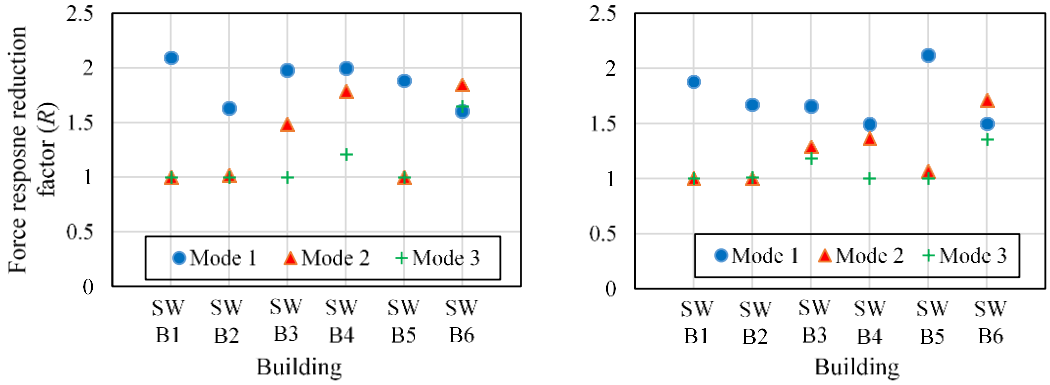

(a) X-direction (b) Y-direction

Figure 4.9 Force response reduction factor of the first-three translational modes for case studies in Bangkok: (a) X-direction; and (b) Y-direction.

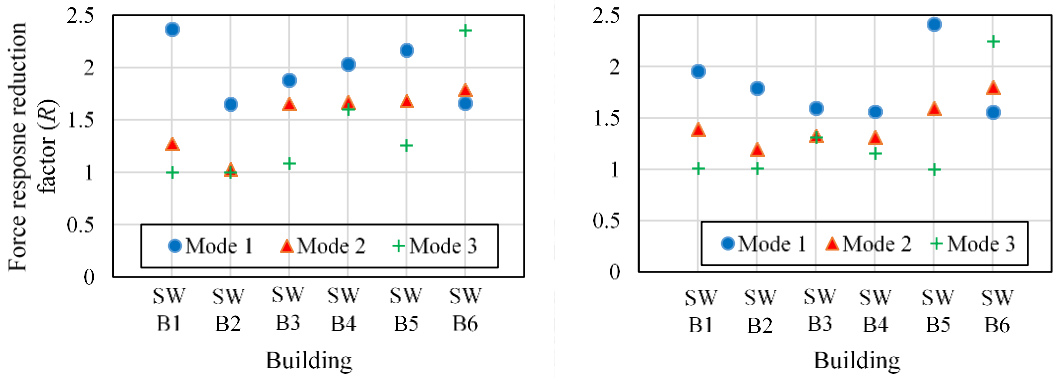

(a) X-direction (b) Y-direction

Figure 4.10 Force response reduction factor of the first-three translational modes for case studies in Chiang Mai: (a) X-direction; and (b) Y-direction.

4.6 Modified response spectrum analysis

As the conventional RSA procedure provided good accuracy in computing floor displacement and story drift demands (Figures 4.1 to 4.4), but on the other hand provided inadequate shear demands for design as shown in Figure 4.7c, a modified response spectrum analysis (MRSA) procedure was proposed to improve the accuracy of the conventional RSA procedure in computing design shear forces in tall RC shear-wall buildings. Two versions of the MRSA method were proposed to compute shear force demands. The first method $MRSA_{HE}$ was based on a higher-mode-elastic (HE) approach and the second method $MRSA_{HI}$ considered the inelasticity of higher modes which requires nonlinear static analysis.

Structural members are normally designed to experience ductile flexural failure mode. By lowering flexural strength, the associated shear force will be lower. However, it is necessary to identify the locations where these ductile failures occur, so that ductile detailing can be implemented. Hence, bending moment demand in the MRSA method was computed and designed for in the same way as conventional RSA procedure (Eq. (4.1)). The RSA in ASCE 7-10 does not provide information on inelastic deformation locations where ductile detailing should be implemented to ensure ductile behavior. In this study, a method based on the equal displacement rule (Veletsos and Newmark 1960) using strain from elastic analysis was proposed to identify the locations of yielding of vertical reinforcement or possible crushing of concrete in RC walls and columns.

4.6.1 Computation of shear forces

4.6.1.1 Modified RSA based on higher-mode-elastic approach

As discussed in the preceding section, higher-mode responses behave elastically for short buildings and can be conservatively assumed to be elastic; hence, the first modified RSA method ($MRSA_{HE}$) was developed based on a higher-mode-elastic (HE) approach. The $MRSA_{HE}$ method is similar to the modified modal superposition (MMS) method of Priestley (2003) and the modified modal pushover analysis (MMPA) method of Chopra et al. (2004) with slight differences in how the first-mode response is computed. Priestley (2003) uses direct displacement-based design and Chopra et al. (2004) uses pushover analysis to compute the inelastic first-mode response, while in the $MRSA_{HE}$ method, the inelastic first-mode shear is obtained by multiplying the elastic first-mode shear with $(SF \times \Omega_0)/R$. Note that this $MRSA_{HE}$ method requires only a linear structural model. In $MRSA_{HE}$, the *SF* is computed in the same way as conventional RSA using Eq. (4.5). The $MRSA_{HE}$ method combines the inelastic first-mode shear with the elastic higher-mode shear by using an appropriate modal combination rule such as the square root of the sum of the squares (SRSS) or the complete quadratic combination (CQC) rule to compute design shear forces in the structure. The shear forces in the structure using the $MRSA_{HE}$ method are computed from

$$V = I\sqrt{\left(\frac{SF \times \Omega_0}{R} V_{1e}\right)^2 + V_{2e}{}^2 + V_{3e}{}^2 + \cdots} \tag{4.12}$$

The bending moments in structures using the higher-mode-elastic (HE) approach M_{HE} are computed from

$$M_{\mathrm{HE}} = I\sqrt{\left(\frac{SF \times \Omega_0}{R} M_{1e}\right)^2 + M_{2e}{}^2 + M_{3e}{}^2 + \cdots} \tag{4.13}$$

But M_{HE} should not be used for design because it will increase shear force due to the increase of flexural strength and will require large vertical reinforcement due to a large bending moment at mid-height level (Figure 4.11b). This can be seen in Figure 4.11a where shear force from NLRHA with flexural strength designed by HE approach, NLRHA (M_{HE}), was larger than shear force from NLRHA with flexural strength designed by RSA procedure, NLRHA (M_{RSA}). Moreover, the HE approach cannot estimate bending moment well when compared with NLRHA (Figure 4.11b) because the provided flexural reinforcements in real practice would not be exactly following the bending moment demands computed from the HE approach, which has smaller demands at some stories between base and mid-height levels (Figure 4.11b).

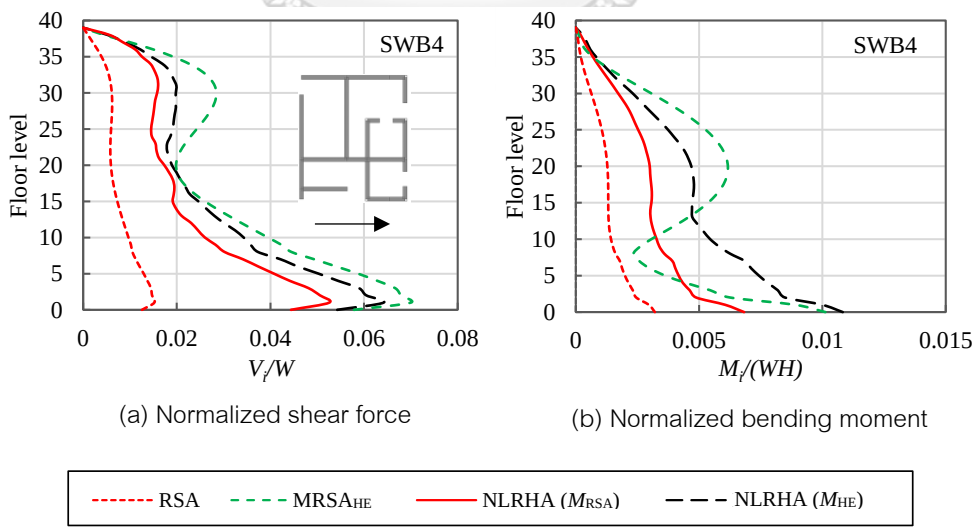

Figure 4.11 Mean values of peak seismic demands (a) shear force; and (b) bending moment of a core wall in the 39-story building (SWB4) in Bangkok with flexural strength designed by RSA and HE. The arrow indicates the direction of seismic excitation.

4.6.1.2 Modified RSA based on higher-mode inelastic approach

The second modified RSA method ($MRSA_{HI}$) was proposed as an alternative method to get higher accuracy for computing shear force demands in case the nonlinear structural model is already available, unlike the $MRSA_{HE}$ method which can be used at the preliminary design stage. The $MRSA_{HI}$ method was developed by modifying the $MRSA_{HE}$ method, such that the inelasticity of higher modes was taken into account by reducing elastic forces contributed from each mode using different force response reduction factors (R_i) which were determined as described in Section 4.5. The $MRSA_{HI}$ method combines the reduced modal forces using an appropriate modal combination rule similar to the $MRSA_{HE}$ method. The $MRSA_{HI}$ method is essentially equivalent to the modal pushover analysis (MPA) method proposed by Chopra and Goel (2002), but $MRSA_{HI}$ does not include the task of extracting the desired response parameters at the target roof displacement from pushover databases as required by the MPA method. In the $MRSA_{HI}$ method, the shear forces in the structure are computed from

$$V = I\sqrt{\left(\frac{V_{1e}}{R_1}\right)^2 + \left(\frac{V_{2e}}{R_2}\right)^2 + \left(\frac{V_{3e}}{R_3}\right)^2 + \cdots} \tag{4.14}$$

where R_i is the force response reduction factor of mode *i*.

4.6.2 Computation of strains in RC walls and columns

As bending moment in the MRSA method is computed and designed for in the same manner as in the conventional RSA procedure, yielding may occur at any location along the height of RC walls or columns. Strain in the walls and columns needs to be determined to identify the locations of yielding of vertical reinforcement or possible crushing of concrete. Based on the equal displacement concept (Veletsos and Newmark 1960), a new method using strain from elastic analysis to predict inelastic strain computed from NLRHA was proposed in this study. Strain from such an elastic analysis was computed using elastic force response determined from linear RSA (*R*=1) combined with factored gravity load, and effective flexural stiffness (EI_{eff}) to represent cracked cross sections of structural members according to ACI 318M-14. The shifting of the neural axis

(NA) location after concrete cracking was also considered in the computation of strain. The shifting of the neutral axis location in an RC wall subjected to cyclic displacement applied at the top of the wall was identified by Orakcal et al. (2004), but the shifting distance of the neutral axis has not yet been addressed.

For inelastic analysis, when tensile strain exceeds cracking strain of concrete, the neutral axis is shifted toward the compressive edge. The shifting distance of the neutral axis (c_{shift}) is the distance between the elastic and inelastic neutral axes. The relative shifting distance of the neutral axis is defined as the ratio between c_{shift} and c_{long} where c_{long} is defined as the longer distance measured from the elastic neutral axis to either edge of the wall as shown in Figure 4.12b.

In this study, the location of the inelastic neutral axis in an RC wall was determined under the assumption of linear strain variation across the cross section. With the known inelastic strains computed from NLRHA, the location of the inelastic neutral axis can be located and actual c_{shift} can be determined from results of NLRHA. It was found that $c_{\text{shift}} / c_{\text{long}}$ was about $1/3$ at the time of peak response for most cases considered in this study. As an example in Figure 4.12a, the time history of $c_{\text{shift}} / c_{\text{long}}$ around the time of peak response in an L-shaped wall of the 15-story building (SWB1) was about constant which was $1/3.33$ and $1/2.50$ when compression occurred at Edge 1 (Figure 4.12c) and Edge 2 (Figure 4.12d), respectively. Therefore, shifting of the neutral axis in the elastic analysis method was taken into account by assuming $c_{\text{shift}} = c_{\text{long}} / 3$. In the MRSA method, the maximum tensile and compressive strains in RC walls and columns are estimated from

$$\varepsilon_t = \frac{P}{E_c A_g} + \frac{M}{E_c I_{eff}}(c + \frac{c_{\text{long}}}{3}) \tag{4.15}$$

$$\varepsilon_c = \frac{P}{E_c A_g} - \frac{M}{E_c I_{eff}}(c - \frac{c_{\text{long}}}{3}) \tag{4.16}$$

where ε_t and ε_c are the maximum tensile and compressive strains, respectively; *M* and *P* are the elastic bending moment and vertical axial force computed from linear RSA

combined with factored gravity load, respectively; c is the distance from the elastic neutral axis to the location where strain is being computed; A_g is the gross cross section of the wall or column; E_c is the Young's modulus of concrete; I_{eff} is the effective moment of inertia of cross section of the wall or column computed by Eq. (4.17), which is taken from Table 6.6.3.1.1(b) of ACI 318M-14.

$$0.35I_g \le I_{eff} = \left(0.80 + 25\frac{A_{st}}{A_g}\right)\left(1 - \frac{M_u}{P_u h} - 0.5\frac{P_u}{P_0}\right)I_g \le 0.875I_g \tag{4.17}$$

where I_g is the gross moment of inertia; A_{st} is the area of vertical reinforcement in the wall or column; M_u and P_u are the design bending moment and axial force of the wall or column that produces the least value of I_{eff}; h is the depth of the column or the length of the wall; and P_0 is the nominal axial strength at zero eccentricity.

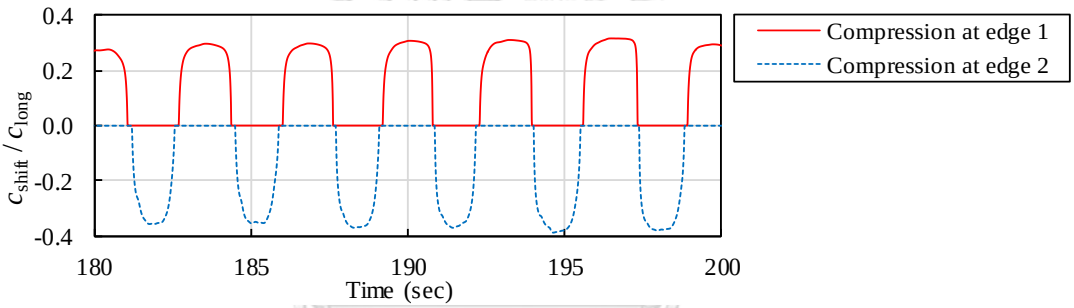

(a) Relative shifting distance of neutral axis in an L-shape wall of 15-story building (SWB1)

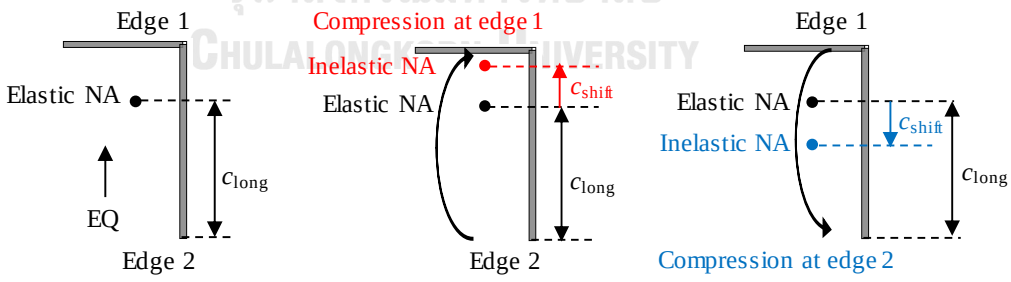

(b) Before shifting of neutral axis

(c) Neutral axis shifted toward edge 1

(d) Neutral axis shifted toward edge 2

Figure 4.12 Shifting of neutral axis in an L-shaped wall of the 15-story building (SWB1) in Bangkok: (a) relative shifting distance of neutral axis computed by using strains from NLRHA; (b) before shifting of neutral axis; (c) neutral axis shifted toward Edge 1; and (d) neutral axis shifted toward Edge 2.

4.6.3 Summary of modified RSA procedure

The general procedure of the MRSA method is summarized below:

1) Modal analysis is conducted on a linear structural model considering cracked cross sections of structural members according to ACI 318M-14.
2) Bending moment is computed in the same way as conventional RSA using Eq. (4.1).
3) Shear force is computed by the $MRSA_{HE}$ method using Eq. (4.12) or by the $MRSA_{HI}$ method using Eq. (4.14) for higher accuracy. Note that the $MRSA_{HE}$ method requires only a linear structural model, but the $MRSA_{HI}$ method requires modal pushover analysis of a nonlinear structural model to compute the force response reduction factor for each mode.
4) Floor displacement and story drift ratio are computed in the same way as conventional RSA using Eq. (4.3) and Eq. (4.4), respectively.
5) Scaling procedure is the same as conventional RSA. The modal base shear used in the scaling is computed from the conventional RSA, not from the MRSA method. Scaling factor is computed by Eq. (4.5).
6) Ductile detailing of RC walls or columns is required at the locations where strain in the walls or the columns computed by Eq. (4.15) and Eq. (4.16) exceeds a prescribed limit.

จุฬาลงกรณ์มหาวิทยาลัย
CHULALONGKORN UNIVERSITY

4.7 Evaluation of modified RSA procedure

4.7.1 Shear forces

To evaluate the accuracy of the $MRSA_{HE}$ and $MRSA_{HI}$ methods, the computed results were compared with the benchmark results obtained from NLRHA. The MMPA method proposed by Chopra et al. (2004) and the EC8 (2004) procedure to compute shear forces using a magnification factor were also included in this comparison because the $MRSA_{HE}$, MMPA, and shear amplification factor in EC8 use the same higher-mode-elastic assumption. The first-four translational modes of the building in the direction of seismic excitation were used for the $MRSA_{HE}$, $MRSA_{HI}$, and MMPA methods. For the

$MRSA_{HI}$ method, the first-three translational modes were reduced by R_i factor and the fourth translational mode was assumed to be elastic. The scaling factors shown in Tables 4.1 and 4.2 for buildings in Bangkok and Chiang Mai, respectively and the over-strength factor of Ω_0=2.5 according to ASCE 7-10 were used in $MRSA_{HE}$. The $MRSA_{HE}$ method requires only a linear structural model with cracked section properties in the same way as the conventional RSA, but the $MRSA_{HI}$ and MMPA methods require a nonlinear structural model. The EC8 (2004) procedure to compute shear force using a magnification factor is given by Eq. (2.35); where *q* was taken as the design force reduction factor used in this study; and $\gamma_{Rd} M_{Rd} / M_{Ed}$ was considered as the over-strength factor used in this study.

The story shear forces computed from RSA, $MRSA_{HE}$, $MRSA_{HI}$, MMPA, EC8, and NLRHA procedures are compared in Figures 4.13 and 4.14 for case studies in Bangkok and Chiang Mai, respectively. It showed that the $MRSA_{HE}$, $MRSA_{HI}$, EC8, and MMPA methods significantly improved the underestimation of the RSA method in computing shear forces for all buildings SWB1-SWB6 in Bangkok and Chiang Mai. The shear magnification factor method in EC8 (2004) generally overestimated the shear forces computed from NLRHA for all buildings, and this trend was consistent with the findings of Khy and Chintanapakdee (2017). The $MRSA_{HE}$ could predict the story shear forces well for the 15- (SWB1) and 20-story (SWB2 and SWB5) buildings, and it provided conservative results for the 31- (SWB3) and 39-story (SWB4 and SWB6) buildings when compared with NLRHA because higher modes were not elastic for these two buildings as discussed in Section 4.5. Despite the use of a simplified equation to compute the inelastic first-mode shear, the accuracy obtained from $MRSA_{HE}$ was similar to MMPA, in which the inelastic first-mode shear was computed by pushover analysis.

Including inelasticity of higher modes as considered in the $MRSA_{HI}$ method could improve the accuracy of the $MRSA_{HE}$ method, as the $MRSA_{HI}$ method provided good accuracy in computing story shear forces for most buildings, except for building SWB6 in Chiang Mai (Figure 4.14) where $MRSA_{HI}$ underestimated results from NLRHA. The accuracy of the $MRSA_{HE}$ and $MRSA_{HI}$ methods is very similar for the 15- and 20-story buildings because their higher-mode responses are in elastic range as found in Section

4.5. However, the $MRSA_{HI}$ method requires a nonlinear structural model to compute the force response reduction factor for each mode, which makes the $MRSA_{HE}$ method more practical than the $MRSA_{HI}$ method.

จุฬาลงกรณ์มหาวิทยาลัย
CHULALONGKORN UNIVERSITY

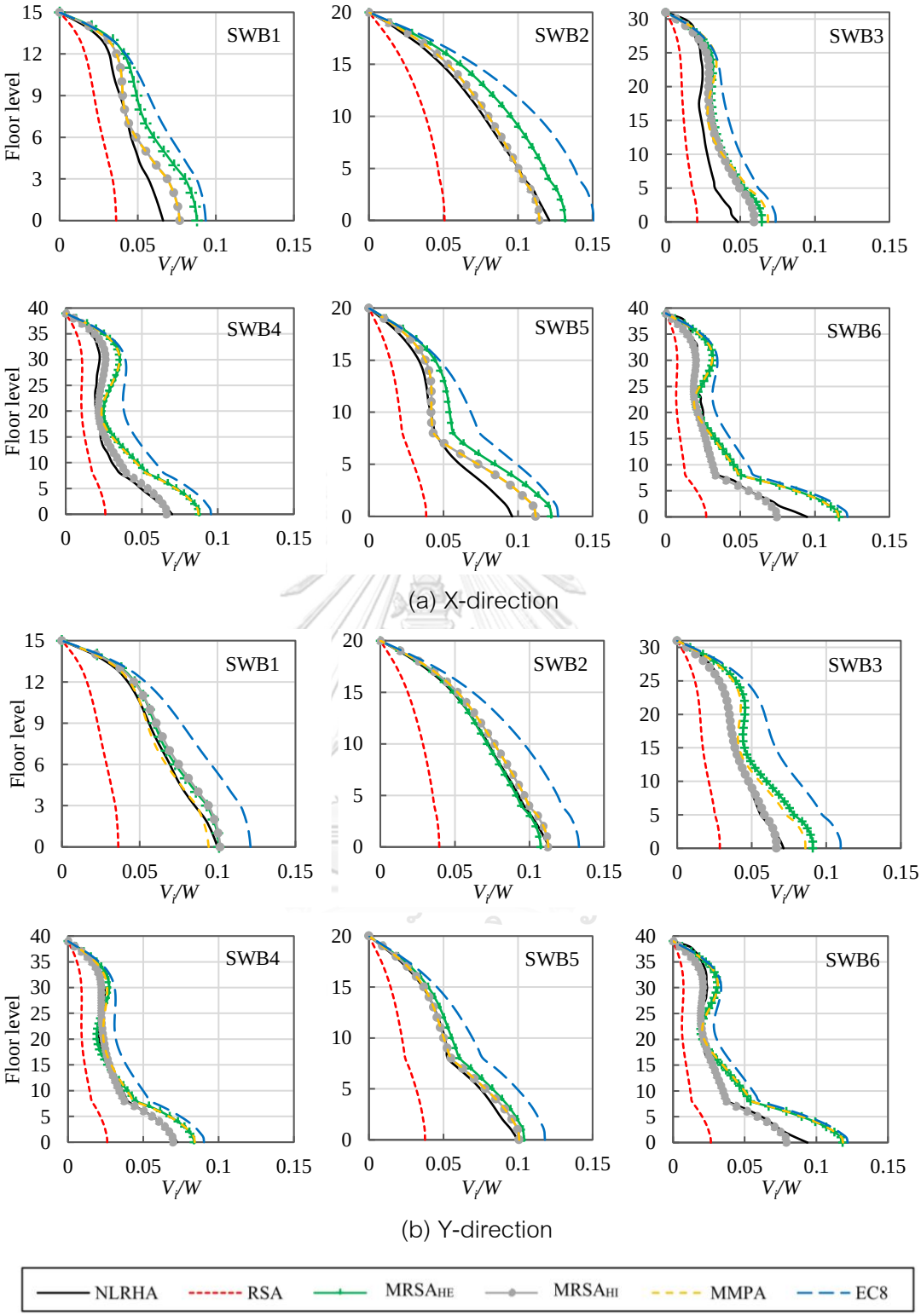

Figure 4.13 Mean values of peak story shear forces computed by RSA, $MRSA_{HE}$, $MRSA_{HI}$, MMPA, EC8, and NLRHA procedures for buildings in Bangkok due to seismic excitation in: (a) X-direction; and (b) Y-direction.

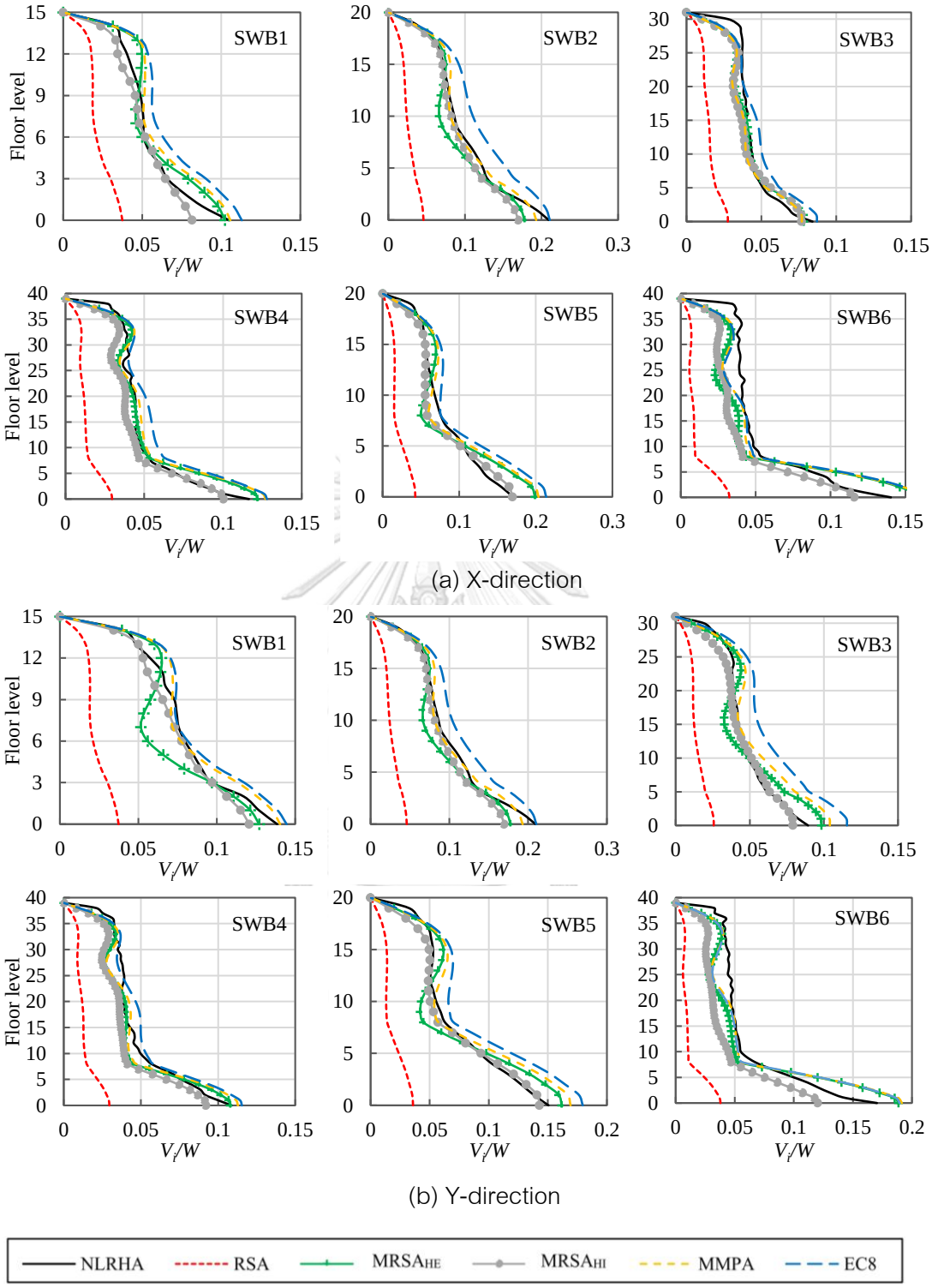

Figure 4.14 Mean values of peak story shear forces computed by RSA, $MRSA_{HE}$, $MRSA_{HI}$, MMPA, EC8, and NLRHA procedures for buildings in Chiang Mai due to seismic excitation in: (a) X-direction; and (b) Y-direction.

The $MRSA_{HE}$ and $MRSA_{HI}$ methods could also compute shear forces in RC walls and columns with reasonable accuracy when compared with NLRHA (Figures 4.15 and 4.16). The $MRSA_{HE}$ and $MRSA_{HI}$ could estimate shear forces reasonably well in RC shear walls and core walls (Figure 4.15) for most buildings in both Bangkok and Chiang Mai, but generally underestimated shear forces in columns for buildings in Chiang Mai (Figure 4.16b) when compared with NLRHA; and the MMPA instead provided good agreement with NLRHA, except for building SWB6 in Chiang Mai where MMPA underestimated results from NLRHA. However, in tall RC shear-wall buildings, shear forces resisted by columns are smaller than those carried by shear walls. The accuracy of the $MRSA_{HE}$ and $MRSA_{HI}$ methods for structural component-force demands is not as good as for story-force demands. This is because the force distribution from story demands to structural components in that story is different for $MRSA_{HE}$, $MRSA_{HI,}$ MMPA, and NLRHA. For $MRSA_{HE}$ and $MRSA_{HI}$, the force distribution is based on initial elastic stiffness of structural members. For MMPA, the first-mode shear accounts for more accurate distribution of nonlinear seismic demand in a way similar to NLRHA, which makes MMPA more accurate than $MRSA_{HE}$ and $MRSA_{HI}$ methods for estimating shear forces in the structural components.

จุฬาลงกรณ์มหาวิทยาลัย
CHULALONGKORN UNIVERSITY

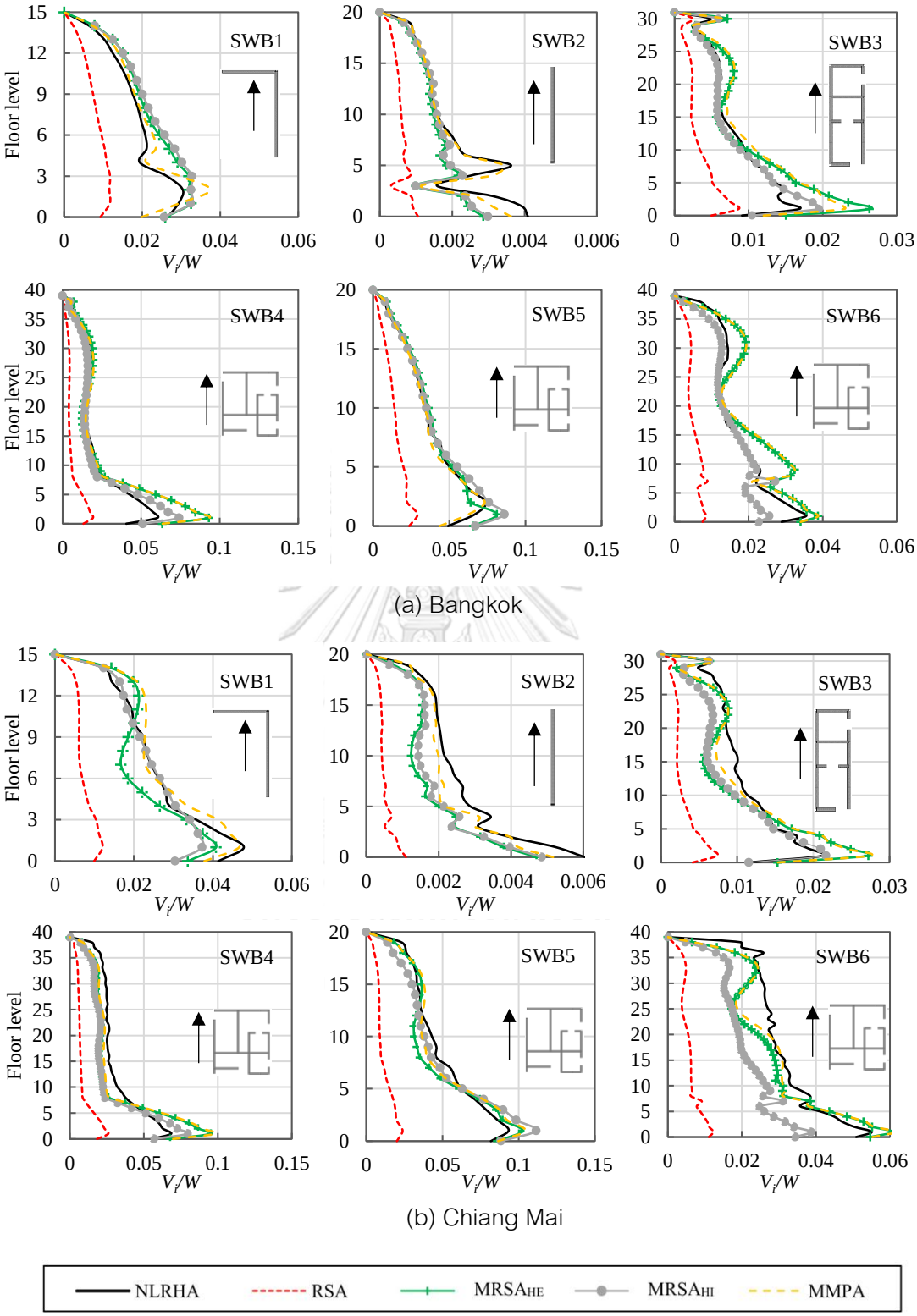

Figure 4.15 Mean values of peak shear forces in RC walls computed by RSA, MRSA$_{HE}$, MRSA$_{HI}$, MMPA, and NLRHA procedures for buildings in: (a) Bangkok; and (b) Chiang Mai. The arrow in each figure indicates the direction of seismic excitation.

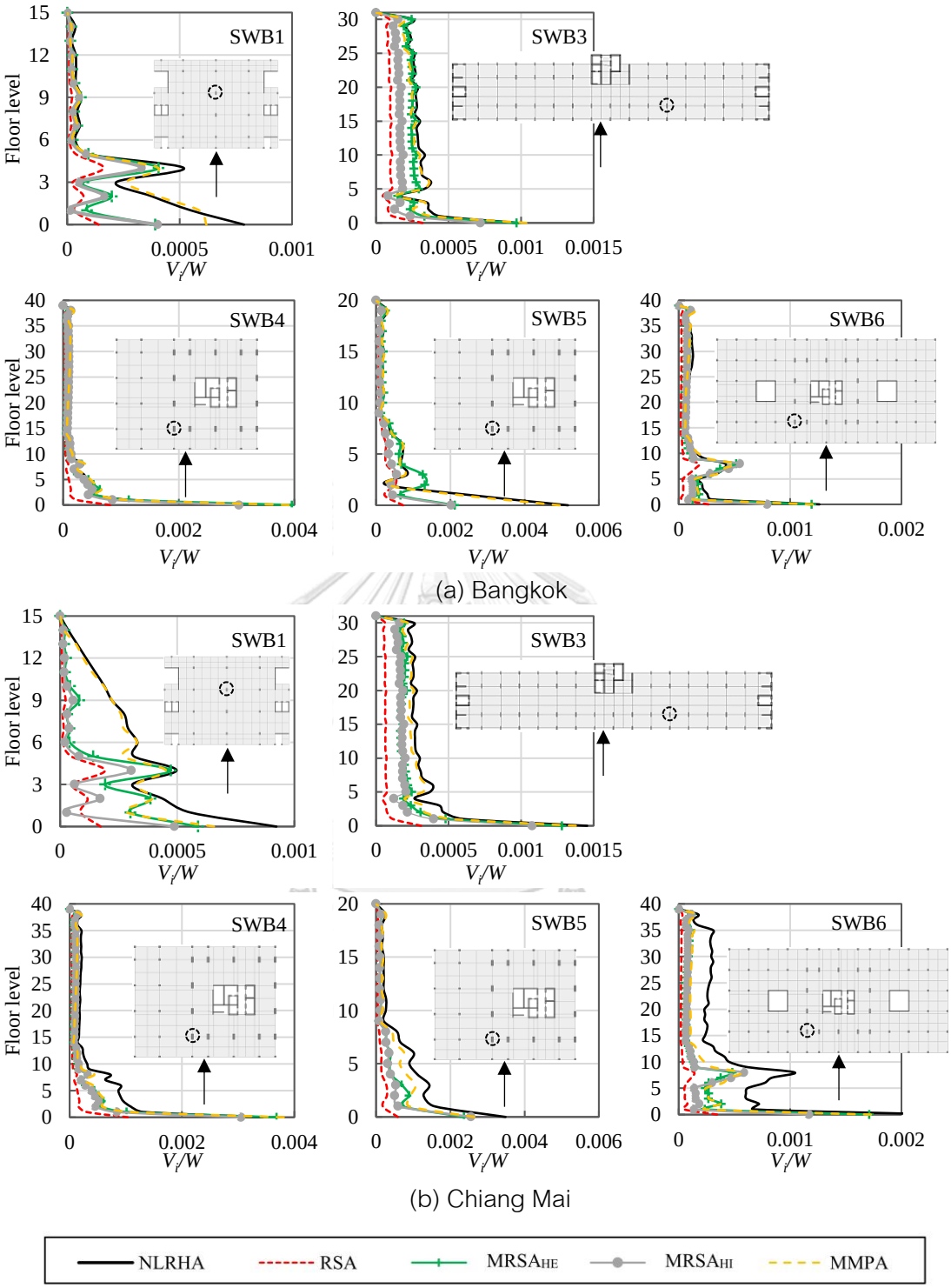

Figure 4.16 Mean values of peak shear forces in RC columns computed by RSA, MRSA$_{HE}$, MRSA$_{HI}$, MMPA, and NLRHA procedures for buildings in: (a) Bangkok; and (b) Chiang Mai. The arrow in each figure indicates the direction of seismic excitation and the circle indicates the location of the column considered.

4.7.2 Strains in RC walls and columns

The variation along the height of predicted strain from MRSA and inelastic strain from NLRHA in RC walls and columns is presented in Figures 4.17 and 4.18 for case studies in Bangkok and Figures 4.19 and 4.20 for case studies in Chiang Mai (where tensile strains are indicated as positive). For RC walls, the contribution from bending strain was significantly larger than that from axial strain because the RC walls in all buildings SWB1-SWB6 resisted more than 75% of the total lateral loads in each story. Due to the shifting of the neutral axis in the wall, the tensile strain was larger than the compressive strain for all buildings (Figures 4.17 and 4.19). For RC columns, the structural members behaved like gravity load resisting members; in this case, the axial force induced strain contributed considerably to the total combined strain. Therefore, the effect of the shifting of the neutral axis was minor and the compressive strain was larger than the tensile strain for all buildings (Figures 4.18 and 4.20). The axial strain in the columns was significantly lower than that in the walls. For most of the studied buildings, it was found that flexural yielding occurs in the walls at the first few stories above the base, and there was no yielding in the columns.

The predicted strain from MRSA method can estimate well the inelastic strain in the walls and columns computed from NLRHA for most cases, except for buildings SWB1 and SWB6 in Chiang Mai (Figure 4.19 for walls and Figure 4.20 for columns) where MRSA underestimated at the upper floors when compared with NLRHA results. It should be noted that the proposed method was developed based on the equal displacement rule (Veletsos and Newmark 1960) which usually works well for long period structures such as tall buildings. If the equal displacement rule does not work well in some cases, the proposed method would also not be accurate in those cases. The error could also due to effective stiffness values of RC walls and columns computed using Eq. (4.17) and the shifting distance of neutral axial along the height of the walls and columns. Note that this study used a constant shifting distance of neutral axis ($c_{\text{shift}} = c_{\text{long}} / 3$) throughout of the height of the walls and columns.

จุฬาลงกรณ์มหาวิทยาลัย
Chulalongkorn University

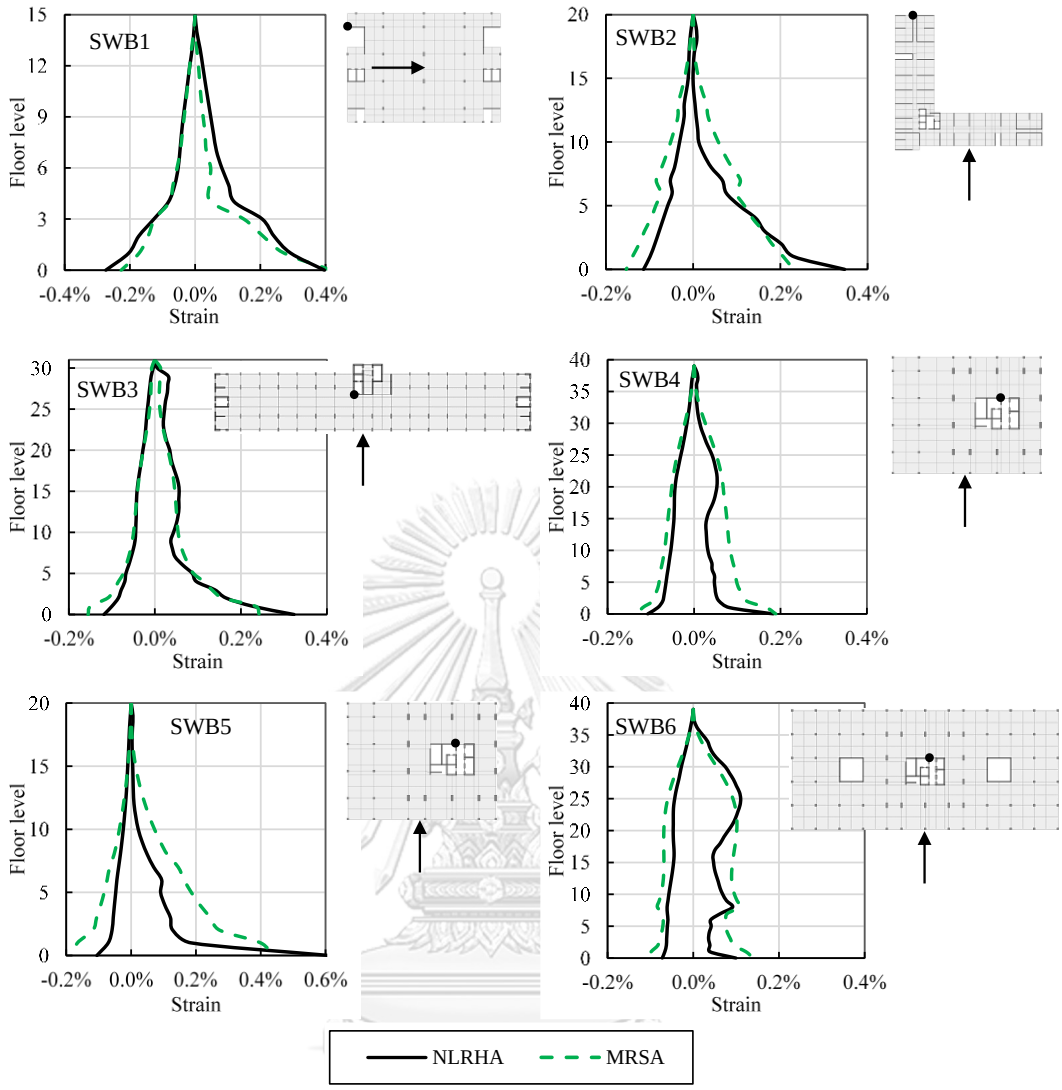

Figure 4.17 Mean values of peak vertical axial strains in RC walls computed by MRSA and NLRHA procedures for buildings in Bangkok. The arrow in each figure indicates the direction of seismic excitation and the black dot indicates the location of strain considered in the wall.

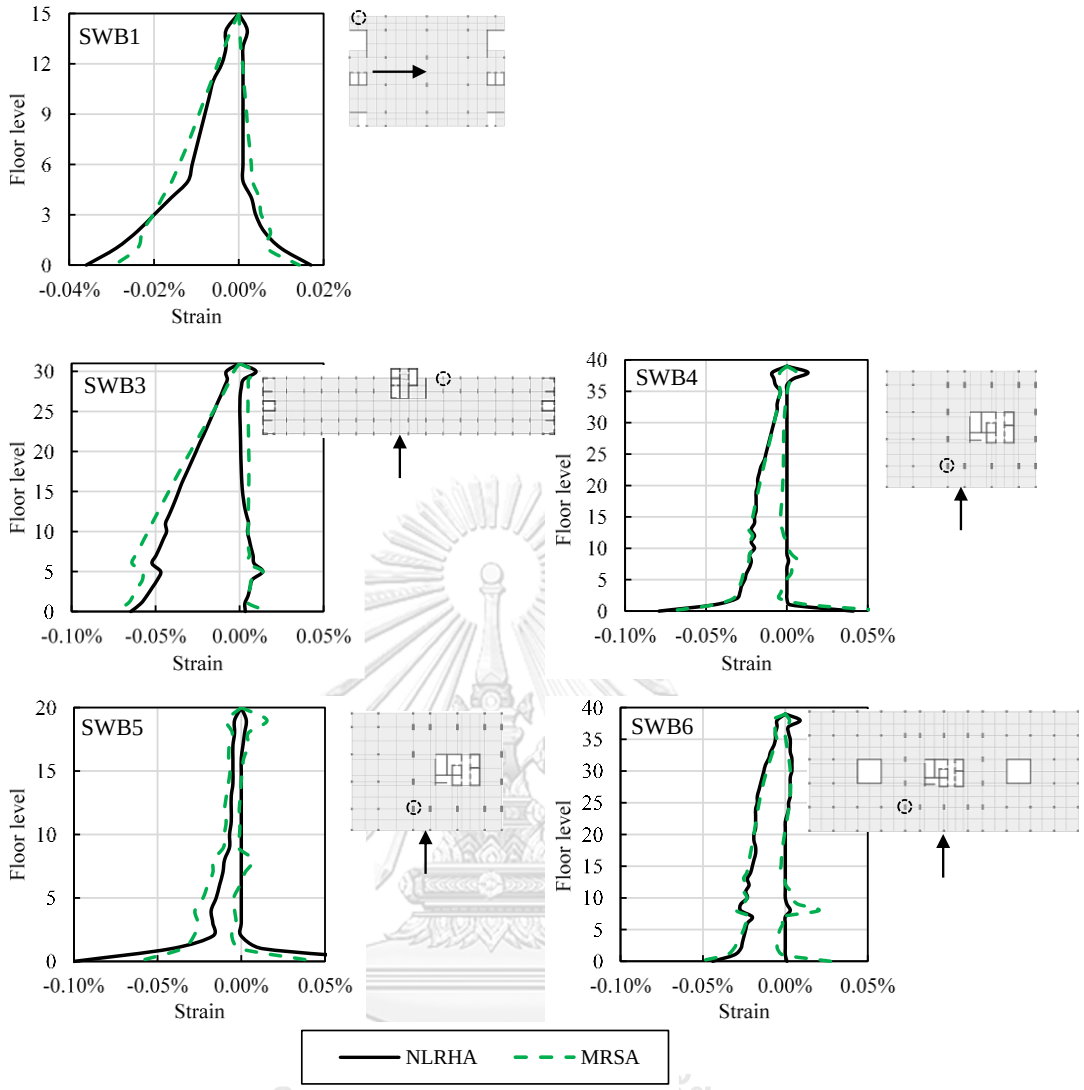

Figure 4.18 Mean values of peak vertical axial strains in RC columns computed by MRSA and NLRHA procedures for buildings in Bangkok. The arrow in each figure indicates the direction of seismic excitation and the circle indicates the location of the column considered.

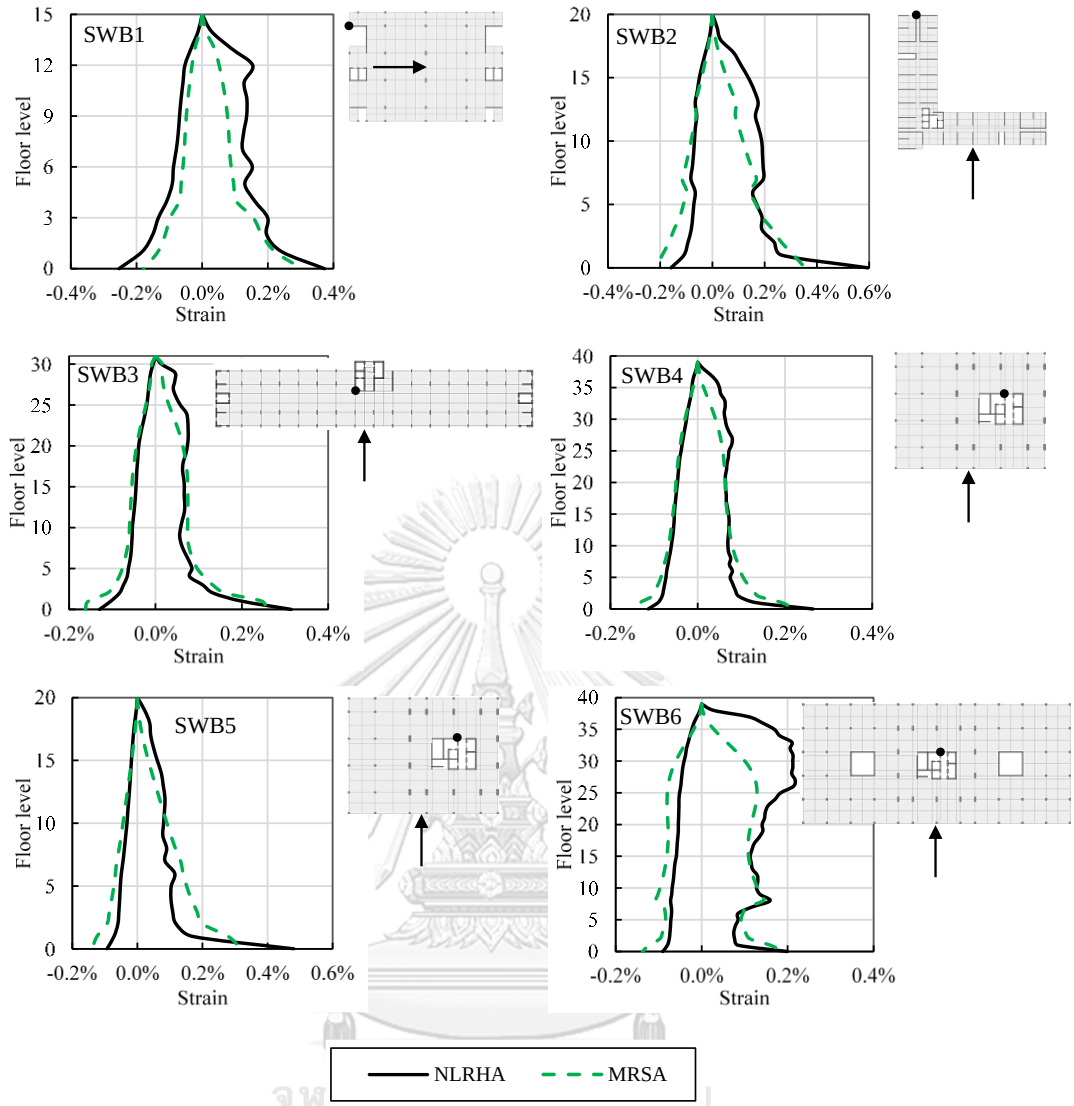

Figure 4.19 Mean values of peak vertical axial strains in RC walls computed by MRSA and NLRHA procedures for buildings in Chiang Mai. The arrow in each figure indicates the direction of seismic excitation and the black dot indicates the location of strain considered in the wall.

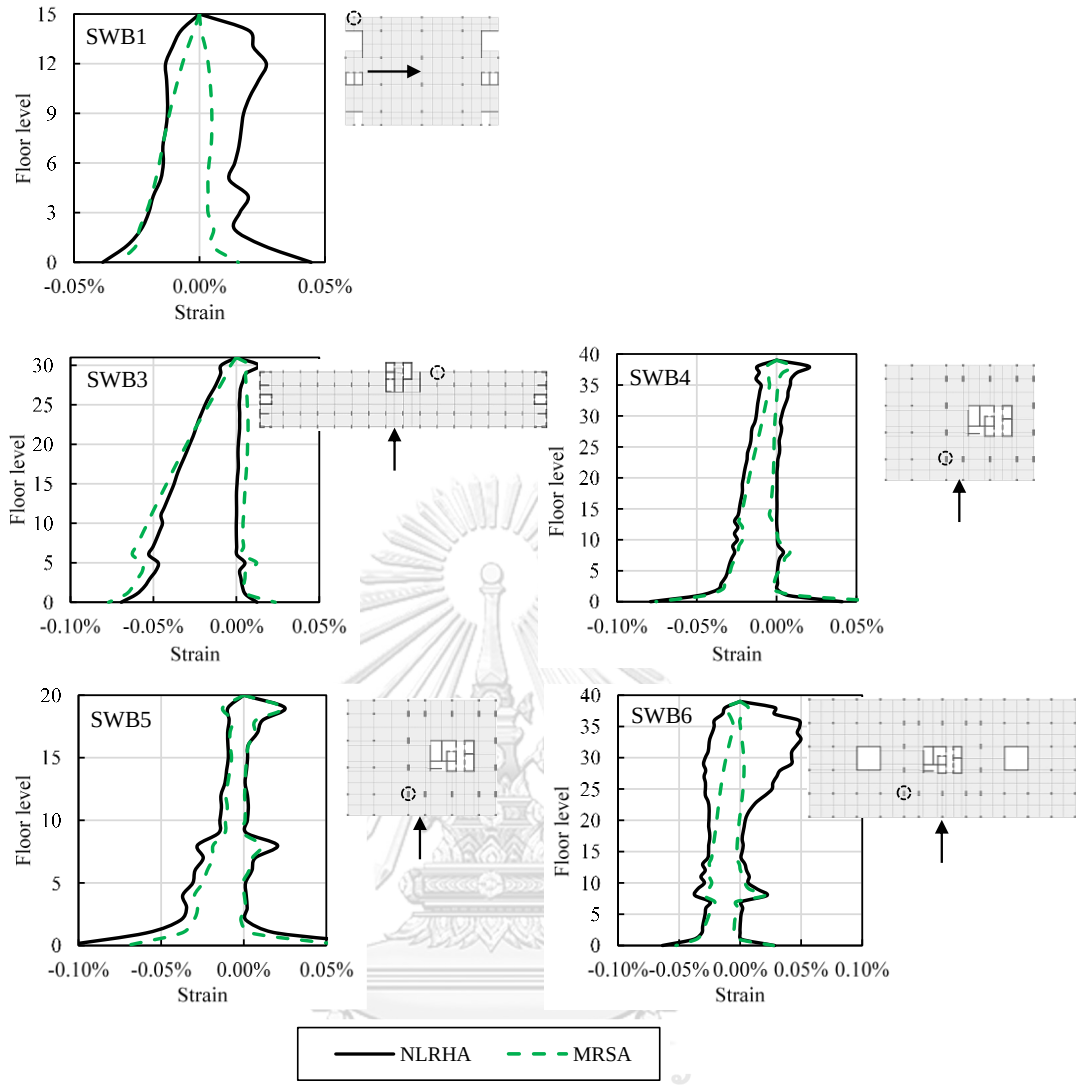

Figure 4.20 Mean values of peak vertical axial strains in RC columns computed by MRSA and NLRHA procedures for buildings in Chiang Mai. The arrow in each figure indicates the direction of seismic excitation and the circle indicates the location of the column considered.

4.8 Summary

The main findings of this Chapter are summarized as the followings:

(1) The RSA procedure can be used to compute floor displacements and story drift ratios for design, as it can provide good estimates of inelastic floor displacements and story drift ratios computed from NLRHA. Shear forces determined from the RSA procedure should not be used for design because it is too small when compared with NLRHA results. As structural walls are designed to experience ductile flexural yielding, bending moments computed from the RSA procedure may be used for design. However, it is necessary to identify the locations where the ductile flexural yielding occurs, so that ductile detailing can be implemented.

(2) The force response reduction factor decreases with increasing mode order and is rather lower than response modification factor used in the design due to the scaling factor required by the code and over-strength factor inherent in the design. Higher-mode responses behave elastically for 15-story and 20-story buildings and deform beyond linear elastic limit for 31-story and 39-story buildings.

(3) The $MRSA_{HE}$ method can predict well shear forces computed from NLRHA for 15- and 20-story buildings and conservatively for 31- and 39-story buildings.

(4) The $MRSA_{HI}$ method can reduce the conservativeness of the $MRSA_{HE}$ method for tall buildings, but it requires a nonlinear structural model to compute force response reduction factor for each mode.

(5) In both MRSA methods, the design bending moment demands are computed in the same way as conventional RSA and ductile detailing of RC walls or columns is required at locations where combined axial and bending strain exceeds a certain limit, for example, 0.002. Strain estimated by the proposed method is found to provide good accuracy in predicting inelastic strain computed from NLRHA for most studied buildings.

จุฬาลงกรณ์มหาวิทยาลัย
Chulalongkorn University

CHAPTER 5
MODIFIED RESPONSE SPECTRUM ANALYSIS FOR DESIGN OF RC FRAME BUILDINGS

5.1 Introduction

This chapter first evaluated the accuracy of the RSA procedure. Then, the proposed MRSA procedure developed in Chapter 4 was applied to RC moment-frame buildings. It should be noted that capacity design approach using probable flexural strength at both ends of beams or columns is used in many design building codes to compute the design shear forces of beams or columns in an RC special moment frame. This could lead to conservative estimation of shear forces in columns and beams in upper stories where their probable flexural strengths are not attained under design earthquake loading. The accuracy of the capacity design method was also evaluated. NLRHA was conducted to evaluate the accuracy of the RSA, MRSA, and capacity design methods.

Here, four special RC moment-frame buildings (Figure 3.2) in Section 3.1.2 were used. For Chiang Mai, ground motions (Figure 3.17) in Section 3.3.2 were used. For Bangkok, due to recent publication of Thailand seismic design standard (DPT 1301/1302-61, 2018), new design spectrum was used, which was different from that in Section 3.3.1. Here, the new design spectrum for 2.5% damping ratio in Bangkok (shown as target spectrum (UHS) in Figure 5.1) was taken from DPT 1301/1302-61 for central Bangkok, zone 5. To obtain UHS spectral matching ground motions for use in NLRHA, CMS ground motions in the set for conditioning period of 3 sec in Section 3.3.1 shown here again in Figure 5.1 were modified by SeismoMatch (SeismoSoft 2016) to have spectral shape matched the target spectrum (UHS). The individual matching spectra, the mean value of matching spectra, and the target spectrum (UHS) for 2.5% damping ratio in Bangkok zone 5 are shown in Figure 5.2. The ground motions were applied separately in each principle direction of the building at a time for all analysis methods and vertical earthquake was not considered.

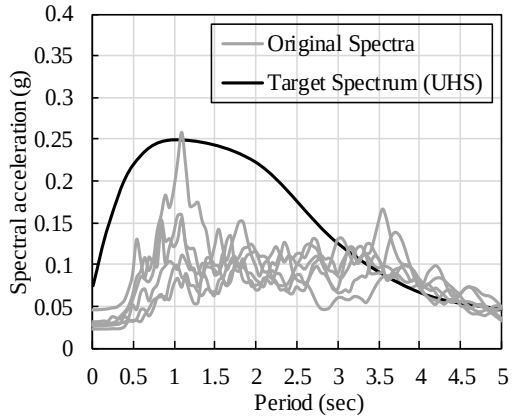

Figure 5.1 Original spectra of CMS ground motions conditioned at 3 sec and target spectrum for 2.5% damping ratio in Bangkok zone 5.

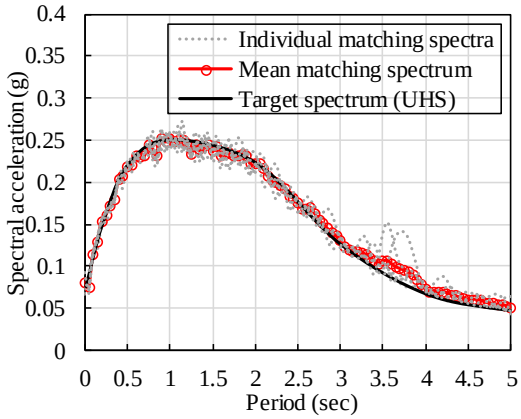

Figure 5.2 Individual matching spectra, mean matching spectrum, and target spectrum for 2.5% damping ratio in Bangkok zone 5.

5.2 Accuracy of response spectrum analysis procedure

The same analysis consideration for RSA and NLRHA as used in Section 4.2 and 4.3, respectively was utilized in this Section. Results from $LRSA_{cracked}$ and $LRSA_{uncracked}$, as used for RC shear-wall buildings in Section 4.4 were also presented.

The RSA modal base shears, ELF base shears, effective response modification factors, and scaling factors for each building are summarized in Table 5.1. The scaling factors varied from 1 to 2.7 and 2.3 to 2.7 for case studies in Bangkok and Chiang Mai, respectively, which depends on the structural modal properties and the characteristic of the design spectrum. For moment-frame buildings, the average mass participating ratio in RSA was 80%, 11%, and 4% for first, second, and third modes, respectively as shown in Table 5.2. The design spectral accelerations at the fundamental period of ELF were larger than those used in RSA as shown in Table 5.3. The level of difference was more significant for case studies in Chiang Mai resulting in larger scaling factors for those cases. The detail modal contribution of each linear response for each building can be found in Appendix C.

Table 5.1 Scaling factors for RC frame buildings.

Building	Bangkok				Chiang Mai			
	$0.85V_s/W$	V_t/W	SF	R_{eff}	$0.85V_s/W$	V_t/W	SF	R_{eff}
MFB1	0.0187	0.0261	1.00	8.00	0.0839	0.0349	2.40	3.33
MFB2	0.0242	0.0238	1.02	7.88	0.0606	0.0234	2.59	3.09
MFB3	0.0262	0.0188	1.39	5.74	0.0406	0.0179	2.27	3.52
MFB4	0.0249	0.0091	2.74	2.92	0.0250	0.0109	2.29	3.49

Table 5.2 Modal mass participating ratio of each mode used in RSA for RC frame buildings.

Building	Translational Modes		
	Mode 1	Mode 2	Mode 3
MFB1	86%	11%	3%
MFB2	83%	10%	4%
MFB3	76%	11%	5%
MFB4	75%	11%	4%

จุฬาลงกรณ์มหาวิทยาลัย
CHULALONGKORN UNIVERSITY

Table 5.3 Spectral accelerations at fundamental periods for ELF and RSA for RC frame buildings.

Building	T_1 (sec)		Sa (T_1) Bangkok		Sa (T_1) Chiang Mai	
	ELF	RSA	ELF	RSA	ELF	RSA
MFB1	0.32	1.23	0.18	0.24	0.79	0.29
MFB2	0.63	1.85	0.23	0.23	0.57	0.20
MFB3	0.95	2.31	0.25	0.19	0.38	0.16
MFB4	1.58	3.90	0.23	0.07	0.24	0.09

Seismic demands computed from $LRSA_{cracked}$, $LRSA_{uncracked}$, and RSA are compared with the mean values of peak seismic demands from NLRHA as shown in Figures 5.3 and 5.4 for case studies in Bangkok and Chiang Mai, respectively. For floor displacements and story drift ratios, $LRSA_{cracked}$ provided good estimates, while $LRSA_{uncracked}$ considerably underestimated when compared with NLRHA for all studied buildings. The RSA procedure ($LRSA_{cracked}$ x C_d/R where C_d=5.5; R=8) resulted in lower estimations of floor displacements and story drift ratios. It should be noted that RSA procedure provided good estimates for RC shear-wall buildings (Figures 4.1 to 4.4). This is because C_d in ASCE 7-10 is slightly smaller than R for RC shear-wall buildings (C_d=4.5, R=5) but is rather smaller than R for RC frame buildings (C_d=5.5, R=8). The $LRSA_{cracked}$ should be used to compute floor displacements and story drift ratios for RC frame buildings. For force demands, RSA ($LRSA_{cracked}$ / R_{eff} where R_{eff} is shown in Table 5.1) significantly underestimated results from NLRHA for all studied buildings in a similar way as the case of RC shear-wall buildings, which is mainly due to the use of a single R factor to reduce the force response of all modes. The ratios between NLRHA and RSA results in terms of base overturning moment, base shear force, and roof displacement are shown in Figure 5.5. The base overturning moment ratios were 2.3 to 6.4 and 2.3 to 2.5 for buildings in Bangkok and Chiang Mai, respectively. The base shear ratios were 2.1 to 6.5 and 2.2 to 2.6 for buildings in Bangkok and Chiang Mai, respectively. The larger base shear ratio corresponded to the buildings designed using larger R_{eff} factor (Table 5.1) used to compute the design base shear force. The base shear ratios for buildings in Bangkok were mostly larger than those in Chiang Mai because R_{eff} factors for buildings in Bangkok were larger than those in Chiang Mai. For example, for the 3-story building (MFB1) in Bangkok, R_{eff} equaled to 8 and the base shear ratio was 6.5 and for the same 3-story building in Chiang Mai, R_{eff} equaled to 3.3 and the base shear ratio was 2.2.

The over-strength factor is defined as the ratio between base probable lateral strength and design base shear force from earthquake using RSA procedure. The base probable lateral strength was computed by pushover analysis using first-mode shape as lateral load pattern. The over-strength factors for RC moment-frame buildings are

presented in Figure 5.6. The over-strength factors for buildings in Bangkok (low seismicity) can be as large as 6 to 7.5 for 3-story (MFB1) and 6-story (MFB2) buildings because the gravity loads and code minimum requirement governed the design strength of these two buildings and the design base shear force from earthquake for these two buildings is quite small, which results in a large lateral over-strength factor for those cases. The over-strength factors for buildings in Chiang Mai (moderate seismicity) vary generally from 2 to 2.5. It should be noted that buildings in Bangkok and Chiang Mai have the same structural sizes and strengths. The over-strength factors for buildings in Bangkok were larger than those in Chiang Mai because the design base shear for buildings in Bangkok were significantly smaller than those for buildings in Chiang Mai (Table 5.1).

จุฬาลงกรณ์มหาวิทยาลัย
CHULALONGKORN UNIVERSITY

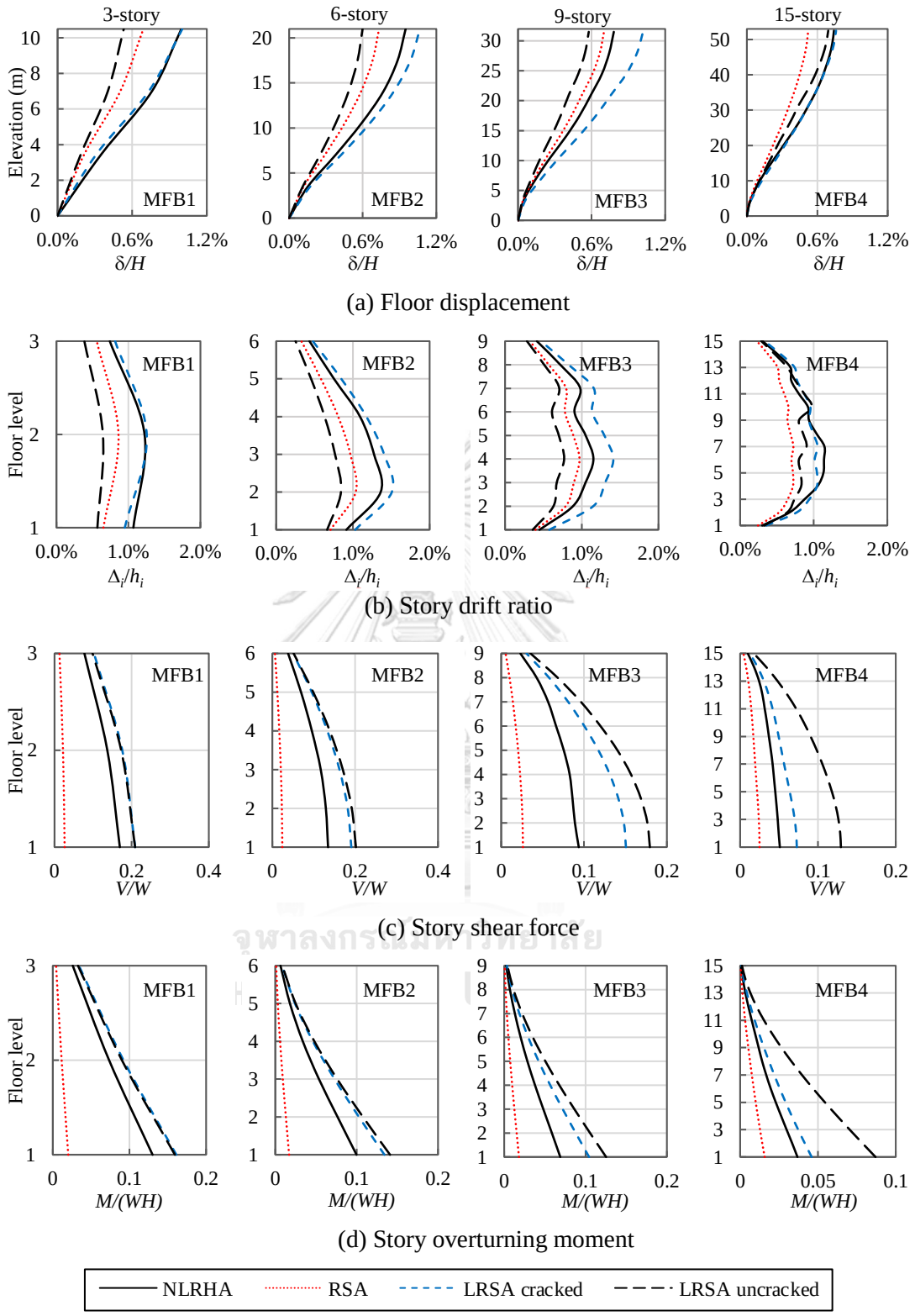

Figure 5.3 Mean values of peak seismic demands computed from RSA, $LRSA_{cracked}$, $LRSA_{uncracked}$, and NLRHA for RC frame buildings in Bangkok: (a) floor displacement; (b) story drift ratio; (c) story shear force; and (d) story overturning moment.

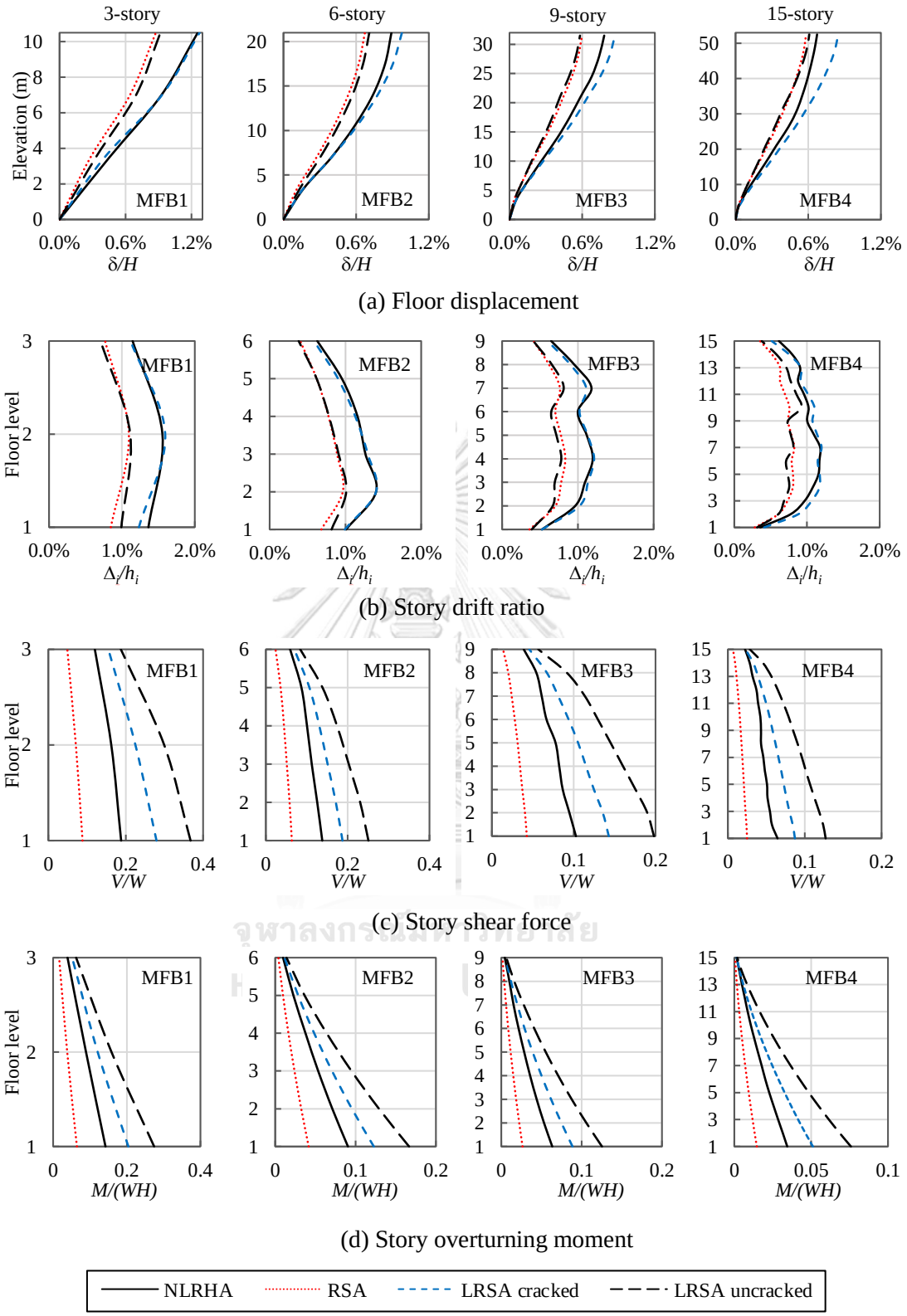

Figure 5.4 Mean values of peak seismic demands computed from RSA, $LRSA_{cracked}$, $LRSA_{uncracked}$, and NLRHA for RC frame buildings in Chiang Mai: (a) floor displacement; (b) story drift ratio; (c) story shear force; and (d) story overturning moment.

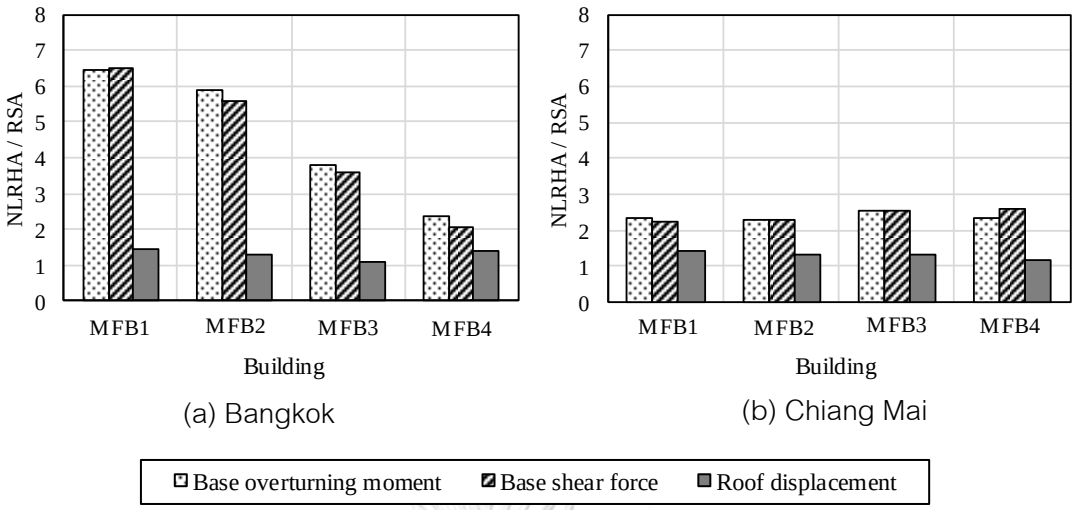

Figure 5.5 Ratio between NLRHA and RSA results: base overturning moment, base shear force, and roof displacement for RC frame buildings in: (a) Bangkok; (b) Chiang Mai.

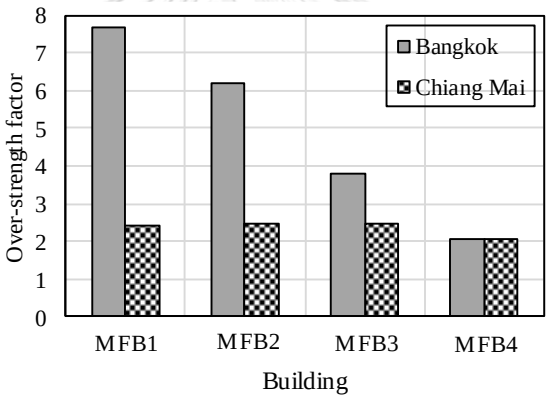

Figure 5.6 Lateral over-strength factors for RC frame buildings.

5.3 Inelasticity of response in each mode

The same methodology as used in Section 4.5 for tall RC shear-wall buildings was used to investigate inelasticity of response in each mode for RC moment-frame buildings.

Base shear-roof displacement curves computed from linear and nonlinear pushover analysis along with the target roof displacements of all moment-frame buildings MFB1-MFB4 are presented in Figure 5.7. The force response reduction factor is summarized in Figure 5.8. It was found that inelasticity of response in different modes was different such that the force response reduction factor decreased with increasing mode order, which was the same trend as for RC shear-wall buildings. The force response reduction factor of the first mode (R_1) was in average about 1.5 for moment-frame

buildings, which was much lower than the response modification factor (R=8) used in computing the design forces of these buildings because of the scaling factor required by ASCE 7-10 and the over-strength inherent in the design process. For moment-frame buildings, higher modes slightly exceeded linear elastic limit for all buildings ($R_{2,3}$ was about 1.1). Therefore, using higher-mode-elastic assumption is appropriate in estimating force demands for moment-frame buildings.

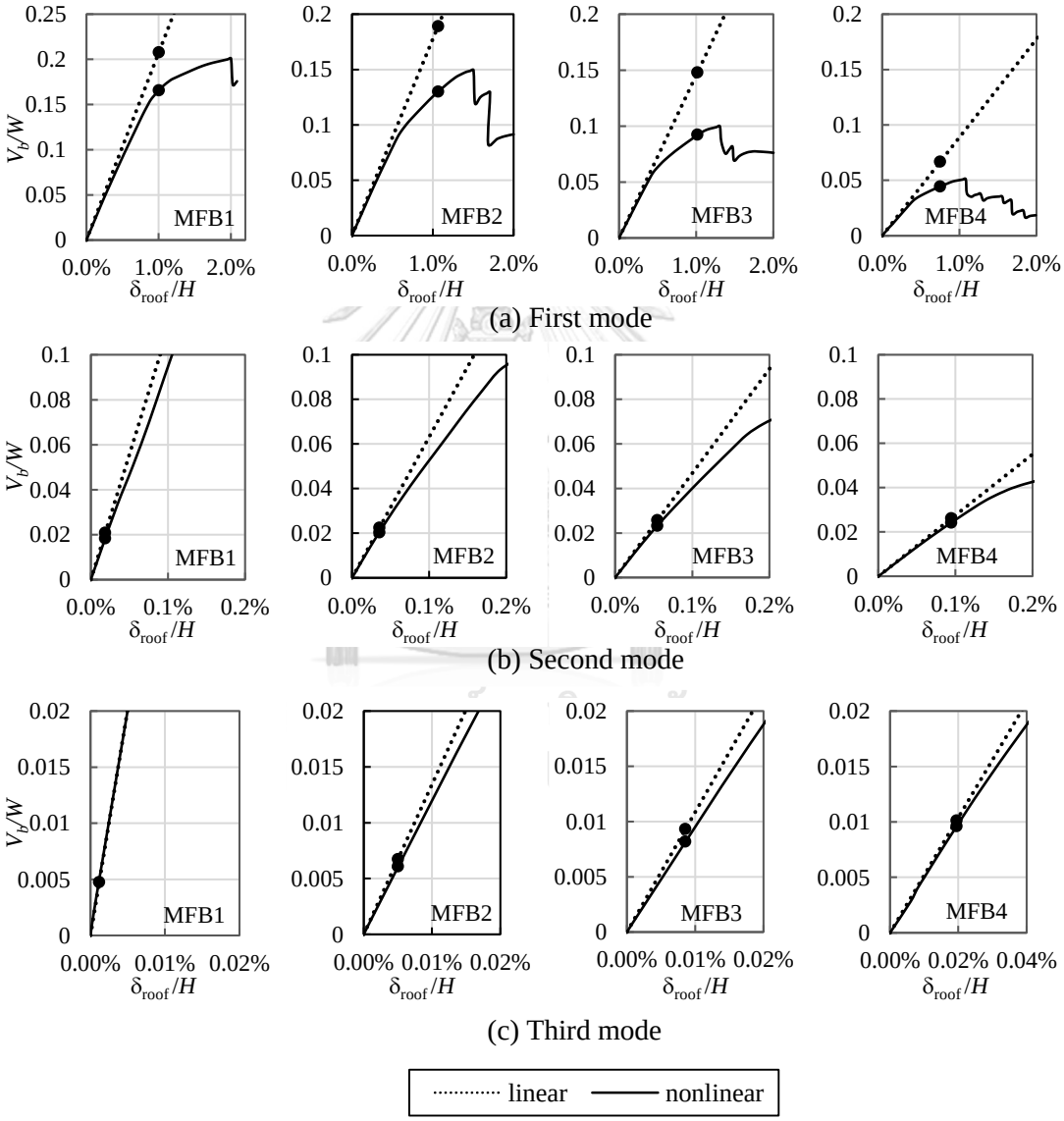

Figure 5.7 Linear and nonlinear pushover curves along with the target roof displacements of the first-three translational modes of RC frame buildings in Bangkok: (a) first mode; (b) second mode; and (c) third mode. The black dots in each figure indicate the target roof displacement.

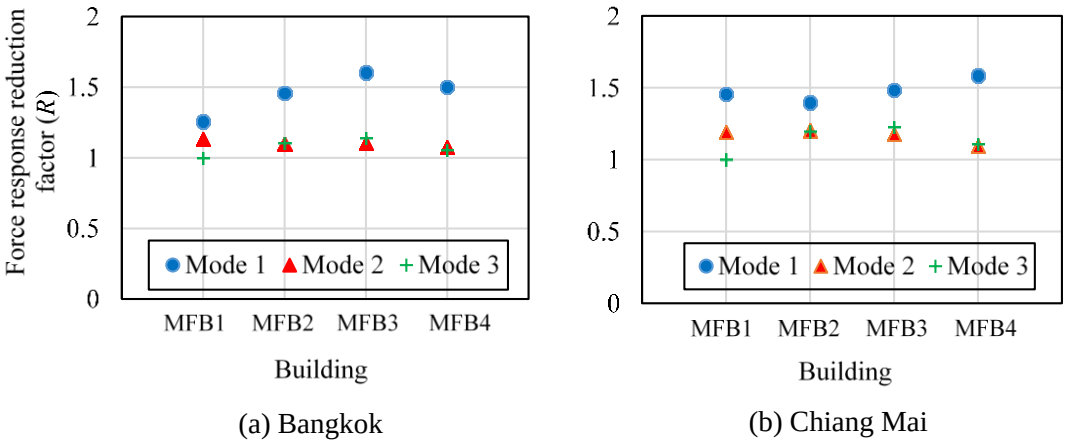

Figure 5.8 Force response reduction factor of each mode for RC frame buildings in: (a) Bangkok; and (b) Chiang Mai.

5.4 Accuracy of modified RSA procedure

5.4.1 Shear forces

The modified RSA procedure based on higher-mode-elastic ($MRSA_{HE}$) as shown in Eq. (4.12) was evaluated in this Section. The scaling factors (*SF*) are shown in Table 5.1. The over-strength factor in ASCE 7-10 (Ω=3) and more actual over-strength factors computed using pushover analysis as shown in Figure 5.6 were used. $MRSA_{HE}$ computed using code over-strength factor and more actual over-strength factor are defined as $MRSA_{HE}(\Omega=3)$ and $MRSA_{HE}(\Omega_{actual})$, respectively. The first-fourth translational modes were used. The capacity design method in ACI 318M-14 using probable flexural strength at both ends of beams or columns to compute their shear forces was also evaluated. The probable strength refers to the actual strength computed using expected material strength as explained in Section 3.2.2.

Story shear forces, column shear forces, and beam shear forces computed from RSA, $MRSA_{HE}$, capacity design, and NLRHA procedures are compared in Figures 5.9, 5.10, and 5.11, respectively. It showed that the $MRSA_{HE}$ and capacity design methods significantly improved the underestimation of the RSA method in computing shear forces for all cases. For frame building, the first-mode response contributes significantly to the total response. Accuracy of $MRSA_{HE}$ is sensitive to the first-mode response which depends on over-strength factor Ω. The $MRSA_{HE}(\Omega_{actual})$ provided good estimates of shear

forces for all cases, while $MRSA_{HE}(\Omega=3)$ underestimated for 3-story (MFB1) and 6-story (MFB2) in Bangkok when compared with NLRHA because actual over-strength factors in these two buildings are significantly larger than over-strength factor in the code ($\Omega=3$) as shown in Figure 5.6. The capacity design method generally provided larger shear forces than NLRHA because the probable flexural strengths were not developed at both ends of all columns and beams at all floors. For columns (Figure 5.10), capacity design method overestimated at the upper floors where columns did not experience flexural yielding, while the $MRSA_{HE}(\Omega_{actual})$ provided good agreement with NLRHA. For beams (Figure 5.11), shear forces were significantly resulted from gravity loads. Shear forces from RSA were lower than NLRHA results, but the underestimation was not as significant as for the case of columns. $MRSA_{HE}(\Omega_{actual})$ can well capture shear forces in beams along the height compared with NLRHA, whereas, capacity design provided conservative results at the upper floors where beams did not experience much yielding.

จุฬาลงกรณ์มหาวิทยาลัย
CHULALONGKORN UNIVERSITY

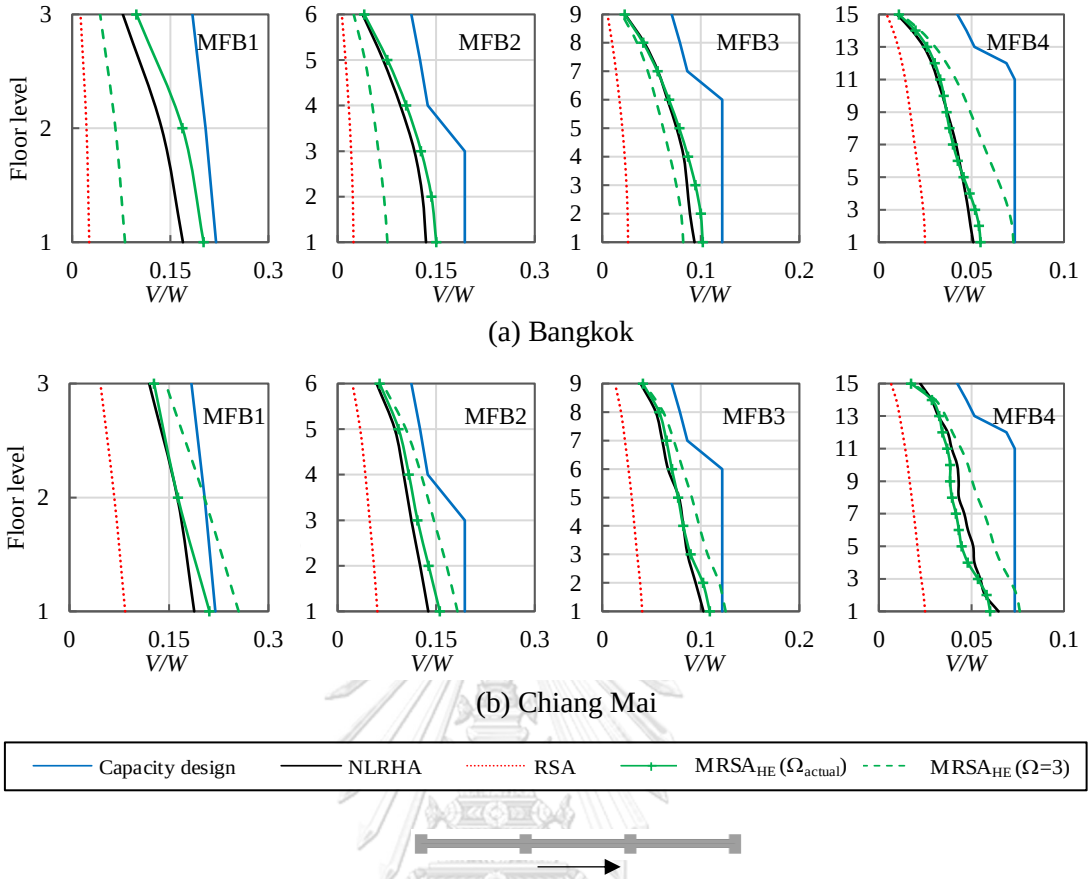

Figure 5.9 Mean values of peak story shear forces computed by RSA, MRSA$_{HE}$, capacity design, and NLRHA procedures for RC frame buildings in: (a) Bangkok; and (b) Chiang Mai.

จุฬาลงกรณ์มหาวิทยาลัย
CHULALONGKORN UNIVERSITY

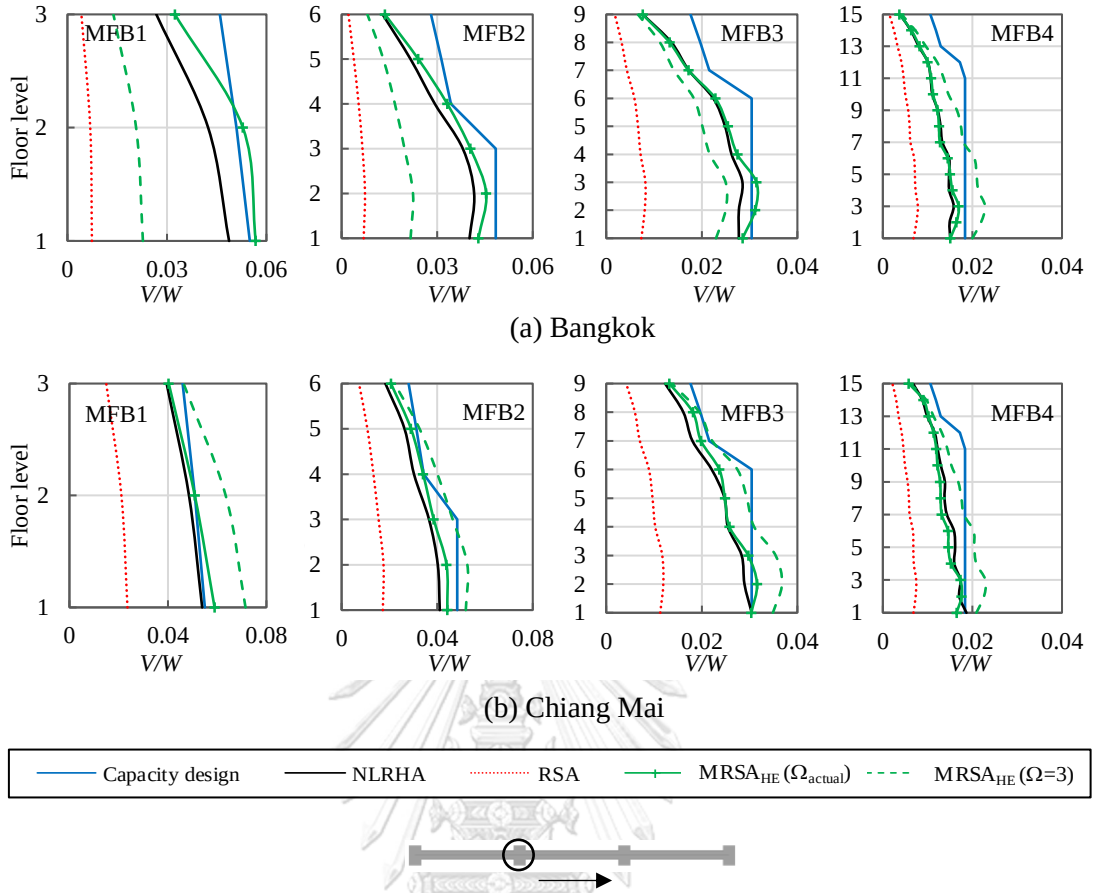

Figure 5.10 Mean values of peak shear forces in RC columns computed by RSA, MRSA$_{HE}$, capacity design, and NLRHA procedures for RC frame buildings in: (a) Bangkok; and (b) Chiang Mai. The circle indicates the location of column considered.

จุฬาลงกรณ์มหาวิทยาลัย
CHULALONGKORN UNIVERSITY

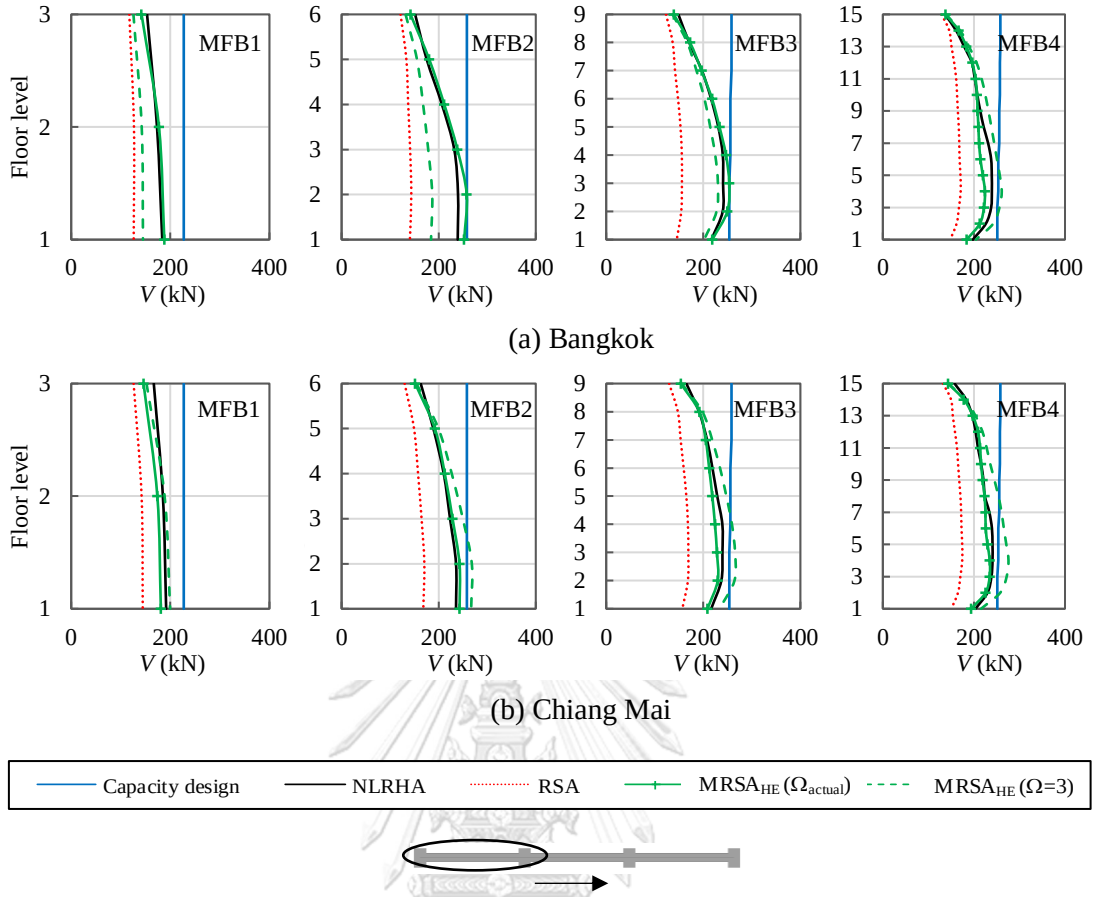

Figure 5.11 Mean values of peak shear forces in RC beams computed by RSA, MRSA$_{HE}$, capacity design, and NLRHA procedures for RC frame buildings in: (a) Bangkok; and (b) Chiang Mai. The circle indicates the location of beam considered.

จุฬาลงกรณ์มหาวิทยาลัย
CHULALONGKORN UNIVERSITY

5.4.2 Strains in columns

The variation along the height of predicted strains and inelastic strains in RC columns computed by MRSA and NLRHA procedures is presented in Figure 5.12. For RC moment-frame buildings MFB1-MFB4, inelasticity mostly occurred in RC beams throughout the height of the building because moment-frame buildings were designed to satisfy with strong column-week beam requirement. As found in this study, plastic hinges occurred in RC beams along the height of the buildings and yielding occurred in columns at the base for 3-, 6-, and 9-story buildings in Bangkok (low seismicity) as shown in Figure 5.12a and at the base and the top floors for 3-, 6-, and 9-story buildings in Chiang Mai

(moderate seismicity) with strains at top floors lower than those at the base (Figure 5.12b), except for the 15-story building (MFB4) in Chiang Mai, where strains at top floors were larger than those at the base and yielding occurred at the top floors because column section sizes were relatively lower than those at the base for the 15-story building. Tensile strains were larger than the compressive strains for all buildings. The predicted strains in MRSA method were in good agreement with inelastic strains in the columns computed from NLRHA for most cases. In practice, the locations of yielding and ductile detailing in RC columns can be estimated by the proposed method.

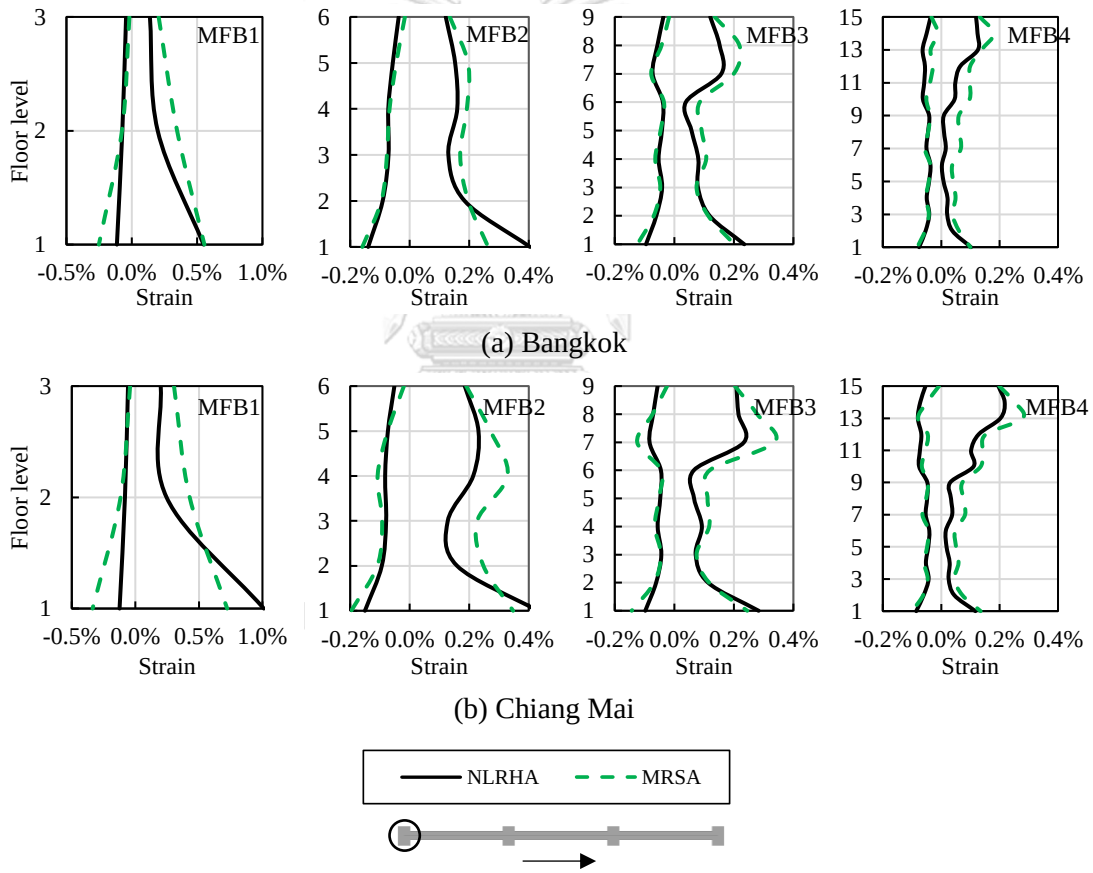

Figure 5.12 Mean values of peak vertical axial strains in RC columns computed by MRSA and NLRHA procedures for RC frame buildings in (a) Bangkok; (b) Chiang Mai. The circle indicates the location of the column considered.

5.5 Summary

The main findings of this chapter are summarized as the followings:

(1) The RSA procedure underestimates floor displacement and story drift ratio for RC moment-frame buildings and linear RSA can well predict floor displacement and story drift ratio when compared with NLRHA.

(2) Shear force determined from RSA procedure should not be used for design because it is too small when compared with NLRHA result.

(3) The force response reduction factor decreases with increasing mode order and is rather lower than response modification factor used in the design due to the scaling factor required by the code and over-strength factor inherent in the design. Higher-mode responses behave almost in the elastic range for all RC frame buildings.

(4) Capacity design method generally overestimates results from NLRHA.

(5) For RC frame buildings, accuracy of $MRSA_{HE}$ is sensitive to the first-mode response which depends on over-strength factor inherent in design. Using an actual over-strength factor, $MRSA_{HE}$ can estimate well NLRHA results for all cases.

(6) The proposed method to compute strain in MRSA procedure can provide good accuracy in predicting inelastic strain in RC columns computed from NLRHA for all studied buildings.

จุฬาลงกรณ์มหาวิทยาลัย
CHULALONGKORN UNIVERSITY

CHAPTER 6
CONCLUSIONS AND RECOMMENDATIONS

6.1 Conclusions

6.1.1 Seismic demands from NLRHA using CMS and UHS as target spectrum

Seismic demands of four tall buildings located on soft-soil Bangkok computed by NLRHA using conditional mean spectrum (CMS) and uniform hazard spectrum (UHS) as target spectrum to select and scale of earthquake records were compared. The results suggested that when using CMS ground motions with tall buildings, it is required to consider more than one conditioning period. Multiple CMSs considering higher-mode periods should be included in the analysis and the design demand values should be determined by enveloping of results computed using multiple CMS ground motions. Using UHS as target spectrum with spectral matching ground motions can provide results close to multiple CMSs and significantly reduces computational effort as only one set of analysis is required as opposed to multiple sets of analysis required when using CMS as target spectrum.

6.1.2 Modified response spectrum analysis procedure

A modified response spectrum analysis (MRSA) procedure with two methods to compute design shear forces was proposed together with a method to compute strains to identify ductile detailing locations in RC walls and columns of tall RC shear-wall buildings and RC moment-frame buildings. The accuracy of the RSA procedure and the proposed MRSA procedure was evaluated by comparing the computed demands to the benchmark results computed from NLRHA using six tall RC shear-wall buildings and four RC moment-frame buildings subjected to large-magnitude long-distance soft-soil ground motions (Bangkok) and moderate-magnitude short-distance stiff-soil ground motions (Chiang Mai). The main findings of this study are summarized as the followings:

(1) The RSA procedure provides good estimates for floor displacements and story drift ratios for RC shear-wall buildings, but underestimates for RC moment-frame buildings. Linear RSA is suggested to use for RC moment-frame buildings as it

can predict well floor displacements and story drift ratios when compared with NLRHA.

(2) Shear forces determined from conventional RSA procedure should not be used for design because it is too small when compared with NLRHA results. As structural wall is normally designed to experience ductile flexural yielding, bending moments computed from RSA procedure may be used for design. However, it is necessary to identify the locations where these ductile flexural yielding occur, so that ductile detailing can be implemented.

(3) Force response reduction factor decreases with increasing mode order and is lower than the response modification factor (R) in ASCE 7-10 used to compute the design force demands of structures due to the over-strength factor inherent in the design and the scaling factor required to scale RSA modal base shear to at least 85% of ELF base shear, which results in an effective modification factor (R_{eff}) smaller than R factor. Using a single R factor to reduce elastic forces from all modes is the primary cause of underestimation in computing force demands in the RSA procedure. Different R factor for each mode should be used to compute more actual force demands in structures.

(4) Higher-mode responses behave mostly in the elastic range for 15-story and 20-story tall RC shear-wall buildings and for all RC frame buildings and deform beyond elastic limit for 31-story and 39-story tall RC shear-wall buildings.

(5) The first modified RSA method ($MRSA_{HE}$) based on higher-mode-elastic approach can predict well shear forces computed from NLRHA for 15- and 20-story tall RC shear-wall buildings and conservatively for 31- and 39-story tall RC shear-wall buildings.

(6) The second modified RSA method ($MRSA_{HI}$) based on higher-mode inelastic approach can reduce the conservativeness of the $MRSA_{HE}$ method for tall buildings, but it requires a nonlinear structural model to compute force response reduction factor for each mode.

(7) For RC frame buildings, accuracy of $MRSA_{HE}$ is sensitive to the first-mode response which depends on over-strength factor inherent in design. Using an actual over-strength factor, $MRSA_{HE}$ can estimate well NLRHA results for all cases.

(8) In both $MRSA_{HE}$ and $MRSA_{HI}$ methods, bending moment demands are computed and designed for in the same way as conventional RSA procedure but with ductile detailing of RC walls or columns required at locations where strain exceeds a certain limit, for example, 0.002. The proposed method to compute strains in the MRSA procedure can provide good accuracy in predicting inelastic strains in RC walls and columns computed from NLRHA for most of the studied buildings.

6.2 Suggestions for design practice

The MRSA procedure is suggested for design practice and for future revision of a seismic design standard to compute design demands in tall RC shear-wall buildings and RC moment-frame buildings. The MRSA procedure will be to ensure that the computed design demands on tall buildings are reasonably accurate and safe to use while maintaining the suitability for practical application.

The $MRSA_{HE}$ method can be used at the preliminary design stage as it requires only a linear structural model. The $MRSA_{HE}$ method can be easily implemented in design practice by multiplying spectral ordinate of elastic spectrum with a factor of $(SF \times \Omega_0)/R$ at the fundamental period of the building in the direction of seismic excitation. Alternatively, many commercial structural analysis software programs provide an option for user-defined scaling factors for each vibration mode, so the $MRSA_{HE}$ method can be implemented in such software programs similar to the conventional RSA procedure but including scaling factors for different modes, which makes the $MRSA_{HE}$ method suitable for design practice. However, when a nonlinear structural model is available, the $MRSA_{HI}$ method is recommended as it can provide higher accuracy than the $MRSA_{HE}$ method. For performance-based design, the $MRSA_{HI}$ method can be useful at the intermediate stage to confirm shear demands and adequate shear strengths, before conducting NLRHA for

verification at the final stage of a design project. The $MRSA_{HE}$ and $MRSA_{HI}$ methods can be used to prevent brittle shear failure in RC walls and columns in a building.

The proposed method to compute strains in RC walls and columns in the MRSA procedure can be used to identify the required ductile detailing locations in RC walls and columns to prevent ductile failure mode and crushing of concrete. Such method is not yet available in the RSA procedure.

6.3 Recommendations for future studies

The following suggestions are recommended for future studies:

(1) The results presented in this study were based on buildings without significant coupling effect between translational and torsional modes such that each dominant translational mode in a building can be identified and inelasticity of each mode can be investigated through uncoupled-mode assumption. Irregular tall buildings having significant coupling between translational and torsional modes are necessary for future studies to evaluate the accuracy of the proposed MRSA procedure.

(2) The current study considered two types of lateral force resisting systems: RC shear wall and RC moment-resisting frame. Further studies using different types of lateral force resisting system should also be carried out.

(3) Stronger ground motions than those used in this study should be used in future studies to investigate the accuracy of the proposed MRSA procedure.

(4) This study focused on soft-soil class in downtown area of Bangkok and site class D in Chiang Mai. Other site classes which strongly affect the spectral shape of design spectrum should be observed.

(5) The present study considered unidirectional earthquake when applied to structures. Tall buildings subjected to bi-directional earthquake ground motions should also be studied.

APPENDIX A
DETAILS OF STUDIED BUILDINGS

A.1 Design loads and load combinations

Gravity loads are shown in Section A.2 separately for each building. Wind loads for all buildings are computed according to the Bangkok Building Control Law (2001) as shown in Table A.1. Seismic loads are presented in Section 3.3.

Table A.1 Wind load according to the Bangkok Building Control Law (2001).

Building height (m)	Design Wind Pressure (kN/m^2)
H>80	2.0
40<H≤80	1.6
20<H≤40	1.2
10<H≤20	0.8
H≤10	0.5

Design load combinations according to DPT (1301/1302-61, 2018) were used.

$$
\begin{aligned}
&1.4D+1.7L \\
&0.75(1.4D+1.7L)+1.0E \\
&0.9D+1.0E \\
&0.75(1.4D+1.7L)+1.6W \\
&0.9D+1.6W
\end{aligned}
$$

where D is the dead loads; L is the live loads; W is the wind load; and E is the seismic load.

จุฬาลงกรณ์มหาวิทยาลัย
Chulalongkorn University

A.2 Details of tall RC shear-wall buildings

➢ 15-story building (SWB1)

Table A.2 Concrete sections of structural members in 15-story building (SWB1).

Floor	Column size (m x m)				Wall thickness (m)			Slab thickness (m)	Coupling beam (m x m)
	C1	C2	C3	C4	SW1	SW2	SW3		
14th-15th	0.6 x 0.6	0.6 x 0.6	0.6 x 0.6	0.6 x 0.6	0.25	0.25	0.25	0.25	0.25 x 1
11th-13th	0.6 x 0.6	0.6 x 0.6	0.6 x 0.6	0.6 x 0.6	0.25	0.25	0.25	0.25	0.25 x 1
8th-10th	0.6 x 0.6	0.6 x 0.6	0.6 x 0.6	0.6 x 0.8	0.25	0.25	0.25	0.25	0.25 x 1
6th-7th	0.6 x 0.6	0.6 x 0.8	0.6 x 0.8	0.6 x 0.8	0.25	0.25	0.25	0.25	0.25 x 1
4th-5th	0.6 x 0.6	0.6 x 0.8	0.6 x 0.8	0.6 x 1.2	0.25	0.25	0.25	0.25	0.25 x 1
1st-3rd	0.6 x 0.6	0.8 x 0.8	0.6 x 1.2	0.6 x 1.2	0.25	0.25	0.25	0.25	0.25 x 1

Table A.3 Design gravity loads.

Floor	Super-imposed dead load (kN/m^2)	Live load (kN/m^2)
1st-15th	2.5	3

จุฬาลงกรณ์มหาวิทยาลัย
CHULALONGKORN UNIVERSITY

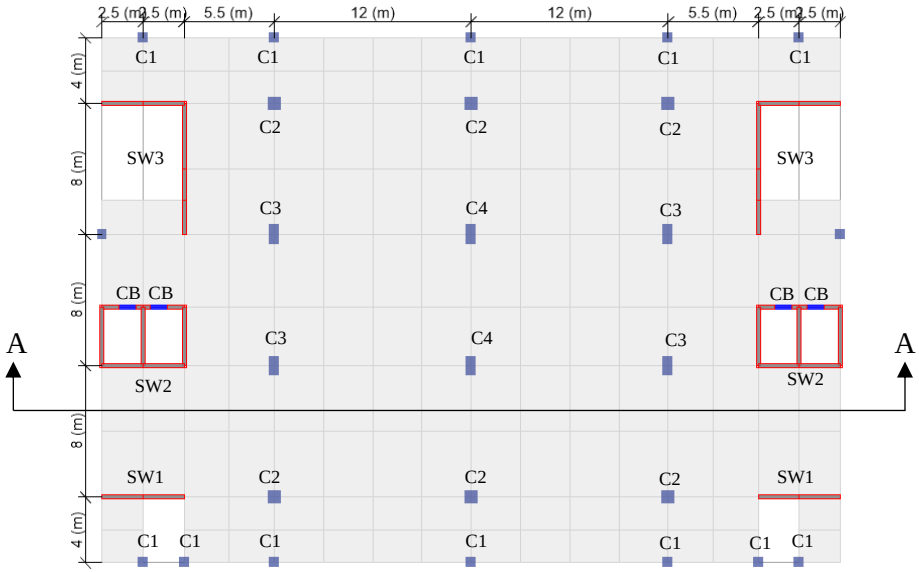

1st to 15th floor

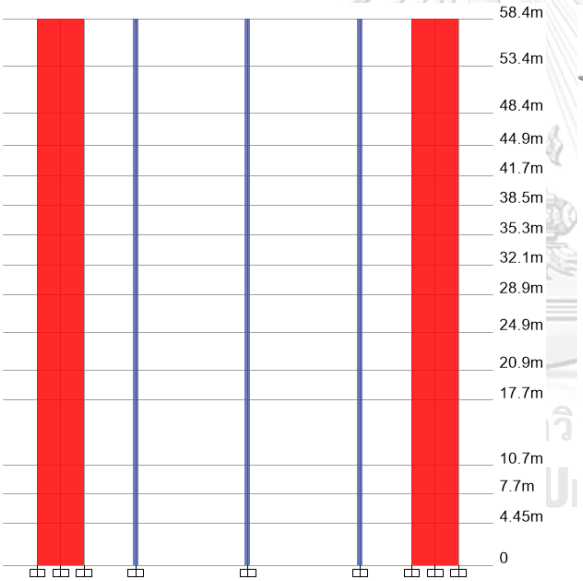

Elevation: cut AA

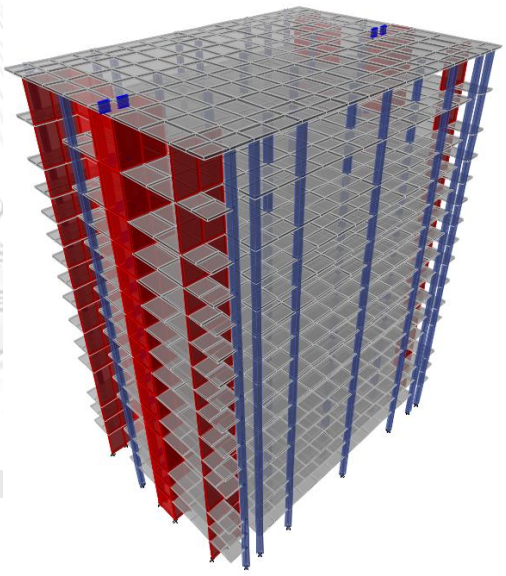

3D model

Figure A.1 15-story building SWB1.

➢ 20-story building (SWB2)

Table A.4 Concrete sections of structural members in 20-story building (SWB2).

Floor	Wall thickness (m)			Slab thickness (m)	Beam section (m x m)			
	SW1	SW2	Core		B1	B2	B3	CB
14th-20th	-	0.12	0.2	0.2	-	-	-	0.2 x 0.5
8th-13th	-	0.15	0.2	0.2	-	-	-	0.2 x 0.5
5th-7th	-	0.2	0.2	0.2	-	-	-	0.2 x 0.5
1st-4th	0.2	0.2	0.2	0.2	0.2 x 0.7	0.15 x 0.6	0.2 x 0.6	0.2 x 0.5

Table A.5 Design gravity loads.

Floor	Super-imposed dead load (kN/m^2)	Live load (kN/m^2)
5th-20th	2.5	2
1st-4th	2.5	4

จุฬาลงกรณ์มหาวิทยาลัย
CHULALONGKORN UNIVERSITY

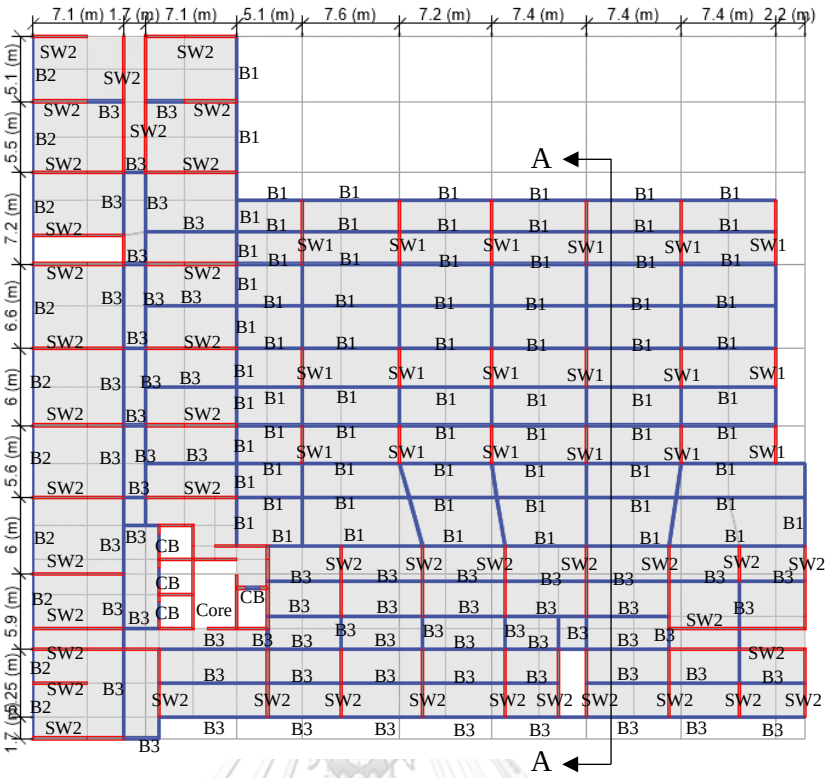

1st to 4th floor

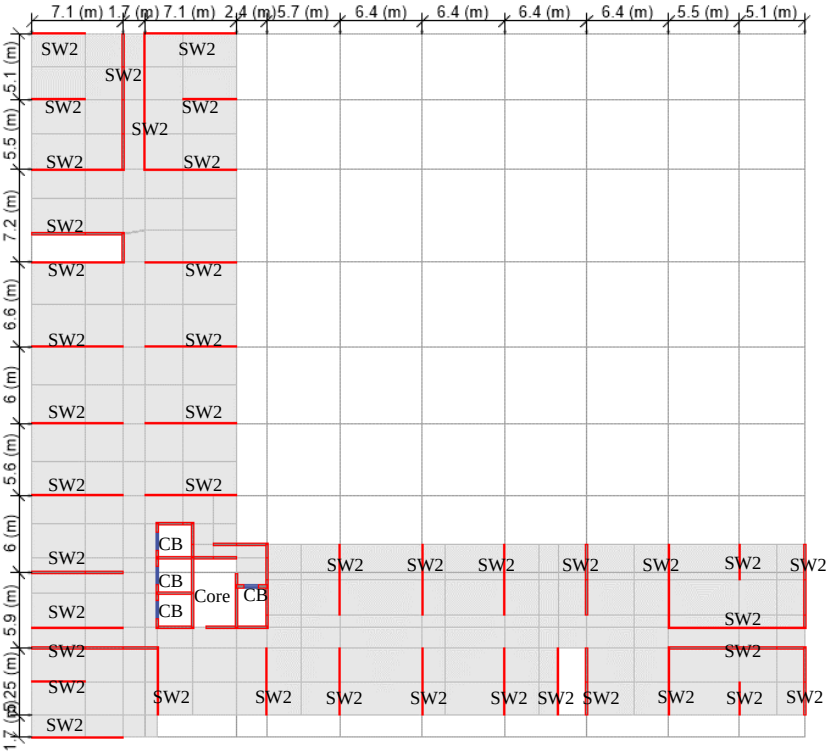

5th to 20th floor

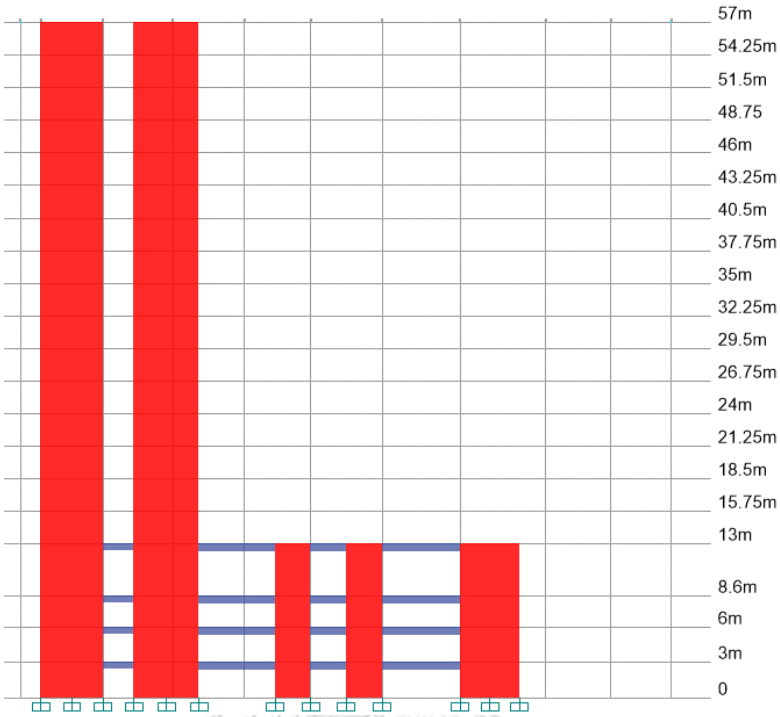

Elevation: cut AA

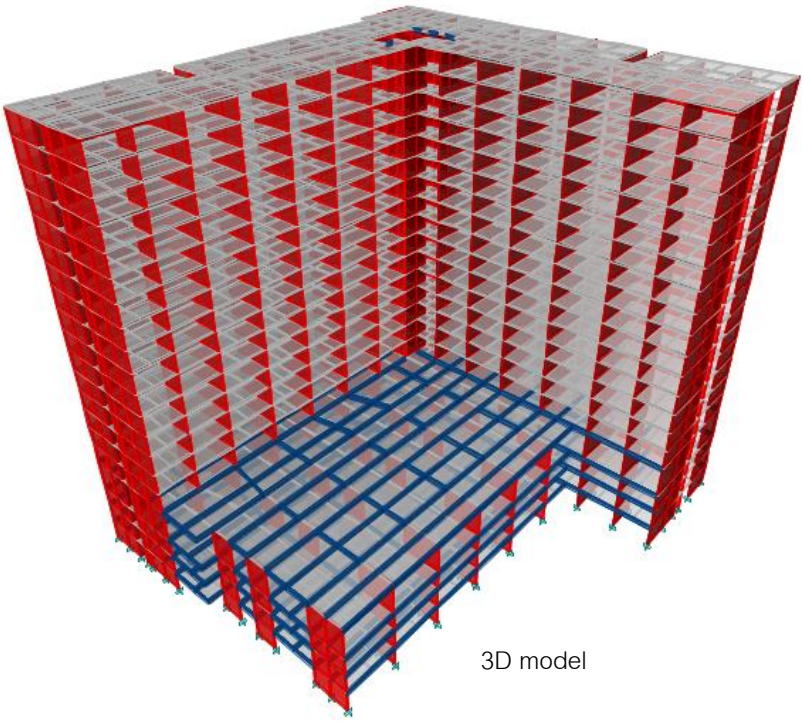

3D model

Figure A.2 20-story building SWB2.

➢ 31-story building (SWB3)

Table A.6 Concrete sections of structural members in 31-story building (SWB3).

Floor	Column size (m x m)				Wall thickness (m)			Slab thickness (m)	Coupling beam (m x m)
	C1	C2	C3	C4	SW1	SW2	SW3		
26th-31st	-	-	1.0 x 0.4	1.0 x 0.4	-	0.3	0.3	0.25	0.3 x 0.8
21th-25th	-	-	1.0 x 0.4	1.2 x 0.4	-	0.3	0.3	0.25	0.3 x 0.8
16th-20th	-	-	1.0 x 0.4	1.4 x 0.4	-	0.3	0.3	0.25	0.3 x 0.8
11th-15th	-	-	1.0 x 0.4	1.6 x 0.4	-	0.3	0.3	0.25	0.3 x 0.8
6th-10th	-	-	1.0 x 0.4	1.8 x 0.4	-	0.3	0.3	0.25	0.3 x 0.8
1st-5th	1.1 x 0.3	1.1 x 0.45	1.0 x 0.5	1.8 x 0.5	0.15	0.3	0.3	0.25	0.3 x 0.8

Table A.7 Design gravity loads.

Floor	Super-imposed dead load (kN/m^2)	Live load (kN/m^2)
6th-31st	3	2
1st-5th	3	4

จุฬาลงกรณ์มหาวิทยาลัย
CHULALONGKORN UNIVERSITY

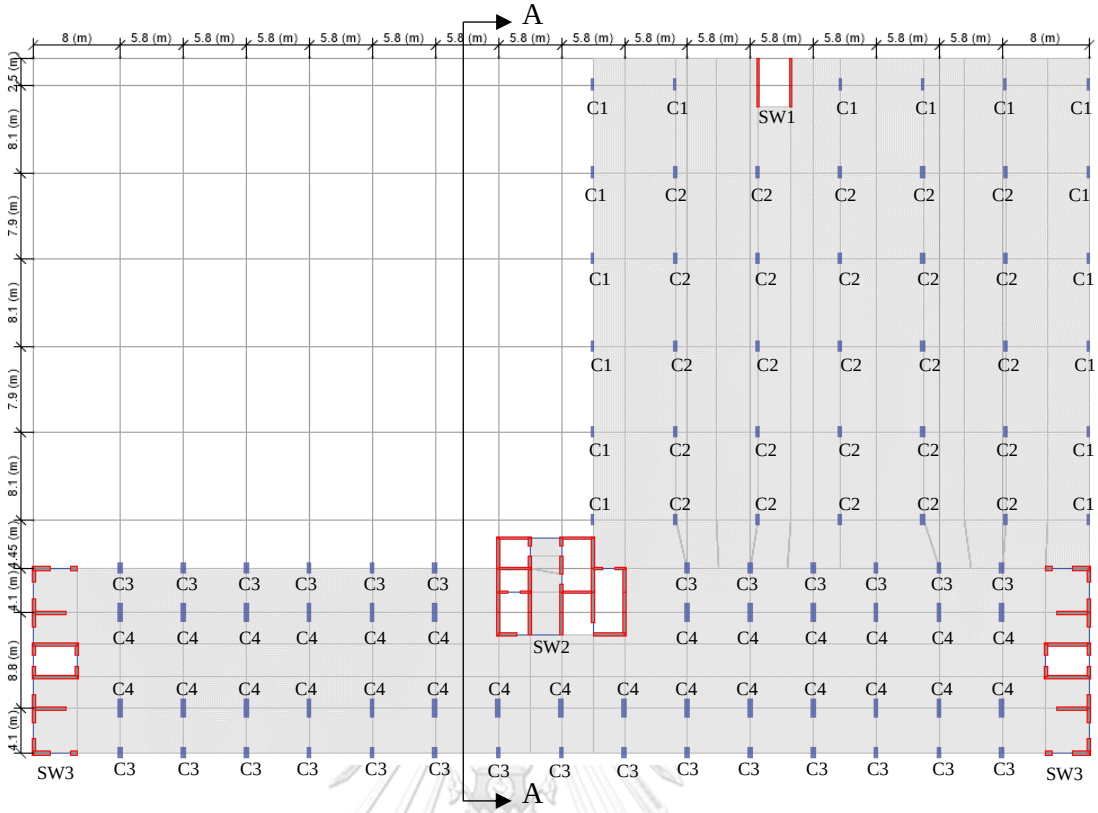

1st to 5th floor

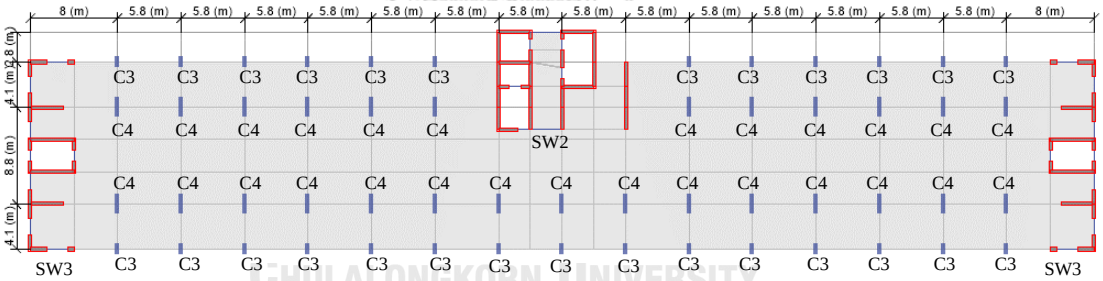

6th to 31st floor

CHULALONGKORN UNIVERSITY

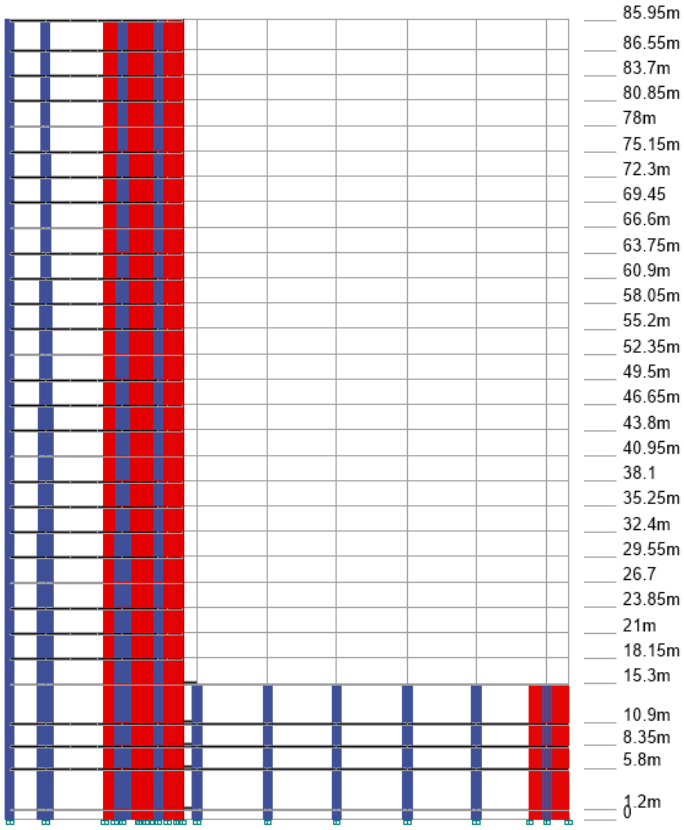

Elevation: cut AA

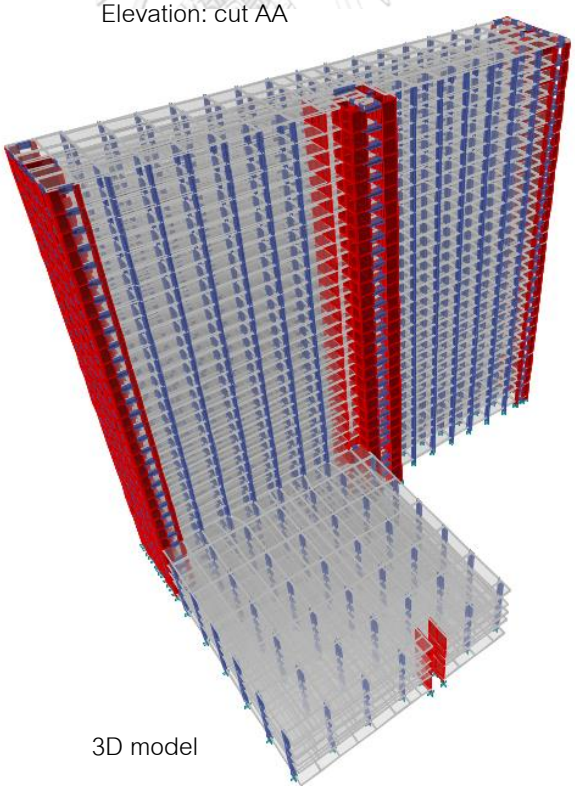

3D model

Figure A.3 31-story building SWB3.

➢ 39-story building (SWB4)

Table A.8 Concrete sections of structural members in 39-story building (SWB4).

Floor	Column size (m x m)			Wall thickness (m)		Slab thickness (m)	Coupling beam (m x m)	
	C1	C2	C3	Core 1	Core 2		CB1	CB2
37th-39th	0.8 x 0.8	-	-	0.3	0.35	0.25	0.3 x 1	0.35 x 1
14th-36th	0.8 x 1.2	-	-	0.3	0.35	0.25	0.3 x 1	0.35 x 1
12th-13th	0.8 x 1.4	-	-	0.3	0.35	0.25	0.3 x 1	0.35 x 1
9th-11th	0.8 x 1.6	-	-	0.3	0.35	0.25	0.3 x 1	0.35 x 1
1st-8th	0.8 x 1.8	0.6 x 0.6	0.6 x 0.6	0.3	0.35	0.3	0.3 x 1	0.35 x 1

Table A.9 Design gravity loads.

Floor	Super-imposed dead load (kN/m^2)	Live load (kN/m^2)
9th-39th	2.5	2
1st-8th	2.5	3

จุฬาลงกรณ์มหาวิทยาลัย
CHULALONGKORN UNIVERSITY

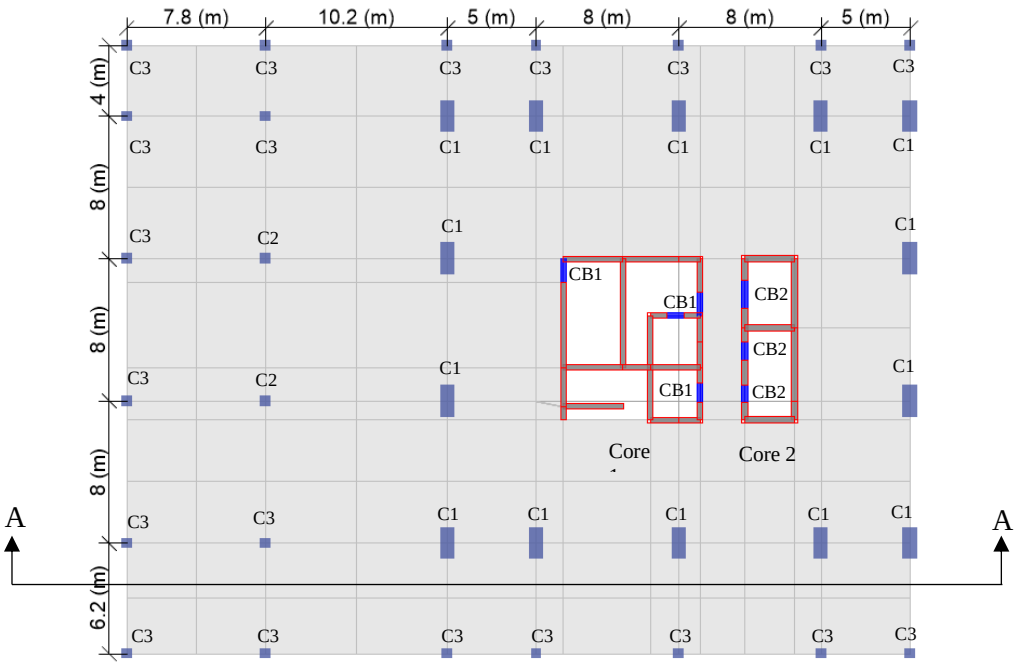

1st to 8th floor

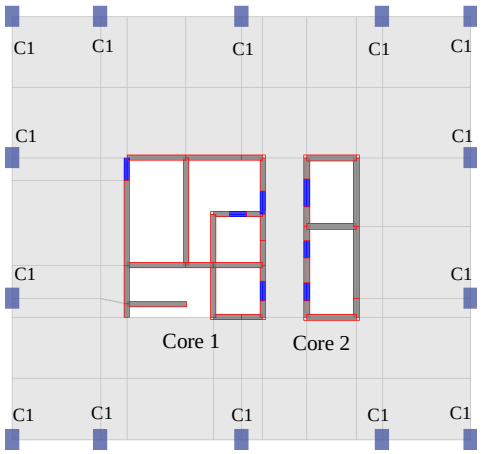

9th to 39th floor

จุฬาลงกรณ์
CHULALONGKO

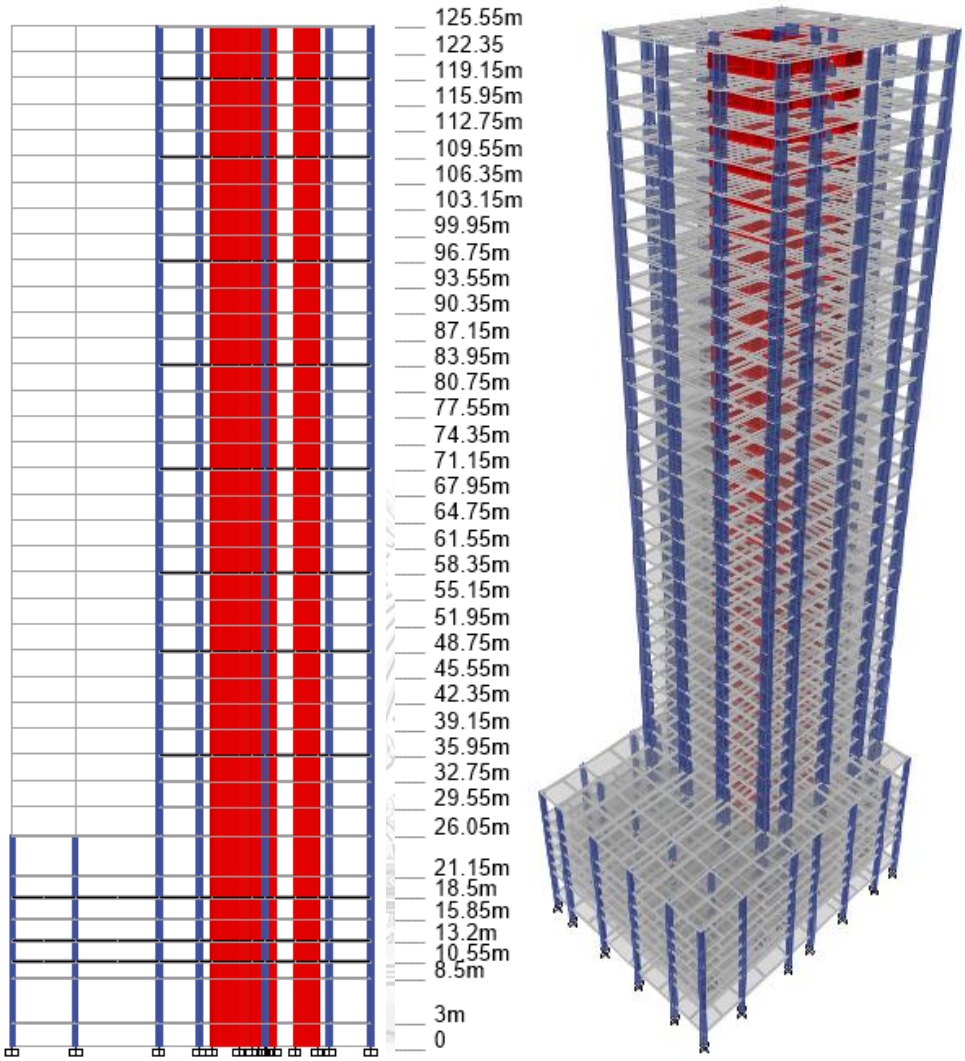

Elevation: cut AA 3D model

จุฬาลงกรณ์มหาวิทยาลัย
CHULALONGKORN UNIVERSITY

Figure A.4 39-story building SWB4

➢ 20-story building (SWB5)

Table A.10 Concrete sections of structural members in 39-story building (SWB5).

Floor	Column size (m x m)			Wall thickness (m)		Slab thickness (m)	Coupling beam (m x m)
	C1	C2	C3	Core 1	Core 2		
17th-20th	0.6 x 0.6	-	-	0.25	0.25	0.25	0.25 x 1
13th-16th	0.6 x 0.8	-	-	0.25	0.25	0.25	0.25 x 1
9th-12th	0.6 x 1.0	-	-	0.25	0.25	0.25	0.25 x 1
5th-8th	0.6 x 1.2	0.6 x 0.6	0.6 x 0.6	0.25	0.25	0.25	0.25 x 1
1st-4th	0.6 x 1.5	0.6 x 0.6	0.6 x 0.6	0.25	0.25	0.3	0.25 x 1

Table A.11 Design gravity loads.

Floor	Super-imposed dead load (kN/m^2)	Live load (kN/m^2)
9th-20th	2.5	2
1st-8th	2.5	3

จุฬาลงกรณ์มหาวิทยาลัย
CHULALONGKORN UNIVERSITY

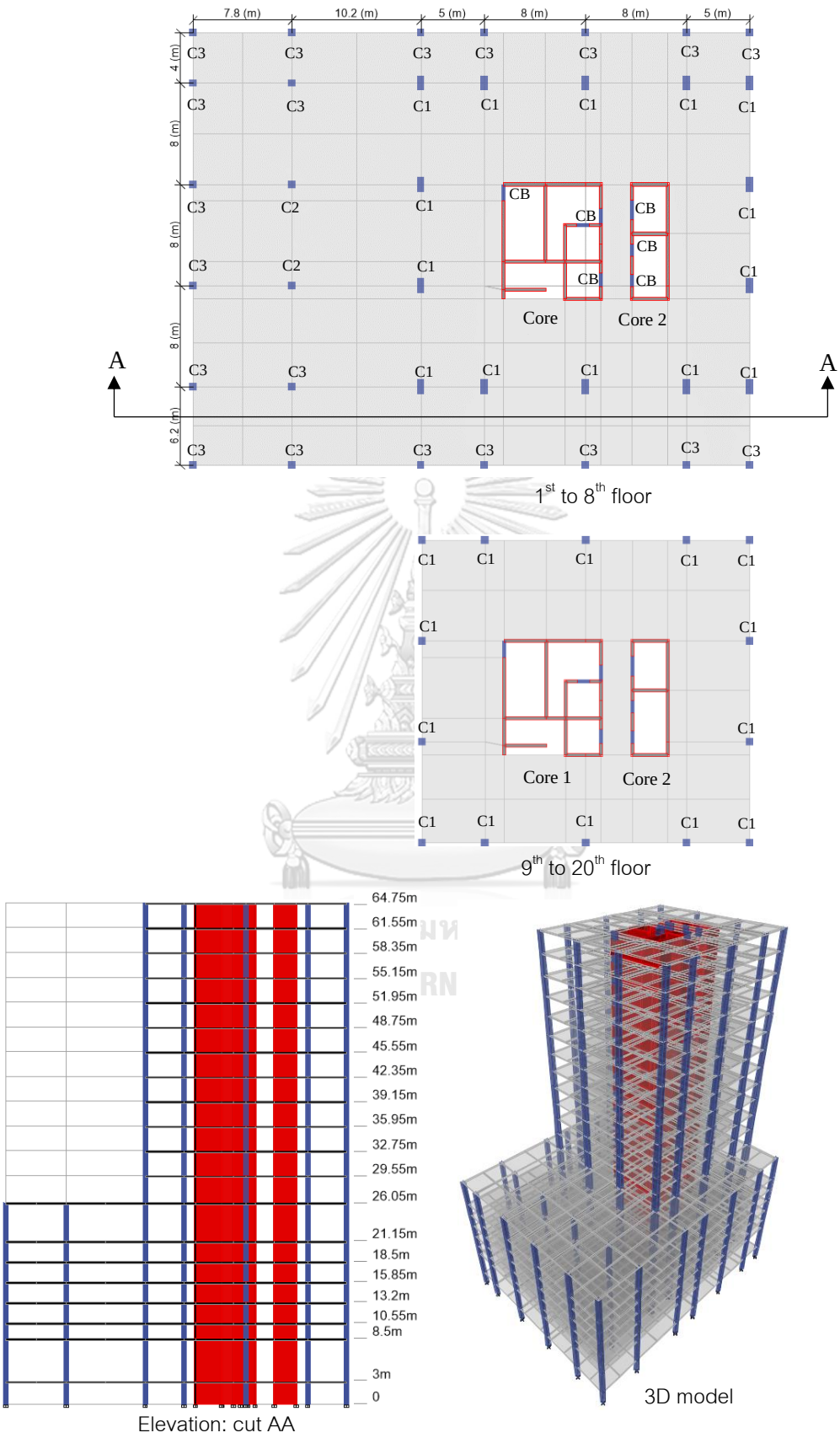

Figure A.5 20-story building SWB5.

➢ 39-story building (SWB6)

Table A.12 Concrete sections of structural members in 39-story building (SWB6).

Floor	Column size (m x m)			Wall thickness (m)			Slab thickness (m)	Coupling beam (m x m)	
	C1	C2	C3	Core 1	Core 2	Core 3		CB1	CB2
37th-39th	0.8 x 0.8	-	-	0.3	0.35	-	0.25	0.3 x 1	0.35 x 1
14th-36th	0.8 x 1.2	-	-	0.3	0.35	-	0.25	0.3 x 1	0.35 x 1
12th-13th	0.8 x 1.4	-	-	0.3	0.35	-	0.25	0.3 x 1	0.35 x 1
9th-11th	0.8 x 1.6	-	-	0.3	0.35	-	0.25	0.3 x 1	0.35 x 1
1st-8th	0.8 x 1.8	0.8 x 0.8	0.8 x 0.8	0.3	0.35	0.25	0.3	0.3 x 1	0.35 x 1

Table A.13 Design gravity loads.

Floor	Super-imposed dead load (kN/m^2)	Live load (kN/m^2)
9th-39th	2.5	2
1st-8th	2.5	3

จุฬาลงกรณ์มหาวิทยาลัย
CHULALONGKORN UNIVERSITY

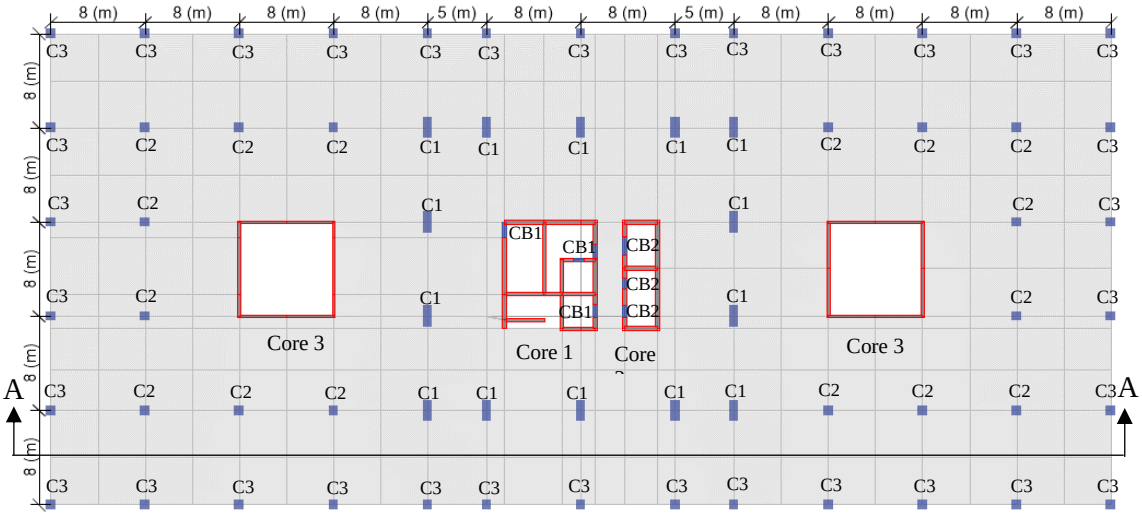

1st to 8th floor

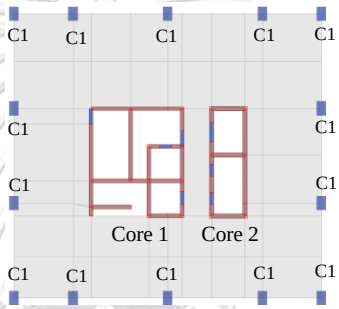

9th to 39th floor

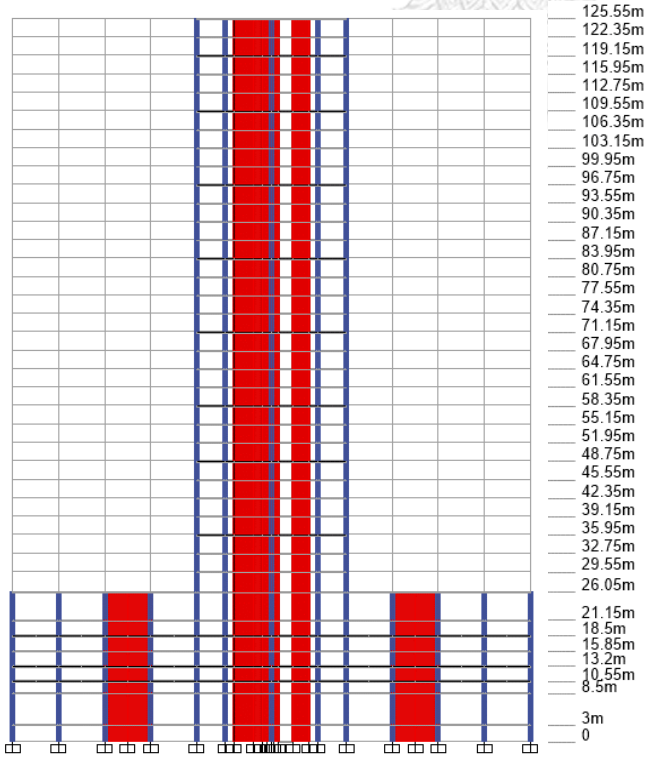

Elevation: cut AA

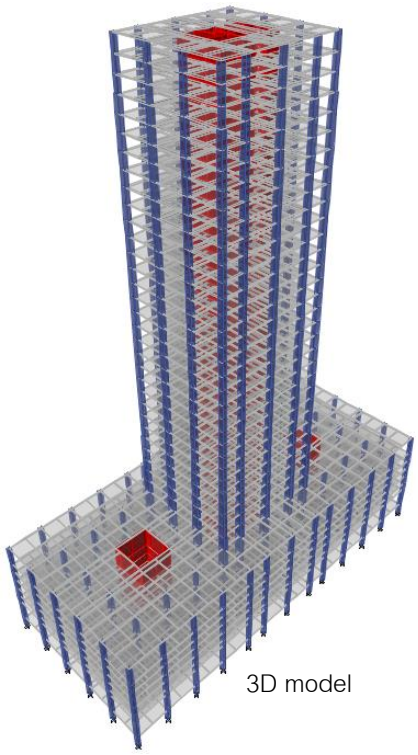

3D model

Figure A.6 39-story building SWB6.

A.3 Details of RC moment-frame buildings

Slabs were not included in the structural model. The thickness of the slab was taken equal to 0.15m. The self-weight of the slab was 24 x 0.15=3.6kN/m^2.

Table A.14 Design gravity loads.

Load case	Value
Super-imposed dead load	2.5 kN/m^2
Live load	2.5 kN/m^2

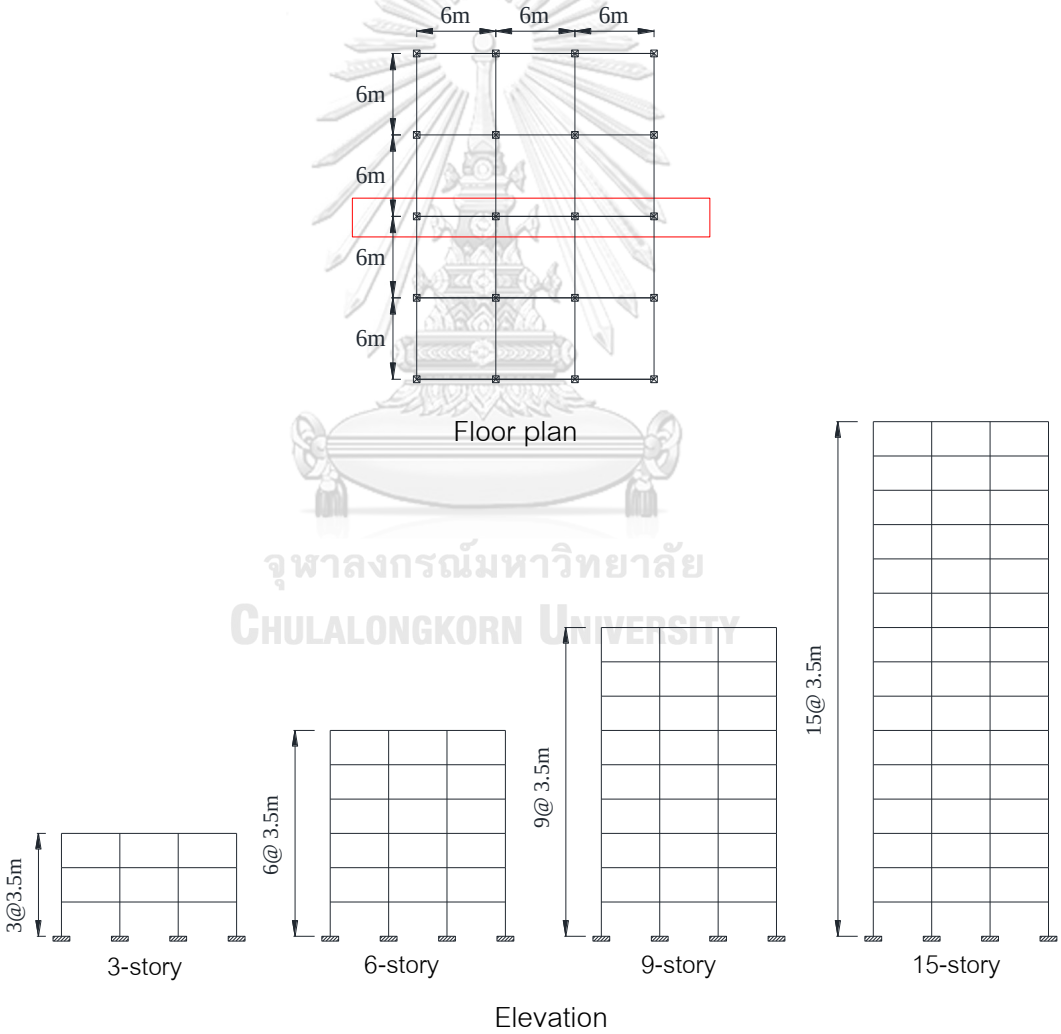

Figure A.7 RC moment-frame buildings

Table A.15 Concrete sections and steel reinforcements of beams and columns of RC frame buildings.

Floor Level	3-story		6-story		9-story		15-story	
	Column (mm x mm)	Beam (mm x mm)	Column (mm x mm)	Beam (mm x mm)	Column (mm x mm)	Beam (mm x mm)	Column (mm x mm)	Beam (mm x mm)
13-15							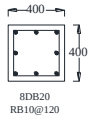	
10-12							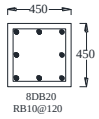	
7-9					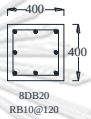		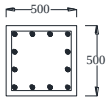	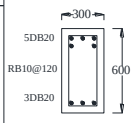
4-6			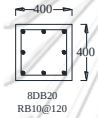	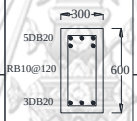	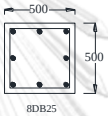	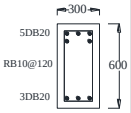	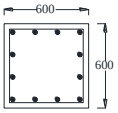	
1-3		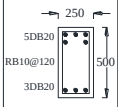			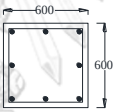		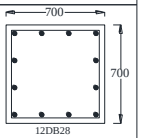	

จุฬาลงกรณ์มหาวิทยาลัย
CHULALONGKORN UNIVERSITY

APPENDIX B

TIME HISTORY OF EARTHQUAKE GROUND ACCELERATIONS

B.1 Bangkok

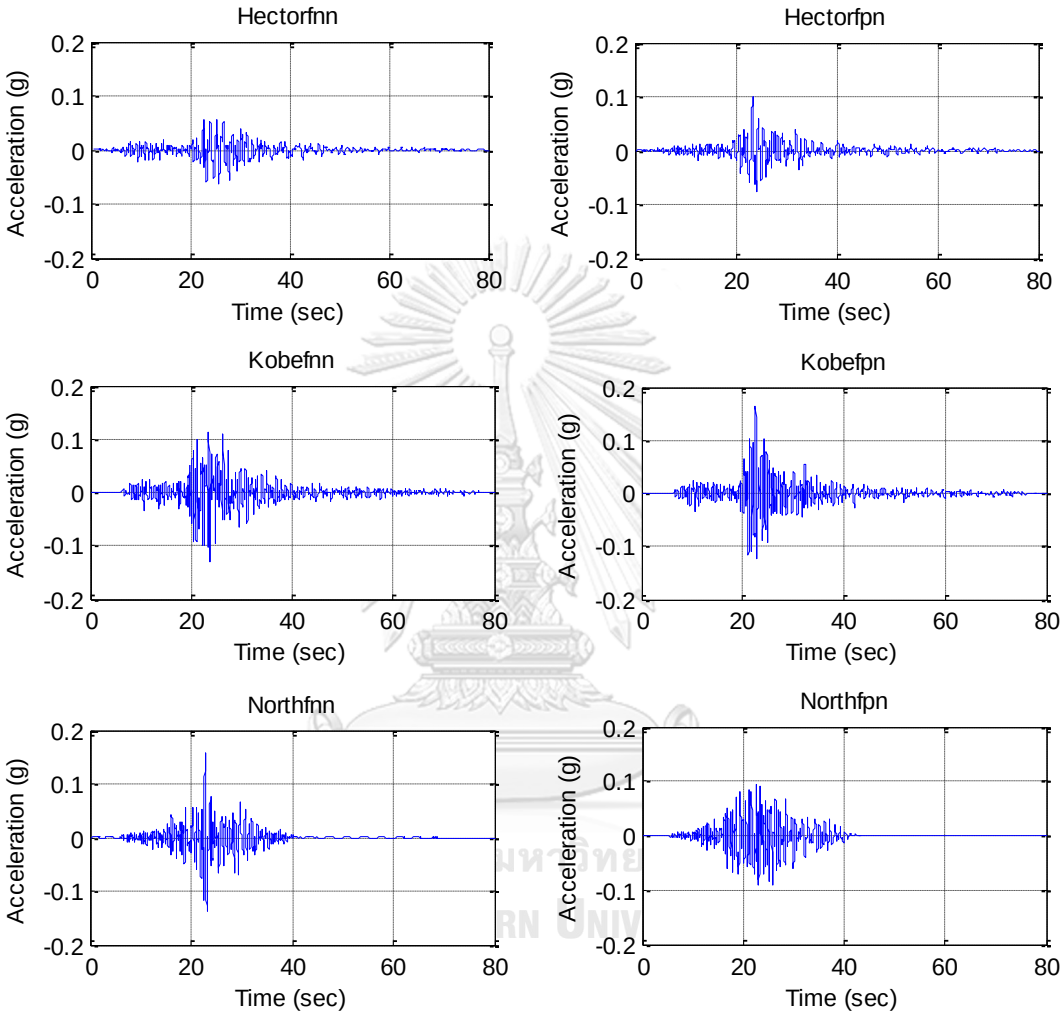

(a) Six soft-soil ground acceleration for CMS at 0.2sec

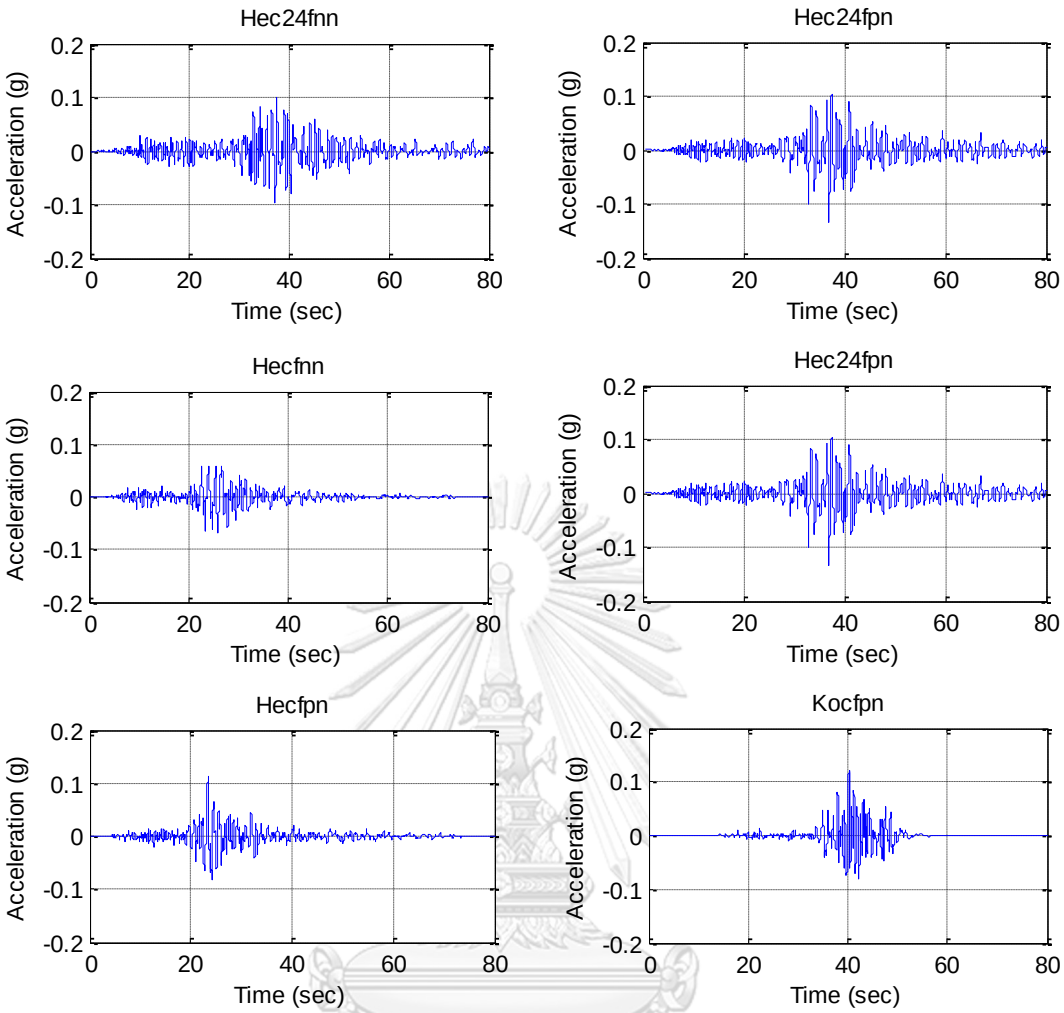

(b) Six soft-soil ground accelerations for CMS at 0.5sec

จุฬาลงกรณ์มหาวิทยาลัย
CHULALONGKORN UNIVERSITY

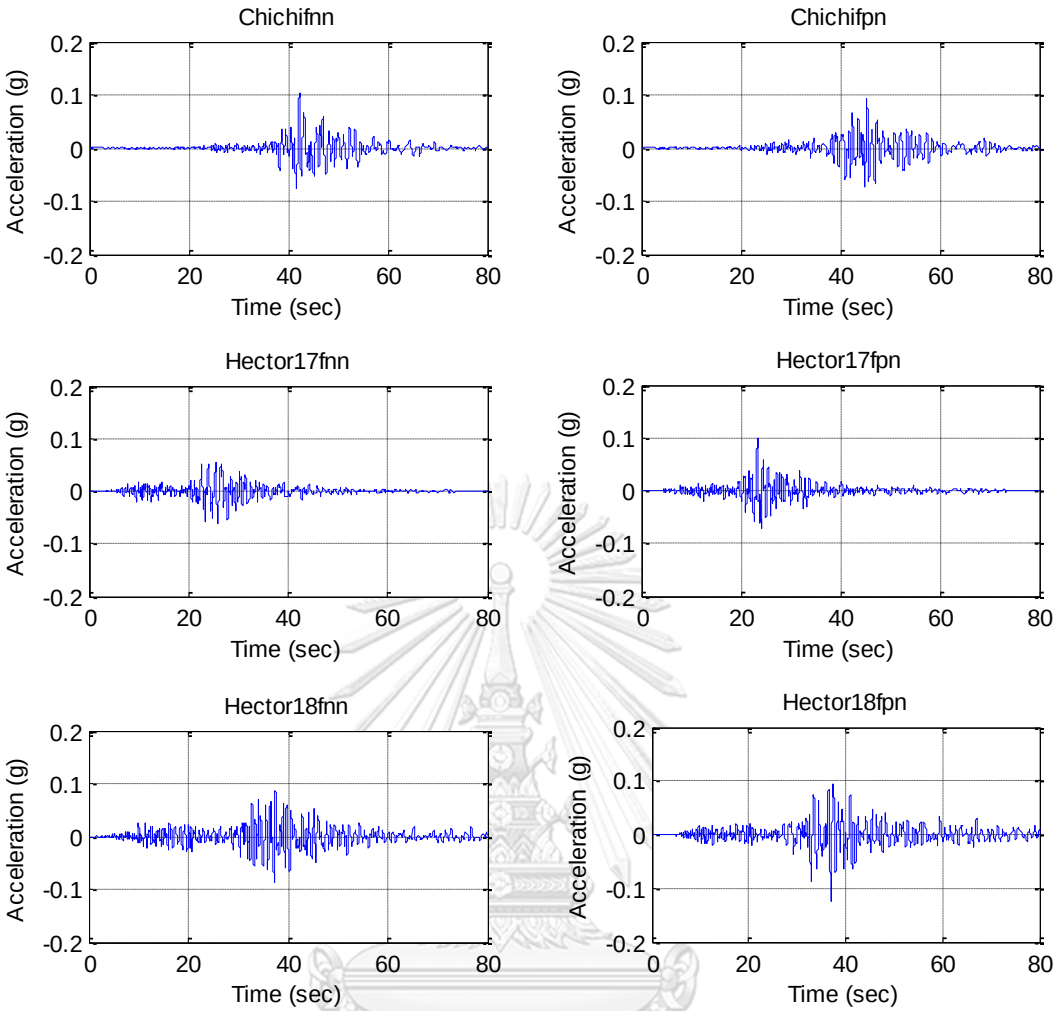

(c) Six soft-soil ground accelerations for CMS at 1.0sec

จุฬาลงกรณ์มหาวิทยาลัย
CHULALONGKORN UNIVERSITY

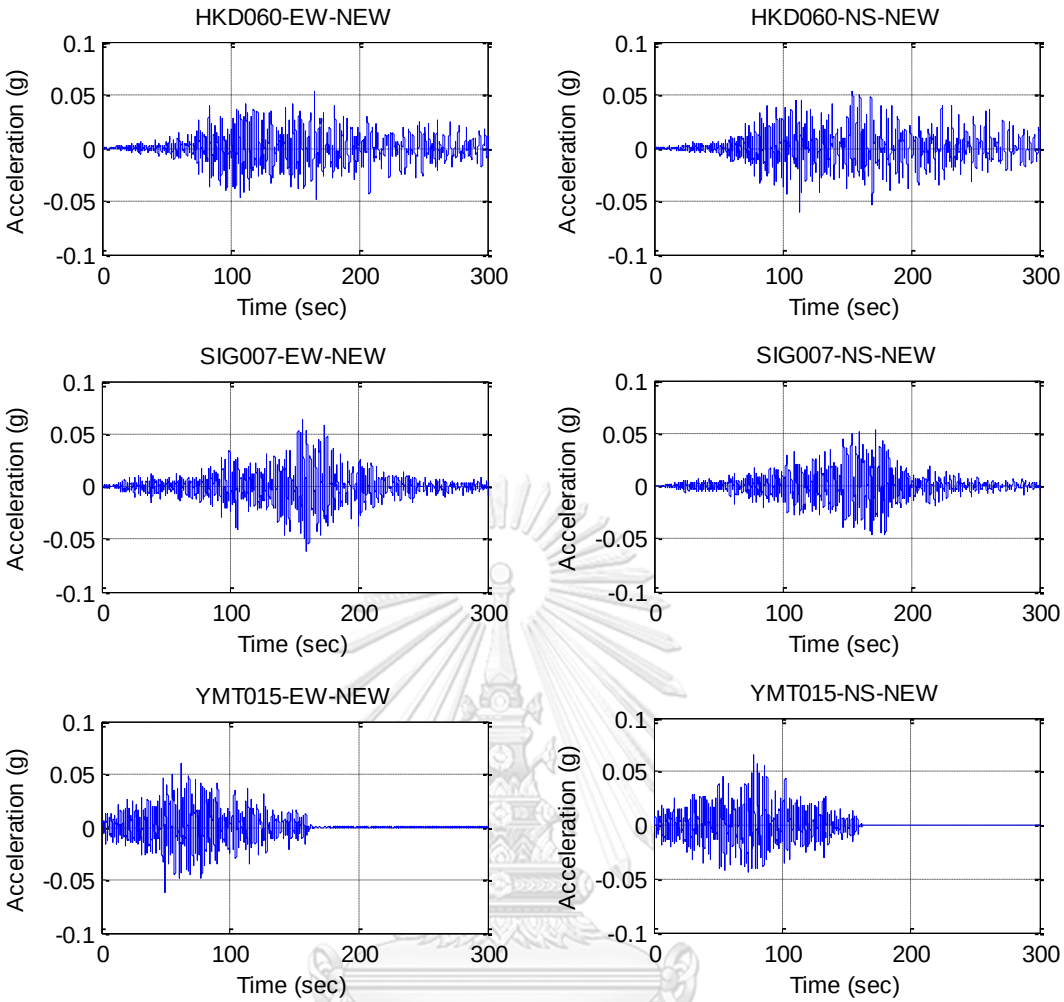

(d) Six soft-soil ground accelerations for CMS at 1.5sec

จุฬาลงกรณ์มหาวิทยาลัย
CHULALONGKORN UNIVERSITY

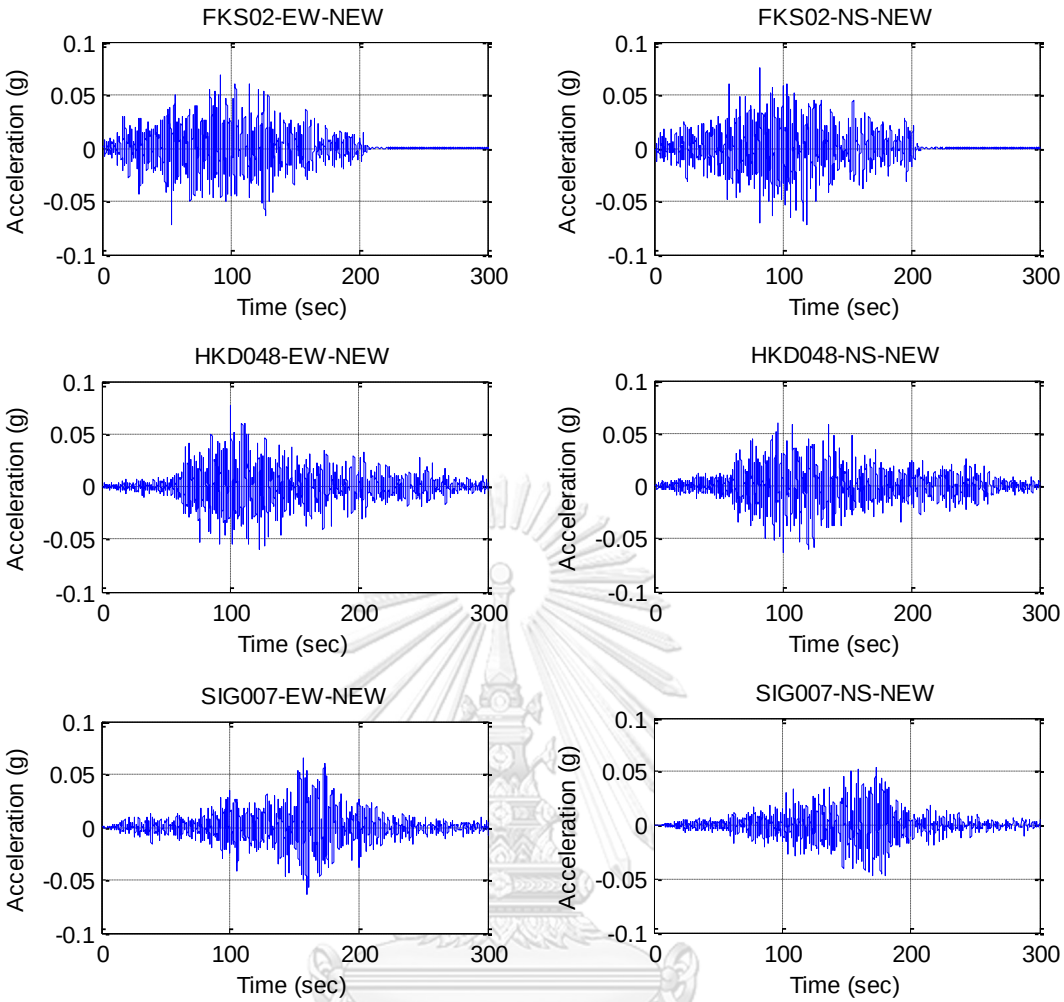

(e) Six soft-soil ground accelerations for CMS at 2.0sec

จุฬาลงกรณ์มหาวิทยาลัย
CHULALONGKORN UNIVERSITY

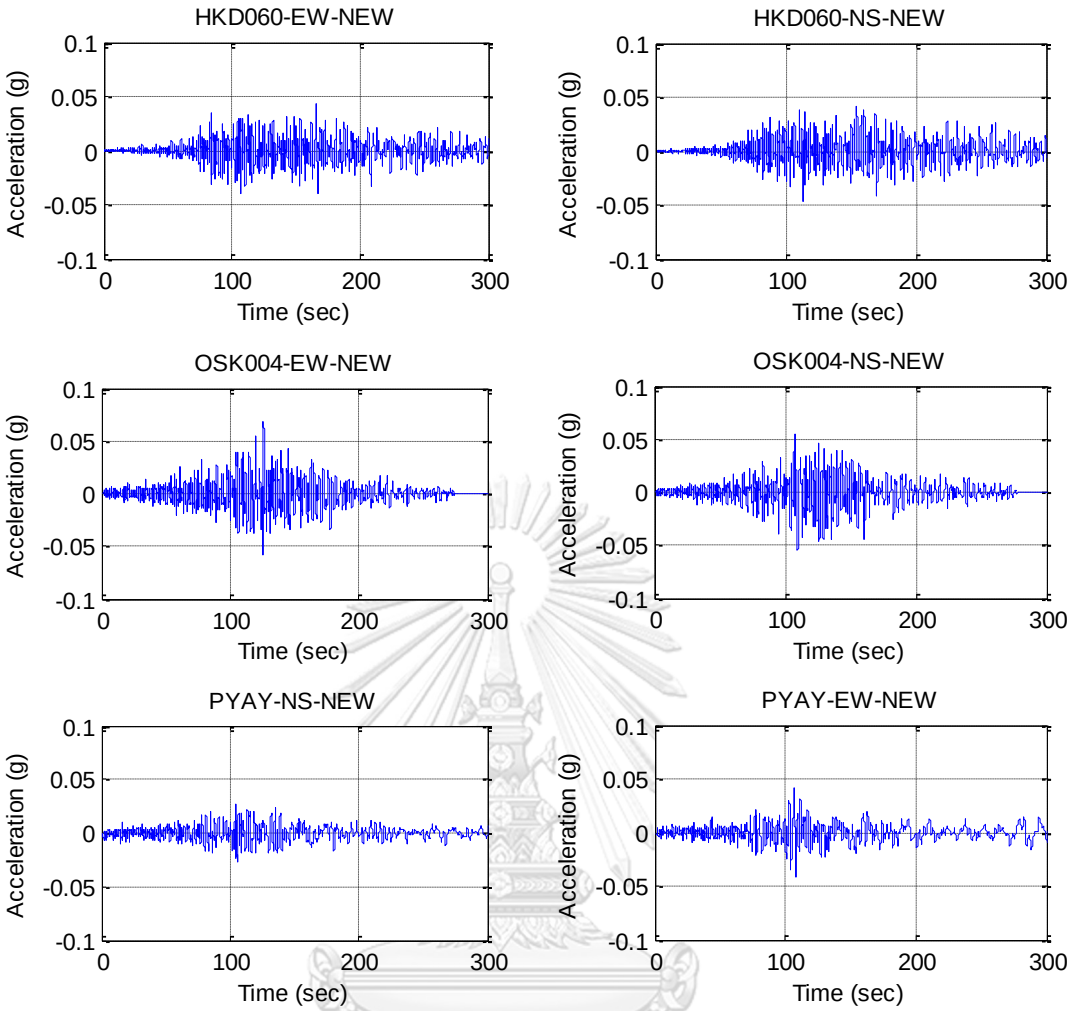

(f) Six soft-soil ground accelerations for CMS at 3.0sec

จุฬาลงกรณ์มหาวิทยาลัย
CHULALONGKORN UNIVERSITY

Figure B.1 Soft-soil ground accelerations for conditional mean spectrum (CMS) at six periods: 0.2; 0.5; 1; 1.5; 2; and 3 sec.

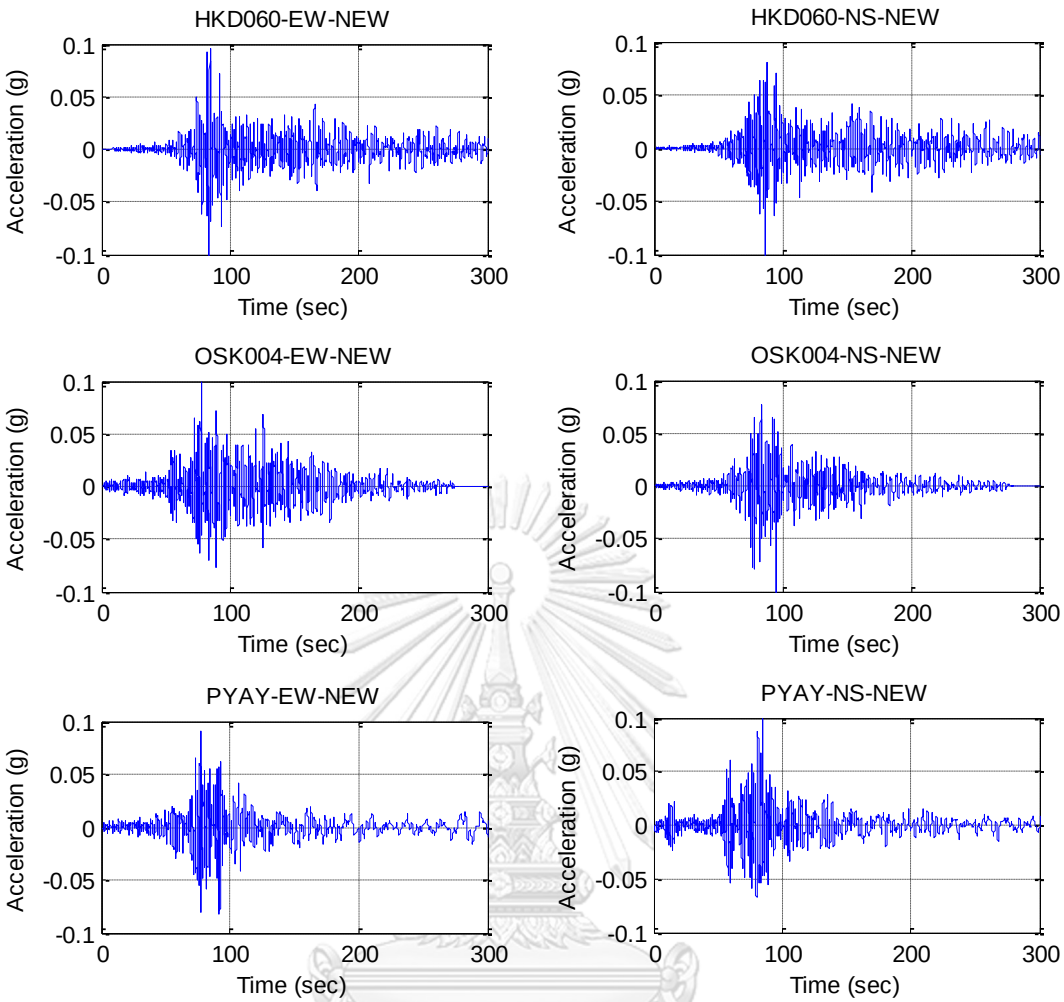

Figure B.2 Six UHS spectral matching soft-soil ground accelerations in Bangkok used in NLRHA.

จุฬาลงกรณ์มหาวิทยาลัย
CHULALONGKORN UNIVERSITY

B.2 Chiang Mai

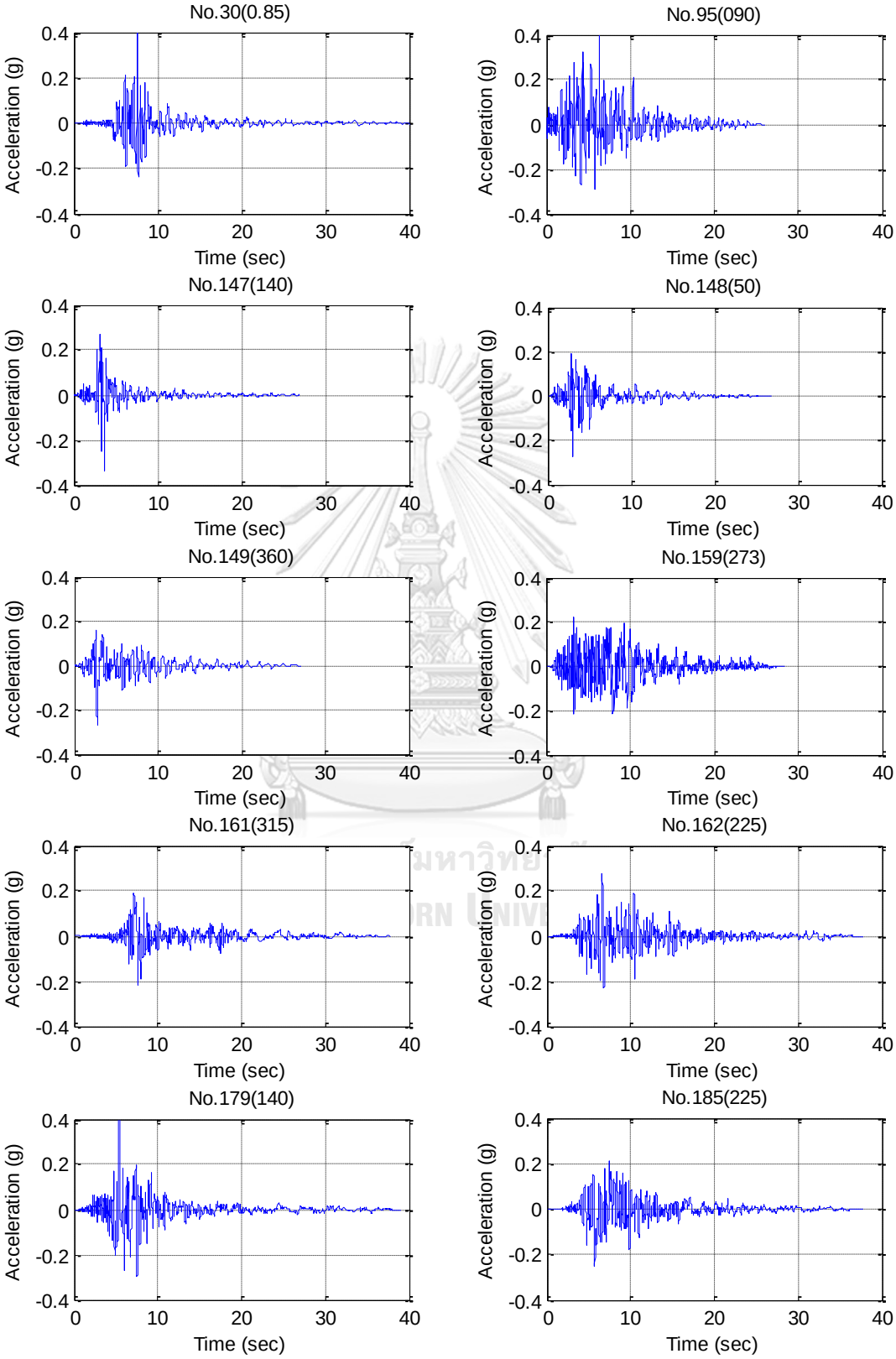

Figure B.3 Ten ground accelerations in Chiang Mai before scaling.

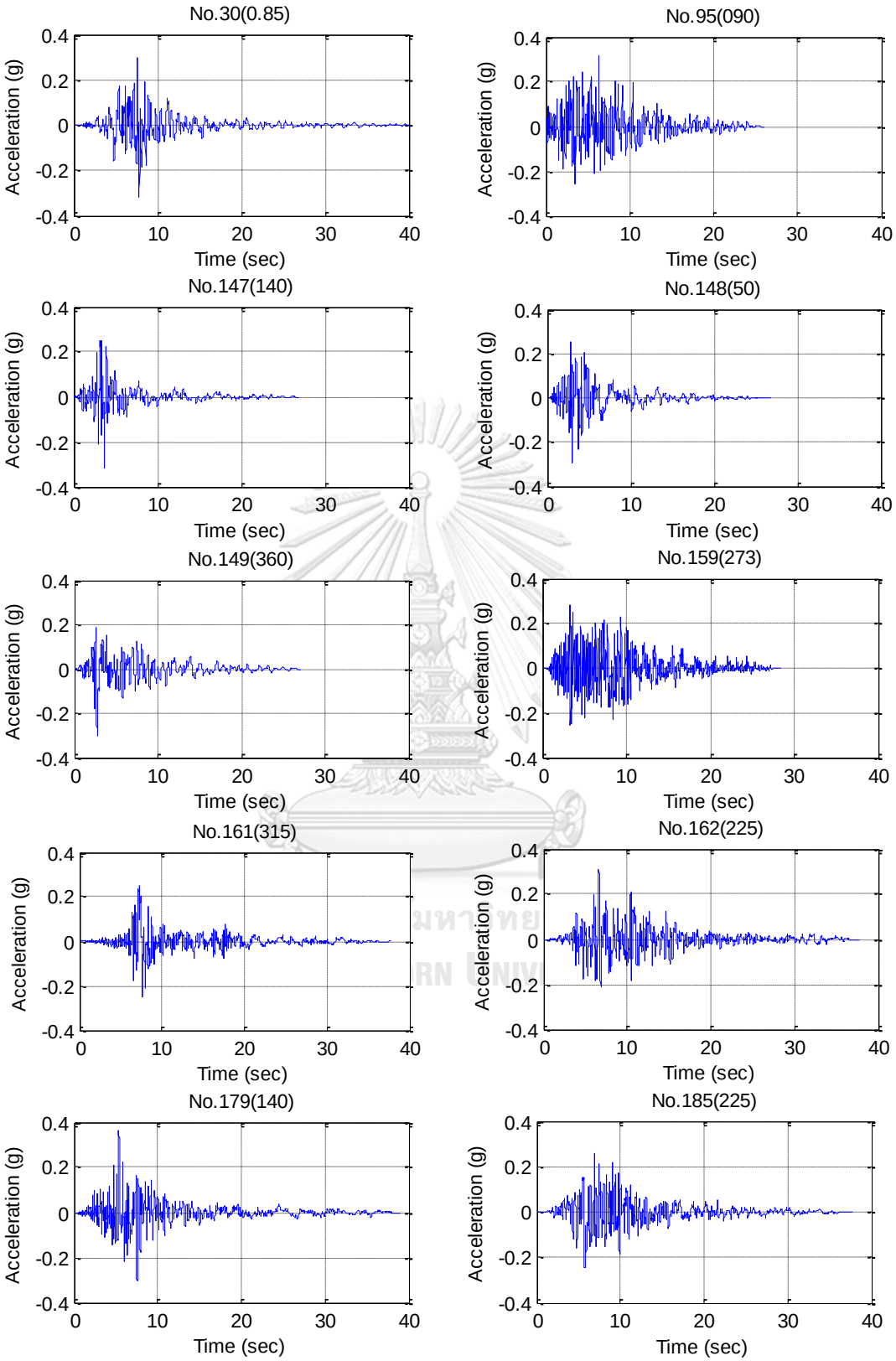

Figure B.4 Ten UHS spectral matching ground accelerations in Chiang Mai used in NLRHA.

APPENDIX C
LINEAR RESPONSE SPECTRUM ANALYSIS AND LINEAR RESPONSE HISTORY ANALYSIS

In this appendix, modal contribution of each linear responses in terms of floor displacement, story drift, story shear force, and story overturning moment was investigated. Then, results from linear response spectrum analysis (LRSA) where total responses were computed by combining modal responses using SRSS modal combination rule and linear response history analysis (LRHA) where total responses were computed by direct summation of modal responses in time history were compared. Four tall RC shear-wall buildings and four RC moment frames buildings subjected to an earthquake ground motion selected and scaled to match the design spectrum in Bangkok (Figure 3.15) and Chiang Mai (Figure 3.17) was used. The history of ground acceleration and spectral acceleration of the selected earthquake are shown in Figure C.1.

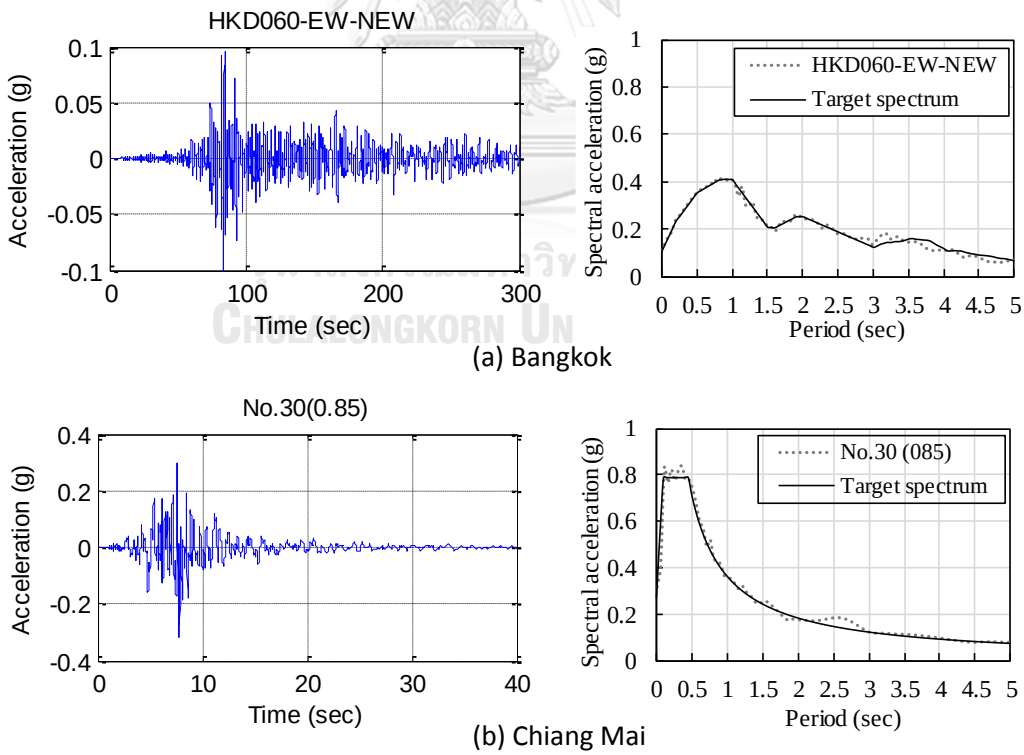

Figure C.1 Earthquake used for comparing LRSA and LRHA of buildings in (a) Bangkok; (b) Chiang Mai

C.1 Modal contribution of each linear response

The modal contributions of each linear response were computed by linear modal analysis described in Section 2.1.1. The response contributed from the nth mode was determined by Eq. (2.10). The total response was approximately computed by SRSS combination rule.

The modal contribution for the first-three translational modes of floor displacement, story drift, story shear force, and story overturning moment of tall RC shear-wall buildings SWB1-SWB6 are plotted in Figures C.2 and C.3 for buildings in Bangkok and in Figures C.4 and C.5 for buildings in Chiang Mai. The modal contributions to the total response envelope were totally different between shear force, overturning moment, story drift, and story displacement responses. For shear force, second-mode contribution was considerably significant at the base. For overturning moment, the first mode was dominant at the base, while higher modes played an important role around mid-height of the structure. Higher modes were more dominant for tall buildings, even though the mass participating ratio of higher modes (20% and 10% for 2nd and 3rd modes) was smaller than that of the first mode (55%) (see Table 4.3). For story drift and story displacement, the first-mode contribution was always dominant along the height of all buildings.

For RC frame buildings (Figures C.6 and C.7), the first-mode response contributed dominantly for all buildings because the mass participating ratio of first mode was about 80% compared to 11% and 4% of mass participating ratio of second and third modes, respectively (see Table 5.2), and the buildings are not tall (less than 15-story).

C.2 Comparison of results from LRSA and LRHA

Results from LRSA and LRHA are compared in Figures C.2 to C.5 for tall RC shear-wall buildings SWB1-SWB4 and in Figures C.6 to C.7 for RC moment-frame buildings MFB1-MFB4. It was found that LRSA generally provides similar results as LRHA for most studied buildings. Hence, the SRSS modal combination rule used in the RSA or the proposed MRSA method could be used to compute total response in these studied buildings with minor error.

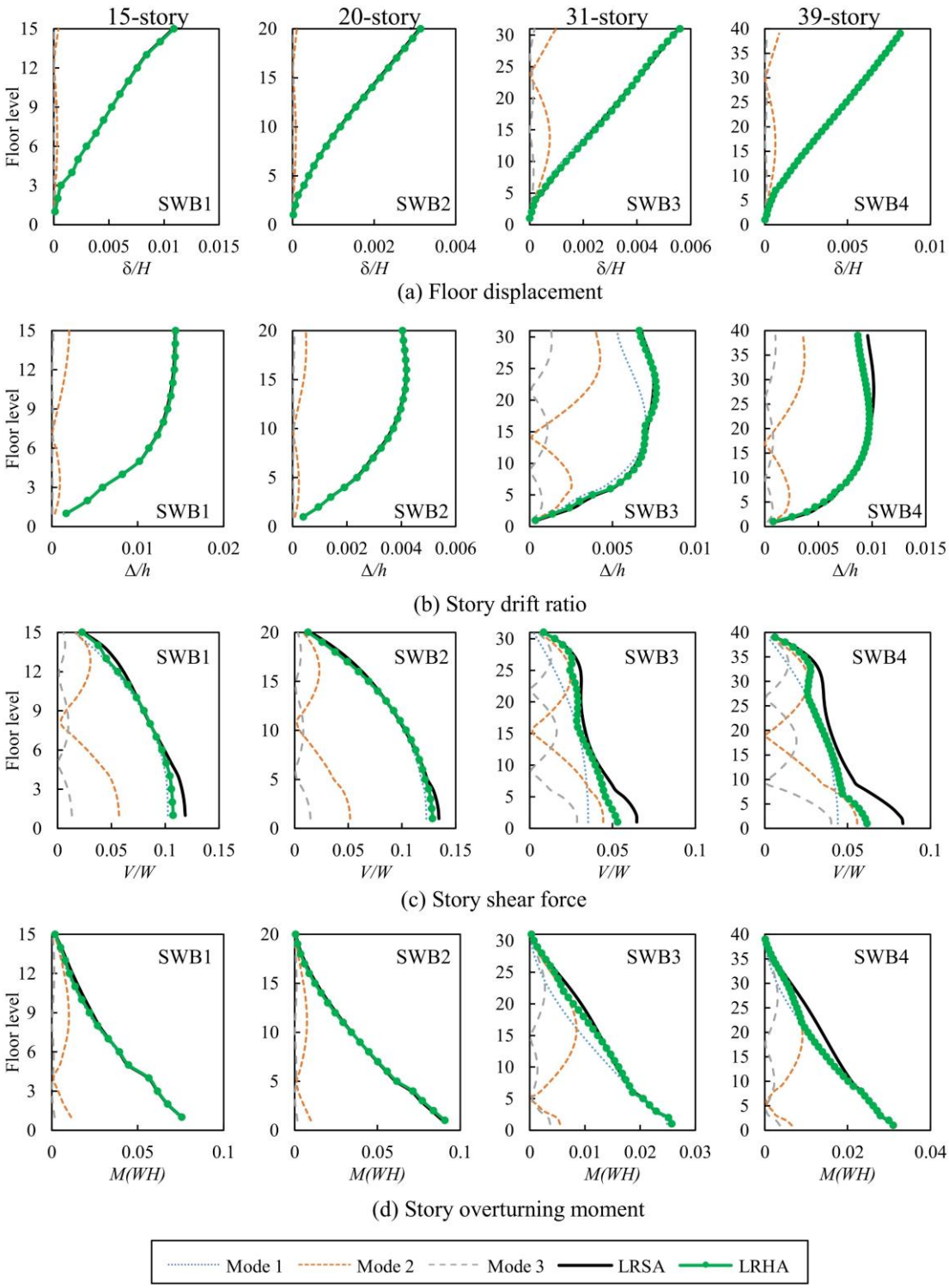

Figure C.2 Results from LRSA and LRHA along with the modal contribution of each linear response in X-direction of tall RC shear-wall buildings SWB1-SWB4 in Bangkok: (a) floor displacement; (b) story drift ratio; (c) story shear force; and (d) story overturning moment.

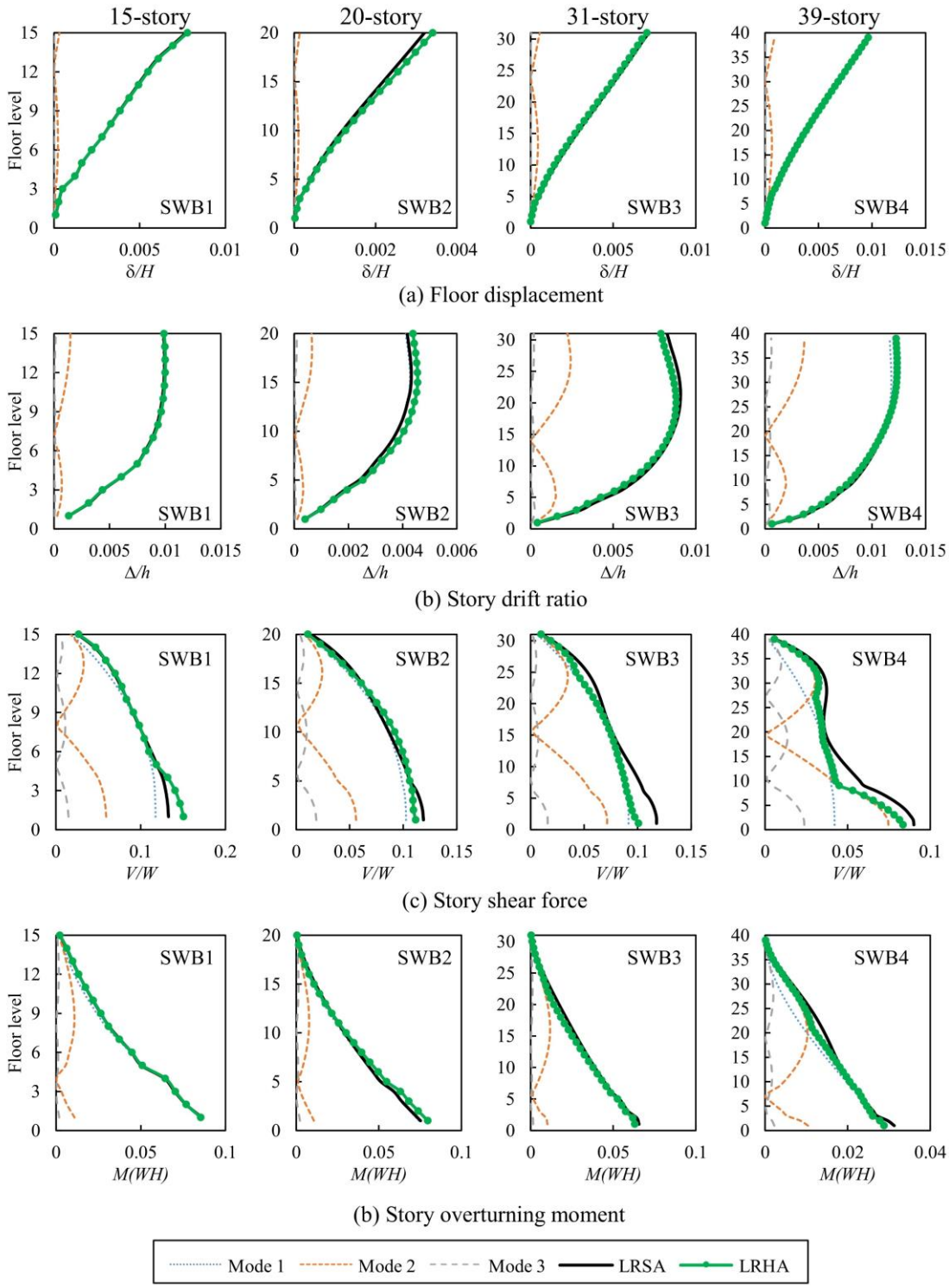

Figure C.3 Results from LRSA and LRHA along with the modal contribution of each linear response in Y-direction of tall RC shear-wall buildings SWB1-SWB4 in Bangkok: (a) floor displacement; (b) story drift ratio; (c) story shear force; and (d) story overturning moment.

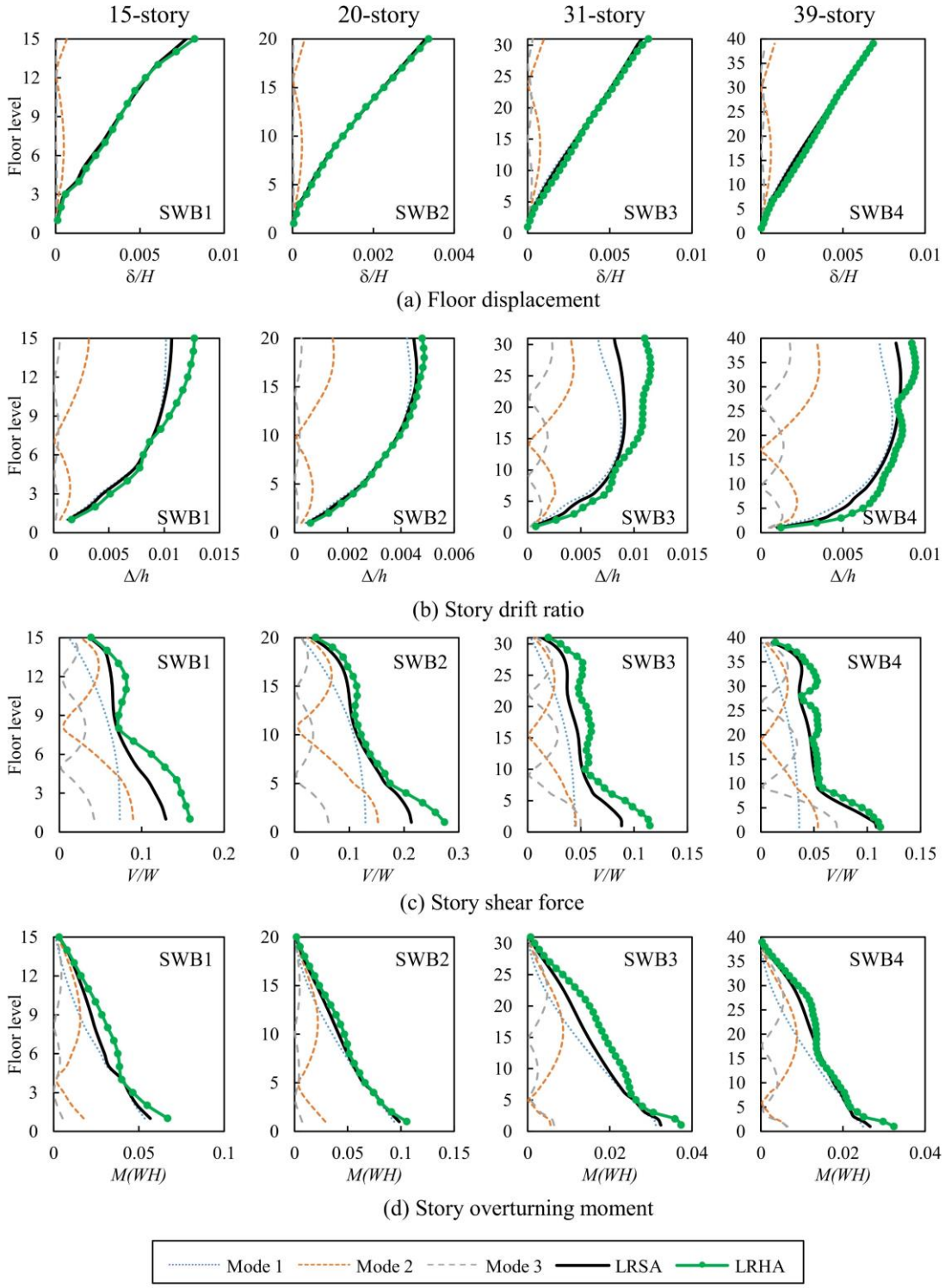

Figure C.4 Results from LRSA and LRHA along with the modal contribution of each linear response in X-direction of tall RC shear-wall buildings SWB1-SWB4 in Chiang Mai: (a) floor displacement; (b) story drift ratio; (c) story shear force; and (d) story overturning moment.

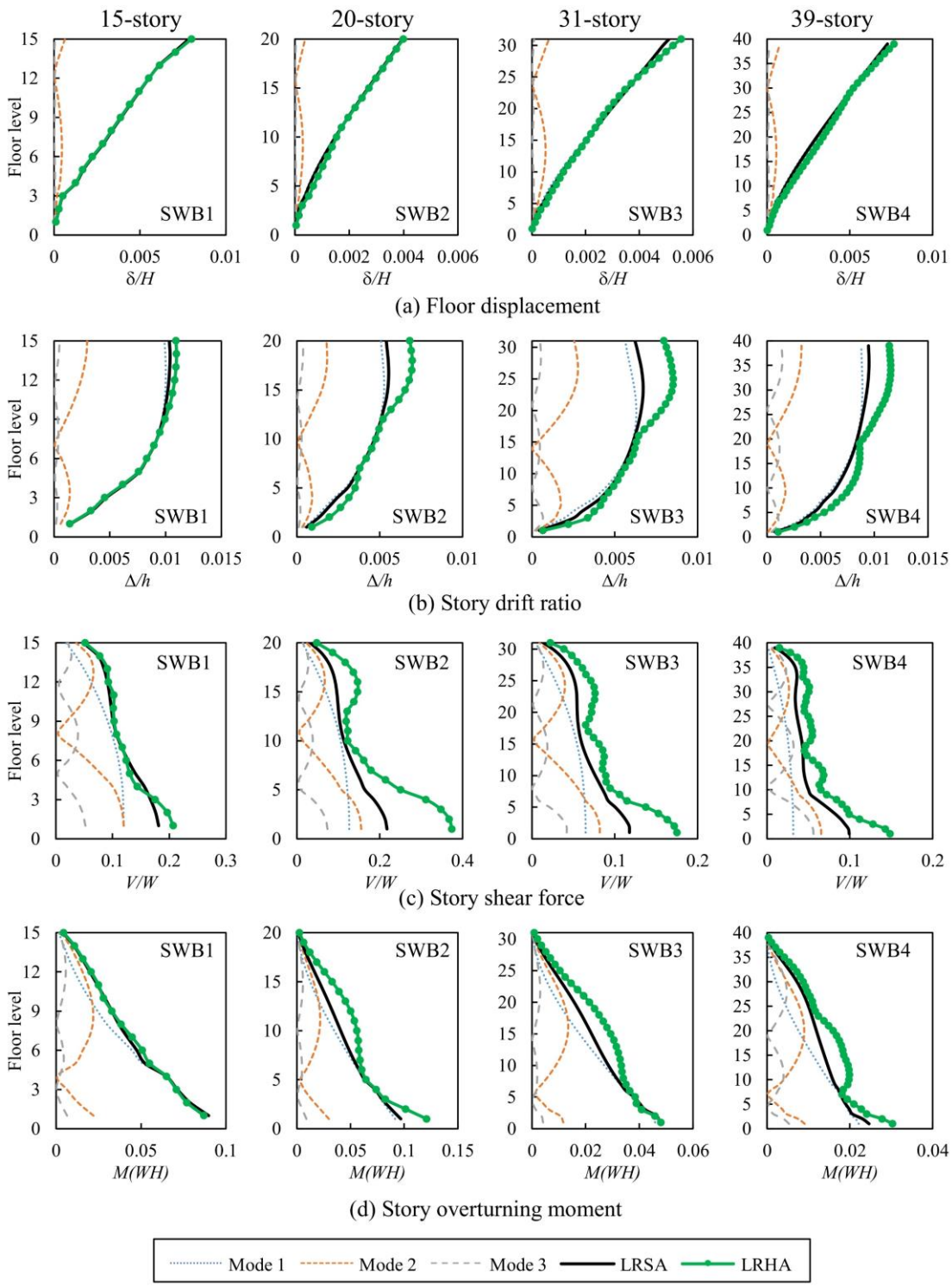

Figure C.5 Results from LRSA and LRHA along with the modal contribution of each linear response in Y-direction of tall RC shear-wall buildings SWB1-SWB4 in Chiang Mai: (a) floor displacement; (b) story drift ratio; (c) story shear force; and (d) story overturning moment.

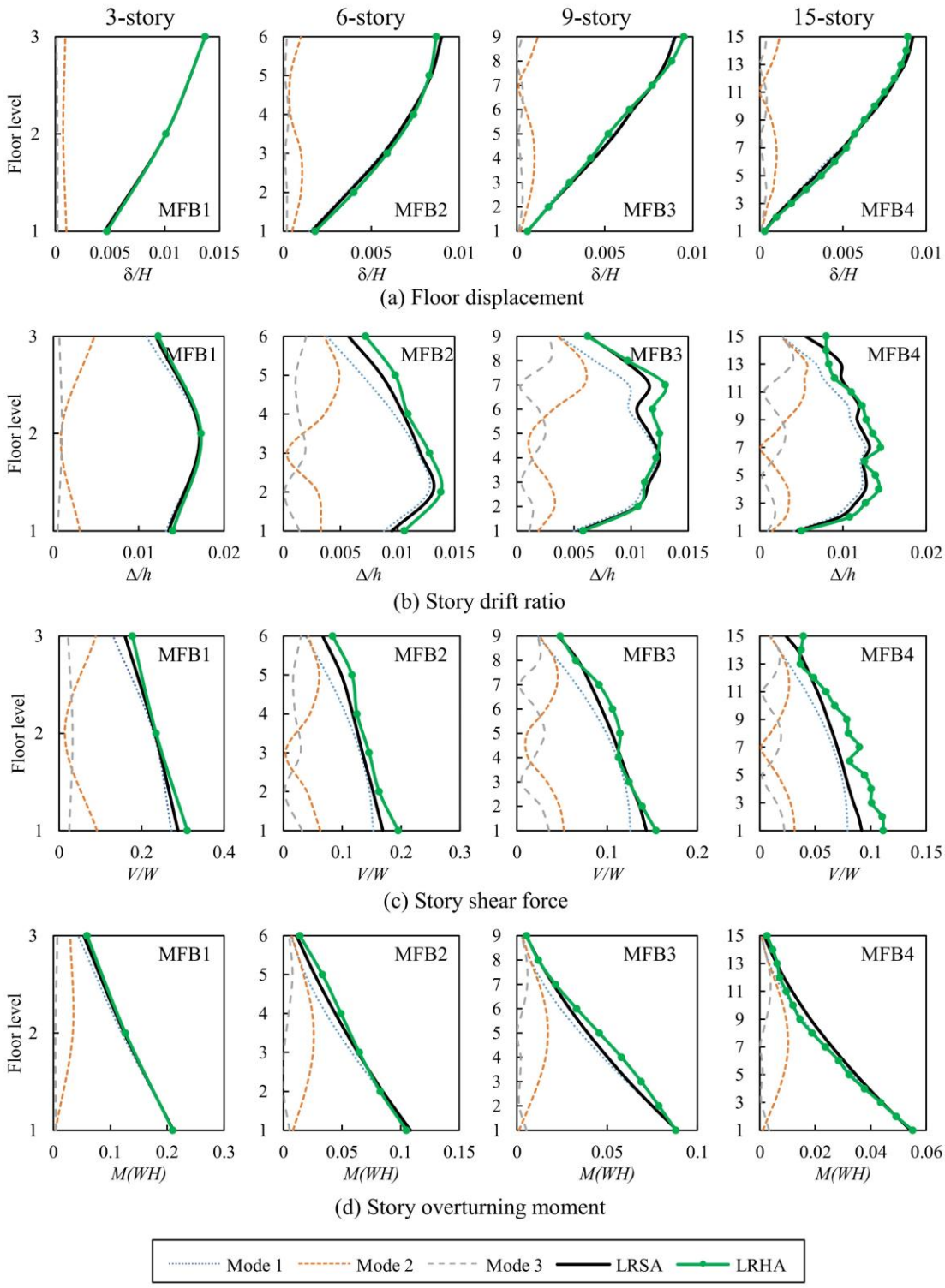

Figure C.6 Results from LRSA and LRHA along with the modal contribution of each linear response for RC frame buildings MFB1-MFB4 in Bangkok: (a) floor displacement; (b) story drift ratio; (c) story shear force; and (d) story overturning moment.

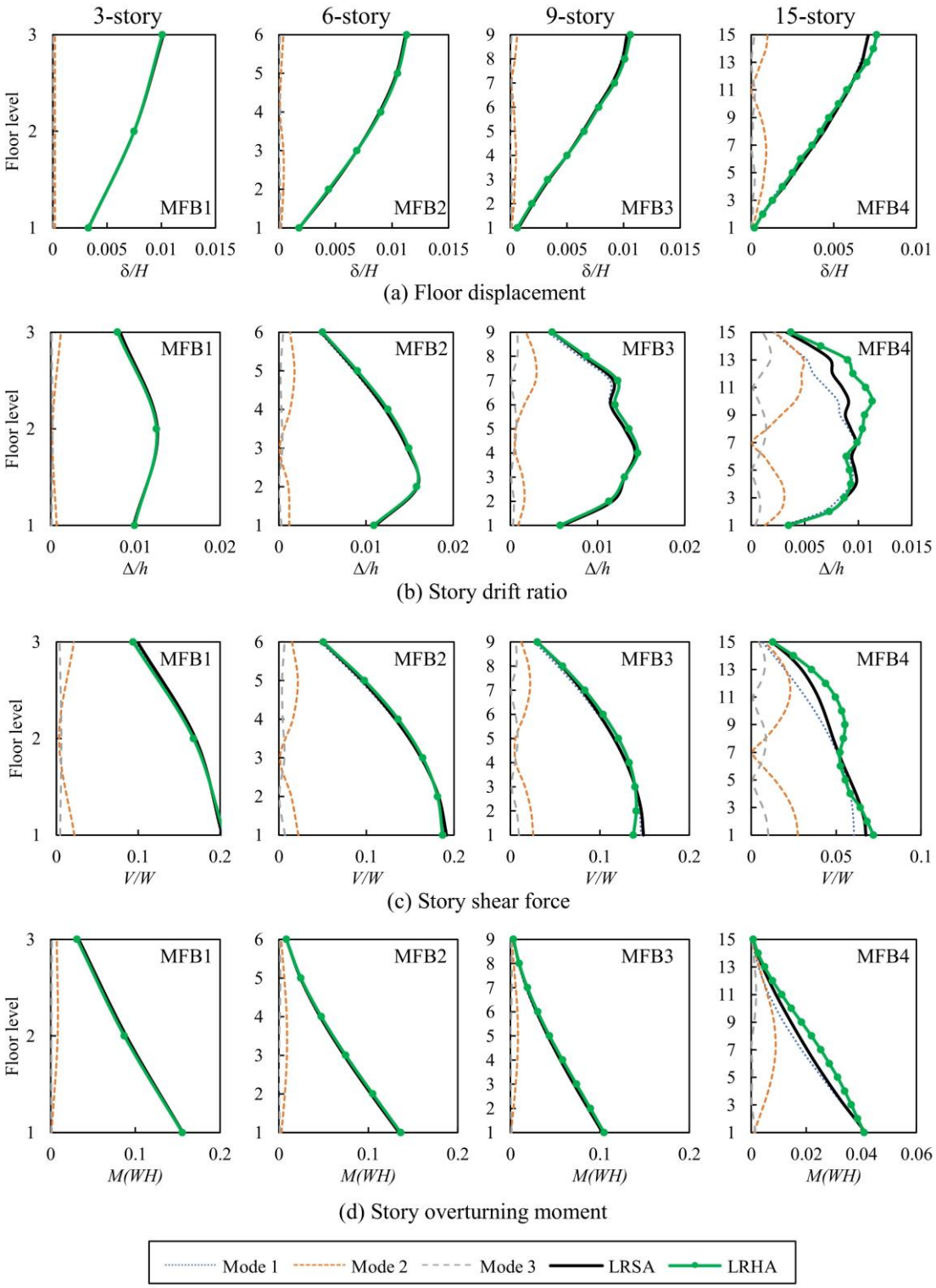

Figure C.7 Results from LRSA and LRHA along with the modal contribution of each linear response for RC frame buildings MFB1-MFB4 in Chiang Mai: (a) floor displacement; (b) story drift ratio; (c) story shear force; and (d) story overturning moment.

APPENDIX D
EXAMPLE OF MODIFIED RESPONSE SPECTRUM ANALYSIS PROCEDURE

D1. Modified response spectrum analysis procedure

1. Construct design spectrum.
2. Construct structural model with reduced stiffness of structural members required by the code.
3. Conduct the analysis to compute modal properties of each mode. The analysis shall include a sufficient number of modes to obtain a combined modal mass participation of at least 90 percent of the actual mass.
4. Compute modal base shear force (V_t) from conventional response spectrum analysis (RSA) procedure.
5. Compute base shear force (V_s) from equivalent lateral force (ELF) procedure.
6. Compute scaling factor (*SF*) to scale up the RSA modal base shear to at least 85% of the ELF base shear.
7. Compute each linear response contributed from each mode.
8. Compute design bending moment from Eq. (4.1), design shear force from Eq. (4.12), design displacement from Eq. (4.3), and drift from Eq. (4.4).
9. Combine earthquake load with other load cases.
10. Determine maximum strain of the wall by Eq. (4.15) and Eq. (4.16). Ductile detailing is required at the locations where the computed strain exceeds elastic limit, for example, 0.002.

Steps 1 to 9 can be implemented in many popular commercial programs in a similar way as the conventional RSA procedure. The flowchart of the MRSA procedure for use in commercial programs is shown in Figure D.1.

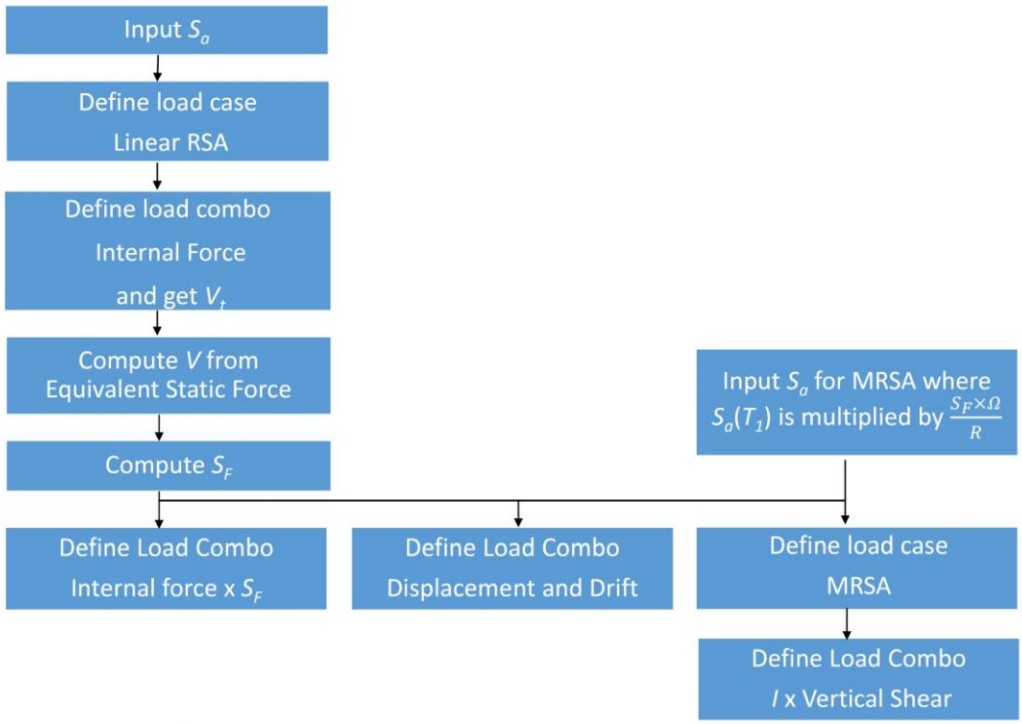

Figure D.1 Flowchart for implementation of MRSA procedure.

D.2 Example of MRSA procedure

D.2.1 Case studied building

A 39-story building (SWB4) was used as example to explain the procedure of MRSA. The detail of this building can be found in Appendix A (Figure A.4). The lateral force resisting system was considered to be special RC shear wall whose design factors are: R=6, C_d=5, Ω_0=2.5. The building is in occupancy III, the importance factor is I=1.25.

D.2.2 Design spectral acceleration

In this example, the location of the building was considered to be in central Bangkok (zone 5). The spectral acceleration values were taken from DPT 1301/1302-61 (2018). For this tall building, damping ratio of 2.5% was used. The obtained elastic spectral acceleration for 2.5% damping ratio is shown in Figure D.2.

S_{DS}=S_a (0.2sec)=0.148, S_{D1}=S_a(1.0sec)=0.25, according to the code, this building is assigned to seismic design category *D*.

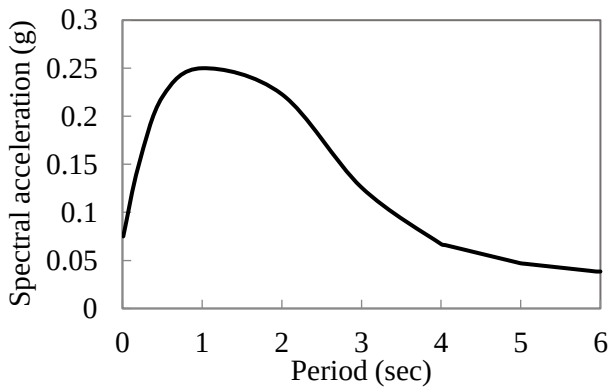

Figure D.2 Elastic spectral acceleration in Bangkok zone 5 for 2.5% damping ratio.

D.2.3 Structural model

Three-dimensional linear structural model considering cracked cross sections of structural members was created in ETABS program (CSI 2015) for analysis. The effective stiffness values of structural members following ACI 318M-14 were used to account for cracked sections of RC members. As allowed in ACI 318M-14, the effective stiffness values of each member can either be taken from Table D.1, or can be assumed I=0.5I_g for all members. In this example, I=0.5I_g was used for all members. The diaphragm was assumed to be rigid. Accidental eccentricity of 0.05 times dimension of the structure perpendicular to the direction of applied earthquake load was used to account for accidental torsional effect as required by the code. Seismic weight was computed from all dead loads and super-imposed dead loads.

จุฬาลงกรณ์มหาวิทยาลัย
CHULALONGKORN UNIVERSITY

Table D.1 Effective stiffness of structural members (ACI 318M-14).

Element		Effective stiffness	
		Moment of inertia	Cross sectional area
Wall	Cracked	0.35 I_g	1.0 A_g
	Uncracked	0.70 I_g	1.0 A_g
Column		0.70 I_g	1.0 A_g
Beam		0.35 I_g	1.0 A_g
Slab		0.25 I_g	1.0 A_g

D.2.4 Modal properties of the building

Modal properties were computed by modal analysis using ETABS program (CSI 2015). The modal properties of the first 20 modes from three-dimensional structural model

is summarized in Table D.2 from which the first-five translational modes in X-direction of the building (Table D.3) can be obtained based on the modal participating mass ratios in X-direction. The mode shapes of the first-five translational modes in X-direction are shown in Figure D.3. Only the results due to earthquake load in X-direction were presented in this example.

Table D.2 Modal properties of the first 20 modes from three-dimensional structural model of building.

Mode	Period (sec)	Modal participating mass ratios		Cumulative mass ratios	
		X	Y	X	Y
1	5.61	0%	52%	0%	52%
2	4.85	54%	0%	54%	52%
3	3.04	0%	0%	54%	52%
4	1.23	0%	21%	54%	73%
5	1.21	19%	0%	73%	73%
6	1.10	0%	0%	73%	73%
7	0.72	0%	3%	73%	76%
8	0.58	12%	0%	85%	76%
9	0.49	0%	8%	85%	85%
10	0.43	0%	0%	85%	85%
11	0.35	6%	0%	90%	85%
12	0.30	0%	1%	90%	86%
13	0.28	0%	4%	90%	90%
14	0.24	1%	0%	92%	91%
15	0.23	1%	0%	93%	91%
16	0.18	0%	2%	93%	93%
17	0.18	0%	0%	93%	93%
18	0.17	1%	0%	94%	93%
19	0.15	0%	0%	94%	93%
20	0.13	0%	1%	94%	95%

จุฬาลงกรณ์มหาวิทยาลัย
CHULALONGKORN UNIVERSITY

Table D.3 Modal properties of the first-five translational modes in X-direction.

Mode	Period (sec)	Modal participating mass ratios	Cumulative mass ratios
1	4.85	54%	54%
2	1.21	19%	73%
3	0.58	12%	84%
4	0.35	6%	90%
5	0.24	1%	91%

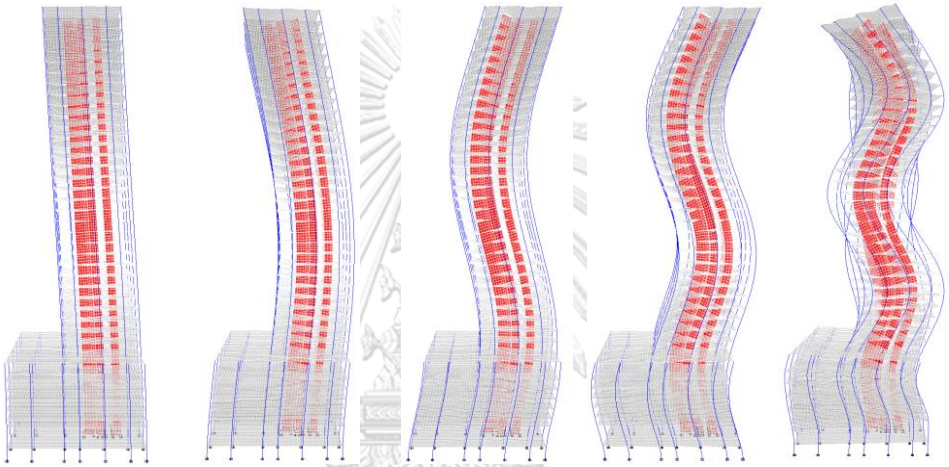

T_1=4.85 sec T_2=1.21 sec T_3=0.58 sec T_4=0.35 sec T_5=0.24 sec

Figure D.3 Mode shapes of the first-five translation modes in X-direction of the building.

จุฬาลงกรณ์มหาวิทยาลัย
CHULALONGKORN UNIVERSITY

D.2.5 Modal base shear force from conventional RSA

The modal base shear force of each mode was computed by $V_{bn} = M_n^* A_n$. The base shear force of each mode in X-direction of the building is summarized in Table D.4.

Table D.4 Base shear force of each mode in X-direction of the building.

Mode	Period (sec)	Effective modal mass M_n^*(ton)	Spectral acceleration S_a (T_n) or A_n (g)	Modal base shear force $V_{bn} = M_n^* A_n$ (kN)
1	4.85	20,409	0.05	10,000
2	1.21	7,062	0.24	16,894
3	0.58	4,417	0.22	9,734
4	0.35	2,109	0.18	3,823
5	0.24	446	0.16	686

The total modal base shear force was computed by combining base shear force of each mode by SRSS combination, and then multiplying by *I*/*R* factor.

$$V_t = \frac{I}{R}\sqrt{V_{1e}{}^2 + V_{2e}{}^2 + V_{3e}{}^2 + \cdots}$$

$$V_t = \frac{1.25}{6}\sqrt{10,000^2 + 16,894^2 + 9,734^2 + 3,823^2 + 686^2} = 4,636kN$$

The modal base shear force from RSA can be implemented in ETABS program. First, define load case for earthquake using design spectral acceleration as shown in Figure D.2. This load case is named as LRSA X as shown in Figure D.4, which is used to computed elastic response from the input earthquake. To get the design internal forces, the elastic demands are multiplied with I/R. This can be done using load combination (Internal Force) as shown in Figure D.5.

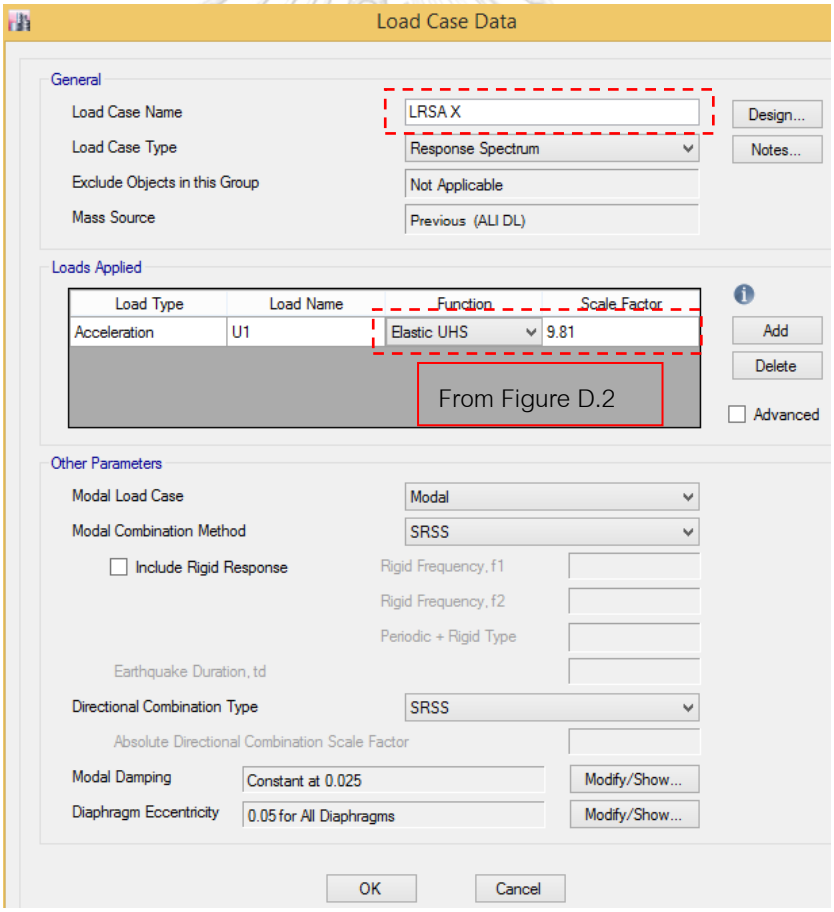

Figure D.4 Load case for earthquake: LRSA X.

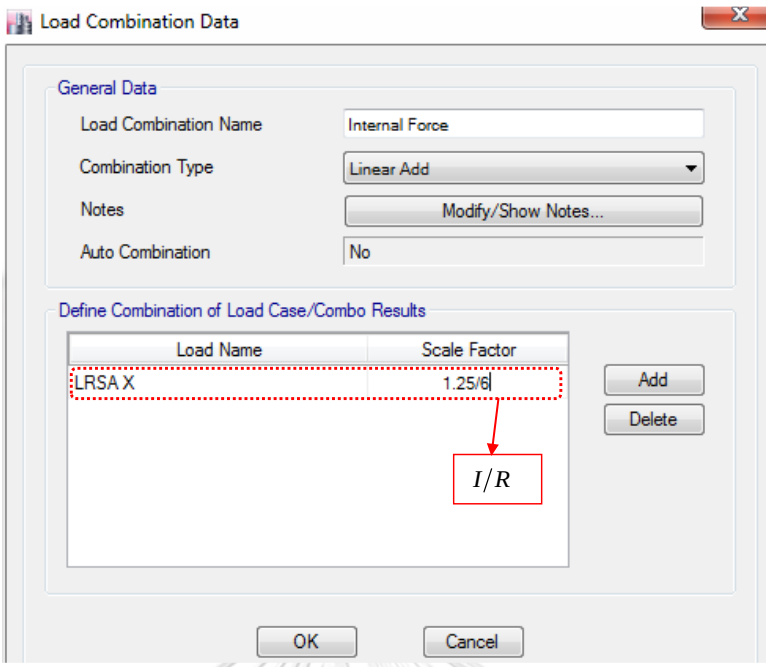

Figure D.5 Load combination: Internal Force.

D.2.6 Static base shear force from ELF

The approximated period from empirical formula in DPT 1301/1302-61 (2018) is computed by

$$T_a = 0.02H = 0.02 \times 125.55 = 2.51\text{sec}$$

The fundamental period used in ELF procedure is computed by

$$T = \min(C_u T_a, T_{etabs}) = \min(1.5 \times 2.51\ ,\ 4.85) = 3.77\,\text{sec}$$

The ELF base shear is computed by

$$V_s = C_s W$$

$$C_s = S_a \frac{I}{R} \geq 0.01$$

From elastic spectrum in Figure D.2, $S_a(3.77\,\text{sec}) = 0.0808$

$$C_s = \frac{0.0808 \times 1.25}{6} = 0.01683$$

Seismic weight of the building: $W = 370{,}566\,kN$

The ELF base shear is

$$V_s = 0.01683 \times 370,566 = 6,236kN$$

D.2.7 Scaling of modal base shear

Because RSA modal base shear is smaller than 85% of ELF base shear, $V_t = 4,636kN < 0.85V_s = 5,300kN$, scaling is required and scaling factor (*SF*) is computed by

$$SF = \frac{0.85V_s}{V_t} = 1.143$$

This scaling requirement is used in ETABS using load combination (Internal Force x SF as shown in Figure D.6).

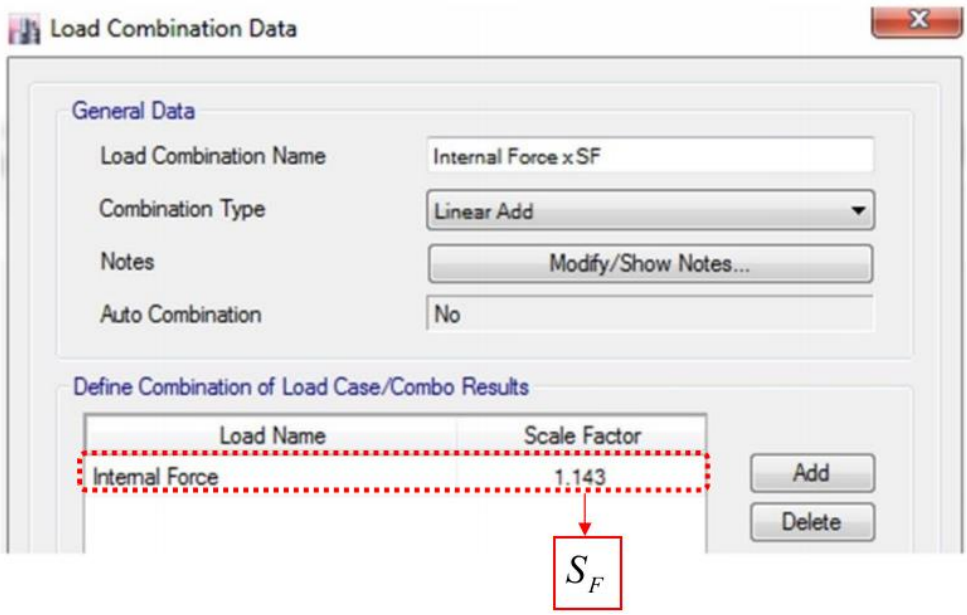

Figure D.6 Load combination: Internal Force x SF.

D.2.8 Design demands from MRSA procedure

Design bending moments are computed using elastic demands multiplied with $(SF \times I)/R$. This can be done using load combination Internal Force x SF (Figure D.6) which corresponds to equation below.

Bending moment: $$M = \frac{SF \times I}{R}\sqrt{M_{1e}^{\ 2} + M_{2e}^{\ 2} + M_{3e}^{\ 2} + \cdots}$$

Floor displacements and drifts are computed using elastic demands multiplied with C_d / R. This can be done using load combination as shown in Figure D.7 which is for equations below

Displacement: $$\delta = \frac{C_d}{R}\sqrt{\delta_{1e}^{\ 2} + \delta_{2e}^{\ 2} + \delta_{3e}^{\ 2} + \cdots}$$

Drift: $$\Delta = \frac{C_d}{R}\sqrt{\Delta_{1e}^{\ 2} + \Delta_{2e}^{\ 2} + \Delta_{3e}^{\ 2} + \cdots}$$

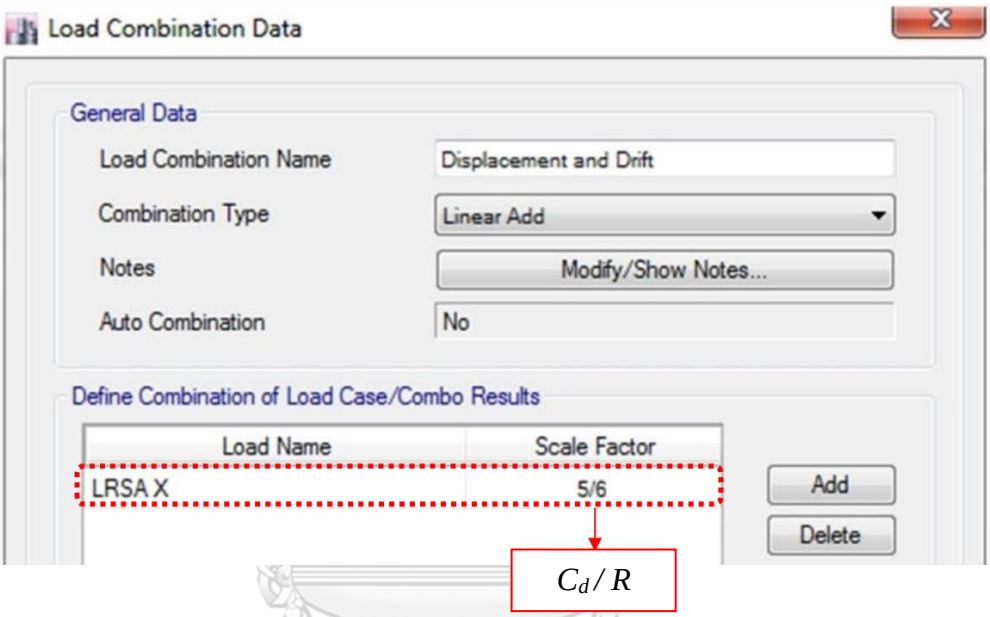

Figure D.7 Load combination for floor displacements and drifts.

Shear forces are computed from modified RSA, $MRSA_{HE}$ method.

Shear force: $$V = I\sqrt{\left(\frac{SF \times \Omega_0}{R} V_{1e}\right)^2 + V_{2e}^{\ 2} + V_{3e}^{\ 2} + \cdots}$$

This can be implemented using a separated design spectrum for shear which is computed by multiplying spectral ordinate of elastic spectrum with a factor of $(SF \times \Omega_0)/R = 0.476$ only at the fundamental period of the building in the direction considered. For this example, fundamental period in X-direction is 4.85 sec; the elastic spectrum is reduced at periods from 4.5 sec to 6 sec to obtain the design spectrum for shear as shown in Figure D.8.

To implement in ETABS, define load case (MRSA X) representing design spectrum for shear as shown in Figure D.9, and then, define load combination (Shear in Vertical Members) with load case MRSA X multiplied with *I* as shown in Figure D.10.

In summary, it requires three load combinations in ETABS program: Figure D.6 for bending moments; Figure D.10 for shear forces; and Figure D.7 for displacements and drifts. The story demands from MRSA procedure due to earthquake in X-direction are shown in Table D.5.

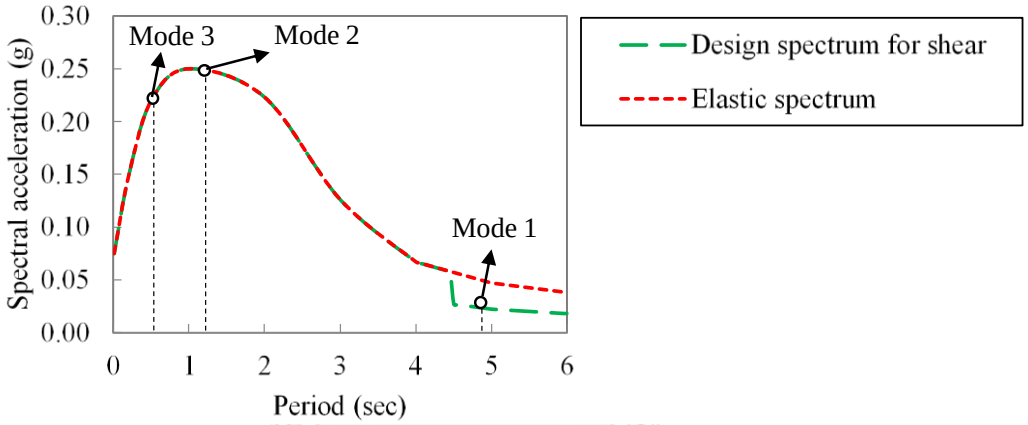

Figure D.8 Elastic spectrum, design spectrum shear.

จุฬาลงกรณ์มหาวิทยาลัย
CHULALONGKORN UNIVERSITY

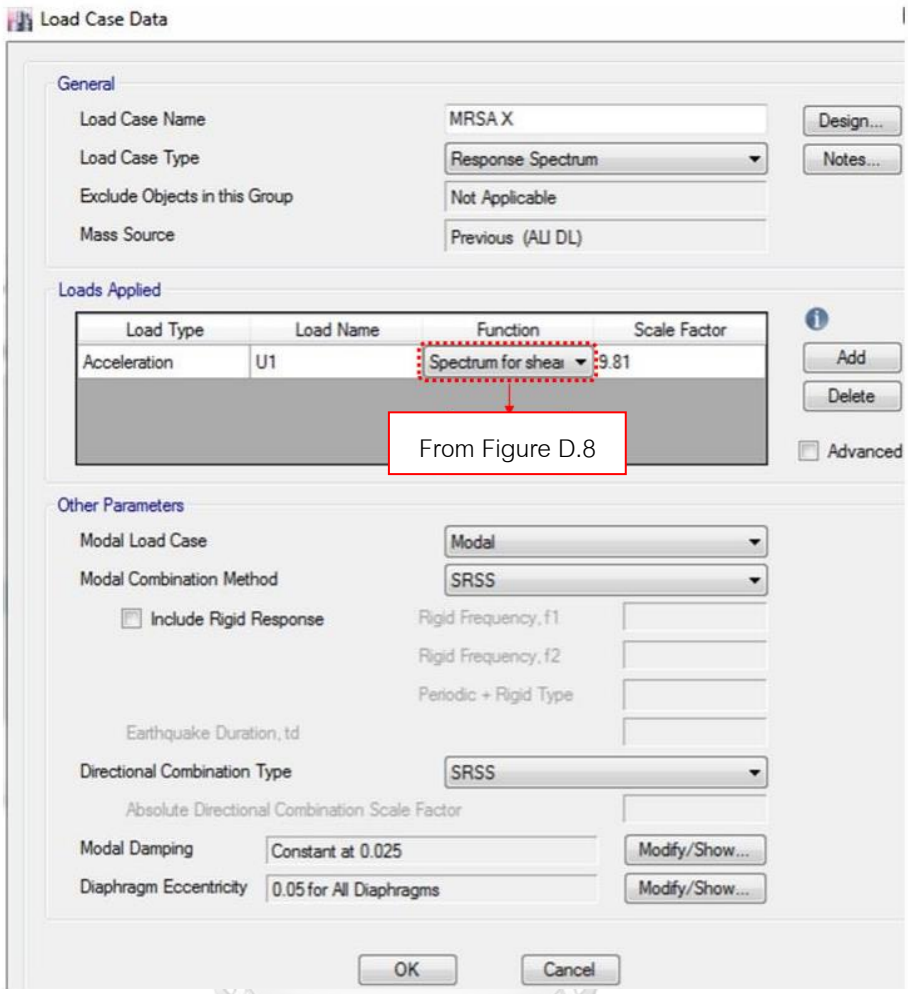

Figure D.9 Load case: MRSA X.

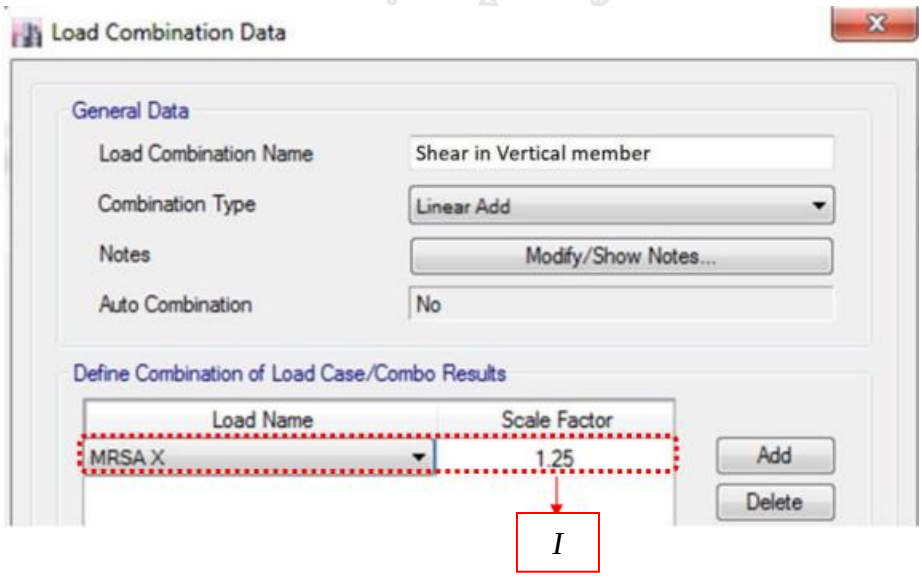

Figure D.10 Load combinaiton: Shear in Vertical Member.

Table D.5 Story demands computed from MRSA procedure due to earthquake in X-direction.

Story	Story shear (kN)	Story overturning moment (kN.m)	Story displacement (m)	Story drift ratio (%)
39	2,231	1,265	0.40	0.39
38	4,326	3,872	0.39	0.39
37	6,087	7,619	0.38	0.40
36	7,558	12,334	0.37	0.41
35	8,737	17,839	0.36	0.41
34	9,613	23,947	0.34	0.42
33	10,212	30,487	0.33	0.43
32	10,565	37,304	0.32	0.43
31	10,702	44,260	0.31	0.43
30	10,655	51,238	0.30	0.43
29	10,453	58,134	0.29	0.43
28	10,129	64,864	0.27	0.43
27	9,715	71,360	0.26	0.43
26	9,245	77,568	0.25	0.43
25	8,752	83,451	0.24	0.42
24	8,273	88,984	0.23	0.42
23	7,845	94,157	0.22	0.41
22	7,505	98,972	0.21	0.41
21	7,294	103,441	0.19	0.40
20	7,247	107,591	0.18	0.40
19	7,390	111,456	0.17	0.39
18	7,726	115,087	0.16	0.39
17	8,242	118,543	0.15	0.38
16	8,907	121,894	0.14	0.38
15	9,685	125,222	0.13	0.37
14	10,535	128,616	0.12	0.36
13	11,454	132,162	0.10	0.36
12	12,409	135,951	0.09	0.35
11	13,381	140,075	0.08	0.34
10	14,346	144,621	0.07	0.33
9	15,307	150,172	0.06	0.31
8	17,525	159,005	0.05	0.30
7	19,398	164,464	0.04	0.27
6	21,087	170,498	0.03	0.25
5	22,596	177,194	0.02	0.23
4	23,866	184,599	0.02	0.21
3	24,827	190,825	0.01	0.19
2	25,647	209,501	0.01	0.14
1	25,810	220,687	0.00	0.06

จุฬาลงกรณ์มหาวิทยาลัย
Chulalongkorn University

D.2.9 Torsional amplification factor

Torsional amplification factor is used to amplify accidental torsional moment when it is larger than 1. Torsional amplification factor is computed by

$$A_x = \left(\frac{\delta_{\max}}{1.2\delta_{\text{ave}}} \right)^2 \qquad 1 \le A_x \le 3$$

where δ_{max} is the maximum displacement at the edge of each story, and δ_{avg} is the average displacement at the two edges of that story.

The locations of computed displacements in this example (δ_1 and δ_2) are shown in Figure D.11. These displacements are computed using design displacement from RSA procedure. The obtained results are summarized in Table D.6. It shows that torsional amplification is not required for this building as A_x is less than 1.0 for all stories.

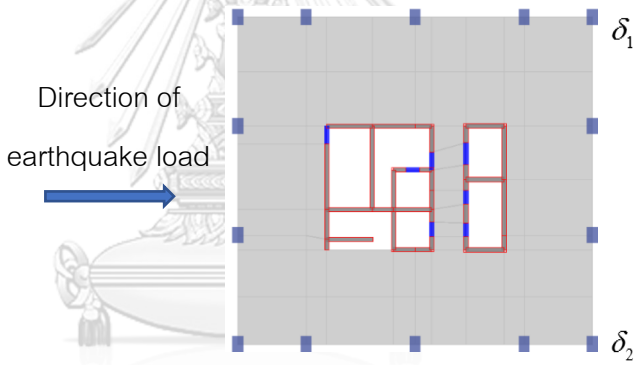

Figure D.11 Location of displacements for computing torsional amplification factor.

CHULALONGKORN UNIVERSITY

Table D.6 Displacements and torsional amplification factors of each story in X-direction.

Story	δ_1	δ_1	δ_{ave}	δ_{max}	A_x
39	0.402	0.397	0.399	0.402	0.70
38	0.390	0.385	0.388	0.390	0.70
37	0.379	0.374	0.377	0.379	0.70
36	0.368	0.363	0.365	0.368	0.70
35	0.356	0.351	0.354	0.356	0.70
34	0.345	0.340	0.342	0.345	0.70
33	0.333	0.328	0.331	0.333	0.71
32	0.321	0.316	0.319	0.321	0.71
31	0.310	0.305	0.307	0.310	0.71
30	0.298	0.293	0.296	0.298	0.71
29	0.286	0.281	0.284	0.286	0.71
28	0.275	0.270	0.272	0.275	0.71
27	0.263	0.258	0.261	0.263	0.71
26	0.252	0.247	0.249	0.252	0.71
25	0.240	0.235	0.238	0.240	0.71
24	0.228	0.224	0.226	0.228	0.71
23	0.217	0.212	0.215	0.217	0.71
22	0.206	0.201	0.203	0.206	0.71
21	0.194	0.189	0.192	0.194	0.71
20	0.183	0.178	0.180	0.183	0.71
19	0.172	0.167	0.169	0.172	0.72
18	0.160	0.155	0.158	0.160	0.72
17	0.149	0.144	0.147	0.149	0.72
16	0.138	0.133	0.135	0.138	0.72
15	0.127	0.122	0.124	0.127	0.72
14	0.116	0.111	0.113	0.116	0.72
13	0.105	0.100	0.102	0.105	0.73
12	0.094	0.089	0.091	0.094	0.73
11	0.083	0.079	0.081	0.083	0.73
10	0.072	0.069	0.070	0.072	0.73
9	0.062	0.059	0.060	0.062	0.73
8	0.051	0.048	0.050	0.051	0.73
7	0.037	0.035	0.036	0.037	0.74
6	0.030	0.028	0.029	0.030	0.74
5	0.024	0.022	0.023	0.024	0.74
4	0.018	0.017	0.017	0.018	0.74
3	0.013	0.012	0.012	0.013	0.75
2	0.009	0.008	0.009	0.009	0.75
1	0.002	0.001	0.002	0.002	0.75

จุฬาลงกรณ์มหาวิทยาลัย
CHULALONGKORN UNIVERSITY

D.2.10 P-Delta effect

In P-Delta effect checking, the stability ratio is computed for each story by

$$\theta = \frac{P_x \Delta}{V_x h_{sx} C_d}$$

where P_x is the unfactored total design gravity load at level x

V_x is the total design shear at level x

Δ is the design story drift (story drift due to V_x multiplied by C_d)

h_{sx} is the story height

C_d is the deflection amplification factor (C_d=5)

There are three cases to check with stability ratio.

$\theta \le 0.1$: P-Delta effect is not required

$0.1 < \theta \le \theta_{\max}$: P-Delta effect is included by multiplying displacement and member forces by $\frac{1}{1-\theta}$

$\theta > \theta_{\max}$: The structure is unstable and shall be redesigned

$\theta_{\max} = \frac{0.5}{\beta C_d} \le 0.25$, where β is the ratio of shear demand to shear capacity. This ratio is conservatively taken as 1.0.

Note that the stability ratio mainly depends on vertical load, story height, and lateral stiffness (V/Δ). It does not depend on magnitude of drift, design earthquake or design spectrum. Even if earthquake becomes very strong, causing very large shear force (V) and drift (Δ). The ratio of V/Δ will just become lateral stiffness. We can avoid P-Delta effect by good proportioning of story height and lateral stiffness. In P-Delta checking, story shears and story drifts are determined using ELF procedure. The vertical distribution of seismic load is computed by

$$F_x = C_{vx} V$$

$$C_{vx} = \frac{w_x h_x^k}{\sum_{i=1}^{n} w_i h_i^k}$$

where C_{vx} is the vertical distribution factor

V is the total design shear at the base of the structure computed by ELF procedure, $V = V_s = 6,236kN$ (see Section D.2.6)

w_i, and w_x, are the portion of the total effective seismic weight of the structure (W) assigned to level i or x

h_i, and h_x, are the height from the base to level i or x

k is an exponent related to the structure period. For this building, fundamental period from ELF procedure is 3.77 sec, k is taken equal to 2.

Vertical distribution of seismic load (F_x) by ELF procedure and stability ratio (θ) are summarized in Table D.7 and Table D.8, respectively. P_x in column 3 of Table D.8 is computed using all dead loads and super-imposed dead loads of the building. Applying F_x to the structure, design story force V_x can be obtained as shown in column 4 of Table D.8. The design story drift, Δ shown in column 5 of Table D.8 is computed by multiplying the story drift due to F_x with C_d factor. $\theta_{\max}$ shown in column 7 of Table D.8 is computed using β=1. It shows that θ<0.1 and $\theta < \theta_{\max} (\beta = 1)$ for all stories; therefore, P-Delta effect is not required for this building.

จุฬาลงกรณ์มหาวิทยาลัย
CHULALONGKORN UNIVERSITY

Table D.7 Vertical distribution of seismic load by ELF procedure in X-direction.

Story	Story height	h_x (m)	W_x (kN)	$w_x h_x^k$	C_{vx}	F_x (kN)
39	3.2	125.55	6,446	1.0E+08	0.065	404
38	3.2	122.35	7,010	1.0E+08	0.067	417
37	3.2	119.15	7,010	1.0E+08	0.063	395
36	3.2	115.95	7,182	9.7E+07	0.062	384
35	3.2	112.75	7,354	9.3E+07	0.060	371
34	3.2	109.55	7,354	8.8E+07	0.056	351
33	3.2	106.35	7,354	8.3E+07	0.053	330
32	3.2	103.15	7,354	7.8E+07	0.050	311
31	3.2	99.95	7,354	7.3E+07	0.047	292
30	3.2	96.75	7,354	6.9E+07	0.044	273
29	3.2	93.55	7,354	6.4E+07	0.041	256
28	3.2	90.35	7,354	6.0E+07	0.038	238
27	3.2	87.15	7,354	5.6E+07	0.036	222
26	3.2	83.95	7,354	5.2E+07	0.033	206
25	3.2	80.75	7,354	4.8E+07	0.031	190
24	3.2	77.55	7,354	4.4E+07	0.028	176
23	3.2	74.35	7,354	4.1E+07	0.026	161
22	3.2	71.15	7,354	3.7E+07	0.024	148
21	3.2	67.95	7,354	3.4E+07	0.022	135
20	3.2	64.75	7,354	3.1E+07	0.020	122
19	3.2	61.55	7,354	2.8E+07	0.018	111
18	3.2	58.35	7,354	2.5E+07	0.016	99
17	3.2	55.15	7,354	2.2E+07	0.014	89
16	3.2	51.95	7,354	2.0E+07	0.013	79
15	3.2	48.75	7,354	1.7E+07	0.011	69
14	3.2	45.55	7,298	1.5E+07	0.010	60
13	3.2	42.35	7,440	1.3E+07	0.008	53
12	3.2	39.15	7,526	1.2E+07	0.007	46
11	3.2	35.95	7,612	9.8E+06	0.006	39
10	3.2	32.75	7,698	8.3E+06	0.005	33
9	3.5	29.55	8,002	7.0E+06	0.004	28
8	4.9	26.05	18,906	1.3E+07	0.008	51
7	2.65	21.15	17,769	7.9E+06	0.005	32
6	2.65	18.50	16,984	5.8E+06	0.004	23
5	2.65	15.85	16,984	4.3E+06	0.003	17
4	2.65	13.20	16,984	3.0E+06	0.002	12
3	2.05	10.55	16,506	1.8E+06	0.001	7
2	5.5	8.50	19,247	1.4E+06	0.001	6
1	3	3.00	19,518	1.8E+05	0.000	0.70
Total			370,566	1.6E+09	1	6,236

Table D.8 Stability ratio for checking of P-Delta effect in X-direction.

Story	h_{sx} (m)	P_x (kN)	V_x (kN)	Δ (m)	θ	θ_{max} (β=1)
39	3.2	7,010	404	0.043	0.05	0.10
38	3.2	14,021	820	0.043	0.05	0.10
37	3.2	21,031	1216	0.044	0.05	0.10
36	3.2	28,385	1599	0.044	0.05	0.10
35	3.2	35,740	1971	0.045	0.05	0.10
34	3.2	43,094	2321	0.046	0.05	0.10
33	3.2	50,448	2652	0.047	0.06	0.10
32	3.2	57,803	2962	0.048	0.06	0.10
31	3.2	65,157	3254	0.048	0.06	0.10
30	3.2	72,511	3528	0.049	0.06	0.10
29	3.2	79,866	3783	0.050	0.07	0.10
28	3.2	87,220	4022	0.050	0.07	0.10
27	3.2	94,574	4244	0.051	0.07	0.10
26	3.2	101,929	4450	0.051	0.07	0.10
25	3.2	109,283	4640	0.051	0.08	0.10
24	3.2	116,637	4816	0.051	0.08	0.10
23	3.2	123,992	4977	0.052	0.08	0.10
22	3.2	131,346	5125	0.051	0.08	0.10
21	3.2	138,700	5260	0.051	0.08	0.10
20	3.2	146,055	5382	0.051	0.09	0.10
19	3.2	153,409	5493	0.050	0.09	0.10
18	3.2	160,764	5592	0.050	0.09	0.10
17	3.2	168,118	5681	0.049	0.09	0.10
16	3.2	175,472	5760	0.048	0.09	0.10
15	3.2	182,827	5830	0.047	0.09	0.10
14	3.2	190,124	5890	0.045	0.09	0.10
13	3.2	197,651	5943	0.044	0.09	0.10
12	3.2	205,177	5989	0.042	0.09	0.10
11	3.2	212,876	6028	0.040	0.09	0.10
10	3.2	220,574	6060	0.037	0.09	0.10
9	3.5	228,755	6088	0.038	0.08	0.10
8	4.9	248,494	6139	0.048	0.08	0.10
7	2.65	265,477	6171	0.022	0.07	0.10
6	2.65	282,461	6194	0.020	0.07	0.10
5	2.65	299,445	6211	0.018	0.06	0.10
4	2.65	316,429	6223	0.015	0.06	0.10
3	2.05	332,678	6230	0.010	0.05	0.10
2	5.5	353,151	6235	0.019	0.04	0.10
1	3	370,564	6236	0.004	0.01	0.10

จุฬาลงกรณ์มหาวิทยาลัย
CHULALONGKORN UNIVERSITY

D.2.11 Design load combinations

The design load combinations are the followings.

$$U_1 = 0.75(1.4D + 1.7L) + 1.0E_x + 0.3E_y$$
$$U_2 = 0.75(1.4D + 1.7L) + 0.3E_x + 1.0E_y$$
$$U_3 = 0.9D + 1.0E_x + 0.3E_y$$
$$U_4 = 0.9D + 0.3E_x + 1.0E_y$$

Two sets for each load combination are required because shear force and bending moment use different design spectrum (see Figure D.8) as explained in Section A.2.9. The first set is for computing bending moment and axial force, in which the earthquake load is from elastic spectrum reduced by *R* factor for the entire periods. The second set is for computing shear force, in which the earthquake load is from elastic spectrum reduced by $R/(SF \times \Omega_0)$ factor only at the fundamental period of the building in the direction considered.

The design force demands from load combination U_1 are presented in Figure D.12 for RC core wall. U_1 (*V*) and U_1 (*M*) refer to load combination U_1 used for computing shear force and axial force/bending moment, respectively.

จุฬาลงกรณ์มหาวิทยาลัย
CHULALONGKORN UNIVERSITY

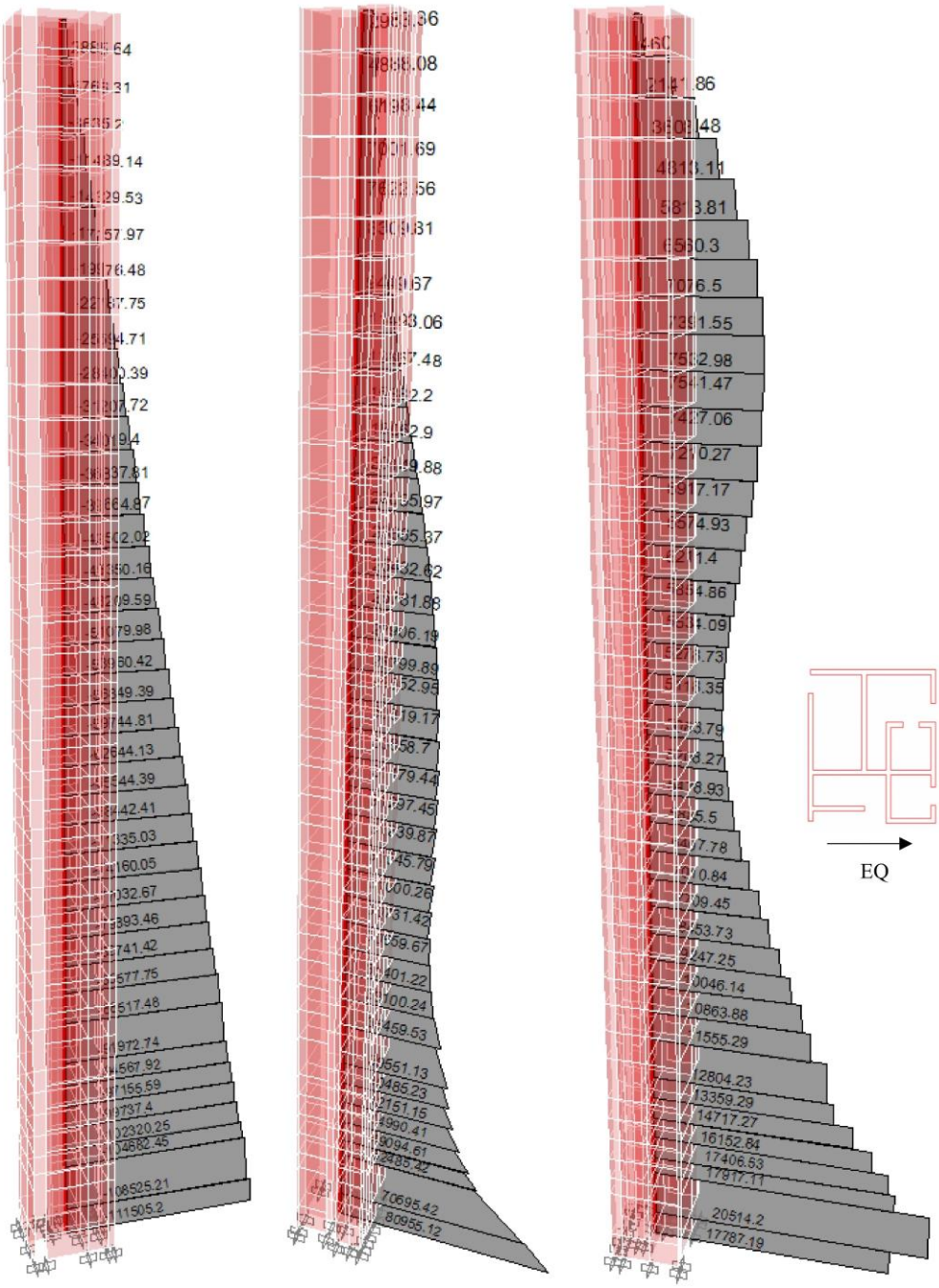

(a) Axial force (kN) (b) Bending moment (kN.m) (c) Shear force (kN)

$U_1(M) = 0.75(1.4D + 1.7L) + 1.0E_x + 0.3E_y$ $U_1(V) = 0.75(1.4D + 1.7L) + 1.0E_x + 0.3E_y$

Figure D.12 (a) Axial force, (b) bending moment, and (c) shear force of RC core wall from load combination $U_1 = 0.75(1.4D + 1.7L) + 1.0E_x + 0.3E_y$

D.2.12 Computation of strain in RC wall

Ductile detailing of an RC wall is required at the locations where strain in that wall exceeds a certain limit; for example, 0.002. Maximum strain in the wall is computed by:

Maximum tensile strain: $$\varepsilon_t = \frac{P}{EA_g} + \frac{M}{EI_{eff}}(c + \frac{c_{long}}{3})$$

Maximum compressive strain: $$\varepsilon_c = \frac{P}{EA_g} - \frac{M}{EI_{eff}}(c - \frac{c_{long}}{3})$$

Below is the detail example for computing strain in an RC core wall (see Figure D.13) at the base floor due to earthquake load in X-direction.

- Core wall cross section's properties

$$A = 14.61m^2$$
$$E = 4700\sqrt{f_c^{'}} = 4700\sqrt{32} = 26587MPa$$
$$I_y = I_g = 102.32m^4$$
$$c = c_{long} = 4.06m$$

- Computation of I_{eff}

$$0.35I_g \le I_{eff} = \left(0.80 + 25\frac{A_{st}}{A_g}\right)\left(1 - \frac{M_u}{P_u h} - 0.5\frac{P_u}{P_0}\right)I_g \le 0.875I_g$$

Vertical reinforcement ratio of core wall: $\frac{A_{st}}{A_g} = 0.25\%$

Design force: $M_u = 80,955kN.m$ $P_u = 111,505kN$. They are taken from load combination $U_1(M) = 0.75(1.4D + 1.7L) + 1.0E_x + 0.3E_y$ that produces minimum value of I_{eff}.

Nominal axial strength at zero eccentricity: $P_0 = 326,222kN$

Length of the wall under loading in X-direction: *h*=7.7m

$$I_{eff} = (0.80 + 25 \times 0.0025)\left(1 - \frac{80,955}{111,505 \times 7.7} - 0.5\frac{111,505}{326,222}\right)I_g = 0.63I_g$$

- Elastic forces from linear RSA combined with factor gravity loads

M and *P* of the wall are computed from linear RSA (*R*=1) combined with factored gravity load of *D*+0.25*L*. For linear RSA, there are positive (E_{max}) and negative (E_{min}) results. Compressive and tensile strains are computed using load combination with E_{min} and E_{max}, that produce maximum compressive and tensile strains, respectively. The *M* and *P* at the base of the wall are shown in Table below.

Internal force	*D*+0.25*L*	E_{max}	E_{min}	$D+0.25L+E_{min}$	$D+0.25L+E_{max}$
P (kN)	-101,698	38,297	-38,297	-139,994	-63,401
M (kN.m)	1,917	324,630	-324,630	-322,713	326,546

Maximum tensile and compressive strains at the base of the wall are

$$\varepsilon_t = \frac{-63,401}{2.6587\times10^7\times14.61} + \frac{326,546}{2.6587\times10^7\times0.63\times102.32}\left(4.06+\frac{4.06}{3}\right)$$
$$\varepsilon_t = -0.00016 + 0.00103$$
$$\varepsilon_t = 0.00087$$

$$\varepsilon_c = \frac{-139,994}{2.6587\times10^7\times14.61} - \frac{322,713}{2.6587\times10^7\times0.63\times102.32}\left(\frac{2\times4.06}{3}\right)$$
$$\varepsilon_c = -0.00036 - 0.00051$$
$$\varepsilon_c = -0.00087$$

The maximum tensile and compressive strains along the height of the wall are shown in Figure D.13. In this building, axial strains of wall are less than 0.002, seismic ductile detailing in RC wall is not required.

จุฬาลงกรณ์มหาวิทยาลัย
Chulalongkorn University

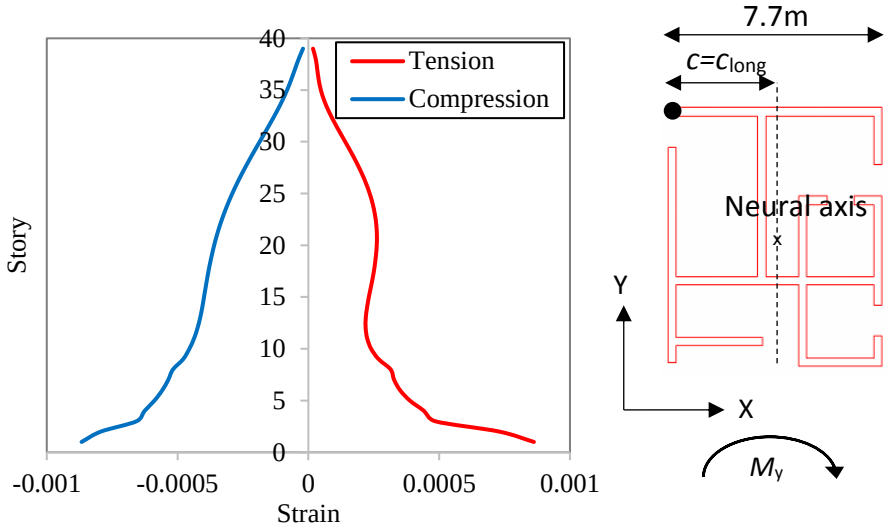

Figure D.13 Maximum compressive and tensile strains in the wall due to earthquake in X-direction.

จุฬาลงกรณ์มหาวิทยาลัย
CHULALONGKORN UNIVERSITY

REFERENCES

Adebar, P., J. Mutrie, R. DeVall and D. Mitchell (2014). Seismic design of concrete buildings: The 2015 Canadian Building Code. 10th US National Conference on Earthquake Engineering, Anchorage, Alaska.

American Concrete Institute (2014). Building code requirements for structural concrete (ACI 318M-14) and commentary (ACI 318RM-14). Farmington Hills, USA.

American Society of Civil Engineers (2010). Minimum design loads for buildings and other structures. ASCE/SEI 7-10. Reston, Virginia.

American Society of Civil Engineers (2013). Seismic evaluation and retrofit of existing buildings. ASCE/SEI 41-13. Reston, Virginia.

American Society of Civil Engineers (2016). Minimum design loads and associated criteria for buildings and other structures. ASCE/SEI 7-16. Reston, Virginia.

Baker, J. W. (2011). "Conditional mean spectrum: Tool for ground-motion selection." Journal of Structural Engineering **137**(3): 322-331.

Baker, J. W. and A. C. Cornell (2006). "Spectral shape, epsilon and record selection." Earthquake Engineering and Structural Dynamics **35**(9): 1077-1095.

Bangkok Metropolitan Administration (2001). Bangkok building control law, B.E. 2544. http://203.155.220.230/bmainfo/law/law.php?t=031.

Blakeley, R. W. G., R. C. Cooney and L. M. Megget (1975). "Seismic shear loading at flexural capacity in cantilever wall structures." Bulletin of the New Zealand Society for Earthquake Engineering **8**(4): 278-290.

Boivin, Y. and P. Paultre (2012). "Seismic force demand on ductile reinforced concrete shear walls subjected to western North American ground motions: Part 2 - new capacity design methods." Canadian Journal of Civil Engineering **39**(7): 738-750.

Bommer, J. J., S. G. Scott and S. K. Sarma (2000). "Hazard-consistent earthquake scenarios." Soil Dynamics and Earthquake Engineering **19**(4): 219-231.

Calugaru, V. and M. Panagiotou (2012). "Response of tall cantilever wall buildings to strong pulse type seismic excitation." Earthquake Engineering and Structural Dynamics **41**(9): 1301-1318.

Canadian Standard Association (2004). Design of concrete structures. CSA standard A23.3-04. Ontario, Canada.

Chopra, A. K. and R. K. Goel (2001). "Direct Displacement-Based Design: Use of Inelastic vs. Elastic Design Spectra." Earthquake Spectra **17**(1): 47-64.

Chopra, A. K. and R. K. Goel (2002). "A modal pushover analysis procedure for estimating seismic demands for buildings." Earthquake Engineering and Structural Dynamics **31**(3): 561-582.

Chopra, A. K., R. K. Goel and C. Chintanapakdee (2004). "Evaluation of a modified MPA procedure assuming higher modes as elastic to estimate seismic demands." Earthquake Spectra **20**(3): 757-778.

Chopra, A. K. and F. McKenna (2016). "Modeling viscous damping in nonlinear response history analysis of buildings for earthquake excitation." Earthquake Engineering and Structural Dynamics **45**(2): 193-211.

Computers and Structures, Inc. (2011). PERFORM-3D, Nonlinear analysis and performance assessment of 3D structures, Version 5.0.1. Berkeley, California.

Computers and Structures, Inc. (2015). ETABS, Integrated building design software, Version 15.2.2. Berkeley, California.

Department of Public Works and Town & Country Planning (2009). Seismic Resistant Design of Buildings and Structures, DPT 1302-52. Bangkok, Thailand. (in Thai).

Department of Public Works and Town & Country Planning (2018). Seismic Resistant Design of Buildings and Structures, DPT 1301/1302-61. Bangkok, Thailand. (in Thai).

จุฬาลงกรณ์มหาวิทยาลัย
CHULALONGKORN UNIVERSITY

Eibl, J. and E. Keintzel (1988). Seismic shear forces in RC cantilever shear walls. 9th World Conference on Earthquake Engineering, Tokyo-Kyoto, Japan.

European Committee for Standardization (2004). Eurocode 8: Design of structures for earthquake resistance - Part 1: General rules, seismic actions and rules for buildings. Brussels, Belgium.

Fox, M. J., T. J. Sullivan and K. Beyer (2014). "Capacity design of coupled RC walls." Journal of Earthquake Engineering **18**(5): 735-758.

Ghorbanirenani, I., R. Tremblay, P. Léger and M. Leclerc (2011). "Shake table testing of slender RC shear walls subjected to eastern North America seismic ground motions." Journal of Structural Engineering, ASCE **138**(12): 1515-1529.

Ghosh, S. K. and V. P. Markevicius (1990). Design of earthquake resistant shear walls to prevent shear failure. 4th US National Conference on Earthquake Engineering, Palm Springs, California.

Haselton, C. B., J. W. Baker, J. P. Stewart, A. S. Whittaker, N. Luco, A. Fry, R. O. Hamburger, R. B. Zimmerman, J. D. Hooper, F. A. Charney and R. G. Pekelnicky (2017). "Response history analysis for the design of new buildings in the NEHRP provisions and ASCE/SEI 7 standard: Part I - Overview and specification of ground motions." Earthquake Spectra **33**(2): 373-395.

Jimenez, F. J. and L. M. Massone (2018). "Experimental seismic shear force amplification in scaled RC cantilever shear walls with base irregularities." Bulletin of Earthquake Engineering **16**(10): 4735-4760.

Jirasakjamroonsri, A., N. Poovarodom and P. Warnitchai (2018). "Seismic site characteristics of shallow sediments in the Bangkok Metropolitan Region, and their inherent relations." Bulletin of Engineering Geology and the Environment: 1-17.

Kappos, A. J. and P. Antoniadis (2007). "A contribution to seismic shear design of R/C walls in dual structures." Bulletin of Earthquake Engineering **5**(3): 443-466.

จุฬาลงกรณ์มหาวิทยาลัย
CHULALONGKORN UNIVERSITY

Kazaz, İ. and P. Gülkan (2016). "Dynamic shear force amplification in regular frame–wall systems." The Structural Design of Tall and Special Buildings **25**(2): 112-135.

Khy, K. and C. Chintanapakdee (2017). "Evaluation of seismic shear demands of RC core walls in Thailand determined by RSA Procedure." Engineering Journal **21**(2): 151-172.

Khy, K., C. Chintanapakdee, P. Warnitchai and A. C. Wijeyewickrema (2019). "Modified response spectrum analysis to compute shear force in tall RC shear wall buildings." Engineering Structures **180**: 295-309.

Klemencic, R., J. A. Fry, J. D. Hooper and B. G. Morgen (2007). "Performance-based design of ductile concrete core wall buildings—issues to consider before detailed analysis." The Structural Design of Tall and Special Buildings **16**(5): 599-614.

Kolozvari, K., G. Piatos and K. Beyer (2017). Practical nonlinear modeling of U-shaped reinforced concrete walls under bi-directional loading. 16th World Conference on Earthquake Engineering, Santiago, Chile.

Koopaee, M. E., R. P. Dhakal and G. MacRae (2017). "Effect of ground motion selection methods on seismic collapse fragility of RC frame buildings." Earthquake Engineering and Structural Dynamics **46**(11): 1875-1892.

Kwong, N. S. and A. K. Chopra (2017). "A generalized conditional mean spectrum and its application for intensity-based assessments of seismic demands." Earthquake Spectra **33**(1): 123-143.

Leng, K., C. Chintanapakdee and T. Hayashikawa (2014). "Seismic shear forces in shear walls of a medium-rise building designed by response spectrum analysis." Engineering Journal **18**(4): 73-95.

Los Angeles Tall Buildings Structural Design Council (2017). An alternative procedure for seismic analysis and design of tall buildings located in the Los Angeles region. Los Angeles, California.

จุฬาลงกรณ์มหาวิทยาลัย
CHULALONGKORN UNIVERSITY

Luu, H., P. Léger and R. Tremblay (2014). "Seismic demand of moderately ductile reinforced concrete shear walls subjected to high-frequency ground motions." Canadian Journal of Civil Engineering **41**(2): 125-135.

Mander, J. B., M. J. Priestley and R. Park (1988). "Theoretical stress-strain model for confined concrete." Journal of Structural Engineering, ASCE **114**(8): 1804-1826.

Maniatakis, C. A., I. N. Psycharis and C. C. Spyrakos (2013). "Effect of higher modes on the seismic response and design of moment-resisting RC frame structures." Engineering Structures **56**: 417-430.

Marius, M. (2013). "Seismic behaviour of reinforced concrete shear walls with regular and staggered openings after the strong earthquakes between 2009 and 2011." Engineering Failure Analysis **34**: 537-565.

Menegotto, M. and E. Pinto (1973). Method of analysis for cyclically loaded reinforced concrete plane frames including changes in geometry and non-elastic behavior of elements under combined normal force and bending. IABSE Symposium, Lisbon, Portugal.

Munir, A. and P. Warnitchai (2012). "The cause of unproportionately large higher mode contributions in the inelastic seismic responses of high-rise core-wall buildings." Earthquake Engineering and Structural Dynamics **41**(15): 2195-2214.

Naish, D., A. Fry, R. Klemencic and J. Wallace (2013). "Reinforced concrete coupling beams - Part II: Modeling." ACI Structural Journal **110**(06): 1067-1075.

Najam, F. A. and P. Warnitchai (2018). "A modified response spectrum analysis procedure to determine nonlinear seismic demands of high-rise buildings with shear walls." The Structural Design of Tall and Special Buildings **27**(1): e1409.

National Building Code of Canada (2010). Commission on building and fire codes, National Research Council of Canada. Ottawa, Canada.

National Institute of Standards and Technology (2011). Selecting and scaling earthquake ground motions for performing response-history analyses, NIST GCR 11-917-15, prepared by the NEHRP Consultants Joint Venture, Gaithersburg, Maryland

จุฬาลงกรณ์มหาวิทยาลัย
CHULALONGKORN UNIVERSITY

New Zealand Standard (2006). Concrete structure standard - Part 2: Commentary on the design of concrete structures. NZS 3101. Wellington, New Zealand.

Orakcal, K., J. W. Wallace and J. P. Conte (2004). "Flexural modeling of reinforced concrete walls-model attributes." ACI Structural Journal **101**(5): 688-698.

Ordonez, G. A. (2012). SHAKE2000-A computer program for the 1-D analysis of geotechnical earthquake engineering problems. GeoMotion, LLC; Lacey, Washington, USA.

Ornthammarath, T., P. Warnitchai, K. Worakanchana, S. Zaman, R. Sigbjörnsson and C. G. Lai (2011). "Probabilistic seismic hazard assessment for Thailand." Bulletin of Earthquake Engineering **9**(2): 367-394.

Pacific Earthquake Engineering Research (2017). Tall Buildings Initiative, Guidelines for performance-based seismic design of tall buildings, PEER-2017/06. Berkeley, California.

Panagiotou, M. and J. I. Restrepo (2011). "Displacement-based method of analysis for regular reinforced-concrete wall buildings: Application to a full-scale 7-story building slice tested at UC–San Diego." Journal of Structural Engineering, ASCE **137**(6): 677-690.

Panagiotou, M., J. I. Restrepo and J. P. Conte (2011). "Shake-table test of a full-scale 7-story building slice. Phase I: Rectangular wall." Journal of Structural Engineering, ASCE **137**(6): 691-704.

Paulay, T. and M. J. N. Priestley (1992). Seismic design of reinforced concrete and masonry buildings. John Wiley and Sons, New York, USA.

Pennucci, D., T. J. Sullivan and G. M. Calvi (2015). "Inelastic higher-mode response in reinforced concrete wall structures." Earthquake Spectra **31**(3): 1493-1514.

Poovarodom, N., A. Jirasakjamroonsri, T. Ornthammarath and P. Warnitchai (2017). New design spectral acceleration of soft and deep deposits in Bangkok. International Conference on Earthquake Eegineering and Structural Dynamics, Reykjavík, Iceland.

จุฬาลงกรณ์มหาวิทยาลัย
Chulalongkorn University

Priestley, M., G. Calvi and M. Kowalsky (2007). Direct displacement-based seismic design of structures. 2007 New Zealand Society for Earthquake Engineering Conference, Palmerston North, New Zealand.

Priestley, M. J. N. (2003). "Does capacity design do the job? An examination of higher mode effects in cantilever walls." Bulletin of the New Zealand Society for Earthquake Engineering **36**(4): 276-292.

Priestley, M. J. N., G. M. Calvi and M. J. Kowalsky (2007). Displacement-based seismic design of structures. IUSS Press, Pavia, Italy.

Rejec, K., T. Isaković and M. Fischinger (2012). "Seismic shear force magnification in RC cantilever structural walls, designed according to Eurocode 8." Bulletin of Earthquake Engineering **10**(2): 567-586.

Research and Consultancy Institute of Thammasat University Drafting of Thai building code project. Report Vol. 2: Building loads, submitted to Department of Public Works and Town & Country Planning. Bangkok, Thailand; 2009. (in Thai).

Rutenberg, A. and E. Nsieri (2006). "The seismic shear demand in ductile cantilever wall systems and the EC8 provisions." Bulletin of Earthquake Engineering **4**(1): 1-21.

SeismoSoft (2016). SeismoMatch, A computer application capable of adjusting earthquake accelerograms to match a specific target response spectrum, Version 2016. http://www.seismosoft.com.

Sinković, N. L., M. Dolšek and J. Žižmond (2018). "Impact of the type of the target response spectrum for ground motion selection and of the number of ground motions on the pushover-based seismic performance assessment of buildings." Engineering Structures **175**: 731-742.

Sullivan, T. J., M. J. N. Priestley and G. M. Calvi (2008). "Estimating the higher-mode response of ductile structures." Journal of Earthquake Engineering **12**(3): 456-472.

Telleen, K., J. Maffei, J. Heintz, P. Bonelli, D. Kelly and M. Willford (2017). Addressing boundary design for reinforced concrete walls, based on studies of the 2010 Chile earthquake. 16th World Conference on Earthquake Engineering, Santiago Chile.

จุฬาลงกรณ์มหาวิทยาลัย
CHULALONGKORN UNIVERSITY

Veletsos, A. and N. M. Newmark (1960). Effect of inelastic behavior on the response of simple systems to earthquake motions. 2nd World Conference on Earthquake Engineering, Tokyo, Japan.

Wallace, J. W., L. M. Massone, P. Bonelli, J. Dragovich, R. Lagos, C. Lüders and J. Moehle (2012). "Damage and implications for seismic design of RC structural wall buildings." Earthquake Spectra **28**(S1): S281-S299.

Yathon, J. S. (2011). Seismic shear demand of reinforced concrete cantilever walls. Master Thesis, University of British Columbia, Vancouver, Canada.

จุฬาลงกรณ์มหาวิทยาลัย
CHULALONGKORN UNIVERSITY

VITA

NAME	Kimleng Khy
DATE OF BIRTH	01 February 1991
PLACE OF BIRTH	Kampot, Cambodia
INSTITUTIONS ATTENDED	PhD (2016-2019): Department of Civil Engineering, Chulalongkorn University, Thailand M.Eng. (2013-2015): Department of Civil Engineering, Chulalongkorn University, Thailand B.Eng. (2008-2013): Department of Civil Engineering, Institute of Technology of Cambodia, Cambodia
HOME ADDRESS	9E, Chrang Chamres 2, Russey Keo, Phnom Penh, 12108, Cambodia
PUBLICATION	Khy, K., Chintanapakdee, C., Warnitchai, P. and Wijeyewickrema, A. C. (2019), "Modified response spectrum analysis to compute shear force in tall RC shear wall buildings", Engineering Structures, Vol 180, pp. 295-309. Khy, K, Chintanapakdee C. and Wijeyewickrema, A. C. (2019), "Application of conditional mean spectrum in nonlinear response history analysis of tall buildings on soft soil", Engineering Journal, Vol 23, Issue 1, pp. 135-150. Khy, K, Chintanapakdee C. (2017), "Evaluation of seismic shear demands of RC core walls in Thailand determined by RSA Procedure", Engineering Journal, Vol 21, Issue 2, pp. 151-172. Khy, K. and Chintanapakdee, C. (2018), "A modified response spectrum analysis procedure for design of tall RC shear wall and RC moment frame buildings", 7th Asia

จุฬาลงกรณ์มหาวิทยาลัย
CHULALONGKORN UNIVERSITY

Conference on Earthquake Engineering, November 22-24, Bangkok, Thailand.

Khy, K., Chintanapakdee, C. and Wijeyewickrema, A. C. (2018), "An improved RSA procedure to compute shear force in tall RC shear wall buildings", Proceedings of EURO-C 2018, February 26 - March 01, Bad Hofgastein, Austria, pp. 993-1002.

Khy, K. and Chintanapakdee, C. (2017), "Application of CMS ground motions in nonlinear dynamic analysis of tall buildings", 30th KKHTCNN Symposium on Civil Engineering, November 02-04, Taiwan.

Khy, K. and Chintanapakdee, C. (2017), "Seismic shear demands of RC core walls for design of tall buildings in Thailand", 16th World Conference on Earthquake Engineering, January 09-13, Santiago Chile.

Khy, K. and Chintanapakdee (2015), "Comparison of seismic demands of RC core walls determined by RSA and NLRHA", 28th KKHTCNN Symposium on Civil Engineering, November 16-18, Bangkok, Thailand.

Khy, K. and Chintanapakdee (2015), "Seismic Shear Demands of Reinforced Concrete Core Walls", 20th National Convention on Civil Engineering, July 08-10, Chonburi, Thailand.

AWARD RECEIVED

JICA AUN/SEED-Net Scholarship for PhD, August 2016-August 2019.

JICA AUN/SEED-Net Scholarship for M.Eng, October 2013-October 2015.

Cambodian Government Scholarship for B.Eng, October 2008-July-2013.

Honda Young Engineers and Scientists Award in Cambodia organized by Honda Company, Japan, 2012.

จุฬาลงกรณ์มหาวิทยาลัย
CHULALONGKORN UNIVERSITY